UNIVERSIDADE FEDERAL DE SANTA CATARINA
CAMPUS FLORIANÓPOLIS
PROGRAMA DE PÓS-GRADUAÇÃO EM ENGENHARIA MECÂNICA

Neider Nadid Romero Nuñez

CONTRIBUTIONS TO THE KINEMATICS AND BALANCING OF MECHANISMS

Florianópolis
2023

Neider Nadid Romero Nuñez

CONTRIBUTIONS TO THE KINEMATICS AND BALANCING OF MECHANISMS

Tese submetida ao Programa de Pós-Graduação em Engenharia Mecânica da Universidade Federal de Santa Catarina para a obtenção do título de doutor em Engenharia Mecânica.
Orientador: Prof. Daniel Martins, Dr. Eng.
Co-orientador: Prof. Rodrigo Vieira, Dr. Eng.

Florianópolis
2023

Ficha de identificação da obra elaborada pelo autor,
através do Programa de Geração Automática da Biblioteca Universitária da UFSC.

Nuñez, Neider Nadid
Contributions to the kinematic and balancing of mechanisms / Neider Nadid Nuñez ; orientador, Daniel Martins, coorientador, Rodrigo S Vieira, 2023.
169 p.

Tese (doutorado) - Universidade Federal de Santa Catarina, Centro Tecnológico, Programa de Pós-Graduação em Engenharia Mecânica, Florianópolis, 2023.

Inclui referências.

1. Engenharia Mecânica. 2. Balanceamento estático. 3. Cinemática. 4. Balanceamento dinâmico. 5. Sistemas equimomentais. I. Martins, Daniel. II. Vieira, Rodrigo S. III. Universidade Federal de Santa Catarina. Programa de Pós-Graduação em Engenharia Mecânica. IV. Título.

Neider Nadid Romero Nuñez

CONTRIBUTIONS TO THE KINEMATICS AND BALANCING OF MECHANISMS

O presente trabalho em nível de doutorado foi avaliado e aprovado por banca examinadora composta pelos seguintes membros:

Prof. Tarcisio Antonio Hess Coelho, Dr. Eng.
Universidade de São Paulo

Prof. Eduardo Alberto Fancello, Dr. Eng.
Universidade Federal de Santa Catarina

Prof. Aníbal Alexandre Campos Bonilla, Dr. Eng.
Universidade do Estado de Santa Catarina

Prof. Eduardo Camponogara, Ph.D.
Universidade Federal de Santa Catarina

Certificamos que esta é a **versão original e final** do trabalho de conclusão que foi julgado adequado para obtenção do título de doutor em Engenharia Mecânica.

Documento assinado digitalmente
Henrique Simas
Data: 30/10/2023 09:16:20-0300
CPF: ***.194.639-**
Verifique as assinaturas em https://v.ufsc.br

Prof. Henrique Simas, Dr. Eng.
Coordenador do Programa

Documento assinado digitalmente
Daniel Martins
Data: 28/10/2023 12:28:47-0300
CPF: ***.746.219-**
Verifique as assinaturas em https://v.ufsc.br

Prof. Daniel Martins, Dr. Eng.
Orientador

Florianópolis, 3 de outubro de 2023.

This work is dedicated to the King of kings and the Lord of lords.

ACKNOWLEDGEMENTS

I am grateful to my wife, Lorena, for her patience and emotional support throughout this challenging journey. I also thank my parents, María and Jorge, for their financial and spiritual assistance.

I am immensely thankful to my advisor Daniel Martins for entrusting me with solving challenging problems. I appreciate his wise advice during moments of frustration and our valuable conversations. I thank professors Henrique Simas, Rodrigo Vieira, Eduardo Camponogara, and Eduardo Fancello for their teachings.

To my friends Alvaro and Carlos, for our discussions about history, music, philosophy, and the ritual of coffee with chocolate that was ever-present. I am grateful to all those individuals who contributed to the realization of this work in one way or another.

Special gratitude goes to the Méndez family for their support, with a special mention to Linda for her invaluable contribution in proofreading the English texts.

I thank to the Programa de Pós-Graduação em Engenharia Mecânica of the Universidade Federal de Santa Catarina and the Coordenação de Aperfeiçoamento de Pessoal de Nível Superior for their financial support.

“Algebra is generous; she often gives more than is asked of her.”
D’Alembert

RESUMO

Um mecanismo estaticamente balanceado permanece em equilíbrio em qualquer posição em sua faixa de movimento, o que é desejável em muitos dispositivos, pois dispensa a ação nos atuadores para suportar o peso do mecanismo. Além disso, uma melhor eficiência energética, controle simplificado e segurança inerente são propriedades adicionais de dispositivos estaticamente balanceados. Embora o balanceamento estático tenha sido formalmente estudado por várias décadas, as aplicações práticas ainda são desafiadoras. Portanto, é necessário desenvolver métodos que permitam aos projetistas enfrentarem sistematicamente o problema de balanceamento estático de mecanismos, utilizando ferramentas matemáticas modernas de modelagem. Os métodos presentes na literatura não são gerais, e, portanto, cada problema de balanceamento é resolvido caso a caso. Também não são relatados métodos para lidar com o balanceamento de mecanismos confinados em espaços de trabalho reduzidos. Essa limitação está presente nos métodos de síntese dimensional, uma vez que as variáveis de projeto são geralmente de natureza geométrica. Em muitos casos, é desejável usar as coordenadas dos pares cinemáticos como variáveis de projeto; esse assunto será discutido em detalhes nesta tese. O principal objetivo deste trabalho é desenvolver uma metodologia para o balanceamento estático de mecanismos, baseada na incorporação das coordenadas naturais na teoria dos helicóides. Existem abordagens na literatura que permitem o balanceamento estático completo mediante a adição de massas ou elos adicionais, tornando o mecanismo resultante volumoso e ineficiente no espaço ocupado. Neste trabalho, um método de balanceamento estático é desenvolvido combinando a teoria dos helicóides e as coordenadas naturais. Primeiramente, as ferramentas de análise cinemática são apresentadas e propostas usando coordenadas naturais e o método de bilateração, que são a base para a formulação das condições de equilíbrio de um mecanismo. Adicionalmente, o método proposto para o balanceamento estático é adaptado no balanceamento dinâmico de mecanismos planos mediante o uso de sistemas equimomentais de massas pontuais. Finalmente, serão propostos casos de estudo com o objetivo de avaliar os métodos de balanceamento estático e dinâmico desenvolvidos.

Palavras-chave: Balanceamento estático. Cinemática. Mecanismos. Balanceamento dinâmico. Sistemas equimomentais.

RESUMO EXPANDIDO

Introdução

Em um mecanismo estaticamente equilibrado, as forças ou os torques que atuam para manter o equilíbrio são mínimos ou nulos em qualquer configuração dentro de sua faixa de movimento. Nos casos de mecanismos completamente equilibrados, o número de posições de equilíbrio é infinito. Em contrapartida, um mecanismo de equilíbrio aproximado está em equilíbrio apenas para um número finito de posições dentro de sua faixa de movimento. O balanceamento aproximado é uma solução satisfatória para a maioria das aplicações práticas de engenharia. Embora alguns métodos forneçam mecanismos completamente equilibrados, eles exigem massas adicionais, elos auxiliares ou todas as molas ligadas ao elo fixo, o que resulta em um mecanismo volumoso e ineficiente em termos de espaço. O balanceamento estático é uma questão importante no projeto de manipuladores e mecanismos paralelos, uma vez que esses mecanismos são frequentemente utilizados em aplicações que envolvem grandes cargas. Nesses casos, o balanceamento estático pode aumentar a eficiência do mecanismo, uma vez que seus atuadores não precisam contribuir para suportar o peso dos elos em nenhuma configuração. Outra aplicação importante do balanceamento estático é o projeto de mecanismos para auxiliar pacientes em reabilitação que enfrentam dificuldades para levantar certos membros. O balanceamento estático tem sido objeto de estudo há várias décadas, e existem vários métodos que fornecem balanceadores de gravidade completamente equilibrados. No entanto, as aplicações práticas ainda representam um desafio. O projeto de mecanismos balanceados estaticamente com esses métodos requer a adição de massas e elos, levando em consideração molas de comprimento inicial zero ou simulando-as por meio de dispositivos adicionais. Poucos estudos na literatura abordam o balanceamento estático utilizando molas convencionais de tensão e torção. Além disso, o projeto de mecanismos estaticamente balanceados, limitado a um espaço de projeto reduzido, continua sendo um desafio. O balanceamento dinâmico de mecanismos pode ser tratado como balanceamento estático quando as forças inerciais são consideradas. Nesse caso, o problema dinâmico é transformado em um problema estático pela aplicação do princípio de D'Alembert. Uma maneira simples de determinar as forças de inércia é utilizar sistemas de massa pontual equimomentais, o que dispensa o uso de matrizes de inércia e apenas requer o conhecimento das acelerações das massas pontuais. A principal aplicação do balanceamento dinâmico é a redução de vibrações em máquinas e mecanismos, especialmente em motores de combustão interna e compressores. Nesta tese, é desenvolvido um método para o balanceamento estático de mecanismos. A técnica de balanceamento estático baseia-se na minimização das forças ou torques necessários para manter o equilíbrio. No método proposto, as coordenadas naturais são incorporadas à teoria de helicóides, o que possibilita uma formulação sistemática do problema de otimização, independentemente da complexidade do mecanismo. Além disso, neste trabalho, um procedimento para determinar sistemas de massa pontual em corpos rígidos planos é desenvolvido usando um formalismo moderno. Isso permite a adaptação do método de balanceamento estático para o balanceamento dinâmico de mecanismos planos.

Objetivos

O principal objetivo desta tese é desenvolver uma metodologia baseada na teoria dos helicóides para o balanceamento de mecanismos.

Os objetivos específicos deste trabalho são:

- Desenvolver um método baseado na incorporação das coordenadas naturais na teoria dos helicóides para o balanceamento estático de mecanismos.
- Desenvolver um procedimento para a obtenção de sistemas equimomentais de massas pontuais de corpos rígidos planos.
- Propor um método para a análise dinâmica de mecanismos planos por meio de sistemas equimomentais de massas pontuais.
- Adaptar o método de balanceamento estático proposto para o balanceamento dinâmico de mecanismos planos.

Metodologia

Inicialmente, a teoria básica do balanceamento estático e suas aplicações é analisada. Na revisão da literatura, torna-se evidente a falta de metodologias gerais para lidar com o problema de balanceamento estático, e as abordagens propostas só funcionam para casos específicos. Antes de tentar resolver o problema de balanceamento estático, é desenvolvido um método conceitual para a síntese dimensional de mecanismos balanceados estaticamente, o que permite obter uma visão global das diferentes alternativas ao desenvolver um método concreto de balanceamento estático. Em seguida, o problema cinemático é abordado, no qual as coordenadas naturais são apresentadas em detalhe. Esse formalismo é utilizado neste trabalho para modelar mecanismos planos e espaciais. O método de bilateração também é apresentado, o qual, em alguns casos, permite a determinação direta e elegante das coordenadas naturais dos mecanismos planos. Propõe-se a incorporação das coordenadas naturais à teoria helicóides, o que simplifica a resolução do problema de velocidade e aceleração de mecanismos planos e espaciais. O método de balanceamento estático proposto baseia-se na minimização das forças de atuação. A formulação do problema de otimização começa com a modelagem cinemática do mecanismo usando coordenadas naturais e, em seguida, a estática do problema é resolvida por meio da incorporação das coordenadas naturais no método de Davies, o que permite obter as equações da estática de forma sistemática. O uso de coordenadas naturais como variáveis de projeto possibilita o balanceamento estático de mecanismos com espaço de trabalho reduzido ou limitado. O método de balanceamento estático foi adaptado para o balanceamento dinâmico de mecanismos planos por meio do desenvolvimento de um procedimento para obter sistemas equimomentais de massas pontuais.

Resultados e Discussão

Foi proposto um método conceitual para o balanceamento estático de mecanismos, o qual permitiu obter uma visão global das diferentes abordagens para lidar com o problema de balanceamento estático. Em relação à análise cinemática, foi proposta a incorporação das coordenadas naturais na teoria de helicóides, o que possibilitou resolver o problema de velocidade e aceleração de forma simples. O método de bilateração também foi introduzido para resolver a cinemática de posição de mecanismos planos, no qual foi proposta uma maneira alternativa de representar matrizes de bilateração utilizando números complexos. Além disso, foi derivada uma matriz de bilateração livre singularidades para um mecanismo plano RRRP. Essa matriz de bilateração pode ser utilizada para resolver a cinemática de posição de mecanismos mais complexos com

sub-cadeias do tipo RRRP. Foi proposto um método sistemático para o balanceamento estático de mecanismos, independentemente de sua complexidade. Isso foi realizado através da incorporação das coordenadas naturais ao método de Davies. O método de balanceamento foi aplicado a um mecanismo de quatro barras para o movimento vertical em linha reta de uma carga externa, ao balanceamento de um mecanismo espacial RSSR-SS e ao balanceamento estático de um robô manipulador serial. Obtiveram-se reduções nos torques de atuação de 99,91%, 99,89% e 95,9%, respectivamente. Utilizando o conceito de matriz de pseudo-inércia, foi possível desenvolver uma metodologia para representar sistemas equimomentais de massas pontuais de corpos rígidos planos. Com o uso de sistemas equimomentais de massas pontuais, o método de balanceamento estático foi adaptado para o balanceamento dinâmico de mecanismos planos. O método de balanceamento dinâmico proposto foi aplicado no balanceamento dinâmico de um mecanismo biela-manivela, resultando em uma redução de 69,97% na força vibratória e uma redução de 99,99% no torque vibratório.

Considerações Finais

O método de balanceamento estático proposto demonstrou ser suficientemente geral para ser aplicado a qualquer mecanismo, independentemente de sua complexidade. O uso de coordenadas naturais em conjunto com a teoria de helicóides facilita a formulação do problema de balanceamento estático ótimo. Os sistemas de massas pontuais equimomentais permitem que o método de Davies possa ser usado para resolver problemas dinâmicos. Embora o método de balanceamento dinâmico tenha sido desenvolvido para mecanismos planos, com algum trabalho adicional, ele pode ser estendido a mecanismos espaciais.

Palavras-chave: Balanceamento estático. Cinemática. Mecanismos. Balanceamento dinâmico. Sistemas equimomentais.

ABSTRACT

A statically balanced mechanism remains in equilibrium at any position in its range of motion, which is desirable in many devices, as it eliminates the need for actuators to support the mechanism's weight. Furthermore, better energy efficiency, simplified control, and inherent safety are additional properties of statically balanced devices. Although static balancing has been formally studied for several decades, practical applications are still challenging. Therefore, it is necessary to develop methods that allow designers to systematically tackle the problem of static balancing of mechanisms using modern mathematical modeling tools. The methods in the literature are not general, so each balancing problem is solved on a case-by-case basis. There are also no reported methods for dealing with the balancing of confined mechanisms in small workspaces. This limitation is present in dimensional synthesis methods since the design variables are generally geometric. This limitation is present in the dimensional synthesis methods since the design variables are usually geometric, and, in many cases, it is desirable to use the coordinates of the kinematic pairs as design variables; this issue will be discussed in detail in this thesis. The main objective of this work is to develop a methodology for the static balancing of mechanisms based on incorporating natural coordinates into screw theory. Some approaches in the literature allow complete static balancing by adding additional masses or links, making the resulting mechanism bulky and inefficient in the space occupied. In this work, a static balancing method is developed that combines screw theory and natural coordinates. First, kinematic analysis tools are presented and proposed using natural coordinates and the bilateration method, which are the basis for formulating the equilibrium conditions of a mechanism. Additionally, the methods proposed for static balancing are adapted to the dynamic balancing of planar mechanisms by using equimomental systems of point masses. Finally, case studies will be proposed to evaluate the static and dynamic balancing methods developed.

Keywords: Static balancing. Kinematic. Mechanisms. Dynamic balancing. Equimomental system.

LIST OF FIGURES

LIST OF TABLES

LIST OF ABBREVIATIONS AND ACRONYMS

DoF	Degree of Freedom
LAR	Laboratory of Applied Robotics Raul Guenther

LIST OF SYMBOLS

V	Total potential energy
V_g	Gravitational potential energy
V_e	Elastic potential energy
$\mathbf{q}$	Generalized coordinates vector
$\mathbf{\Phi}$	Constraint equations vector
n_c	Number of constraint equations
n_v	Number of coordinates
M	Mobility of a mechanism
$\mathbf{\Phi_q}$	Jacobian matrix for constraint equations
$\mathbf{N}_{ijk}$	Bilateration matrix of the oriented triangle with vertices i, j, k
z_{pqr}	Bilaterator for the triangle with vertices p, q, r
$\mathbf{Y}_{ijk}$	Bilateration matrix for a RRRP kinematic chain
$\mathbf{\$}$	Screw
$\hat{\mathbf{\$}}$	Normalised screw
h	Screw pitch
$\hat{\mathbf{M}}_N$	Network unit motion matrix
${}^d\hat{\mathbf{M}}_N$	Dependent network unit motion matrix
${}^i\hat{\mathbf{M}}_N$	Independent network unit motion matrix
$\delta_{\mathbf{q}}$	Virtual displacement vector
$\dot{\mathbf{q}}^*$	Virtual velocity vector
$\hat{\mathbf{A}}_N$	Network unit action matrix
$\mathbf{\Psi}$	Vector of magnitudes of action screws
$\hat{\mathbf{A}}_D$	Unit action matrix
$\mathbf{Q}_A$	Action graph fundamental cutset matrix
${}^a\mathbf{\Psi}$	Vector of the forces supply by each actuator
$\mathbf{z}$	Design variables vector
$\underline{\mathbf{z}}$	Lower bounds of design variables vector
$\overline{\mathbf{z}}$	Upper bounds of design variables vector
$\otimes$	Kronecker product
$\widetilde{\mathbf{\Xi}}$	Pseudo-inertia matrix
$\widetilde{\mathbf{p}}$	Homogeneous position vector
$\mathbf{G}$	Homogeneous transformation matrix
$\widetilde{\mathbf{D}}$	Non-rigid transformation
$\mathbf{U}$	Orthogonal matrix
$\mathbf{\$}_i^{in}$	Inertia screw of the body i
$\mathbf{\$}_{sh}$	Shaking screw
$\boldsymbol{\eta}$	Normalization matrix
$\boldsymbol{\nu}$	Weight matrix

CONTENTS

1 INTRODUCTION

A mechanism is statically balanced in a range of motion if it remains in equilibrium in any position in that range of motion, or it can also be said that a mechanism is statically balanced if the weight of the links does not produce any torque or force on the actuators under static conditions, for any configuration of the mechanism (MOORE, 2009). The complete balanced mechanism remains in equilibrium for an infinite number of positions in its range of motion, whereas an approximate balancer mechanism is in equilibrium only for a finite number of positions in its range of motion. For the majority of practical engineering applications, an approximate balancer mechanism is a satisfactory solution. Although there are methods that provide exactly balanced mechanisms, they require additional masses or auxiliary links, or all springs attached to the fixed link, resulting in a bulky and space-inefficient mechanism (VEER; SUJATHA, 2015).

Static balancing is an important issue in the design of parallel manipulators and mechanisms, since parallel mechanisms are often used in applications where large loads are involved, where static balancing can improve the efficiency of the mechanism since its actuator does not contribute to supporting the weight of the links in any configuration. Another important application of static balancing is the design of mechanisms to help patients in rehabilitation with difficulties lifting some of their limbs.

Static balancing has been studied for several decades, and there are several methods that provide exact gravity balancers, but practical applications have been elusive (VEER; SUJATHA, 2015). Designing statically balanced mechanisms with these methods requires the addition of masses and links, in addition to considering zero-free-length springs or simulated them through additional devices. There are still few works in the literature that can deal with static balancing using conventional tension and torsion springs. Furthermore, the design of statically balanced mechanisms confined to a reduced design space is still a challenge to overcome.

In this thesis, several methods are proposed in order to allow the dimensional synthesis of statically balanced mechanisms on practical implementations of handling large payloads or exoskeletons for industry and devices for patient rehabilitation. This is achieved by integrating the following methods and tools: natural coordinates method, bilateration method, screw theory, principles of virtual works and powers, and unconventional optimization techniques.

1.1 OBJECTIVES

The main objective of this thesis is to develop a methodology based on screw theory for balancing mechanisms.

The specific objectives of this work are:

- To develop a method based on the incorporation of natural coordinates into the screw theory for the static balancing of mechanisms.

- Develop a procedure for obtaining equimomental systems of point masses of flat rigid bodies.
- To propose a method for the dynamic analysis of planar mechanisms by means of equimomental systems of point masses.
- To adapt the proposed static balancing method for dynamic balancing of planar mechanisms.

1.2 MOTIVATION AND APPLICATIONS

The genesis of this work arose from a specific balancing challenge that a company entrusted to the Laboratory of Applied Robotics, Raul Guenther (LAR). Our team developed a specific technique using the design tools we developed in our laboratory. This scenario led us to ask ourselves: Is it possible to create a versatile method to balance any mechanism?

Exploring the specialized literature, an extensive study devoted to static balancing of mechanisms was found, with numerous articles published. However, many of the proposed methods apply only to particular cases. The existence of tools such as Davies' method, born within LAR, which allow the methodical analysis of mechanisms regardless of their level of complexity, provided us with the motivation to develop a sufficiently generic tool that can address the static balancing of mechanisms in practical applications, without requiring auxiliary devices such as additional links, cables, and pulleys, and special springs.

Furthermore, mechanisms that achieve static balancing exhibit highly desirable characteristics, such as the ability to operate with minimal or no actuation to support the weight of their links. In this context, the dimensional synthesis procedures we propose in this thesis represent significant contributions to future research and the industry itself.

Statically balanced mechanisms are highly desirable for many engineering applications:

- Static balancing of mechanisms is present in many devices of daily life. The most recognizable example is the Anglepoise lamp (see Figure 1), which is a work lamp that can move effortlessly and balance in arbitrary positions (TAKAHASHI et al., 2019).
- Statically balanced mechanisms are used in surgical devices as they allow the manipulation of a payload with minimal effort, thereby reducing human fatigue due to the long operation time. Figure 2a shows a stackable mechanism architecture for otologic surgery (WOO; SEO; YI, 2019).
- Many people are affected by conditions that cause profound muscle weakness or impaired motor control. However, the equipment available to facilitate this is very limited. Therefore, it can be said that statically balanced devices can accelerate rehabilitation of patients with difficulty moving any of their limbs (BANALA et al., 2006). Figure 2b shows a static balancing mechanism for lower limb rehabilitation.

Figure 1 – Anglepoise lamp model 1227.

Source: Adapted from (WIKIPEDIA, 2020).

Figure 2 – Stackable balancing mechanism for otologic surgery (a) and gravity-balancing leg Orthosis (b).

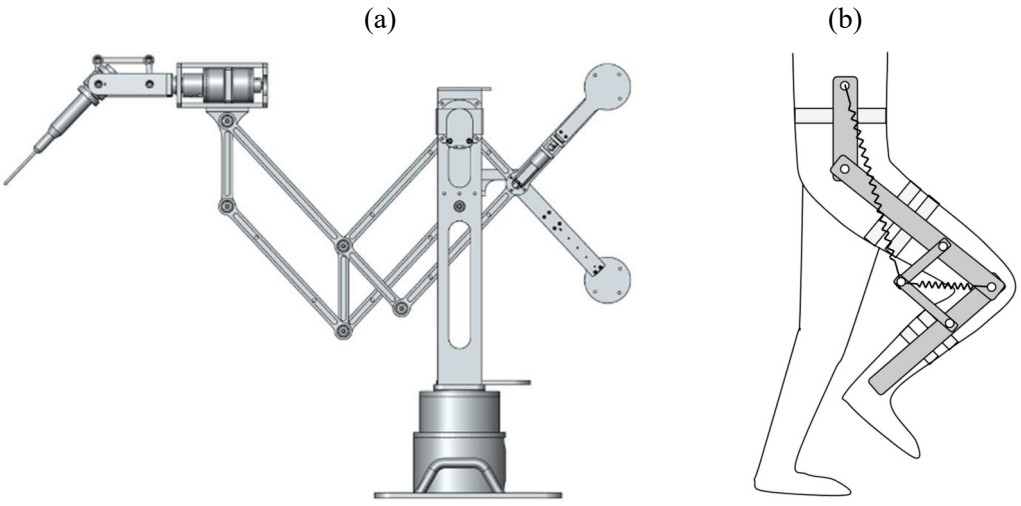

Source: Adapted from (WOO; SEO; YI, 2019; BANALA et al., 2006).

- An interesting application of statically balanced mechanisms is the simulation of environments with low gravity or gravity; this is especially useful in the training of cosmonauts or in the testing of space devices such as satellites. Figure 3 shows a 6-Dof platform for testing a free-floating spacecraft or space object in a zero-gravity environment (MA, 2013).

Figure 3 – Concept design of the 6-Dof zero-gravity test platform.

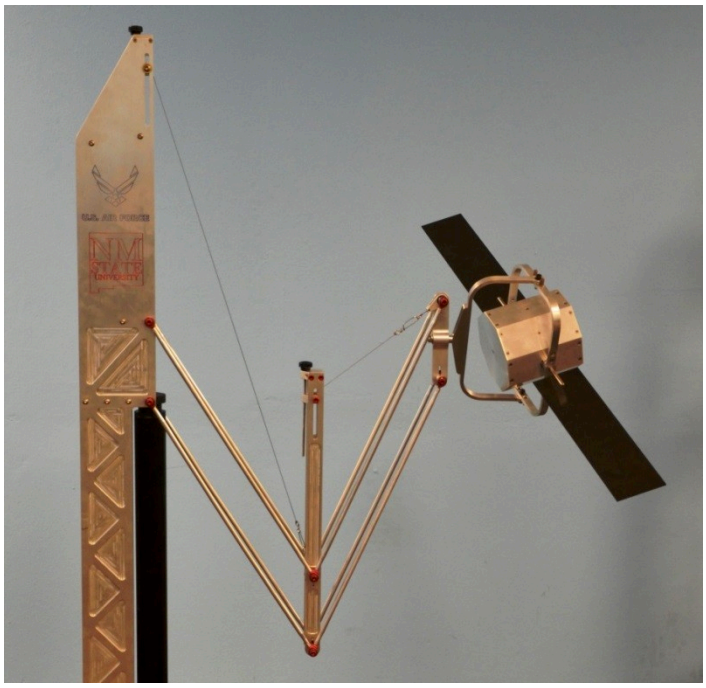

Source: Ma (2013).

1.3 THESIS CONTRIBUTIONS

This thesis mainly contributes to the static balancing of mechanisms and the dynamic balancing of planar mechanisms. Static and dynamic balancing methods are based on incorporating natural coordinates into screw theory, thus facilitating kinematic modeling and static and dynamic analysis. Combining natural coordinates and screw theory makes it possible to systematically approach static and dynamic balancing problems.

The specific contributions are as follows.

1.3.1 Kinematic analysis

New approaches for the kinematic analysis of mechanisms are proposed based on Davies' method, natural coordinates, and the bilateration method. Specific contributions are as follows:

- The kinematic analysis by means of natural coordinates, bilateration, and screw theory is reviewed. Then, a combination of natural coordinates and screw theory is proposed, facilitating the kinematic analysis of velocities and accelerations of mechanisms. The analysis of accelerations by incorporating natural coordinates in the Davies method allows the determination of relative angular accelerations in a simple way. Moreover, a simultaneous solution of the position and velocity problem is proposed.

- In this thesis, the bilateration method was formulated in an alternative way using complex numbers and showing that some properties can be easily demonstrated in the complex form of bilateration matrices, called bilaterators. It also proposed a bilateration matrix for a planar RRRP mechanism which can be used to solve the position kinematics of more complex planar mechanisms.

1.3.2 Static balancing

A screw theory-based static balancing method is proposed that is applicable to planar and spatial mechanisms. The static balancing problem is formulated as an optimization problem that allows optimization techniques based on the computation of gradient and evolutionary approaches. The specific contributions are:

- A conceptual algorithmic method for static balancing mechanisms was developed to serve as a guide for the development of specific balancing methods. An approach was also proposed to deal with the static balancing of mechanisms with limited workspaces.
- A screw theory-based static balancing method founded on incorporating natural coordinates into Davies' method is developed where the application of Davies' method in conjunction with natural coordinates permits finding of actuator forces in a systematic form. The proposed method is helpful in practical engineering problems since there are no excessive simplifications necessary.
- Using natural coordinates as design variables in the optimal static balancing of mechanisms is also proposed. The main advantage of using natural coordinates as design variables is that it facilitates static balancing of mechanisms confined to a reduced working space.

1.3.3 Equimomental systems representation of planar rigid bodies

Based on the description of equimomental systems of four point-masses of three-dimensional rigid bodies proposed by Laus and Selig (2020), a procedure is developed to determine an equimomental system of three point-masses of a given rigid body. Specific contributions are as follows:

- In this work, the equimomental systems of three point-masses of planar rigid bodies are investigated using the concept of pseudo-inertia matrix. It is found that, given a planar rigid body, it is always possible to determine an equimomental system of three equal masses located at the vertices of an isosceles triangle.
- A procedure is presented to determine equimomental systems with different masses, guaranteeing that the masses are positive. It is shown that it is always possible to choose an equimomental system of three point-masses located at the vertices of an isosceles triangle with a prescribed position of one mass.

1.3.4 Dynamic balancing

Based on the equimomental systems of three point-masses of planar rigid bodies, the static balancing method is adapted for the dynamic balancing of planar mechanisms. Specific contributions are as follows:

- The equation of motion of a planar rigid body is obtained from an equimomental system of three point-masses, which is straightforward using Plücker coordinates. Based on the concept of an inertial screw Frantz et al. (2018), a procedure is developed to solve the inverse dynamics of mechanisms using Davies' method.
- This thesis introduces the concept of a shaking screw. This new concept enables us to adapt the static balancing method to the dynamic balancing of planar mechanisms. In this case, as in static balancing, the mathematical formulation is based on incorporating natural coordinates into the screw theory.

1.4 OVERVIEW OF THIS WORK

In this chapter, an introduction on statically balanced mechanisms is presented, in addition to the objectives and contributions of this thesis, the motivation to carry out this work, and finally, some important applications of statically balanced mechanisms are mentioned.

Chapter 2 presents the applications and features of static balancing. Methods or principles for balancing a system are presented. The basic theory on static balancing is also discussed. At the end of the chapter, a bibliographical review classified by methods of complete and approximate static balancing is presented.

Chapter 3 presents an overview of the synthesis of statically balanced mechanisms, where a conceptual method of static balancing is proposed, on which the method developed in Chapter 5 is based.

Chapter 4 is one of the most important chapters of this thesis, since it presents and develops the kinematic analysis methods which are the basis of the static balancing methods developed in Chapter 5.

In Chapter 5, a new screw theory-based static balancing method is developed. The method is based on the incorporation of natural coordinates into the theory of screws.

In Chapter 6, the equimomental systems of three point-masses of planar rigid bodies are investigated using the concept of pseudo-inertia matrix.

Chapter 7 proposes an adaptation of the static balancing method developed in Chapter 5 for the dynamic balancing of planar mechanisms using equimomental systems of point masses.

The conclusions of this thesis and future work are presented in Chapter 8.

2 STATIC BALANCING

This chapter presents the basic theory of static balancing and a preliminary bibliographic review. Initially, the main applications and features of static balancing are presented, as well as some static balancing methods based on the use of counterweights and/or springs. In a similar manner, the equilibrium conditions and their classification are posed. Finally, a review of the bibliography is presented where the works are classified in complete balance and approximate balance.

2.1 APPLICATIONS AND FEATURES

Typical applications of static balancing are gravity compensation of mechanisms, vibration isolation, and stiffness reduction in compliant mechanisms (GALLEGO SANCHEZ, 2013).

Figure 4 – Typical applications of static balancing.

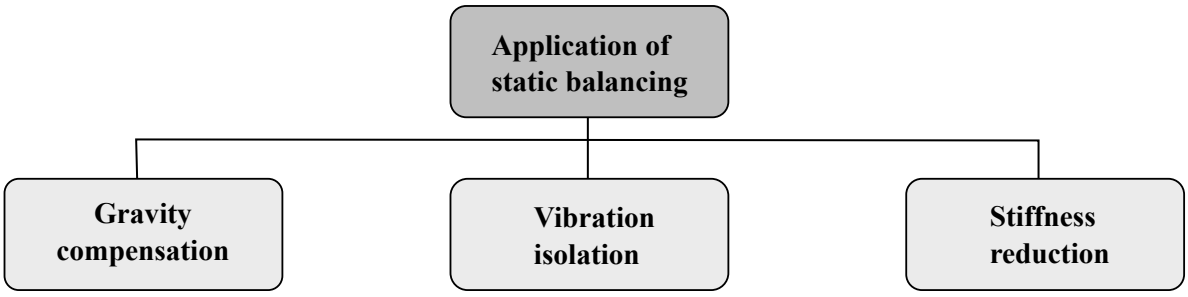

Source: Adapted from (GALLEGO SANCHEZ, 2013).

- **Gravity compensation**: Static balancing for gravity compensation can be found in applications ranging from daily lives devices such as monitor supports, lamps, to more sophisticated devices such as rehabilitation medical devices, serial and parallel manipulators, antigravity devices in space applications. Typically, the idea is to compensate for the weight of a mechanism in order to achieve an effortless actuation. Design methods for gravity compensation are based on the use of springs and/or stationary centers of gravity. This is the main subject of this thesis.

- **Vibration isolation**: Another basic application of static balancing is vibration isolation. In theory, a statically balanced mechanism has a natural frequency equal to zero; therefore, if it is subjected to a perturbation, it does not oscillate. Thus, they are ideal for passive systems in vibration isolation. Some design methods for vibration isolation are presented by Alabuzhev (1989), Park and Luu (2007), Eugene Rivin (1999), Freakley and Payne (1978), Eugene I Rivin (2003), David L Platus (1993), DL Platus (1993).

- **Stiffness reduction**: There are situations where a reduction in the operational stiffness of compliant mechanisms is desirable, such as in the case of increasing energy efficiency or the ability to keep the force feedback between the input and output of a compliant tool. Imagine a mechanism where its actuator cannot exert high forces; in this case it is convenient that all the energy from the actuator goes to the payload and it is not wasted deforming the mechanism just to achieve motion (GALLEGO SANCHEZ, 2013). Some works on this subject are presented by Herder and Van Den Berg (2000), Stapel and Herder (2004), Trease and Dede (2004), Radaelli, Gallego, and Herder (2011), Tolou, Henneken, and Herder (2010).

Herder (2001), lists the distinctive features of a statically balanced mechanism, of which the following are highlighted:

- **Energy-free motion**: Statically balanced systems can be moved in the presence of considerable conservative forces, but they require no operating force or energy.
- **Improved information transmission**: In manually operated instruments, such as body-powered hand prostheses and surgical forceps, the elimination of undesired forces, such as weight or undesired spring forces, not only reduces operating effort but also improves feedback.
- **Neutral buoyancy**: By using gravity equilibrators, forces due to gravity are compensated. This allows zero-gravity simulation, for instance, for space research applications.
- **Improved performance**: In general, the precision of operation is improved if the loading characteristics are reduced. Furthermore, if undesired forces are eliminated, smaller actuators are needed (if any), the whole construction can become more light-weight, and control is simplified leading to better performance, also lower power consumption and reduced heat rise.
- **Inherent safety**: The fact that statically balanced mechanisms are in equilibrium when they are not actuated represents a form of safety. For example, in an electrically powered robot arm with passive gravity balancing, a power failure does not result in a dramatic breakdown of the mechanism.

2.2 STATIC BALANCING METHODS

In this section, the main balancing methods used in practical applications are shown. In this case, we refer to the balancing method as the device or medium to store and exchange energy, so that the total potential energy remains constant.

2.2.1 Balancing with counterweights

A mechanism can be statically balanced by adding masses so that the energy of the entire system is constant. One example is the Mechane, this device was used in classical Greek theater to surprise the audience. The device consisted of a beam pivoted so that the weight of the man at one extreme representing a hero or a god, was equilibrated by a counterweight at the other extreme. In this way, a single person could operate the device without much effort 5.

The condition for the mechanism to be balanced is that the global center-of-mass of the mechanism is fixed. This property is useful in manipulators or mechanisms where it is required that they are balanced for any orientation.

$$M\bar{\mathbf{r}} = \sum_i m_i \bar{\mathbf{r}}_i = \textbf{constant}, \tag{1}$$

Figure 5 – Deus ex Machina. Reconstruction of the 'mechane' for the Athens theater of Dionysos.

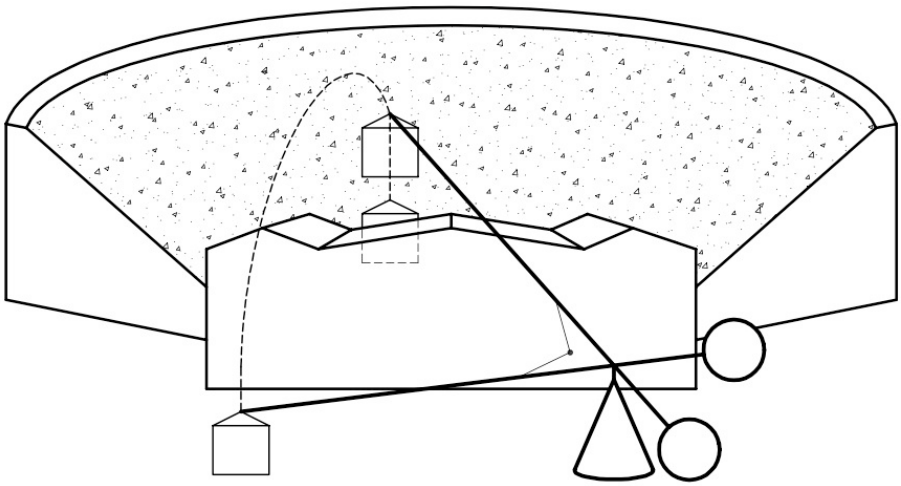

Source: Adapted from (HERDER, 2001).

where M is total mass, $\bar{\mathbf{r}}$ is position of the center of mass, m_i and $\bar{\mathbf{r}}_i$ are the mass and position of i-th mass.

2.2.2 Balancing with springs

Static balancing with springs consists in ensuring that the total potential energy of the mechanism remains constant, which means that the weight of the mechanism has no effect on the actuators. In addition, with this approach, the weight of the entire mechanism can be balanced with a much lower total mass than when counterweights are used. See, for example, a six-degree-of-freedom parallel manipulator Figure 6, which was developed to be used in motion simulators. The moving platform is carried in any position by the three spring-actuated legs using parallelogram linkages, so that the actuators only need to accelerate and decelerate the

system. As the desired accelerations are considerable, it was preferred to use springs instead of counterweights.

In this case, the condition for the mechanism to be statically balanced is that the total potential energy V from the sum of the gravitational potential energy V_g and the elastic potential energy V_e must be constant.

$$V = V_g + V_e = constant. \tag{2}$$

Figure 6 – Statically balanced parallel manipulator.

Source: Adapted from (LAVAL UNIVERSITY ROBOTICS LABORATORY, 2002).

2.3 THEORY ON STATIC BALANCE

The literature on theoretical aspects of equilibrium focuses mainly on the identification of instability in structures and how to avoid it to ensure a stable equilibrium. But static balancing is a special case of equilibrium called neutral or indifferent equilibrium, for which very few works in the literature are devoted to this topic (GALLEGO SANCHEZ, 2013). Due to the above and the fact that this thesis is not intended to deep into theoretical aspects of equilibrium, in this

section the basic theory to understand the equilibrium of a mechanical system is presented, and therefore it is far from being exhaustive and complete.

The basic idea behind static balancing is that if the potential energy in a system is constant, then it remains in equilibrium at any position in its range of motion.

$$V(\mathbf{q}) = constant, \tag{3}$$

where $\mathbf{q}$ is the vector of generalized coordinates.

Definition 1 *A mechanical system with constant potential energy along a certain range of motion is a statically balanced system along such a range of motion (GALLEGO SANCHEZ, 2013).*

2.3.1 Stability of equilibrium

It can be intuited that the equilibrium state of the three bars shown in Figure 7 is different. The bar in Figure 7(a) tends to return to its equilibrium position if subjected to a small change of position, while the bar in Figure 7(b) will move away from its equilibrium position under a small change of position, and the bar in Figure 7(c) will remain in equilibrium in its new position. These three types of equilibrium are classified, respectively, as stable equilibrium, unstable equilibrium, and neutral equilibrium.

Figure 7 – Illustration of the types of equilibrium.

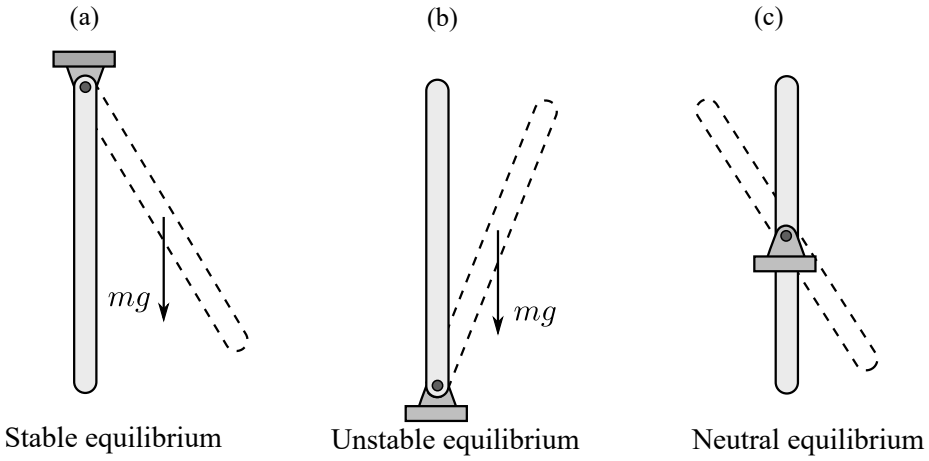

Source: Adapted from (BEER, 2010).

- **Stable equilibrium**: A system is said to be in stable equilibrium if it has a tendency to return to its original position when the system is given a small displacement.
- **Unstable equilibrium**: A system is said to be in unstable equilibrium if it has a tendency to move even farther from its original equilibrium position when given a small displacement.

- **Neutral equilibrium**: A system is said to be in neutral equilibrium if the system remains in equilibrium even when given a small displacement from its original position.

The potential function V of a system can be used to investigate the stability of equilibrium by applying the principle of virtual work, which states that a mechanical system is in equilibrium if the virtual work of external forces is zero (GOLDSTEIN; POOLE; SAFKO, 2013). Then

$$\delta_W = 0, \tag{4}$$

If all external forces are conservative, then the following relation can be written

$$dW = -dV, \tag{5}$$

and applying the virtual operator to Equation 5, yields

$$\delta_W = -\delta_V. \tag{6}$$

Consider that the potential energy is a function of the degrees of freedom grouped in the vector $\mathbf{q}$, that is, $V = V(\mathbf{q})$. Then the potential energy variation can be expressed as

$$\begin{aligned} \delta_V &= \frac{\partial V}{\partial \mathbf{q}} \delta_{\mathbf{q}} \\ &= \delta_{\mathbf{q}}^T \left[\frac{\partial V}{\partial q_i} \right]. \end{aligned} \tag{7}$$

From Equation 4, Equation 6 and due to the fact that the virtual displacements $\delta_{\mathbf{q}}$ are independent, we can deduce the equilibrium condition for a mechanic system,

$$\left[\frac{\partial V}{\partial q_i} \right] = \mathbf{0}. \tag{8}$$

To determine the stability of equilibrium, the criterion of the second derivative can be used to determine the maxima and minima of a function; for more details, see (KAPLAN, 2002). Thus, a complete classification is:

$$\left[\frac{\partial V}{\partial q_i}\right] = \mathbf{0}; \quad \left[\frac{\partial^2 V}{\partial q_j \partial q_i}\right] > \mathbf{0}: \quad \text{Stable equilibrium}$$

$$\left[\frac{\partial V}{\partial q_i}\right] = \mathbf{0}; \quad \left[\frac{\partial^2 V}{\partial q_j \partial q_i}\right] < \mathbf{0}: \quad \text{Unstable equilibrium}$$

$$\left[\frac{\partial V}{\partial q_i}\right] = \mathbf{0}; \quad \left[\frac{\partial^2 V}{\partial q_j \partial q_i}\right] = \mathbf{0}: \quad \text{Neutral equilibrium}$$

$$\text{Otherwise}: \quad \text{Partially stable or partially neutral equilibrium}$$

Figure 8 – Potential energy for the three types of equilibrium in a 1-DoF system.

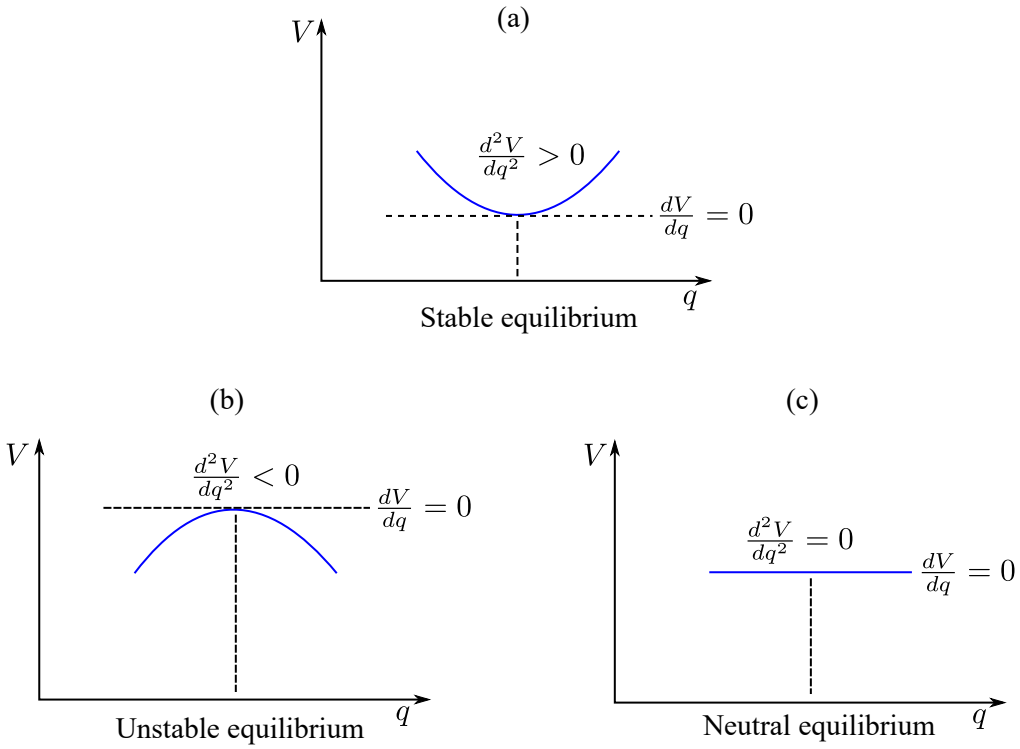

Source: Adapted from (HIBBELER, 2010).

Figure 8 illustrates the three types of equilibrium stability for a one-degree-of-freedom system. Here it can be seen that in the stable equilibrium position the potential function is a minima, in the unstable equilibrium position the potential function is a maxima and the potential function corresponding to the neutral equilibrium is constant.

2.4 BIBLIOGRAPHIC REVIEW

In this section a bibliography review of the literature on statically balanced mechanisms of the last four decades is shown, classified as perfect static balancing and approximate static balancing.

2.4.1 Complete static balancing

In (SHIN, Eungsoo; STREIT, Donald A., 1991), a study is presented for the static balancing of planar pantographs using a potential energy approach. The study presents complete balancers with both kinematic pairs of revolution and prismatic, where one of the applications is on walking machine legs, since they provide relatively good energy efficiency. Walsh, Streit, and Gilmore (1991), present a general methodology for the design of all possible balancers of two degrees of freedom in a spatial arrangement, with two revolution pairs, where the system may

consist of n-springs, each attached to the ground at one end. Streit and Shin (1993), show the fact that any planar mechanism with lower and/or higher kinematic pairs can be, in theory, fully balanced. Balance is achieved by adding a two degree-of-freedom mechanism to each center of gravity of each link. Another interesting work on a balancer used on the legs of a quadruped to improve its efficiency is presented in (SHIN, E.; STREIT, D. A., 1993). Dynamic simulation demonstrates that proper balancer design can reduce peak torque of leg actuators by more than 90 percent and offer a vehicle specific resistance 70 percent smaller than that of tracked vehicles.

An important contribution on statically balanced manipulators is found in (WANG, 1997), the author presents a dimensional synthesis formulation for balancing with counterweights and balancing with springs, planar and spatial parallel manipulators with revolute actuators, from two to six-degrees of freedom. Moreover, it is also found that balancing is always possible for any given value of the design variables, which is an interesting result since it allows the kinematic design of a mechanism to be completed using any criterion and the balancing to be performed a posteriori.

Complete balancing using higher kinematic pairs is possible by variable shape of the pairs as is presented by Simionescu and Ciupitu (2000b), where some constructional solutions for the balancing of robotic arms are presented, and exact balancing is performed for all points of the workspace by using mechanisms with higher pairs.

A theoretical viewpoint on static balancing is presented by Herder (2001), whereby the use of different principles is derived from the relationship between geometrical parameters for the neutral equilibrium of some basic balancer mechanisms. Moreover, basic composition rules are proposed in order to generate new balance mechanisms from the basic balancers.

The stationary center-of-mass method for static balancing of hexapods is addressed in (RUSSO; SINATRA; XI, 2005), where static balancing is defined as a mechanism in which the weight of the links does not produce any force on the actuators for any configuration of the manipulator. Moore (2009), presents an algebraic method for static and dynamic balancing for $4R$ mechanisms, where the necessary and sufficient conditions for the static balancing of spherical $4R$ linkages and Bennet linkages are established, in both cases, the balancing is achieved by the addition of masses.

Banala et al. (2006) presents a statically balanced mechanism for leg orthosis, which is designed to assist persons with hemiparesis to walk by eliminating the effects of gravity. The balancing conditions are derived from the potential energy approach.

Po Yang Lin, Win Bin Shieh, and Dar Zen Chen (2010), develop a methodology to determine the location of the springs of a statically balanced planar manipulator without auxiliary links. Static equilibrium analysis is formulated using the potential energy approach, which is determined through a constant block stiffness matrix. The main advantage of the method is that singularities that may be present due to the addition of additional links are avoided.

Deepak and Ananthasuresh (2012) present three techniques to statically balance a four-bar mechanism loaded with a zero-free length spring. The authors state that the number of

necessary linkages and auxiliary springs is less than or equal to that found in the literature. In addition, the Roberts–Chebyshev cognate theorem is extended to static balancing of four-bar linkages. Applications of perfect static balancing to support the upper or lower limbs of patients in rehabilitation or people with some type of disability that limits the ability to move are shown in (LIN, P.-Y.; SHIEH, W.-B.; CHEN, D.-Z., 2013; TSENG et al., 2017; KUO; NGUYEN, et al., 2021). Other medical applications are surgical devices based on static balancing that are discussed in (WOO; SEO; YI, 2019; KUO; LAI, 2016; KIM et al., 2019).

2.4.2 Approximate static balancing

Segla, Kalker-Kalkman, and Schwab (1998), show that the static balancing of a robot mechanism can be formulated as an optimization problem by using a Computer Algebra System. A general program based on the Monte-Carlo method and a genetic algorithm is also developed, and it is shown that a practical problem can be solved without the need for simplifications.

Simionescu and Ciupitu (2000a), present some constructional solutions for statically balanced robot arms. The formulation developed by the authors permits the balancing for a discrete number of work field positions.

Procedures for static balancing of mechanisms with torsion spring are proposed in Radaelli, Gallego, and Herder (2011), Gallego and Herder (2011), Gallego Sanchez (2013). In these works, static balancing is formulated as an optimization problem where geometric parameters of the mechanism are also considered as design variables.

Perreault, Cardou, and Gosselin (2014), present a novel method to approximate the static balancing of a planar parallel cable-driven mechanism based on four-bar linkages and spring. The author proposed the use of nonlinear spring to generate minimum torques and thus keep the cable taut. In this paper, we have first determined the best non-linear tension profile in the cables in order to approximate neutral equilibrium over the workspace. The objective was to minimize over the workspace the Euclidean norm of the resultant of all forces applied on the end effector while ensuring a minimum tension in the cables. Then, the desired four-bar linkage input–output relationship was determined.

Carrabotta et al. (2015), propose different solutions for static balancing of a commercial robot for palletizing. The solutions consist of using only counterweights, springs, and the combination of counterweights and springs. In all cases, the design variables are determined by two proposed optimization procedures. Simionescu, Ciupitu, and Ionita (2015), present a new solution and its respective mathematical model for the static balancing of a parallel delta robot. The results showed that the maximum torque required by the actuators was reduced about 20 times that of the unbalanced robot.

Denizhan (2015) presents an interesting application of the statically balanced mechanisms that deals with a procedure of optimal synthesis of three positions for static balancing of the hood of a vehicle. Veer and Sujatha (2015) prove that exact static balancing in a serial kinematic chain with springs connected to consecutive links is impossible. The authors propose

an optimization procedure based on minimizing the variance of the potential energy for discretized configurations with which an approximate static balance is achieved. Similar work (ROSYID; EL-KHASAWNEH; ALAZZAM, 2019; TAKAHASHI et al., 2019; WANG; KONG, 2020) uses the minimization of a measure derived from the potential energy or by minimizing the force of the actuators (RAO; WAGHMARE, 2018; ROSYID; EL-KHASAWNEH; ALAZZAM, 2019; ALAMDARI; HAGHIGHI; KROVI, 2019; MARTINI; TRONCOSSI; RIVOLA, 2019; ZHOU et al., 2020).

Developing techniques for static balancing of mechanisms through screw theory is incipient, and published works are scarce. Ma et al. (2019) show the kinetostatics of the TriMule parallel robot using screws, although the kinetostatic model has a small discrepancy with the Solidworks model. The balancing is performed by two sets of gas springs. A geometric method based on screws for static balancing of mechanisms constructed using spherical chain units is presented in (WANG; KONG, 2019). Shekarforoush, Eghtesad, and Farid (2013) present the static balancing of a spatial tensegrity mechanism with compliant active components. In this work, the kinetostatic problem is solved using screws. In the works cited above, no systematic procedure is presented to generate the equations of statics through screw theory, unlike the method proposed in this thesis, which systematically determines the constitutive equations of statics. Moreover, in the literature consulted, there is no evidence of the use of graph theory in the context of static balancing.

3 STATIC BALANCING SYNTHESIS OVERVIEW

In Chapter 2, the theoretical bases of equilibrium needed to understand the static balancing of a mechanism were briefly addressed, but it was not said how the dimensions and parameters necessary for a mechanism to be statically balanced can be found, this aspect is called static balancing synthesis and will be conceptually approached in this chapter. Although the neutral equilibrium conditions for static balancing are simple this cannot be used majority directly to synthesize mechanisms, due that in general, the mechanisms' structure is highly nonlinear.

3.1 KINEMATIC MODELING

Since a mechanism is composed of links interconnected by kinematic pairs, before considering synthesis it is necessary to choose how to mathematically describe the relationship between the links. This mathematical description constitutes the model on which it will be built later in the formulation of the optimal synthesis. This subject will be covered in more detail in Chapter 4.

To modeling a mechanism, we need description variables to know the position of all the links. All these positions at a given moment constitute a linkage configuration. Description variables, also called generalized coordinates, can be independent or dependent. In fact, since bodies are interconnected by joints, their movements are not completely free and this can cause restrictions between some generalized coordinates.

It must be emphasized here that the kinematic modeling is crucial for the behavior of the optimal synthesis process. During the optimization, the model will be evaluated with various values of the dimensions (angles or lengths) leading to various configurations of the mechanism. For closed-loop linkages, these evaluations also involve the assembly of the mechanism and problems of singularity that may occur.

3.1.1 Types of generalized coordinates

This subsection will briefly describe the three types of coordinates most used in the bibliography on the definition of mechanisms (JEAN-FRANÇOIS COLLARD, 2007; JALÓN; BAYO, 1994), namely, relative coordinates, Cartesian or reference point coordinates, and natural coordinates.

3.1.1.1 Relative coordinates

Relative coordinates are defined in each kinematic pair and each one of them measures the position of an element with respect to the previous one in the kinematic chain. With the relative coordinates, the constraint equations basically come from the loop closure conditions.

Table 1 shows the main advantages and disadvantages of this type of coordinates.

Table 1 – Advantages and disadvantages of relative coordinates.

Advantages	**Disadvantages**
They are the minimum number of dependent coordinates that can be define.	Complex mathematical formulation, since the absolute position of an element, depends on the previous ones in the chain.
They are especially recommended for the study of open chain mechanisms.	The closed-loop equations are reduced in number, but highly non-linear.
As they are defined in the kinematic pairs, the movement of the input coordinates can be directly controlled.	May require some postprocessing work to determine the absolute kinematics of a point, for example.

Source: Adapted from (ANA MAGDALENA DE JUAN DE LUNA, 2011; JEAN-FRANÇOIS COLLARD, 2007).

3.1.1.2 Reference point coordinates

The reference point coordinates place the position and orientation of each element of the mechanism absolutely. There are several possible choices. The most direct consists of defining a reference system rigidly attached to the element and taking, on the one hand, the coordinates of its origin to define the translation and, on the other, the Euler angles (or another way of parameterizing the rotations) to define its orientation. The constraint equations arise by examining each pair and writing mathematically the restrictions to the movement imposed by the own pair on the two elements joined by it.

Table 2 shows the main advantages and disadvantages of this type of coordinates.

Table 2 – Advantages and disadvantages of reference point coordinates.

Advantages	**Disadvantages**
The position and orientation of each element are defined directly.	It is not taken into account if the mechanism is open or closed chain.
The constraint equations are much more simple than in the case of relative coordinates, leading to a more efficient calculation process.	More coordinates are needed, and therefore equations are much higher than in the case of relative coordinates.

Source: Adapted from (ANA MAGDALENA DE JUAN DE LUNA, 2011; JEAN-FRANÇOIS COLLARD, 2007).

3.1.1.3 Natural coordinates

Natural coordinates also absolutely define the position of each element, but instead of being located in the origin of the reference system of the element, like reference point coordinates, they are usually placed in the pairs. With natural coordinates, the constraint equations are of two types: rigid body and kinematic pair, the latter only in certain pairs.

Table 3 shows the main advantages and disadvantages of this type of coordinates.

Table 3 – Advantages and disadvantages of natural coordinates.

Advantages	**Disadvantages**
The position and orientation of each element are defined directly.	It is not taken into account if the mechanism is open or closed chain.
Trigonometric functions do not appear in the restriction equations.	May require some post processing work to determine angular values whether these are necessary.
Natural coordinates are particularly well adapted to sensitivity analysis and optimization.	More coordinates are needed, and therefore equations are much higher than in the case of relative coordinates.

Source: Adapted from (ANA MAGDALENA DE JUAN DE LUNA, 2011; JEAN-FRANÇOIS COLLARD, 2007).

3.1.1.4 Discussion on the choice of the type of coordinates

Given the advantages of the natural coordinates mentioned above, these are the formalism chosen for the description of mechanisms in this thesis. Another advantage of this choice is that this type of coordinates can naturally be integrated into screw theory, as will be shown in later chapters.

Figure 9 – Classification of static balancing synthesis of mechanisms.

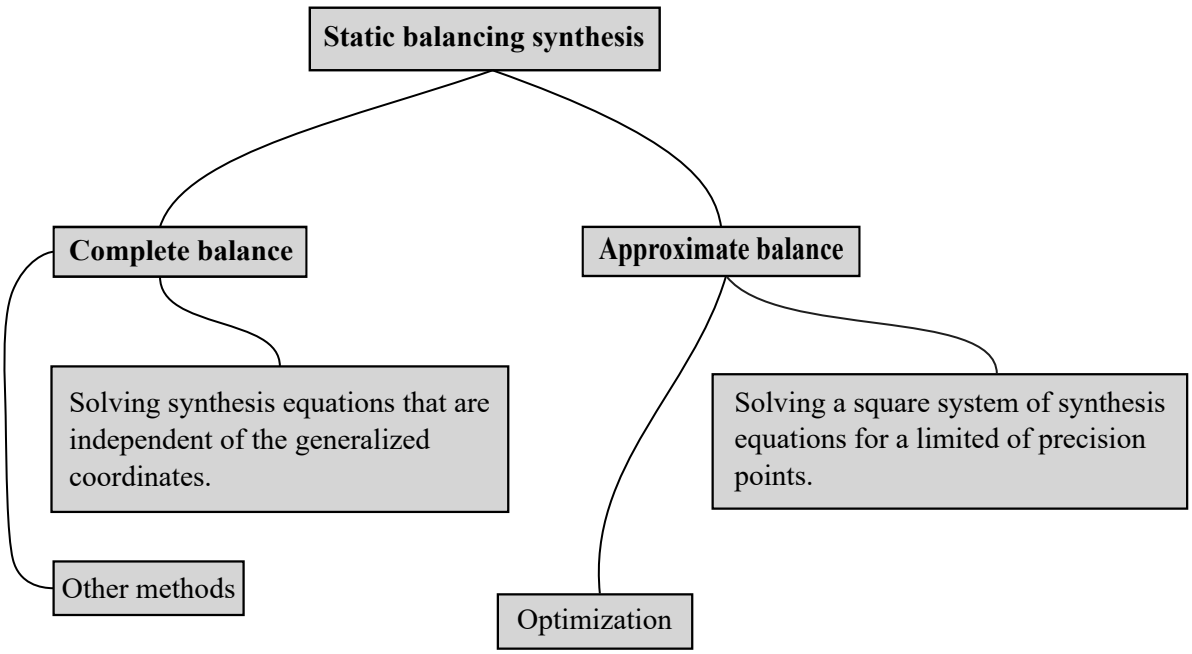

Source: The author.

3.2 STATIC BALANCING SYNTHESIS

In this thesis, we refer to the static balancing synthesis as the process of determining the dimensions of the mechanism, the position and properties of the springs and / or counterweights. The dimensional synthesis of statically balanced mechanisms can be classified into two categories: complete balance and approximate balance as shown in Figure 9.

3.2.1 Complete balance

In theory, any planar or spatial mechanism with lower and/or higher kinematic pairs can be completely balanced (HERDER, 2001). To demonstrate this intuitively consider a basic mechanism that keeps the center of mass of a link balanced as represented in the graph (Figure 10). The basic balanced mechanisms are obtained either by solving synthesis equations that are independent of the generalized coordinates or using other methods, see Figure 9.

Figure 10 – Graph of isolate link equilibrated by a basic balanced mechanisms.

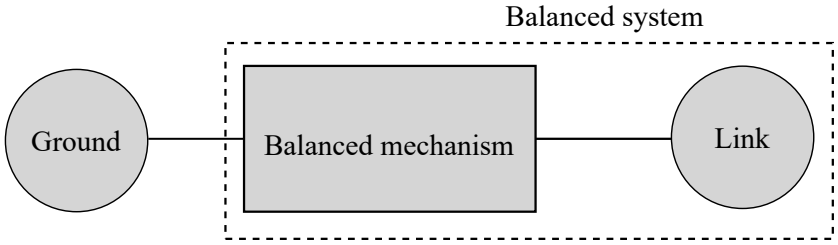

Source: The author.

Now we consider the generic mechanism shown in Figure 11, which is composed of $n + 1$ links. Then this system can be exactly balanced by adding a basic balancing mechanism for each link. If each basic balancing mechanism is composed by m links then the resultant mechanism is formed by $nm + 1$.

Although the ideal balancing system is an exact balancer mechanism, this in practice leads to the following disadvantages:

- The use of zero-free-length springs that are not common and more complicated to manufacture than normal springs.
- It is necessary to add links that make the mechanism more complicated and therefore increase the total cost.
- Generally, the final mechanism becomes bulkier, which is a problem if the workspace is tight.
- Singularity problems can occur due to the additional links.

Figure 11 – Graph of generic rigid body system balanced by basic balanced mechanisms.

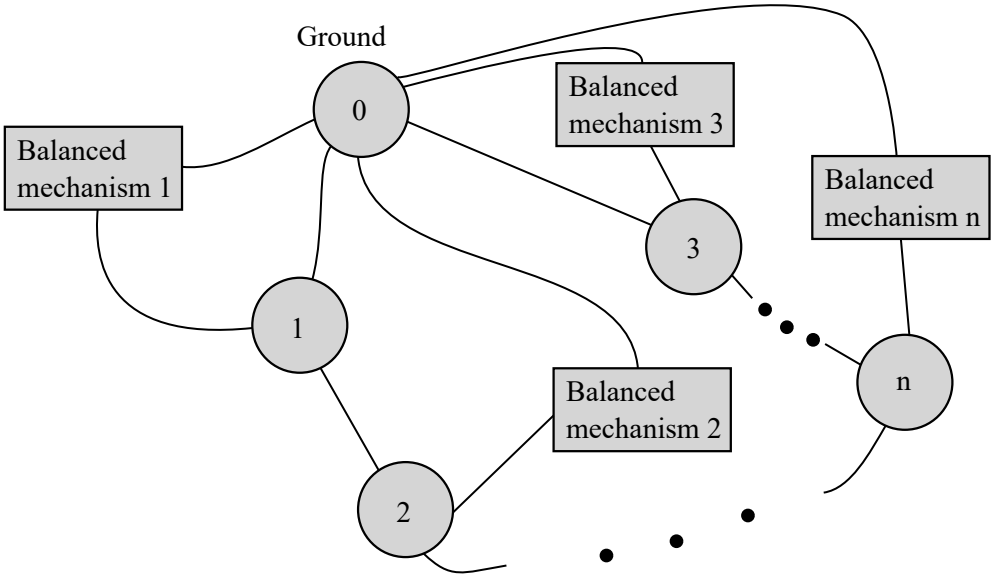

Source: The author.

In accordance with the objectives of this thesis, the perfect balance will not choose due to the aforementioned. All our efforts will be focused on approximate balance where the bases of conceptual synthesis are detailed in the following sections.

3.2.2 Approximate balance

As normal springs usually are cheapest to produce, it is worthwhile to consider their use in a simple non-linear linkage converting the spring forces as desired. Although normal springs can often be used to obtain the behavior of zero-free-length springs, this, therefore, requires the use of additional cables and links that make the mechanism more complex, and in some cases, it does not meet space requirements (HERDER, 2001).

Approximate balance can be faced by two approaches: Solving a square system of synthesis equations for a limited of precision points, or using optimization, see Figure 9. The first one is limited to a number of precision points while the second one is more general and can be used to synthesize balanced mechanisms with complicated design restrictions.

In this thesis, we refer to the dimensional optimization of statically balanced mechanisms simply as optimal synthesis.The wedding between optimization and synthesis (Figure 12), permits us to tackle complicate balanced multi-loop mechanisms where it is necessary to solve simultaneously the position or assembly problem, moreover avoiding singularity positions and multiple assembly modes separated by bifurcation configurations.

Figure 12 – Wedding between optimization and synthesis.

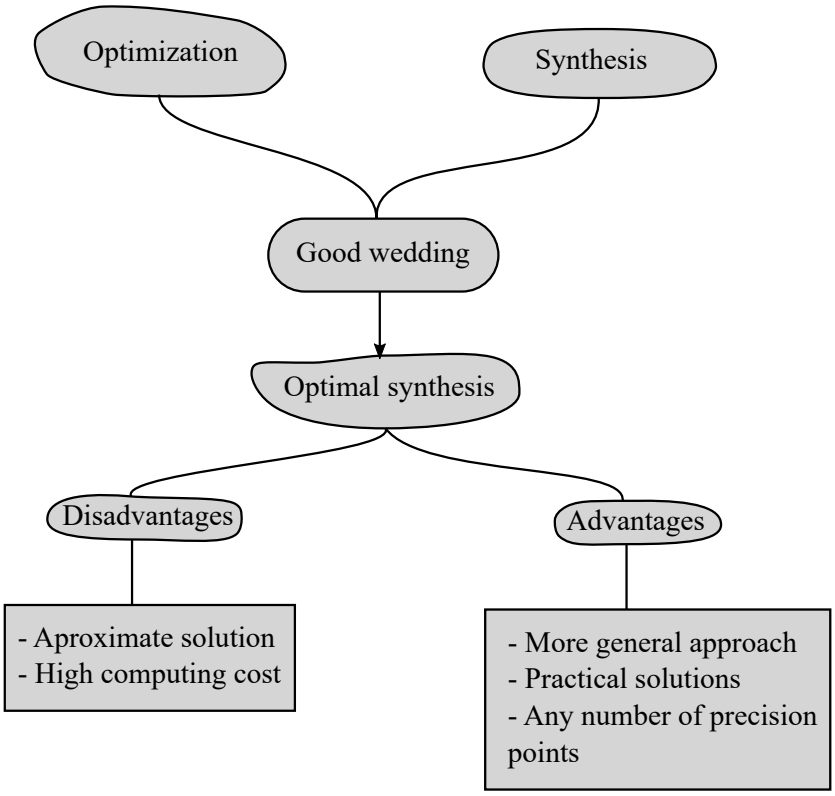

Source: The author.

3.2.3 Optimal synthesis problem

The optimization problem is conformed of an objective function whose minimization results in the dimensions of the balanced mechanism, in addition to some constraints that can be classified as constraints of the design variables and constraints of the generalized coordinates as it shows in the Figure 13.

Figure 13 – Construction of the optimal synthesis problem.

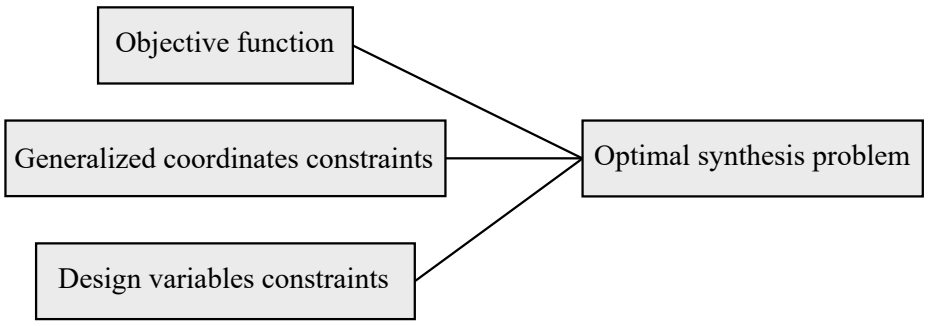

Source: The author.

The objective function is formulated from the equilibrium conditions mentioned in Chapter 2. Then the constraints of the design variables are formulated, which generally correspond to the limit dimensions of the links and the values of the parameters of the counterweights and/or springs. Finally, the generalized coordinates constraints are formulated, which can be mainly associated with space constraints as illustrated in the Figure 14. These restrictions can also be associated with the maximum travels of the springs.

Figure 14 – Mechanism with space constraints.

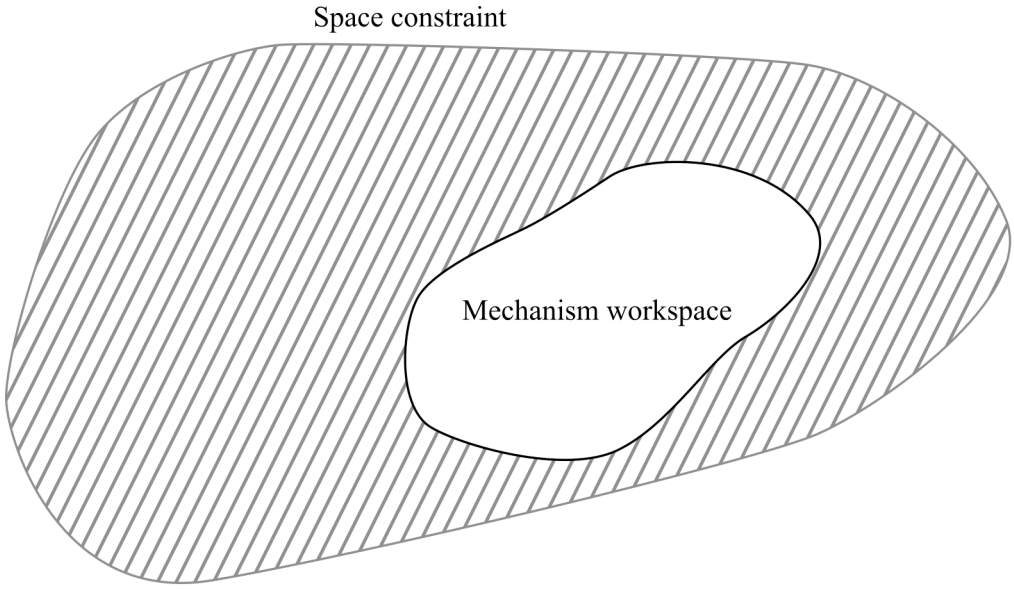

Source: The author.

Once the optimization problem is formulated, we can use deterministic, hybrid or stochastic methods to find an optimal solution, see Figure. 15. Theoretical details about these methods and their implementation are found in (ARORA, J., 2012), (ARORA, R. K., 2015).

Figure 15 – Classification of the optimization algorithms.

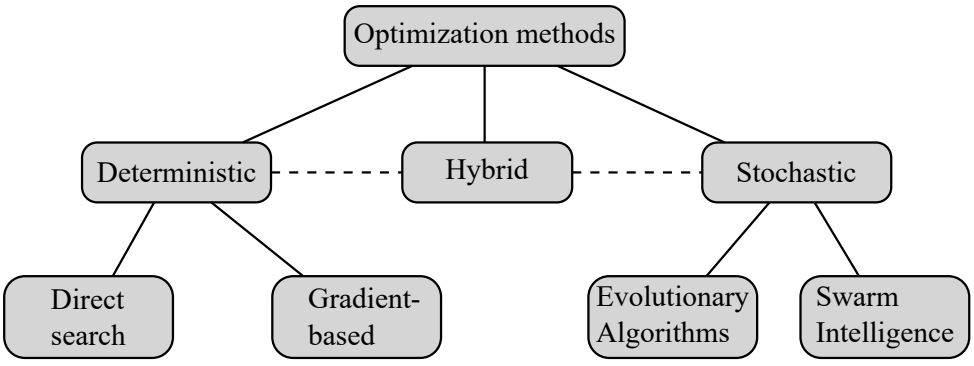

Source: Adapted from (JEAN-FRANÇOIS COLLARD, 2007).

3.2.4 The conceptual method proposed for the static balancing synthesis

In this section, we propose a conceptual static balancing synthesis method, from which the methods proposed in Chapter 5 are derived. The step by step of the proposed method is the following:

- The first step is to select a mechanism topology that it guarantees a permissible approximate balancing. One way to do this is by selecting a mechanism previously balanced by complete balancing methods.
- The second step is kinematic modeling. First, we model the mechanism using adequate generalized coordinates, then as far as possible we solve the position in closed form, otherwise, it is obtained a numerical solution. Immediately we performed the velocity analysis either by screw theory or using differentiation. The velocity analysis is only necessary if we used virtual work or virtual power principles to formulate the equilibrium conditions.
- In the third step, we select the appropriate equilibrium conditions in order to make an objective function in the next step. The equilibrium conditions can be formulated from:
  - Constant potential energy condition.
  - Virtual work or virtual power principle.
  - Zero input forces or torques condition. This can be systematically performed by solving the static problem via screw theory or using the natural coordinates formulation.
- The fourth step is to formulate static balancing synthesis as an optimization problem. To solve the optimization problem can be used gradient-based methods, stochastic methods, and hybrid methods.
- Finally, we analyze the optimal mechanism in order to find any singularity problem and verify that the balancing is acceptable for a practical application.

The method described above is illustrated in the Figure 16.

3.2.5 Proposal to deal with the static balancing synthesis of mechanisms with space constraints

To deal with the problem of static balancing synthesis of mechanisms with space constraints, in this thesis it is proposed to use the generalized coordinates as design variables, which makes it much easier to deal with this type of constraints. The use of generalized coordinates as design variables has already been used in (GARCÍA-MARINA et al., 2018), (BUSTOS, 2004), and (SUH; RADCLIFFE, 1978), in these works, the design variables correspond to the generalized coordinates of the initial position of the mechanism. To date no studies have been

Figure 16 – The conceptual method proposed for the static balancing synthesis.

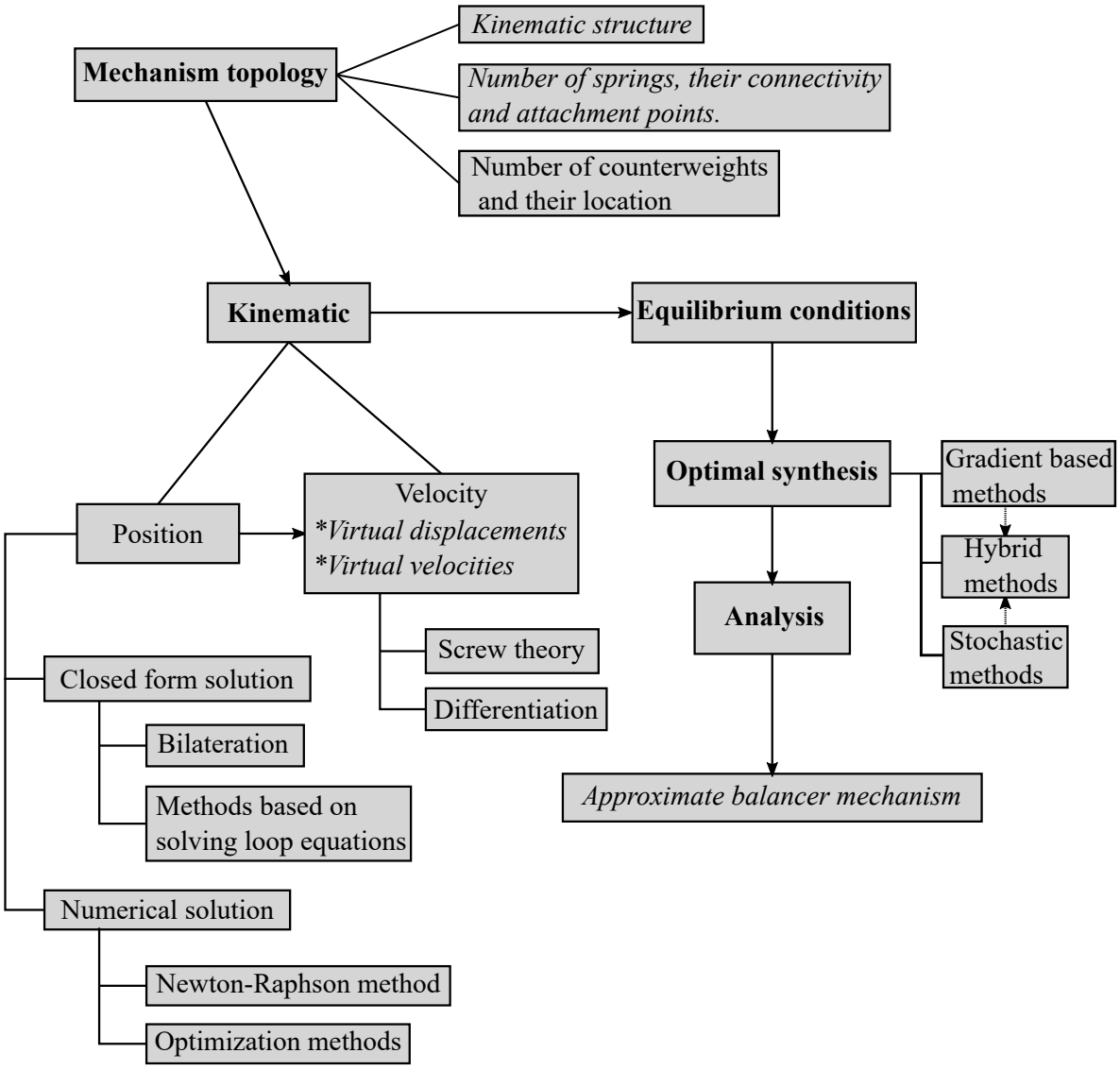

Source: The author.

reported that use the above approach to static balancing, and in the studies consulted there is no evidence of an efficient method to address space constraints.

Conceptually this method consists of the following steps:

- First of all, we must choose from the generalized coordinates those that will be part of the design variables.
- Then the objective function is formulated suitably in such a way that it allows an efficient computation and also that a sensitivity analysis is possible in the case that a hybrid optimization method is used.
- The next step is to represent the space constraints of the mechanism by using the generalized

coordinate constraints. Also, restrictions on the design variables of the counterweights and / or springs are included.

- Finally, the optimization problem is solved through an optimization method of those shown in the Figure 16.

The Figure 17 illustrates the method described above.

Figure 17 – The conceptual method proposed for static balancing synthesis with space constraints.

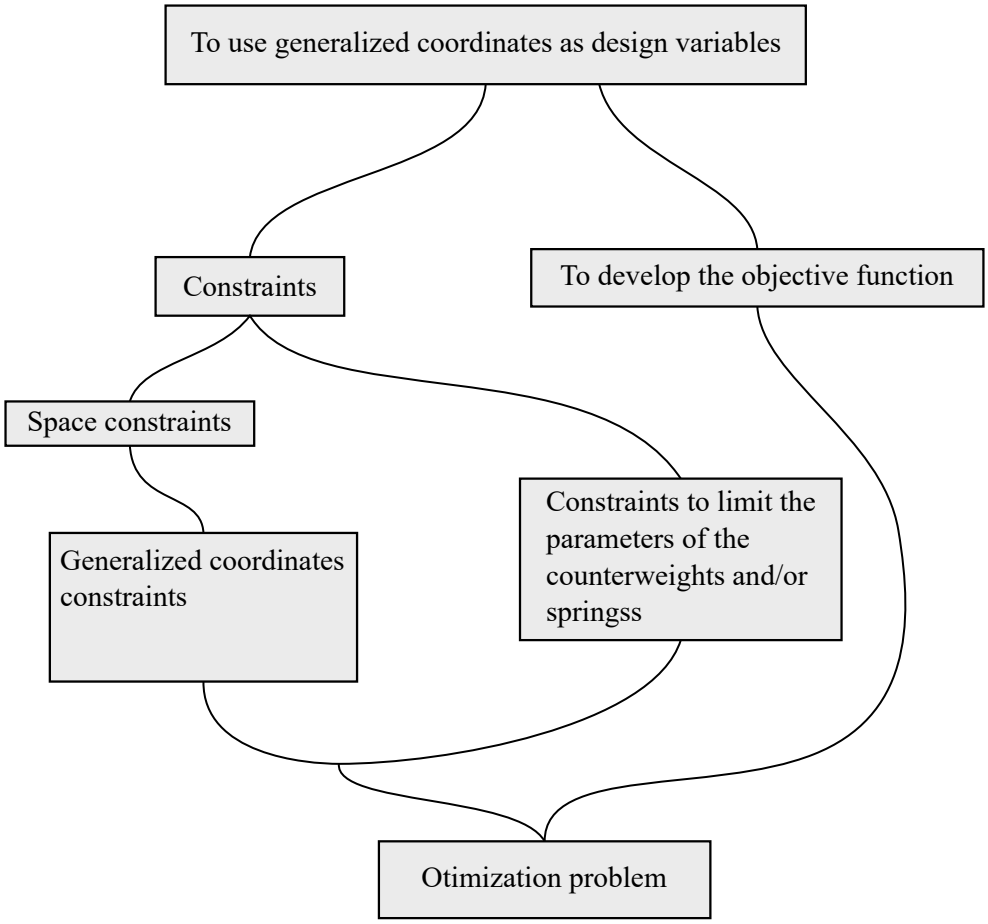

Source: The author.

4 KINEMATIC ANALYSIS

As described in Chapter 3, kinematic modeling or kinematic analysis is the most important stage in static balancing synthesis, since the behavior of the optimization or optimal synthesis process depends on the approach to the kinematic description of a mechanism. Therefore, this subject is covered in detail in this chapter.

Kinematics is the study of motions of objects in the Euclidean plane or space. Furthermore, kinematics can be defined accurately, as the study of the geometry of motion, since kinematics is geometry with the addition of the time dimension (WALDRON; KINZEL; AGRAWAL, 2016). In our case, in the following sections we study the position, velocity, virtual displacements, and virtual velocities of a mechanism.

4.1 POSITION ANALYSIS

The position analysis consists basically of finding the feasible assembly modes that a kinematic chain can adopt. An assembly mode is a possible relative transformation between the geometrical elements, i.e. the links of a kinematic chain. When a position and orientation assignment is made for all links, an assembly mode is called a configuration (ROJAS, 2012).

Next, the position analysis using natural coordinates and the bilateration method is described, which will be widely used throughout this thesis.

4.1.1 Natural coordinates in the plane

Natural coordinates were originally introduced by García De Jalón and collaborators (JALÓN; UNDA; AVELLO, 1986; JALÓN; BAYO, 1994), In planar mechanisms natural coordinates are mostly cartesians coordinates located at kinematic pairs or points of interest. The main advantage in the use of natural coordinates is its simplicity and intuitive physical interpretation. Moreover, it is not necessary to define angular type coordinates to define the orientation of each elements to the mechanism, avoiding all the complexity that this entails (AVELLO, 2014).

To correctly model a mechanism in natural coordinates, you can follow the following rules:

1. A point must be placed on each joint.
2. In prismatic pairs, there must be at least three collinear points: two to define the axis and one for the sliding joint.
3. Each link must contain at least two points. If this condition is not met, it is impossible to determine the orientation of the link.
4. In addition to the above, as many additional points as necessary can be used.

Once the points are defined, we can add another type of coordinates and group in the vector $\mathbf{q}$. Then the position is represented by the constraint equations vector as

$$\mathbf{\Phi}(\mathbf{q}) = \mathbf{0}, \tag{9}$$

where the number of constraint equations n_c, the number of coordinates n_v and mobility M are related by

$$n_c = n_v - M. \tag{10}$$

Figure 18 – Slider-crank mechanism modeled with natural coordinates.

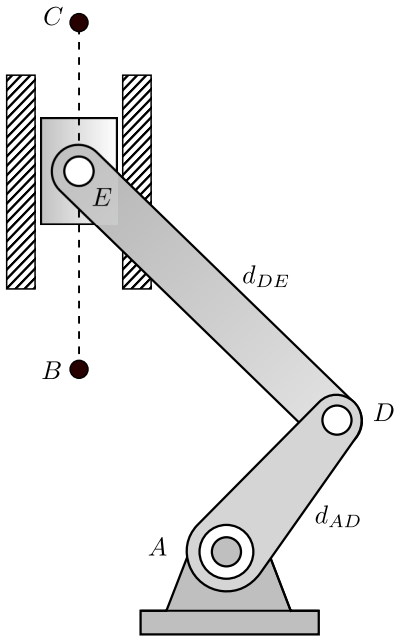

Source: The author.

Example 1 (Slider-crank mechanism modeling with natural coordinates)

For modeling of the slider-crank mechanism shown in Figure 18, the points D and E are taken. Fixed points A, B, and C are necessary for the formulation of the constraint equations, but do not belong to the natural coordinates, because they are not variables. Therefore the vector of natural coordinates is,

$$\mathbf{q} = \begin{bmatrix} D \\ E \end{bmatrix} = \begin{bmatrix} x_D \\ y_D \\ x_E \\ y_E \end{bmatrix}. \tag{11}$$

As the mobility of the mechanism is $M = 1$ and it is modeled with $n_v = 4$ natural coordinates, by Equation (10) we have that three constraint equations are necessary that are:

$$\mathbf{r}_{AD}^T \mathbf{r}_{AD} - d_{AD}^2 = 0, \tag{12}$$

$$\mathbf{r}_{DE}^T \mathbf{r}_{DE} - d_{DE}^2 = 0, \tag{13}$$

$$\mathbf{r}_{BE} \times \mathbf{r}_{BC} = 0. \tag{14}$$

Equations (12) and (13) are obtained from the rigidity condition of the links. Equation (14) corresponds to the collinearity condition of points A, B, and C. Now, writing this equations in the form of Equation (9) we have that

$$\mathbf{\Phi}(\mathbf{q}) = \begin{bmatrix} (x_D - x_A)^2 + (y_D - y_A)^2 - d_{AD}^2 \\ (x_E - x_D)^2 + (y_E - y_D)^2 - d_{DE}^2 \\ (x_E - x_B)(y_C - y_B) - (y_E - y_B)(x_C - x_B) \end{bmatrix} = \mathbf{0}. \tag{15}$$

4.1.1.1 Rigid body constraints

The rigid body constraints are those necessary so that the points of the same element do not have relative displacements. In a planar element defined by n points, there must be $2n - 3$ constraint equations, since the element has three degrees of freedom.

Figure 19 – Planar rigid body constraints.

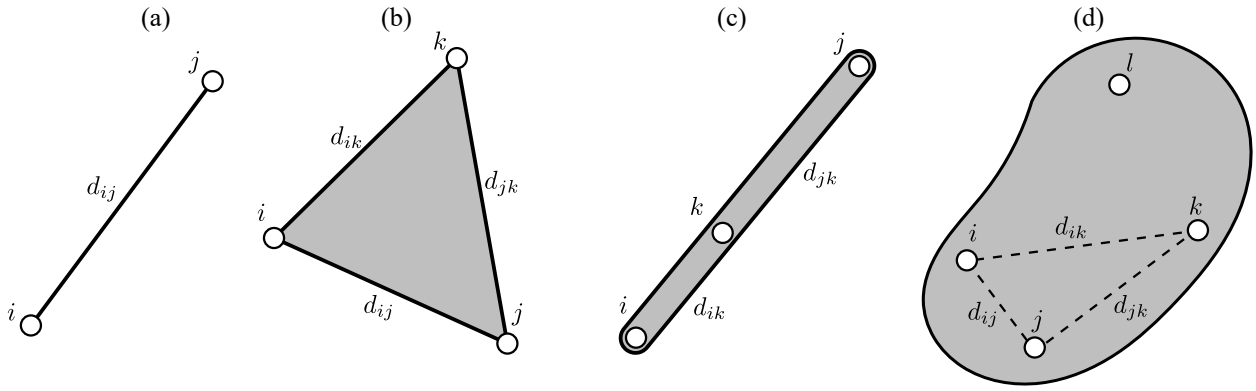

Source: The author.

- **Two points** (Figure 19a): In this case, the distance between points i and j is constant, therefore, we have a unique constraint equation that can be written as:

$$\mathbf{r}_{ij}^T \mathbf{r}_{ij} - d_{ij}^2 = 0, \tag{16}$$

$$\begin{bmatrix} (x_j - x_i) & (y_j - y_i) \end{bmatrix} \begin{bmatrix} (x_j - x_i) \\ (y_j - y_i) \end{bmatrix} - d_{ij}^2 = 0, \tag{17}$$

$$\phi = (x_j - x_i)^2 + (y_j - y_i)^2 - d_{ij}^2 = 0. \tag{18}$$

- **Three non collinear points** (Figure 19b): Now, we need three constraints equations to maintain constant distances on the triangle $\triangle ijk$, that are:

$$\mathbf{r}_{ij}^T \mathbf{r}_{ij} - d_{ij}^2 = 0, \tag{19}$$

$$\mathbf{r}_{ik}^T \mathbf{r}_{ik} - d_{ik}^2 = 0, \tag{20}$$

$$\mathbf{r}_{jk}^T \mathbf{r}_{jk} - d_{jk}^2 = 0, \tag{21}$$

written in expanded form as,

$$\phi_1 = (x_j - x_i)^2 + (y_j - y_i)^2 - d_{ij}^2 = 0, \tag{22}$$

$$\phi_2 = (x_k - x_i)^2 + (y_k - y_i)^2 - d_{ik}^2 = 0, \tag{23}$$

$$\phi_3 = (x_k - x_j)^2 + (y_k - y_j)^2 - d_{jk}^2 = 0. \tag{24}$$

- **Three collinear points** (Figure 19c): When the three points are collinear, the three distance constraint equations do not guarantee the condition of a rigid body because the three equations would not be independent. The solution to this problem is to replace two distance constraint equations with two proportionality constraint equations,

$$\mathbf{r}_{ij}^T \mathbf{r}_{ij} - d_{ij}^2 = 0, \tag{25}$$

$$\mathbf{r}_{ij} - \frac{d_{ij}}{d_{ik}} \mathbf{r}_{ik} = 0, \tag{26}$$

expanding Equation (25) and Equation (26), yields

$$\phi_1 = (x_j - x_i)^2 + (y_j - y_i)^2 - d_{ij}^2 = 0, \tag{27}$$

$$\phi_2 = (x_j - x_i) - \frac{d_{ij}}{d_{ik}}(x_k - x_i) = 0, \tag{28}$$

$$\phi_3 = (y_j - y_i) - \frac{d_{ij}}{d_{ik}}(y_k - y_i) = 0. \tag{29}$$

- **Four points** (Figure 19d): To model a rigid body with four points it is necessary five constraint equations, that are:

$$\mathbf{r}_{ij}^T \mathbf{r}_{ij} - d_{ij}^2 = 0, \tag{30}$$

$$\mathbf{r}_{ik}^T \mathbf{r}_{ik} - d_{ik}^2 = 0, \tag{31}$$

$$\mathbf{r}_{jk}^T \mathbf{r}_{jk} - d_{jk}^2 = 0, \tag{32}$$

$$\mathbf{r}_{il} - \alpha \mathbf{r}_{ij} - \beta \mathbf{r}_{ik} = 0, \tag{33}$$

where the Equations (30) to (32) are constant distance constraints and Equation (33) is the result of writing $\mathbf{r}_{il}$ as linear combination of the vectors $\mathbf{r}_{ij}$ and $\mathbf{r}_{ik}$, where α and β are constants of proportionality. Writing these equations in expanded form, we have that

$$\phi_1 = (x_j - x_i)^2 + (y_j - y_i)^2 - d_{ij}^2 = 0, \tag{34}$$

$$\phi_2 = (x_k - x_i)^2 + (y_k - y_i)^2 - d_{ik}^2 = 0, \tag{35}$$

$$\phi_3 = (x_k - x_j)^2 + (y_k - y_j)^2 - d_{jk}^2 = 0, \tag{36}$$

$$\phi_4 = (x_l - x_i) - \alpha(x_j - x_i) - \beta(x_k - x_i) = 0, \tag{37}$$

$$\phi_5 = (y_l - y_i) - \alpha(y_j - y_i) - \beta(y_k - y_i) = 0. \tag{38}$$

- **More than four points**: Three constraint equations are set for three noncollinear points, and two linear combination constraint equations are added for each additional point.

4.1.1.2 Kinematic pair constraints

The kinematic pair constraints are necessary so that the coordinates of the elements that are joined through a pair can move according to the degrees of freedom allowed by the pair. Figure 20 shows the main pairs in a mechanism.

Figure 20 – Planar kinematic pair constraints.

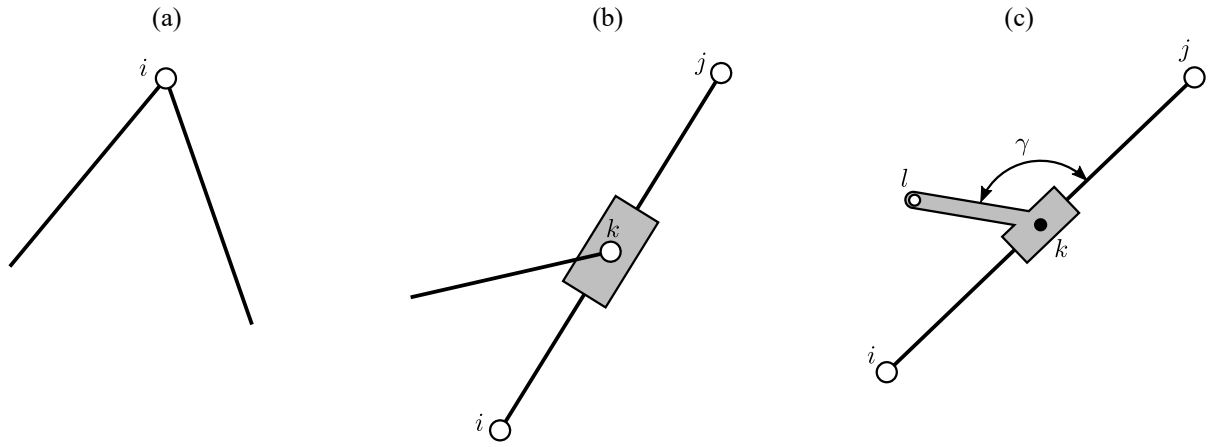

Source: The author.

- **Revolute pair** (Figure 20a): Since in the revolute pair the two elements are sharing the same point, it is not necessary to establish constraint equations. In the case that we want to use constraints to model a revolute pair, we can consider the coordinates of each pair element as different and then the coordinates of each point are forced to be equal, resulting in two constraint equations.

- **Revolute-prismatic pair association** (Figure 20b): To model this pair it is necessary to have three collinear points. The equation that guarantees that the points i, j and k are collinear, is achieved through the equation of null vector product between the vectors $\mathbf{r}_{ij}$ and $\mathbf{r}_{ik}$.

$$\mathbf{r}_{ij} \times \mathbf{r}_{ik} = 0, \tag{39}$$

$$\begin{bmatrix} (x_j - x_i) \\ (y_j - y_i) \\ 0 \end{bmatrix} \times \begin{bmatrix} (x_k - x_i) \\ (y_k - y_i) \\ 0 \end{bmatrix} = 0, \tag{40}$$

$$\phi = (x_j - x_i)(y_k - y_i) - (y_j - y_i)(x_k - x_i) = 0. \tag{41}$$

- **Rigid prismatic pair** (Figure 20c): The rigid prismatic pair can be modeled as revolute-prismatic pair, but in this case, is necessary to add a second constraint that guarantees constant angle between vector $\mathbf{r}_{ij}$ and $\mathbf{r}_{kl}$. The constraint equations are:

$$\mathbf{r}_{ij} \times \mathbf{r}_{ik} = 0, \tag{42}$$

$$\mathbf{r}_{ij}^T \mathbf{r}_{kl} - d_{ij} d_{kl} \cos\gamma = 0, \tag{43}$$

expanding Equation (42) and Equation (43), we have

$$\phi_1 = (x_j - x_i)(y_k - y_i) - (y_j - y_i)(x_k - x_i) = 0, \tag{44}$$

$$\phi_2 = (x_j - x_i)(x_l - x_k) + (y_j - y_i)(y_l - y_k) - d_{ij} d_{kl} \cos\gamma = 0. \tag{45}$$

4.1.1.3 Initial position problem and successive displacements

Coordinates vector $\mathbf{q}$ can be split as

$$\mathbf{q} = \begin{bmatrix} {}^{K}\mathbf{q} \\ {}^{D}\mathbf{q} \end{bmatrix}, \tag{46}$$

where ${}^{D}\mathbf{q}$ and ${}^{K}\mathbf{q}$ are driving and driven coordinates respectively. When driving coordinates are independent, these represent degrees of freedom. Now we define two type of constraints written as

$$\mathbf{\Phi}(\mathbf{q}) = \mathbf{0}, \tag{47}$$

$${}^{D}\mathbf{\Phi}(\mathbf{q}) = \mathbf{0}, \tag{48}$$

where expression in Equation (47) represents the kinematic constraints and expression in Equation (48) represents the driving constraints. To solve the position problem, one of the following two methods can be used (NIKRAVESH, Parviz E., 1988, 2007):

1. **Coordinate partitioning method**: First, determine the known coordinates, ${}^{D}\mathbf{q}$, from the driver expressions of Equation (48). Then solve Equation (47) for the unknown coordinates, ${}^{K}\mathbf{q}$.

2. **Appended constraints method**: In this method, the driving constraints are appended to the kinematic constraints to form the system,

$$\mathbf{\Phi}(\mathbf{q}, t) = \begin{bmatrix} \mathbf{\Phi}(\mathbf{q}) \\ {}^{D}\mathbf{\Phi}(\mathbf{q}) \end{bmatrix} = \mathbf{0}, \tag{49}$$

and solve this equation for unknown coordinates, $\mathbf{q}$.

Method 1 is more efficient in the kinematic analysis of a specific mechanism since the number of equations and restrictions is smaller than that of Method 2, but in the development of general

purpose kinematic analysis programs, Method 2 is more efficient (NIKRAVESH, Parviz E, 2007).

To solve the initial position problem we must solve the constraint equations given in the coordinate partitioning method or the appended constraints method. The solution of the constraint equations can be found through the Newton-Raphson method, that is based in the linearization of the constraints equations.Taking the first two terms of the expansion in a Taylor series around a certain approximation $\mathbf{q}_i$,

$$\mathbf{\Phi}(\mathbf{q}) \cong \mathbf{\Phi}(\mathbf{q}_i) + \mathbf{\Phi}_\mathbf{q}(\mathbf{q}_i)\Delta\mathbf{q}_i = \mathbf{0}, \tag{50}$$

where

$$\mathbf{\Phi}_\mathbf{q} = \frac{\partial \mathbf{\Phi}}{\partial \mathbf{q}} = \left[\frac{\partial \Phi_i}{\partial q_j}\right], \tag{51}$$

then, to approximate the solution, the next iterative procedure is followed,

Assume a solution $\mathbf{q}_i = \mathbf{q}_0$:

- Evaluate the function $\mathbf{\Phi} = \mathbf{\Phi}(\mathbf{q}_i)$;
- If $\sqrt{\mathbf{\Phi}^T\mathbf{\Phi}} \leq \varepsilon$, then $\mathbf{q}_i$ is the solution to $\mathbf{\Phi}(\mathbf{q}) = \mathbf{0}$, stop iteration;
- Otherwise, evaluate $\mathbf{\Phi}_\mathbf{q}(\mathbf{q}_i)$;
- Solve $\mathbf{\Phi}_\mathbf{q}(\mathbf{q}_i)\Delta\mathbf{q}_i = -\mathbf{\Phi}(\mathbf{q}_i)$ for $\Delta\mathbf{q}_i$;
- Improve the estimate solution as $\mathbf{q}_{i+1} = \mathbf{q}_i + \Delta\mathbf{q}_i$.

Repeat the process.

Depending on the choice of $\mathbf{q}_0$, the Newton-Raphson method converges to one configuration or the other, and in some cases, the method diverges. To ensure the convergence to a configuration, the vector $\mathbf{q}_0$ must be close to the desired configuration.

Once the initial position of the mechanism has been determined, the next position of the mechanism is obtained giving a small finite displacement to the driving coordinates. One way of determining successive displacements is by using the anterior position as an approximation to find a posterior position through the Newton-Raphson method, whenever the increments of the displacements are small enough.

Example 2 (Modeling a planar multi-loop mechanism using natural coordinates)

Figure 21 shows a 1-DoF mechanism modeled with natural coordinates, where A, B, C and D are fixed points and φ is an independent input angular coordinate. Then the natural

coordinates vector is,

$$\mathbf{q} = \begin{bmatrix} F \\ G \\ E \end{bmatrix} = \begin{bmatrix} x_F \\ y_F \\ x_G \\ y_G \\ x_E \\ y_E \end{bmatrix}. \tag{52}$$

Let x_E and y_E be two dependent driving coordinates described through the driving constraints,

$$\mathbf{r}_{BE} - d_{BE}\mathbf{u} = \mathbf{0}, \tag{53}$$

where $\mathbf{u} = \begin{bmatrix} \cos\varphi & \sin\varphi \end{bmatrix}^T$, therefore the point E is a function of φ. Let us suppose that link BE is frozen, then the mobility of the mechanism becomes $M = 0$, and according to Equation (10) it is necessary $n_c = 4 - 0 = 4$ kinematic constraints, that are:

$$\mathbf{r}_{AG}^T\mathbf{r}_{AG} - d_{AG}^2 = 0, \tag{54}$$

$$\mathbf{r}_{AG} \times \mathbf{r}_{AE} = 0, \tag{55}$$

$$\mathbf{r}_{AG} \times \mathbf{r}_{AF} = 0, \tag{56}$$

$$\mathbf{r}_{CD} \times \mathbf{r}_{CF} = 0. \tag{57}$$

Now using the coordinate partitioning method we have that,

$${}^D\mathbf{q} = \begin{bmatrix} x_E \\ y_E \end{bmatrix} = \begin{bmatrix} x_B + d_{BE}\cos\varphi \\ y_B + d_{BE}\sin\varphi \end{bmatrix}, \tag{58}$$

$$\mathbf{\Phi}(\mathbf{q}) = \begin{bmatrix} (x_G - x_A)^2 + (y_G - y_A)^2 - d_{AG}^2 \\ (x_G - x_A)(y_E - y_A) - (y_G - y_A)(x_E - x_A) \\ (x_G - x_A)(y_F - y_A) - (y_G - y_A)(x_F - x_A) \\ (x_D - x_C)(y_F - y_C) - (y_D - y_C)(x_F - x_C) \end{bmatrix} = \mathbf{0}. \tag{59}$$

In case it is necessary to use appended constraints method, then we write the constrains as,

$$\mathbf{\Phi}(\mathbf{q}) = \begin{bmatrix} (x_G - x_A)^2 + (y_G - y_A)^2 - d_{AG}^2 \\ (x_G - x_A)(y_E - y_A) - (y_G - y_A)(x_E - x_A) \\ (x_G - x_A)(y_F - y_A) - (y_G - y_A)(x_F - x_A) \\ (x_D - x_C)(y_F - y_C) - (y_D - y_C)(x_F - x_C) \\ (x_E - x_B) - d_{BE}\cos\varphi \\ (y_E - y_B) - d_{BE}\sin\varphi \end{bmatrix} = \mathbf{0}. \tag{60}$$

4.1.2 Natural coordinates in the space

In the case of multibody three-dimensional systems, the natural coordinates describe the position of each element with the Cartesian coordinates of some points located in the pairs of

Figure 21 – Example of modeling with natural coordinates.

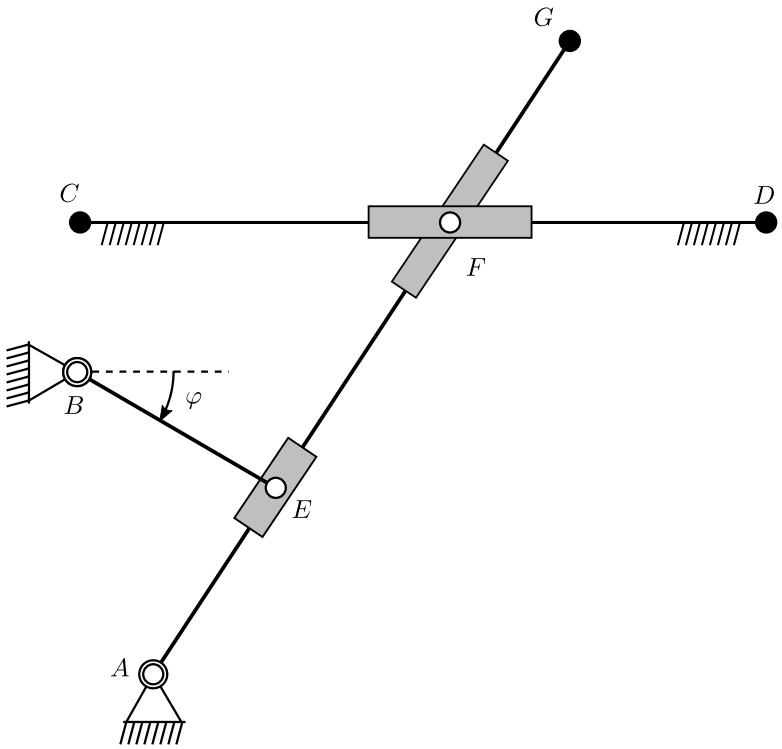

Source: The author.

the elements and with the Cartesian components of multiple unit vectors. Each element of the system must have enough points and vectors linked to it that its movement completely defines the movement of the element (JALÓN; BAYO, 1994).

The modeling of a three-dimensional mechanism with natural coordinates can be carried out following these general rules and recommendations:

1. The elements must contain a sufficient number of points and unit vectors so that their motion is completely defined.

2. A point shall be located at the joints in which there is a point common to the two linked elements. This occurs at the spherical joint (S), at the revolute joint (R), at the universal joint (U), and at other kinematic joints.

3. A unit vector must be placed at those joints having a rotational or translational axis and should have the direction of the corresponding axis. Sometimes, the role performed by a unit vector can also be performed by a couple of basic points.

4. All points of interest, whose positions are to be considered as a primary unknown variable of the problem, can likewise be defined as natural coordinates.

5. Each unit vector is associated with a specific point, and the same single unit vector can be associated with several points.

4.1.2.1 Rigid body constraints

The natural coordinates of a multibody system in space correspond to the Cartesian coordinates of the kinematic pairs, the Cartesian coordinates of some points of interest, and the Cartesian coordinates of some unit vectors. Therefore, the coordinates of a rigid body in space are formed by a set of points and unit vectors rigidly attached to the element. There are different ways to define the natural coordinates of a rigid body, depending on the pair of elements present in the body. The following are the combinations of points and unit vectors that define some rigid bodies.

- **Element with two points** (Figure 22(a)): The constraint equation is similar to the planar case. The only difference is the additional z-coordinate of the points; therefore, the constraint equation can be written as

Figure 22 – Spatial elements: (a) two points, (b) three non-collinear points, and (c) three collinear points.

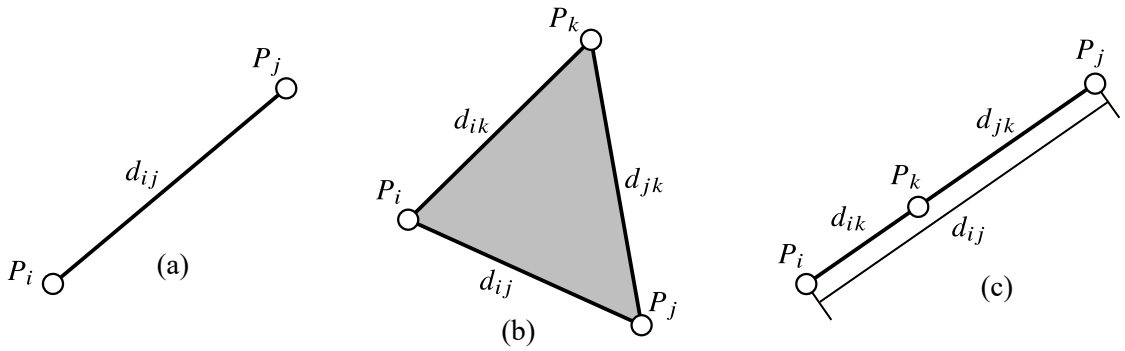

Source: The author.

$$\mathbf{r}_{ij}^T \mathbf{r}_{ij} - d_{ij}^2 = 0, \tag{61}$$

$$\begin{bmatrix} (x_j - x_i) & (y_j - y_i) & (z_j - z_i) \end{bmatrix} \begin{bmatrix} (x_j - x_i) \\ (y_j - y_i) \\ (z_j - z_i) \end{bmatrix} - d_{ij}^2 = 0, \tag{62}$$

$$\phi = (x_j - x_i)^2 + (y_j - y_i)^2 + (z_j - z_i)^2 - d_{ij}^2 = 0. \tag{63}$$

- **Element with three non-collinear points** (Figure 22(b)): The constraint equations for three non-collinear points can be defined with three equations of constant distance. Then the constraint equations are as follows:

$$\mathbf{r}_{ij}^T \mathbf{r}_{ij} - d_{ij}^2 = 0, \tag{64}$$
$$\mathbf{r}_{ik}^T \mathbf{r}_{ik} - d_{ik}^2 = 0, \tag{65}$$
$$\mathbf{r}_{jk}^T \mathbf{r}_{jk} - d_{jk}^2 = 0, \tag{66}$$

written in expanded form as,

$$\phi_1 = (x_j - x_i)^2 + (y_j - y_i)^2 + (z_j - z_i)^2 - d_{ij}^2 = 0, \tag{67}$$
$$\phi_2 = (x_k - x_i)^2 + (y_k - y_i)^2 + (z_k - z_i)^2 - d_{ik}^2 = 0, \tag{68}$$
$$\phi_3 = (x_k - x_j)^2 + (y_k - y_j)^2 (z_k - z_j)^2 - d_{jk}^2 = 0. \tag{69}$$

Note that this alternative way to model this element is to use the fact that the angles of the triangle are constant. Although more complicated, this alternative way can be advantageous in optimizing mechanisms, since it is more general.

- **Element with three collinear points** (Figure 22(c)): When all three points lie on the same line, the three distance constraint equations cannot ensure the rigid body condition, since they are not independent. To address this issue, two of the distance constraint equations are replaced with three proportionality constraint equations.

$$\mathbf{r}_{ij}^T \mathbf{r}_{ij} - d_{ij}^2 = 0, \tag{70}$$
$$\mathbf{r}_{ij} - \alpha \mathbf{r}_{ik} = 0, \tag{71}$$

expanding Equation (70) and Equation (71), yields

$$\phi_1 = (x_j - x_i)^2 + (y_j - y_i)^2 + (z_j - z_i)^2 - d_{ij}^2 = 0, \tag{72}$$
$$\phi_2 = (x_j - x_i) - \alpha(x_k - x_i) = 0, \tag{73}$$
$$\phi_3 = (y_j - y_i) - \alpha(y_k - y_i) = 0, \tag{74}$$
$$\phi_4 = (z_j - z_i) - \alpha(z_k - z_i) = 0, \tag{75}$$

where α is constant and only needs to be calculated once.

- **Element with two points and one unit vector** (Figure 23): The element in Figure 23(a) has two points and one non-collinear unit vector. It has nine natural coordinates and six degrees of freedom, resulting in three constraint equations. The constraint equations are a distance equation between points P_i and P_j, a constant angle equation between vectors $\mathbf{u}_m$ and $\mathbf{r}_{ij}$, and a unit vector condition, respectively.

$$\mathbf{r}_{ij}^T \mathbf{r}_{ij} - d_{ij}^2 = 0, \tag{76}$$

Figure 23 – Element with two basic points and a unit vector.

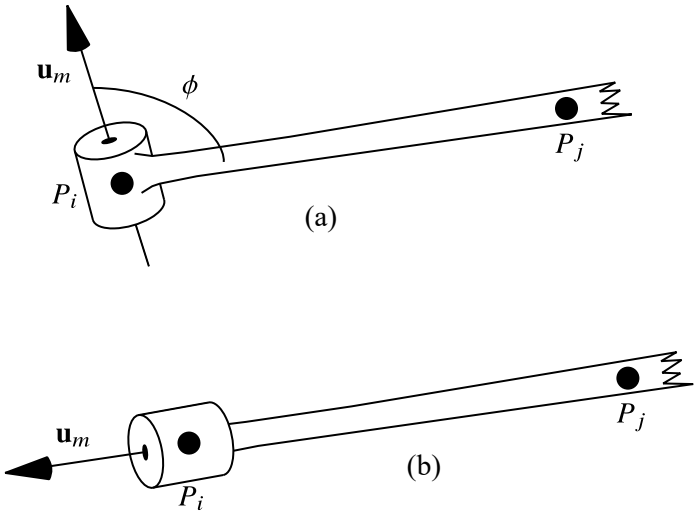

Source: The author.

$$\mathbf{r}_{ij}^T \mathbf{u}_m - d_{ij} \cos\phi = 0, \tag{77}$$

$$\mathbf{u}_m^T \mathbf{u}_m - 1 = 0. \tag{78}$$

If the unit vector is aligned with the points P_i and P_j (angle ϕ equal to zero), the element will have five degrees of freedom. In this case, the four constraint equations will be

$$\mathbf{r}_{ij}^T \mathbf{r}_{ij} - d_{ij}^2 = 0, \tag{79}$$

$$\mathbf{r}_{ij} - \alpha \mathbf{u}_m = 0, \tag{80}$$

where α is a constant. Defining a unit vector in the direction of a known segment is not very necessary, as unit vectors are primarily employed to establish directions. In this particular case, the direction has already been determined. However, introducing a unit vector may still be feasible for other purposes, such as ensuring compatibility with an adjacent body.

- **Element with two points and two unit vectors** (Figure 24): The body has two points and two non-coplanar vectors of units. Therefore, it has 12 natural coordinates and 6 degrees of freedom. The six constraint equations must be found. These six conditions are one constant distance equation, three constant angle conditions (between two vectors and segment and between two vectors themselves) and two unit module conditions for unit vectors. The corresponding equations are the following:

$$\mathbf{r}_{ij}^T \mathbf{r}_{ij} - d_{ij}^2 = 0, \tag{81}$$

Figure 24 – Element with two points and two unit vectors.

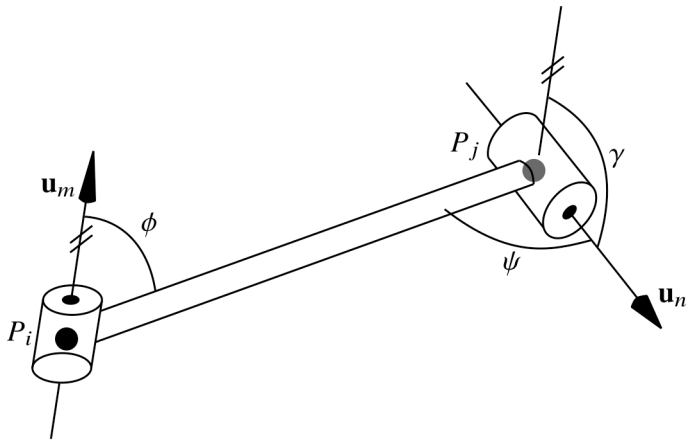

Source: The author.

$$\mathbf{r}_{ij}^T\mathbf{u}_m - d_{ij}\cos\phi = 0, \tag{82}$$
$$\mathbf{r}_{ij}^T\mathbf{u}_n - d_{ij}\cos\psi = 0, \tag{83}$$
$$\mathbf{u}_n^T\mathbf{u}_m - \cos\gamma = 0, \tag{84}$$
$$\mathbf{u}_m^T\mathbf{u}_m - 1 = 0, \tag{85}$$
$$\mathbf{u}_n^T\mathbf{u}_n - 1 = 0. \tag{86}$$

If the two unit vectors are coplanar, then the constraint equations are as follows:

$$\mathbf{r}_{ij}^T\mathbf{r}_{ij} - d_{ij}^2 = 0, \tag{87}$$
$$\mathbf{r}_{ij}^T\mathbf{u}_m - d_{ij}\cos\phi = 0, \tag{88}$$
$$\mathbf{u}_m^T\mathbf{u}_m - 1 = 0, \tag{89}$$
$$\mathbf{u}_n - \alpha_1\mathbf{r}_{ij} - \alpha_2\mathbf{u}_n = \mathbf{0}, \tag{90}$$

where α_1 and α_2 are the constant scalar coefficients of the linear combination.

- **More complex elements**: To streamline the derivation of constraint equations and enhance the accuracy of results, the following steps can be employed for more intricate elements.
  - Three vectors are selected to form a basis in the three-dimensional space. These vectors can be either segments, denoted as $\mathbf{r}_{ij}$, connecting two fundamental points, or unit vectors.
  - The constraint equations are established to ensure that the three chosen vectors form a rigid body.

– The remaining vectors of the body, including both segments and unit vectors, are expressed as linear combinations of the three base frame vectors. This approach offers the advantage of obtaining linear constraints.

4.1.2.2 Joint constraints

After incorporating the constraint equations to ensure the rigid body motion of each element, it becomes essential to formulate additional constraints to enforce the relative motions between the bodies based on the kinematic joints that connect them. It will be demonstrated that for certain joints, no additional equations are required, while for others, additional equations need to be introduced. The types of joints discussed include spherical (S), revolute (R), cylindrical (C), and prismatic (P).

- **Spherical joint** (Figure 25): In a spherical pair, defining constraint equations is unnecessary, since two elements share the same point. Therefore, the only relative motion between the elements is rotations around the shared point, which corresponds to a spherical pair.

Figure 25 – Spherical joint.

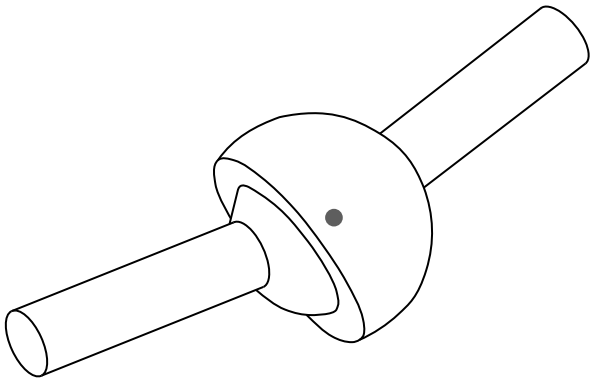

Source: The author.

If the spherical joint is going to be broken during the simulation at a specific moment and the points are not shared, we can still define the constraint equations. To do this, we need to match the coordinates of points P_i and P_j that belong to different bodies.

$$\mathbf{r}_{ij} = \mathbf{0}. \tag{91}$$

- **Revolute joint** (Figure 26): When two adjacent elements share a point and a unit vector, the revolute joint is automatically considered without the need for constraint equations. The only possible relative motion is rotation around the unit vector (Figure 26(a)).

Figure 26 – Revolute joint.

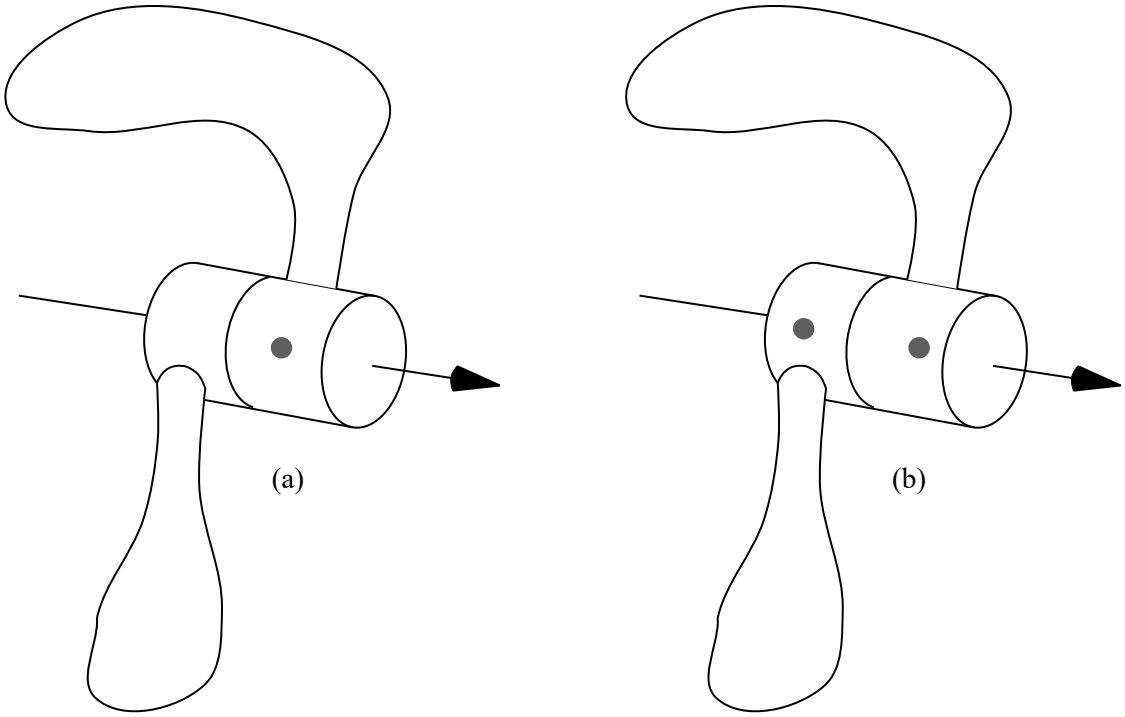

Source: The author.

One way to introduce the revolute joint automatically is by having two adjacent elements share two points, as shown in Figure 26(b). This allows for only one type of relative motion: rotation around the axis passing through those two points.

- **Cylindrical joint** (Figure 27): When a cylindrical joint is used, it is necessary to create four constraint equations to constrain four degrees of freedom. In Figure 27, the two joint elements share a unit vector in the direction of the joint axis, resulting in two constraint equations. The two additional constraint equations are created by ensuring that two points on the joint axis, each belonging to a different element, are aligned with the unit vector. This condition is expressed mathematically by a cross-product

$$\mathbf{r}_{ij} \times \mathbf{u} = \mathbf{0}, \tag{92}$$

  where only two of the three algebraic equations are independent.

- **Prismatic joint** (Figure 28): The prismatic joint allows only one degree of freedom; and generates five constraint equations. These equations are the same as those generated by the cylindrical joint. In fact, all the degrees of freedom restricted by the cylindrical joint are also restricted by the prismatic joint. In addition, one equation prevents relative rotation

Figure 27 – Revolute joint.

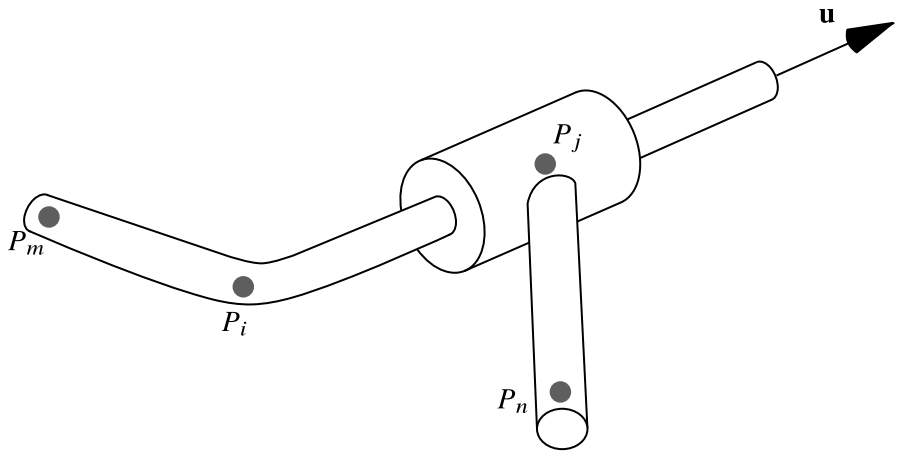

Source: The author.

between the elements with respect to the joint axis.

$$\mathbf{r}_{im}^{T}\mathbf{r}_{jn} - \alpha = 0, \tag{93}$$

where α is a scalar constant.

Figure 28 – Prismatic joint.

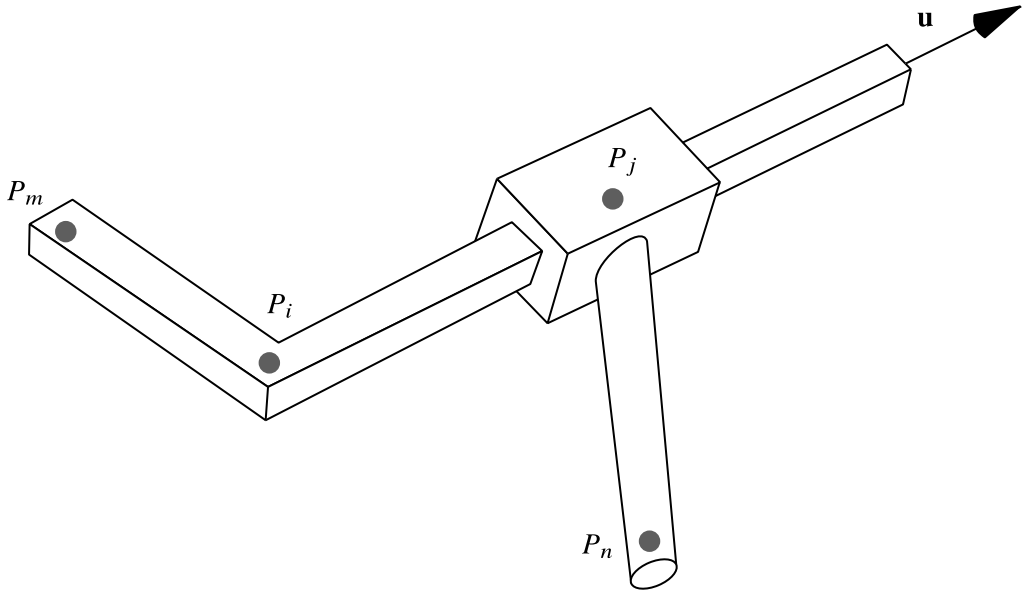

Source: The author.

Example 3 (RSCR mechanism modeled with natural coordinates)

Figure 29 – RSCR spatial mechanism.

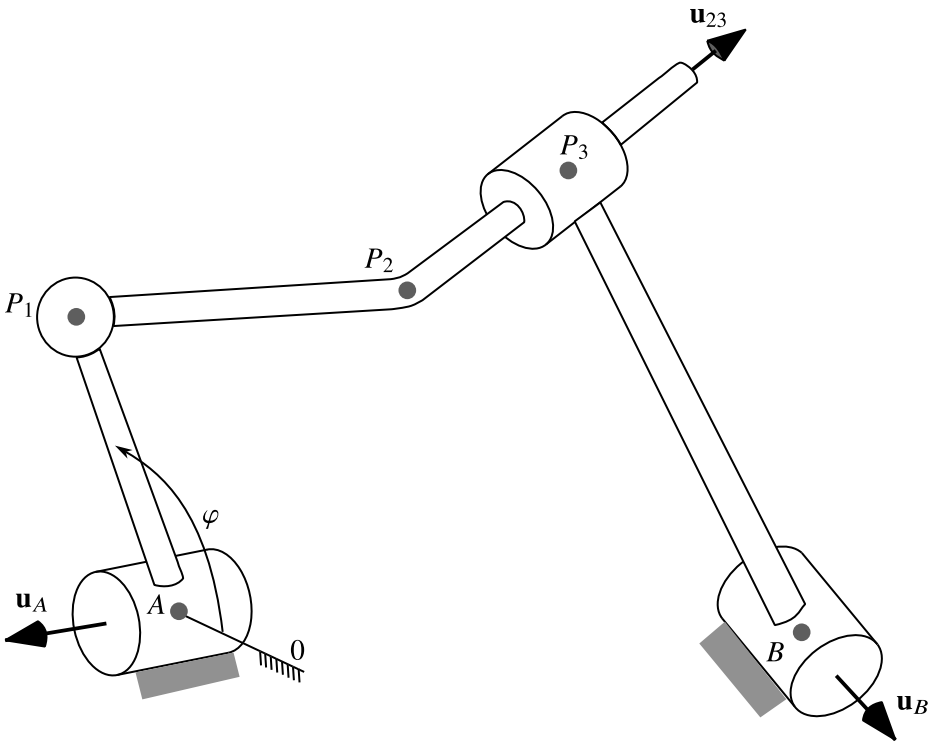

Source: The author.

In Figure 29, a 3D four-bar mechanism called RSCR (Revolute-Spherical-Cylindrical-Revolute) is modeled using natural coordinates. This mechanism has three points and one unit vector that can move, resulting in 12 dependent Cartesian coordinates and one degree of freedom. An input angle y has also been added as an externally driven coordinate. The following are the constraint equations related to this mechanism:

$$(x_1 - x_A)(x_0 - x_A) + (y_1 - y_A)(y_0 - y_A) + (z_1 - z_A)(z_0 - z_A) - k_1 \cos\varphi = 0, \tag{94}$$

$$(x_1 - x_A)^2 + (y_1 - y_A)^2 + (z_1 - z_A)^2 - k_2 = 0, \tag{95}$$

$$(x_1 - x_A)\,u_{Ax} + (y_1 - y_A)\,u_{Ay} + (z_1 - z_A)\,u_{Az} - k_3 = 0 \tag{96}$$

$$(x_2 - x_1)^2 + (y_2 - y_1)^2 + (z_2 - z_1)^2 - k_4 = 0, \tag{97}$$

$$(x_2 - x_1)\,u_{23x} + (y_2 - y_1)\,u_{23y} + (z_2 - z_1)\,u_{23z} - k_5 = 0, \tag{98}$$

$$u_{23x}^2 + u_{23y}^2 + u_{23z}^2 - 1 = 0, \tag{99}$$

$$(x_3 - x_B)^2 + (y_3 - y_B)^2 + (z_3 - z_B)^2 - k_6 = 0, \tag{100}$$

$$(x_3 - x_B)\,u_{23x} + (y_3 - y_B)\,u_{23y} + (z_3 - z_B)\,u_{23z} - k_7 = 0, \tag{101}$$

$$(x_3 - x_B)\,u_{Bx} + (y_3 - y_B)\,u_{By} + (z_3 - z_B)\,u_{Bz} - k_8 = 0, \tag{102}$$

$$u_{Bx}u_{23x} + u_{By}u_{23y} + u_{Bz}u_{23z} - k_9 = 0, \tag{103}$$

$$(y_3 - y_2)\,u_{23z} - (z_3 - z_2)\,u_{23y} = 0, \tag{104}$$

$$(z_3 - z_2)\, u_{23x} - (x_3 - x_2)\, u_{23z} = 0, \tag{105}$$

$$(x_3 - x_2)\, u_{23y} - (y_3 - y_2)\, u_{23x} = 0. \tag{106}$$

This system of non-linear equations governs the position problem for the RSCR mechanism. The first equation corresponds to the input angle definition; equations 95 and 96 represent rigid body conditions for element $P_A P_1$; equations 97 to 99 represent rigid body constraints for element $P_1 P_2$; equations 99 to 103 represent the same for element $P_3 P_B$, and equations 104 to 106 (only two are independent) contribute to defining the cylindrical joint. Finally, k_i for $i = 1, ..., 9$ represents constant values.

4.1.3 Bilateration

Bilateration consists of determining the coordinates of a vertex of a triangle, where the coordinates of two vertices are known and their respective distances to the vertex with unknown coordinates (ROJAS, 2012). Let us use the generic triangle illustrated in Figure 30, to deduce the necessary equations and thus to solve the bilateration problem. Here lowercase and capital bold letters denote vector and matrix, respectively.

Figure 30 – Bilateration problem.

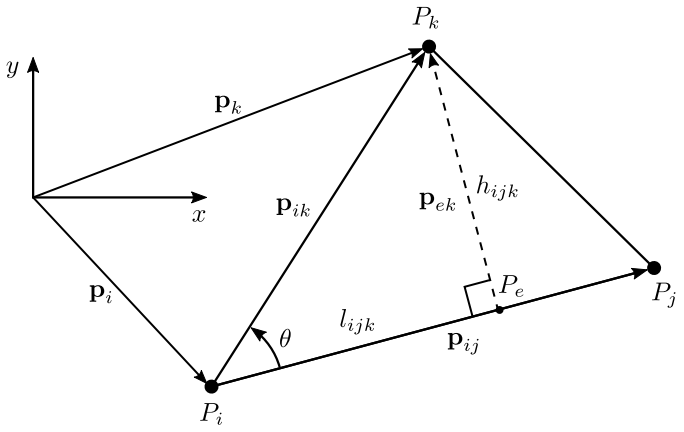

Source: The author.

Let l_{ijk} be the scalar projection of the vector $\mathbf{p}_{ik}$ onto the vector $\mathbf{p}_{ij}$ and let h_{ijk} be the scalar rejection of the same vector from $\mathbf{p}_{ij}$, then we have that

$$l_{ijk} = \mathbf{p}_{ik} \cdot \mathbf{u}_{ij} = d_{ik} \cos\theta, \tag{107}$$

where $\mathbf{u}_{ij}$ is unit vector in the same direction of $\mathbf{p}_{ij}$ and d_{ik} is the Euclidean norm of the vector $\mathbf{p}_{ik}$. From law of cosines it can be written

$$\cos\theta = \frac{d_{ik}^2 + d_{ij}^2 - d_{jk}^2}{2 d_{ij} d_{ik}}, \tag{108}$$

and replacing Equation (108) into Equation (107), yields

$$l_{ijk} = \frac{d_{ik}^2 + d_{ij}^2 - d_{jk}^2}{2d_{ij}}, \tag{109}$$

now applying Pythagoras' theorem to the triangle $\triangle P_i P_e P_k$, it results in

$$h_{ijk} = \pm\sqrt{d_{ik}^2 - l_{ijk}^2} = \pm\frac{\sqrt{4d_{ik}^2 d_{ij}^2 - (d_{ik}^2 + d_{ij}^2 - d_{jk}^2)^2}}{2d_{ij}} \tag{110}$$

rearranging the Equation (110) gives

$$h_{ijk} = \pm\frac{\sqrt{(d_{ik}^2 + d_{ij}^2 + d_{jk}^2)^2 - 2(d_{ik}^4 + d_{ij}^4 + d_{jk}^4)}}{2d_{ij}}. \tag{111}$$

Notice that l_{ijk} and h_{ijk} depend on the distances only, that is, both scalar projection and rejection do not depend on the reference frame chosen. Now according to vectors in Figure 30, we can write the following expression

$$\mathbf{p}_{ik} = \mathbf{p}_{ie} + \mathbf{p}_{ek}, \tag{112}$$

where

$$\mathbf{p}_{ie} = \frac{l_{ijk}}{d_{ij}}\mathbf{p}_{ij}, \tag{113}$$

$$\mathbf{p}_{ek} = \frac{h_{ijk}}{d_{ij}}\mathbf{R}\mathbf{p}_{ij}, \tag{114}$$

here $\mathbf{R}$ is a $\pi/2$ counterclockwise 2×2 rotation matrix. Substituting Equation (113) and Equation (114) into Equation (112), yields

$$\mathbf{p}_{ik} = \frac{l_{ijk}}{d_{ij}}\mathbf{p}_{ij} + \frac{h_{ijk}}{d_{ij}}\mathbf{R}\mathbf{p}_{ij} = \left(\frac{l_{ijk}}{d_{ij}}\mathbf{I} + \frac{h_{ijk}}{d_{ij}}\mathbf{R}\right)\mathbf{p}_{ij}, \tag{115}$$

where $\mathbf{I}$ is a 2×2 identity matrix. The Equation (115) can be written as

$$\mathbf{p}_{ik} = \mathbf{N}_{ijk}\mathbf{p}_{ij}, \tag{116}$$

where

$$\mathbf{N}_{ijk} = \begin{bmatrix} \frac{l_{ijk}}{d_{ij}} & -\frac{h_{ijk}}{d_{ij}} \\ \frac{h_{ijk}}{d_{ij}} & \frac{l_{ijk}}{d_{ij}} \end{bmatrix} = \frac{1}{2dij^2}$$
$$\begin{bmatrix} d_{ik}^2 + d_{ij}^2 - d_{jk}^2 & \mp\sqrt{(d_{ik}^2 + d_{ij}^2 + d_{jk}^2)^2 - 2(d_{ik}^4 + d_{ij}^4 + d_{jk}^4)} \\ \pm\sqrt{(d_{ik}^2 + d_{ij}^2 + d_{jk}^2)^2 - 2(d_{ik}^4 + d_{ij}^4 + d_{jk}^4)} & d_{ik}^2 + d_{ij}^2 - d_{jk}^2 \end{bmatrix}, \tag{117}$$

is named a bilateration matrix. Finally we have that

$$\mathbf{p}_k = \mathbf{p}_i + \mathbf{N}_{ijk}\mathbf{p}_{ij}. \tag{118}$$

4.1.3.1 Bilateration matrices as normal matrices

Bilateration matrices can be seen as 2×2 normal matrices since they are of the form $\mathbf{A} = \begin{bmatrix} a & -b \\ b & a \end{bmatrix}$ and therefore holds that $\mathbf{A}\mathbf{A}^T = \mathbf{A}^T\mathbf{A} = \det(\mathbf{A})\mathbf{I}$, (HORN; JOHNSON, 2012). Some fundamental properties of 2×2 normal matrices are:

Let two perpendicular matrices $\mathbf{A} = \begin{bmatrix} a & -b \\ b & a \end{bmatrix}$ and $\mathbf{B} = \begin{bmatrix} c & -d \\ d & c \end{bmatrix}$, then

1. **Normal matrix addition is closed and commutative**. $\mathbf{A} + \mathbf{B} = \mathbf{B} + \mathbf{A}$ and $\mathbf{A} + \mathbf{B}$ is a normal matrix

   Proof. The expansion of $\mathbf{A} + \mathbf{B}$ and $\mathbf{B} + \mathbf{A}$ yields $\begin{bmatrix} (a+c) & -(b+d) \\ (b+d) & (a+c) \end{bmatrix}$, that is, a normal matrix. □

2. **Normal matrix product is closed and commutative**. $\mathbf{AB} = \mathbf{BA}$ and $\mathbf{AB}$ is a normal matrix

   Proof. The expansion of $\mathbf{AB}$ and $\mathbf{BA}$ yields $\begin{bmatrix} (ac-bd) & -(ad+cb) \\ (ad+cb) & (ac-bd) \end{bmatrix}$, that is, a normal matrix. □

3. **Scaling**. If $\mathbf{u} = \mathbf{A}\mathbf{v}$ with $\mathbf{u}$ and $\mathbf{v}$ appropriate vectors, then $\|\mathbf{u}\|^2 = \det(\mathbf{A})\|\mathbf{v}\|^2$

   Proof. Square of Euclidean norm of vector $\mathbf{u}$ is $\|\mathbf{u}\|^2 = \mathbf{u}^T\mathbf{u}$, therefore,

$$\begin{aligned} \|\mathbf{u}\|^2 &= (\mathbf{A}\mathbf{v})^T(\mathbf{A}\mathbf{v}) = \mathbf{v}^T\mathbf{A}^T\mathbf{A}\mathbf{v} \\ &= \mathbf{v}^T \det(\mathbf{A})\mathbf{I}\mathbf{v} \\ &= \det(\mathbf{A})\mathbf{v}^T\mathbf{v} \\ &= \det(\mathbf{A})\|\mathbf{v}\|^2 \end{aligned}$$

   □

In the next two examples, the enormous potential of the bilateration on the position analysis of mechanisms or kinematic chains with complex geometry is evidenced. The first example corresponds to the Theo Jansen mechanism and the second example is a Baranov chain.

Example 4 (Position analysis of a Theo Jansen mechanism)

The position analysis of the Theo Jansen mechanism Figure 31, begins computing the point C as,

$$C = A + d_{AC}\mathbf{u}_{AC}, \tag{119}$$

where $\mathbf{u}_{AC} = \begin{bmatrix} \cos\varphi & \sin\varphi \end{bmatrix}^T$. To calculate the remaining points, the following sequence of bilateration is sufficient:

$$D = C + \mathbf{N}_{CBD}(B - C), \tag{120}$$

$$G = C + \mathbf{N}_{CBG}(B - C), \tag{121}$$

$$E = B + \mathbf{N}_{BDE}(D - B), \tag{122}$$

$$F = E + \mathbf{N}_{EGF}(G - E), \tag{123}$$

$$P = F + \mathbf{N}_{FGP}(G - F). \tag{124}$$

Since each bilateration equation has two possible solutions, the mechanism would have 32 possible assembly modes or configurations. Considering the sign of the bilateration matrices $\mathbf{N}_{BDE}$ and $\mathbf{N}_{FGP}$ constant that corresponds to ternary link and left leg respectively, the assembly modes will be 8, this is to maintain the orientation of triangles $\triangle BDE$ and $\triangle FGP$.

The position analysis of the right side of the mechanism is similar to the procedure above.

Figure 31 – Theo Jansen mechanism.

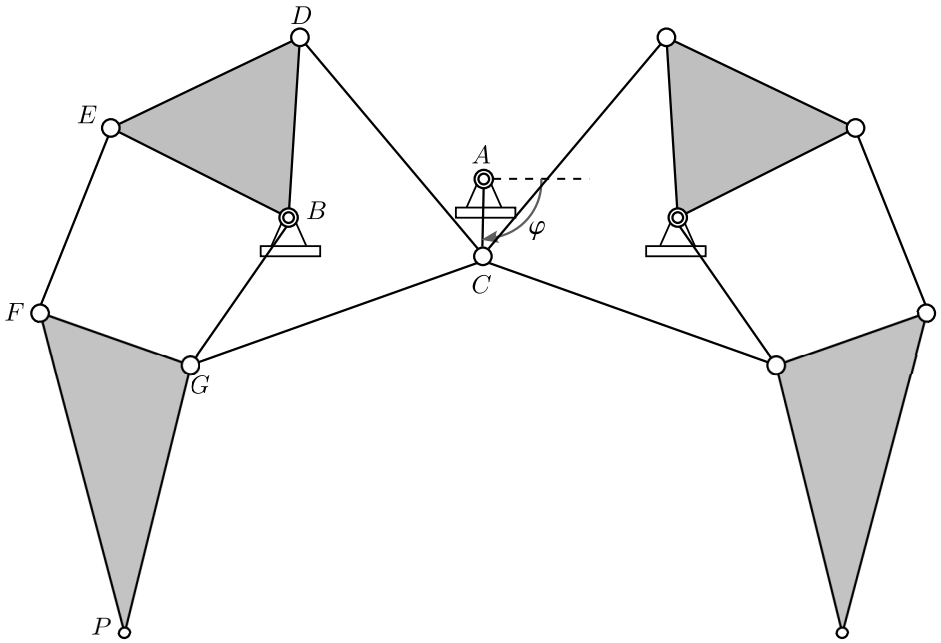

Source: Adapted from (ROMERO NUÑEZ et al., 2018).

Example 5 (Position analysis of five-bar Baranov chain)

To solve the position of the Baranov chain shown in Figure 32, it is necessary to find a closure equation because it is not possible to determine all the points using a bilateration sequence only. Let us use $\mathbf{p}_{16}$ as a reference, then we have

$$\mathbf{p}_{25} = -\mathbf{p}_{12} + \mathbf{p}_{16} + \mathbf{p}_{65}$$

$$
\begin{aligned}
&= -\mathbf{N}_{132}\mathbf{p}_{13} + \mathbf{p}_{16} + \mathbf{N}_{645}\mathbf{p}_{64} \\
&= -\mathbf{N}_{132}\mathbf{N}_{163}\mathbf{p}_{16} + \mathbf{p}_{16} + \mathbf{N}_{645}\mathbf{N}_{164}\mathbf{p}_{16} \\
&= (\mathbf{I} - \mathbf{N}_{132}\mathbf{N}_{163} + \mathbf{N}_{645}\mathbf{N}_{164})\mathbf{p}_{16}. \qquad (125)
\end{aligned}
$$

Applying the scaling property to Equation (125), yields

$$d_{25}^2 = \det(\mathbf{I} - \mathbf{N}_{132}\mathbf{N}_{163} + \mathbf{N}_{645}\mathbf{N}_{164})d_{16}^2, \qquad (126)$$

that is a single variable scalar equation in d_{16}. This equation can be used to derive the characteristic polynomial that can be solved numerically and to determine the possible configurations.

Figure 32 – Five links Baranov chain $(5/B_1)$

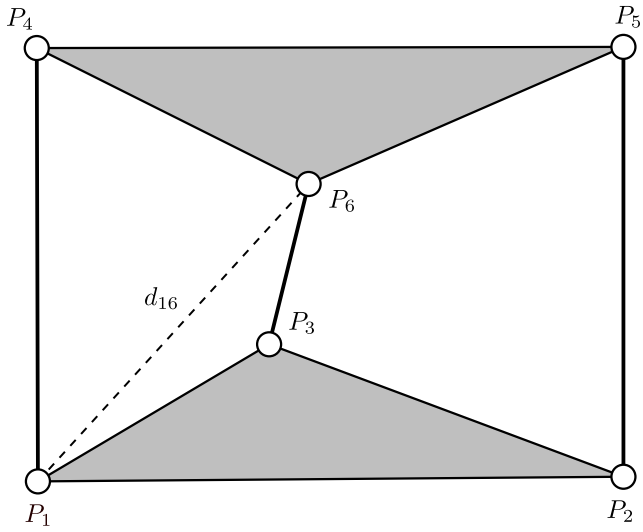

Source: Adapted from (ROJAS, 2012)

Assuming that triangle $\triangle P_1P_2P_3$ is fixed, then the position of the rest of the points can be computed using the following bilateration sequence:

$$\mathbf{p}_6 = \mathbf{p}_1 + \mathbf{N}_{136}\mathbf{p}_{13}, \qquad (127)$$

$$\mathbf{p}_4 = \mathbf{p}_1 + \mathbf{N}_{164}\mathbf{p}_{16}, \qquad (128)$$

$$\mathbf{p}_5 = \mathbf{p}_4 + \mathbf{N}_{465}\mathbf{p}_{46}. \qquad (129)$$

4.1.4 Bilateration via complex numbers

In the Section 4.1.3 bilateration was performed by means of vector and matrix representation. In this section, we propose an alternative way of solving the problem of bilateration through complex numbers. To this we consider the following notation: Let $z_p = x_p + y_p i$ denote a point in the complex plane, where i is the imaginary unit, $z_{pr} = z_r - z_p = (x_r - x_p) + (y_r - y_p)i$

is the vector that goes from z_p to z_r, $d_{pr}^2 = z_{pr}\bar{z}_{pr}$ is the square distance between z_p and z_r and $z_{pr}e^{\theta i}$ is the counterclockwise rotation through an angle θ of the vector z_{pr}.

According to the previous notation and Figure 33, the relative position of the point r with respect to point p can be expressed as

$$z_{pr} = z_{pe} + z_{er}, \tag{130}$$

where

$$z_{pe} = \frac{l_{pqr}}{d_{pq}} z_{pq}, \tag{131}$$

$$z_{er} = \frac{h_{pqr}}{d_{pq}} z_{pq} e^{\frac{\pi}{2}i} = \frac{h_{pqr}}{d_{pq}} z_{pq} i, \tag{132}$$

Figure 33 – Bilateration problem using complex numbers

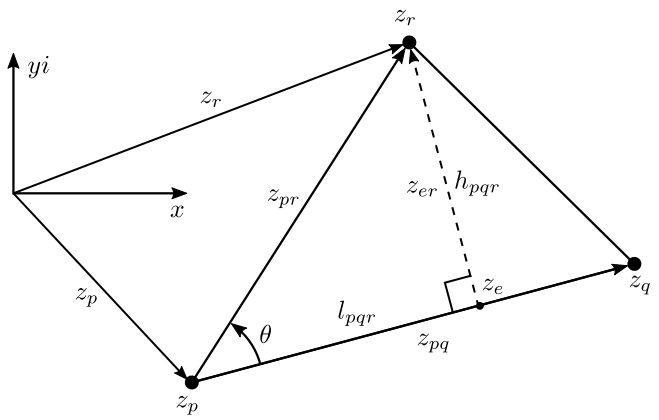

Source: The author

then, substituting Equation (131) and Equation (132), we get

$$z_{pr} = \frac{l_{pqr}}{d_{pq}} z_{pq} + \frac{h_{pqr}}{d_{pq}} z_{pq} i \tag{133}$$

$$= \left(\frac{l_{pqr}}{d_{pq}} + \frac{h_{pqr}}{d_{pq}} i \right) z_{pq}, \tag{134}$$

where

$$\left(\frac{l_{pqr}}{d_{pq}} + \frac{h_{pqr}}{d_{pq}} i \right) = z_{pqr}. \tag{135}$$

Therefore the solution of the bilateration problem can be expressed as:

$$z_{pr} = z_{pqr} z_{pq}, \tag{136}$$

$$z_r = z_p + z_{pqr} z_{pq}. \tag{137}$$

The complex number z_{pqr} will be called the bilaterator. Since the bilaterator obviously has all the properties of complex numbers, some properties demonstrated in the previous section

can be easily proofed here. For example we can write

$$\begin{aligned} z_{pr}\bar{z}_{pr} &= (z_{pqr}z_{pq})\overline{(z_{pqr}z_{pq})} \\ |z_{pr}|^2 &= z_{pqr}\bar{z}_{pqr}z_{pq}\bar{z}_{pq} \\ |z_{pr}|^2 &= |z_{pqr}|^2|z_{pq}|^2 \\ d_{pr}^2 &= |z_{pqr}|^2 d_{pq}^2, \end{aligned}$$

this is exactly the scaling property in the complex numbers version. Where the following equivalence is evident:

$$|z_{pqr}|^2 = \det(\mathbf{N}_{pqr}). \tag{138}$$

4.1.5 Bilateration matrix for a RRRP planar mechanism

The forward position problem of the planar RRRP mechanism illustrated in Figure 34(a) is equivalent to the circle-line interception problem described in Figure 34(b). Rojas (2012) presents a bilateration matrix for the intersection between a line and a circle, but this matrix has a singularity when the line passes through the center of the circle. The matrix that will be deduced to continuation solves the singularity problem described above.

Figure 34 – (a) Planar RRRP mechanism, (b) interception between circle and line.

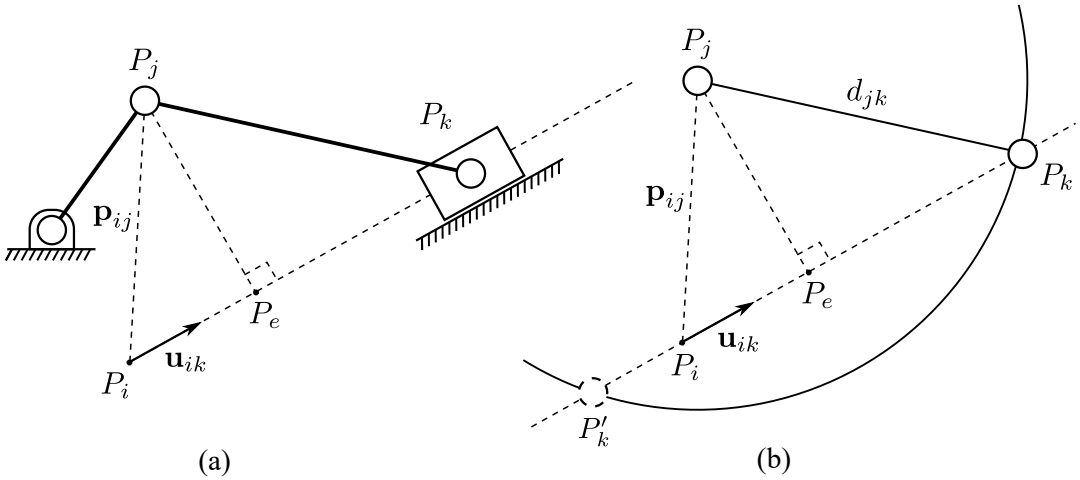

Source: The author.

The idea is to determine the distances d_{ie} and d_{ek} and compute the vector $\mathbf{p}_{ik}$ as a function of s_{ij}, s_{jk}, $\mathbf{p}_{ij}$, and $\mathbf{u}_{ik}$. The distance d_{ie} is the projection $\mathbf{p}_{ij}$ on the line defined by P_i and $\mathbf{u}_{ik}$, then $d_{ie} = \mathbf{p}_{ij} \cdot \mathbf{u}_{ik}$. Now it is applied Pythagoras' theorem in triangles $\triangle P_i P_j P_e$ and $\triangle P_e P_j P_k$ as follows

$$s_{ij} = (\mathbf{p}_{ij} \cdot \mathbf{u}_{ik})^2 + s_{je}, \qquad s_{jk} = s_{je} + s_{ek},$$

$$s_{je} = s_{ij} - (\mathbf{p}_{ij} \cdot \mathbf{u}_{ik})^2, \qquad s_{ek} = s_{jk} - s_{je},$$

where $s_{ie} = (\mathbf{p}_{ij} \cdot \mathbf{u}_{ik})^2$, then

$$s_{ek} = s_{jk} - s_{ij} + (\mathbf{p}_{ij} \cdot \mathbf{u}_{ik})^2. \tag{139}$$

Moreover, the vector $\mathbf{p}_{ik}$ can be expressed as follows:

$$\begin{aligned} \mathbf{p}_{ik} &= (\mathbf{p}_{ij} \cdot \mathbf{u}_{ik})\mathbf{u}_{ik} \pm \sqrt{s_{jk} - s_{ij} + (\mathbf{p}_{ij} \cdot \mathbf{u}_{ik})^2}\mathbf{u}_{ik} \\ &= \left[(\mathbf{p}_{ij} \cdot \mathbf{u}_{ik})\mathbf{I} \pm \sqrt{s_{jk} - s_{ij} + (\mathbf{p}_{ij} \cdot \mathbf{u}_{ik})^2}\mathbf{I}\right]\mathbf{u}_{ik}, \end{aligned} \tag{140}$$

where $\mathbf{I}$ is the 2×2 identity matrix. Writing the Equation (140) in a compact form yields:

$$\mathbf{p}_{ik} = \mathbf{Y}_{ijk}\mathbf{u}_{ik}. \tag{141}$$

Where $\mathbf{Y}_{ijk}$ is the bilateration matrix

$$\mathbf{Y}_{ijk} = \begin{bmatrix} (\mathbf{p}_{ij} \cdot \mathbf{u}_{ik}) \pm \sqrt{s_{jk} - s_{ij} + (\mathbf{p}_{ij} \cdot \mathbf{u}_{ik})^2} & 0 \\ 0 & (\mathbf{p}_{ij} \cdot \mathbf{u}_{ik}) \pm \sqrt{s_{jk} - s_{ij} + (\mathbf{p}_{ij} \cdot \mathbf{u}_{ik})^2} \end{bmatrix}. \tag{142}$$

The signs $\pm$ in Equation (142) correspond to the two possible configurations represented by the points P_k and P'_k, as shown in Figure 34(b). Applying the scaling property (ROJAS; THOMAS, 2012) to Equation (141) yields $s_{ik} = \det(\mathbf{Y}_{ijk})$; this property is essential to derive closure equations.

4.2 VELOCITY ANALYSIS

Velocity analysis of a mechanism consists of formulating the necessary equations to determine angular and/or linear velocities that permit one to specify each link's velocity state. In this section, two methods widely studied by kinematicians to perform the velocity analysis of a mechanism systematically are shown. Furthermore, a method is proposed that incorporates the natural coordinates into the screw theory for the analysis of position and velocity simultaneously.

One method for velocity analysis is to derive the constraint vector (Equation (10)) respect to time

$$\frac{d}{dt}(\mathbf{\Phi}(\mathbf{q})) = \frac{\partial \mathbf{\Phi}}{\partial \mathbf{q}}\frac{d\mathbf{q}}{dt} = \mathbf{0}, \tag{143}$$

$$\mathbf{\Phi}_{\mathbf{q}}\dot{\mathbf{q}} = \mathbf{0}. \tag{144}$$

The velocity vector $\dot{\mathbf{q}}$ can be split as $\dot{\mathbf{q}} = \begin{bmatrix} {}^{d}\dot{\mathbf{q}} & {}^{i}\dot{\mathbf{q}} \end{bmatrix}^{T}$, where ${}^{d}\dot{\mathbf{q}}$ is a vector of dependent velocities and ${}^{i}\dot{\mathbf{q}}$ is a vector of as many independent velocities as degrees of freedom. Therefore the Equation (144) can be written in the form:

$$\left[\begin{array}{c|c} {}^{d}\mathbf{\Phi}_{\mathbf{q}} & {}^{i}\mathbf{\Phi}_{\mathbf{q}} \end{array} \right] \left[\begin{array}{c} {}^{d}\dot{\mathbf{q}} \\ \hline {}^{i}\dot{\mathbf{q}} \end{array} \right] = \mathbf{0}. \tag{145}$$

Then

$${}^{d}\mathbf{\Phi}_{\mathbf{q}}\,{}^{d}\dot{\mathbf{q}} = -{}^{i}\mathbf{\Phi}_{\mathbf{q}}\,{}^{i}\dot{\mathbf{q}}. \tag{146}$$

To illustrate the procedure to perform the velocity analysis, let us consider a simple mechanism shown in Figure 35. If this system is modeled by coordinates $\mathbf{q} = \begin{bmatrix} x_P & y_p & \theta \end{bmatrix}^{T}$, then the constraint vector is

$$\mathbf{\Phi}(\mathbf{q}) = \begin{bmatrix} x_P - d\cos\theta \\ y_P - d\sin\theta \end{bmatrix} = \mathbf{0}, \tag{147}$$

and applying the Equation (144) results in the expression:

$$\left[\begin{array}{cc|c} 1 & 0 & d\sin\theta \\ 0 & 1 & -d\cos\theta \end{array} \right] \left[\begin{array}{c} \dot{x}_P \\ \dot{y}_P \\ \hline \dot{\theta} \end{array} \right] = \begin{bmatrix} 0 \\ 0 \end{bmatrix}. \tag{148}$$

This equation can also be written as:

$$\begin{bmatrix} 1 & 0 \\ 0 & 1 \end{bmatrix} \begin{bmatrix} \dot{x}_P \\ \dot{y}_P \end{bmatrix} = -\begin{bmatrix} d\sin\theta \\ -d\cos\theta \end{bmatrix} \dot{\theta}, \tag{149}$$

therefore the velocity of the point P can be expressed as

$$\mathbf{v}_P = \begin{bmatrix} \dot{x}_P \\ \dot{y}_P \end{bmatrix} = \begin{bmatrix} -d\sin\theta \\ d\cos\theta \end{bmatrix} \dot{\theta}. \tag{150}$$

It is worth mentioning that the linear system (Equation (146)) can be redundant. Therefore, in this case, the system can be solved by a numerical method or by eliminating the system's redundant rows to determine the inverse of the Jacobian of the system.

A second method to perform the velocity analysis of a mechanism is through screw theory, which allows building the Jacobian of the system without taking derivatives. A screw in the kinematic case represents the state of the velocity of a rigid body as an angular velocity around an axis and a linear velocity on the same axis, as illustrated in Figure 36 (DAVISON; HUNT, 2004). The state of the velocity of the body j seems from the body i can be expressed in vector form as

$$\$_{ij} = \begin{bmatrix} \boldsymbol{\omega}_{ij} \\ S_0 \times \boldsymbol{\omega}_{ij} + h\boldsymbol{\omega}_{ij} \end{bmatrix} = \begin{bmatrix} \boldsymbol{\omega}_{ij} \\ \mathbf{v}_O \end{bmatrix}, \tag{151}$$

Figure 35 – The velocity of a single rotatable link.

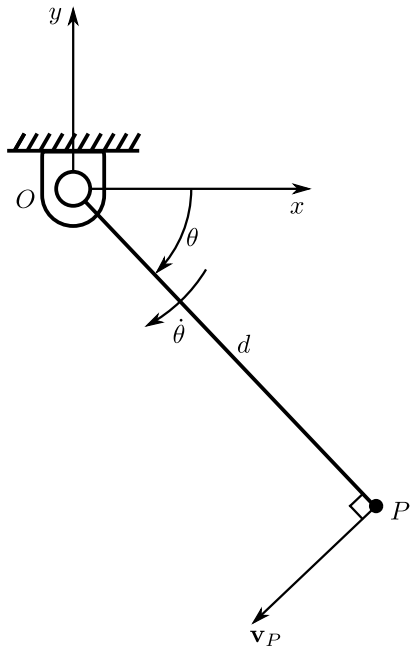

Source: The author.

where the coordinates of this vector are called Plücker coordinates of the screw (BOTTEMA; ROTH, 1990). It is also common to write Equation (151) in normalized form, which is useful in formulating the velocity constraints equations of a mechanism,

$$\$_{ij} = \hat{\$}_{ij}\omega_{ij} = \begin{bmatrix} \mathbf{s} \\ S_0 \times \mathbf{s} + h\mathbf{s} \end{bmatrix} \omega_{ij}, \tag{152}$$

where $\hat{\$}_{ij}$ is the normalized screw, $\mathbf{s}$ is a unit vector in the direction of the angular velocity $\boldsymbol{\omega}_{ij}$, ω_{ij} is the magnitude of the vector $\boldsymbol{\omega}_{ij}$ and h is the pitch of the screw.

In a serial kinematic chain, the screw of the final link n with respect to the initial link 0 can be expressed as

$$\$_{0n} = \sum_{i=0}^{n-1} \$_{i,n+1} = \hat{\$}_{01}\omega_{01} + \hat{\$}_{12}\omega_{12} + \cdots + \hat{\$}_{n-1,n}\omega_{n-1,n}. \tag{153}$$

(154)

Now let us consider the closed kinematic chain shown in Figure 37, where is verified that $\$_{0n} = \mathbf{0}$, then the equation that corresponds to the velocity analysis of a closed kinematic chain is given by

$$\$_{01} + \$_{12} + \cdots + \$_{n-2,n-1} + \$_{n-1,n} = \mathbf{0}, \tag{155}$$

which can be written in compact form as

$$\hat{\mathbf{M}}_N \boldsymbol{\varphi} = \mathbf{0}, \tag{156}$$

Figure 36 – Representation of the velocity state of a rigid body j with respect to a rigid body i through a screw.

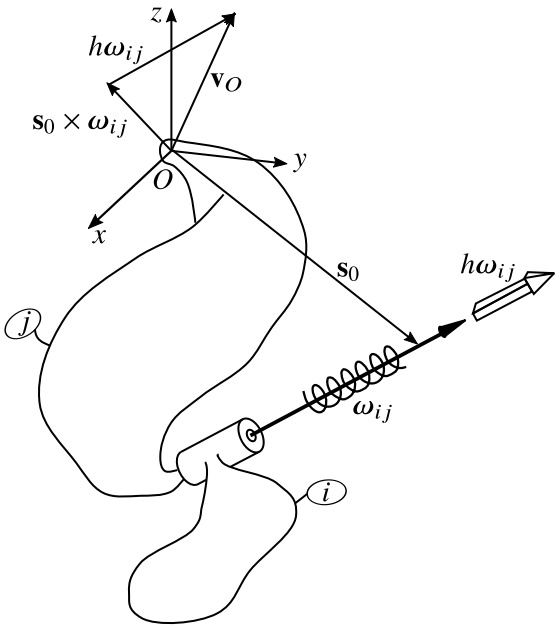

Source: The author.

where $\hat{\mathbf{M}}_N$ is the network unit motion matrix,

$$\hat{\mathbf{M}}_N = \begin{bmatrix} \hat{\$}_{0,1} & \hat{\$}_{1,2} & \cdots & \hat{\$}_{n-2,n-1} & \hat{\$}_{n-1,n}, \end{bmatrix}$$

and $\boldsymbol{\varphi}$ is the velocity vector,

$$\boldsymbol{\varphi} = \begin{bmatrix} \omega_{01} & \omega_{12} & \cdots & \omega_{n-2,n-1} & \omega_{n-1,n} \end{bmatrix}^T.$$

For mechanisms with several loops, the matrix $\hat{\mathbf{M}}_N$ is calculated systematically by the Davies method (DAVIES, 2006). For the reader who did not have been introduced with the Davies method, it is recommended to read (CAZANGI, 2008) and (ERTHAL, 2010).

To solve the velocity Equation (156) we split the vector $\boldsymbol{\varphi}$ into dependent and independent velocities. Therefore we have that

$$\left[\begin{array}{c|c} {}^d\hat{\mathbf{M}}_N & {}^i\hat{\mathbf{M}}_N \end{array} \right] \left[\begin{array}{c} {}^d\boldsymbol{\varphi} \\ \hline {}^i\boldsymbol{\varphi} \end{array} \right] = \mathbf{0}, \tag{157}$$

where ${}^d\hat{\mathbf{M}}_N$ and ${}^i\hat{\mathbf{M}}_N$ are the dependent and independent network unit motion matrix respectively.The above equation is rewritten as

$${}^d\hat{\mathbf{M}}_N {}^d\boldsymbol{\varphi} = {}^i\hat{\mathbf{M}}_N {}^i\boldsymbol{\varphi}, \tag{158}$$

that can either solve numerically or symbolically.

Figure 37 – A closed kinematic chain forms by n bodies.

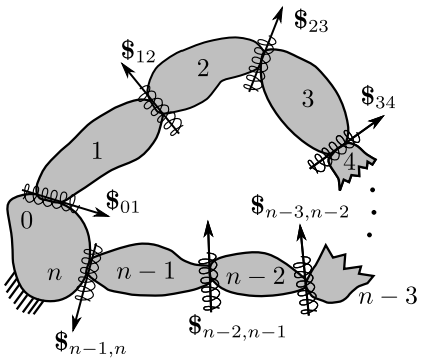

Source: The author.

4.2.1 Incorporation of natural coordinates into the screw theory

The Cartesian coordinates of a point on the axis of the screw of each kinematic pair are necessary to determine the screw's coordinates. Recalling that the natural coordinates are Cartesian points located in the kinematic pairs, it is natural to use the natural coordinates and screws together to analyze a mechanism.

To illustrate the combination of natural coordinates and screw theory, we will use the mechanism shown in Figure 38 as an example. Let us define the natural coordinates vector as follow

$$\mathbf{q} = \begin{bmatrix} x_C \\ y_C \\ x_D \\ y_D \end{bmatrix}.$$

So we can define the following vector of constraints

$$\mathbf{\Phi}(\mathbf{q}) = \begin{bmatrix} (x_D - x_C)^2 + (y_D - y_C)^2 - d_{AC}^2 \\ (x_D - x_B)^2 + (y_D - y_B)^2 - d_{BD}^2 \\ (x_C - x_A) - d_{AC}\cos\varphi \\ (y_C - y_A) - d_{AC}\sin\varphi \end{bmatrix} = \mathbf{0}. \tag{159}$$

Now of the screws of the mechanism, we have the following expression

$$\$_{01} + \$_{12} + \$_{23} + \$_{30} = \mathbf{0}, \tag{160}$$

$$\begin{bmatrix} 1 \\ y_A \\ -x_A \end{bmatrix}\omega_{01} + \begin{bmatrix} 1 \\ y_C \\ -x_C \end{bmatrix}\omega_{12} + \begin{bmatrix} 1 \\ y_D \\ -x_D \end{bmatrix}\omega_{23} + \begin{bmatrix} 1 \\ y_B \\ -x_B \end{bmatrix}\omega_{30} = \mathbf{0},$$

Figure 38 – Four-bar mechanism.

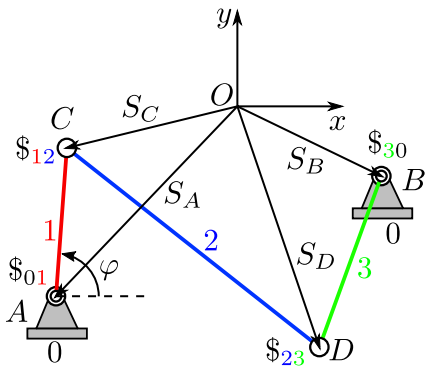

Source: The author.

$$\begin{bmatrix} 1 & 1 & 1 & 1 \\ y_A & y_C & y_D & y_B \\ -x_A & -x_C & -x_D & -x_B \end{bmatrix} \begin{bmatrix} \omega_{01} \\ \omega_{12} \\ \omega_{23} \\ \omega_{30} \end{bmatrix} = \mathbf{0},$$

therefore we can write the Equation (160) in the form

$$\hat{\mathbf{M}}_N(\mathbf{q})\boldsymbol{\varphi} = \mathbf{0} \tag{161}$$

The Equation (159) and Equation (161) can be grouped in the vector

$$\boldsymbol{\Omega}(\mathbf{q}, \boldsymbol{\varphi}) = \begin{bmatrix} \boldsymbol{\Phi}(\mathbf{q}) \\ \hat{M}_N(\mathbf{q})\boldsymbol{\varphi} \end{bmatrix} = \mathbf{0}. \tag{162}$$

And therefore, the position and velocity analysis are performed simultaneously by combining natural coordinates and screw theory, thus obtaining the advantages of both methods.

4.3 VIRTUAL DISPLACEMENTS AND VIRTUAL VELOCITY

A virtual displacement is defined as an imaginary infinitesimal change in the position of a system at a fixed time that is consistent with its boundary conditions and constraints (JALÓN; BAYO, 1994). If the position is represented by the vector $\mathbf{q}$, the vector of virtual displacements is represented by $\delta_{\mathbf{q}}$. The symbol $\delta_{\mathbf{q}}$ is called a variational operator because it represents the variation or change of a quantity. The variational operator acts like a differential operator, but with respect to the dependent variables. Therefore, the laws of variations of sum, ratios, powers, and so forth are analogous to the laws of differentiation (REDDY, 2017).

The driving and driven constraints can be combined in the vector

$$\boldsymbol{\Phi}(\mathbf{q}, t) = \mathbf{0}, \tag{163}$$

then the derivative with respect to time results in the following expression:

$$\mathbf{\Phi_q}\dot{\mathbf{q}} + \mathbf{\Phi}_t = \mathbf{0}, \tag{164}$$

and using the analogy between varational and differential operators we obtain

$$\mathbf{\Phi_q}\delta_{\mathbf{q}} = \mathbf{0}, \tag{165}$$

note that the term $\mathbf{\Phi}_t$ vanishes because the time is maintained fixed. Virtual displacements and real velocities are similar and satisfy the same equations. Then, for this reason, the easiest way to calculate virtual displacements is, frequently, to compute real velocities and, from there, to get virtual displacements applying the virtual operator where appropriate.

Consider the simple mechanism shown in Figure 39. The vector of natural coordinates is $\mathbf{q} = \begin{bmatrix} x_P & y_P & \theta \end{bmatrix}^T$, then the position is modeled by the constraints vector,

$$\mathbf{\Phi}(\mathbf{q}) = \begin{bmatrix} x_P - d\cos\theta \\ y_P - d\sin\theta \end{bmatrix} = \mathbf{0}. \tag{166}$$

From Equation (165),

$$\begin{bmatrix} 1 & 0 & d\sin\theta \\ 0 & 1 & -d\cos\theta \end{bmatrix} \begin{bmatrix} \delta_{x_p} \\ \delta_{y_p} \\ \delta_\theta \end{bmatrix} = \begin{bmatrix} 0 \\ 0 \end{bmatrix}. \tag{167}$$

Considering δ_θ as the independent virtual displacements, then the above expression is rewritten as

$$\begin{bmatrix} \delta_{x_p} \\ \delta_{y_p} \end{bmatrix} = \begin{bmatrix} -d\sin\theta \\ d\cos\theta \end{bmatrix} \delta_\theta, \tag{168}$$

note the similarity of this equation with velocity Equation (150). In mechanisms with more than one degree of freedom, it is necessary to apply as many independent virtual displacements as degrees of freedom to determine all the unknown virtual displacements.

The procedure used above to find the virtual displacements of the mechanism shown in Figure 39 can be generalized as follows: The virtual displacement vector $\delta_{\mathbf{q}}$ can be split as $\delta_{\mathbf{q}} = \begin{bmatrix} \delta_{d_{\mathbf{q}}} & \delta_{i_{\mathbf{q}}} \end{bmatrix}^T$, where $\delta_{d_{\mathbf{q}}}$ is the vector of dependent virtual displacements and $\delta_{i_{\mathbf{q}}}$ is the vector of independent virtual displacements. Hence the Equation (165) is written as

$$\left[\begin{array}{c|c} {}^d\mathbf{\Phi_q} & {}^i\mathbf{\Phi_q} \end{array}\right] \left[\begin{array}{c} \delta_{d_{\mathbf{q}}} \\ \hline \delta_{i_{\mathbf{q}}} \end{array}\right] = \mathbf{0},$$

$${}^d\mathbf{\Phi_q}\delta_{d_{\mathbf{q}}} + {}^i\mathbf{\Phi_q}\delta_{i_{\mathbf{q}}} = \mathbf{0}.$$

If ${}^d\mathbf{\Phi_q}$ is nonsingular then, we have that

$$\delta_{d_{\mathbf{q}}} = -{}^d\mathbf{\Phi}_q^{-1\,i}\mathbf{\Phi_q}\delta_{i_{\mathbf{q}}}. \tag{169}$$

Figure 39 – Virtual displacements of a single rotatable link.

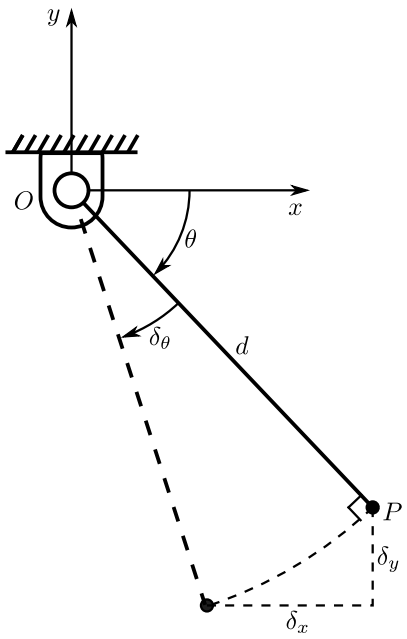

Source: The author.

Therefore, one can write the vector $\delta_{\mathbf{q}}$ as

$$\delta_{\mathbf{q}} = \begin{bmatrix} -{}^{d}\mathbf{\Phi}_{q}^{-1\,i}\mathbf{\Phi}_{\mathbf{q}} \\ \mathbf{I} \end{bmatrix} \delta_{i}\mathbf{q}, \tag{170}$$

where $\mathbf{I}$ is an identity matrix, with dimension $n_v - n_c$.

Instead of talking about virtual displacements, we can also talk about virtual velocities obtained by dividing the virtual displacement by the virtual time. It can be thought that virtual time is a temporal magnitude whose law of variation is completely independent of real time, to which the rest of the mechanical laws are subjected. Contrary to virtual displacements, virtual velocities do not have to be infinitesimal, and like virtual displacements, virtual velocities and real velocities are similar and satisfy the same equations (AVELLO, 2014; JALÓN; BAYO, 1994).

The virtual velocity vector is denoted as $\dot{\mathbf{q}}^{*}$ and must satisfy the constraint equation:

$$\mathbf{\Phi}_{\mathbf{q}}\dot{\mathbf{q}}^{*} = \mathbf{0}, \tag{171}$$

and similarly to the Equation (170) we have that,

$$\dot{\mathbf{q}}^{*} = \begin{bmatrix} -{}^{d}\mathbf{\Phi}_{q}^{-1\,i}\mathbf{\Phi}_{\mathbf{q}} \\ \mathbf{I} \end{bmatrix} {}^{i}\dot{\mathbf{q}}^{*}, \tag{172}$$

where ${}^{i}\dot{\mathbf{q}}^{*}$ is the vector of independent virtual velocities.

Figure 40 – Virtual velocity screw representation.

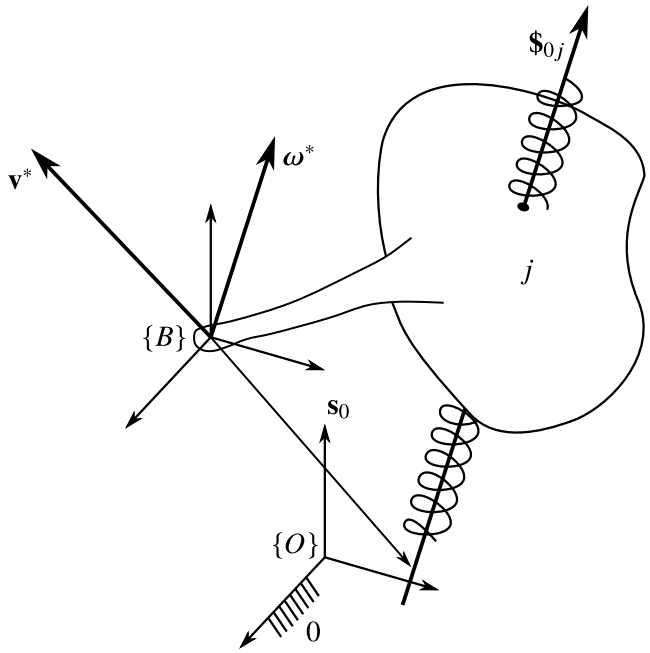

Source: The author.

The virtual velocities associated with the particles of a rigid body satisfy the expression

$$\mathbf{v}_B^* = \mathbf{v}_A^* + \boldsymbol{\omega}^* \times \mathbf{r}_{AB}, \tag{173}$$

where $\boldsymbol{\omega}^*$ is the virtual angular velocity of the rigid body (FOIX, 2000). Let us now consider the body j belonging to the generic mechanism shown in Figure 40. Suppose that the virtual velocity of the body j is defined by the screw $\$_{0j}$,

$$\$_{0j} = \begin{bmatrix} \boldsymbol{\omega}^* \\ S_0 \times \boldsymbol{\omega}^* + h\boldsymbol{\omega}^* \end{bmatrix} = \begin{bmatrix} \boldsymbol{\omega}^* \\ \mathbf{v}^* \end{bmatrix}, \tag{174}$$

then $\mathbf{v}^* = S_0 \times \boldsymbol{\omega}^* + h\boldsymbol{\omega}^*$, where $\mathbf{v}_0^* = h\boldsymbol{\omega}^*$, thus

$$\mathbf{v}^* = \mathbf{v}_0^* + S_0 \times \boldsymbol{\omega}^*. \tag{175}$$

Note that Equation (173) and Equation (175) are equivalent, therefore the screw $\$_{0j}$ really describes the virtual velocity of the rigid body j.

4.4 ACCELERATION ANALYSIS

Our objective in the acceleration problem is to determine the acceleration $\ddot{\mathbf{q}}$ for all the mechanisms variables. We achieve this by utilizing the position $\mathbf{q}$, velocity $\dot{\mathbf{q}}$ and degrees of

freedom accelerations. The desired result can be obtained by deriving the Equation (144) of velocities with respect to time.

$$\mathbf{\Phi_q}\ddot{\mathbf{q}} + \dot{\mathbf{\Phi}}_\mathbf{q}\dot{\mathbf{q}} = \mathbf{0}. \tag{176}$$

Equation (176) can be divided into dependent and independent variables. Then the above equation can be written as follows

$$\left[\begin{array}{c|c} {}^d\mathbf{\Phi_q} & {}^i\mathbf{\Phi_q} \end{array}\right] \left[\begin{array}{c} {}^d\ddot{\mathbf{q}} \\ \hline {}^i\ddot{\mathbf{q}} \end{array}\right] + \dot{\mathbf{\Phi}}_\mathbf{q}\dot{\mathbf{q}} = \mathbf{0}. \tag{177}$$

Rearranging the terms, one can write

$${}^d\mathbf{\Phi_q}\,{}^d\ddot{\mathbf{q}} = -\dot{\mathbf{\Phi}}_\mathbf{q}\dot{\mathbf{q}} - {}^i\mathbf{\Phi_q}\,{}^i\ddot{\mathbf{q}}. \tag{178}$$

Through this method, we can directly know the linear accelerations of some points. If we need to know the angular accelerations of the links, post-processing is necessary. In the following section, we propose a procedure to directly determine the angular accelerations of the links.

4.4.1 Acceleration analysis through the combination of natural coordinates and screw theory

Combining natural coordinates and screw theory can solve the acceleration problem. While the approach described below involves calculating derivatives, this task is simplified because natural coordinates are used. However, solving the acceleration problem through an entirely geometric approach will require additional research and will be explored in upcoming work.

The derivation of the Equation (161) respect to time produces

$$\begin{aligned} \frac{d}{dt}\left(\hat{\mathbf{M}}_N\boldsymbol{\varphi}\right) &= \mathbf{0}, \\ \frac{\partial}{\partial\mathbf{q}}\left(\hat{\mathbf{M}}_N\boldsymbol{\varphi}\right)\dot{\mathbf{q}} + \frac{\partial}{\partial\boldsymbol{\varphi}}\left(\hat{\mathbf{M}}_N\boldsymbol{\varphi}\right)\dot{\boldsymbol{\varphi}} &= \mathbf{0}, \\ \left(\hat{\mathbf{M}}_N\boldsymbol{\varphi}\right)_\mathbf{q}\dot{\mathbf{q}} + \hat{\mathbf{M}}_N\boldsymbol{\alpha} &= \mathbf{0}, \end{aligned} \tag{179}$$

where $\boldsymbol{\alpha} = \dot{\boldsymbol{\varphi}}$ is the acceleration vector. Let us rewrite Equation (179) as follows:

$$\begin{aligned} \left[\begin{array}{cc} {}^d\left(\hat{\mathbf{M}}_N\boldsymbol{\varphi}\right)_\mathbf{q} & {}^i\left(\hat{\mathbf{M}}_N\boldsymbol{\varphi}\right)_\mathbf{q} \end{array}\right] \left[\begin{array}{c} {}^d\dot{\mathbf{q}} \\ {}^i\dot{\mathbf{q}} \end{array}\right] + \left[\begin{array}{cc} {}^d\hat{\mathbf{M}}_N & {}^i\hat{\mathbf{M}}_N \end{array}\right] \left[\begin{array}{c} {}^d\boldsymbol{\alpha} \\ {}^i\boldsymbol{\alpha} \end{array}\right] &= \mathbf{0}, \\ {}^d\left(\hat{\mathbf{M}}_N\boldsymbol{\varphi}\right)_\mathbf{q}\,{}^d\dot{\mathbf{q}} + {}^i\left(\hat{\mathbf{M}}_N\boldsymbol{\varphi}\right)_\mathbf{q}\,{}^i\dot{\mathbf{q}} + {}^d\hat{\mathbf{M}}_N\,{}^d\boldsymbol{\alpha} + {}^i\hat{\mathbf{M}}_N\,{}^i\boldsymbol{\alpha} &= \mathbf{0}, \\ {}^d\hat{\mathbf{M}}_N\,{}^d\boldsymbol{\alpha} = -{}^d\left(\hat{\mathbf{M}}_N\boldsymbol{\varphi}\right)_\mathbf{q}\,{}^d\dot{\mathbf{q}} - {}^i\left(\hat{\mathbf{M}}_N\boldsymbol{\varphi}\right)_\mathbf{q}\,{}^i\dot{\mathbf{q}} - {}^i\hat{\mathbf{M}}_N\,{}^i\boldsymbol{\alpha}. \end{aligned} \tag{180}$$

Finally from Equation (180) the dependent acceleration vector can be isolated, resulting in the equation:

$$ {}^{d}\boldsymbol{\alpha} = {}^{d}\hat{\mathbf{M}}_N^{-1}\left[{}^{d}\left(\hat{\mathbf{M}}_N\boldsymbol{\varphi}\right)_{\mathbf{q}}\,{}^{d}\boldsymbol{\Phi}_{\mathbf{q}}^{-1}\boldsymbol{\Phi}_{\mathbf{q}} - {}^{i}\left(\hat{\mathbf{M}}_N\boldsymbol{\varphi}\right)_{\mathbf{q}}\right]{}^{i}\dot{\mathbf{q}} - {}^{d}\hat{\mathbf{M}}_N^{-1}{}^{i}\hat{\mathbf{M}}_N{}^{i}\boldsymbol{\alpha}. \tag{181} $$

4.4.1.1 Acceleration analysis of a four-bar mechanism

To illustrate the procedure developed to perform the acceleration analysis using the Davies' method, the analysis of the four-bar mechanism shown in Figure 41 is performed.

Figure 41 – Acceleration analysis of a four-bar mechanism.

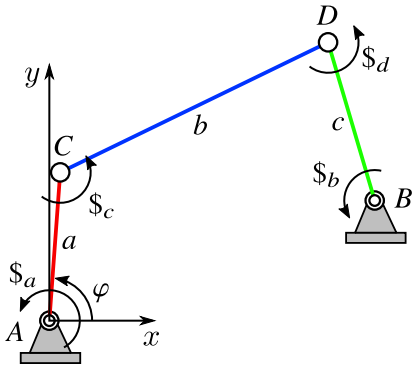

Source: The author.

The vector of constraints of the four-bar mechanism is,

$$ \boldsymbol{\Phi}(\mathbf{q}) = \begin{bmatrix} (x_D - x_C)^2 + (y_D - y_C)^2 - b^2 \\ (x_D - x_B)^2 + (y_D - y_B)^2 - c^2 \\ (x_C - x_A) - a\cos\varphi \\ (y_C - y_A) - a\sin\varphi \end{bmatrix} = \mathbf{0}, \tag{182} $$

where $\mathbf{q} = \begin{bmatrix} x_C & y_C & x_D & y_D & \varphi \end{bmatrix}^T$. From Equation (146) we have that,

$$ \begin{bmatrix} -2(x_D - x_C) & -2(y_D - y_C) & 2(x_D - x_C) & 2(y_D - y_C) \\ 0 & 0 & 2(x_D - x_B) & 2(y_D - y_B) \\ 1 & 0 & 0 & 0 \\ 0 & 1 & 0 & 0 \end{bmatrix} \dot{\mathbf{q}} = \begin{bmatrix} 0 \\ -a\sin\varphi \\ a\cos\varphi \end{bmatrix} \omega_a. \tag{183} $$

Where ω_a is the input velocity, and $\dot{\mathbf{q}} = \begin{bmatrix} \dot{x_C} & \dot{y_C} & \dot{x_D} & \dot{y_D} \end{bmatrix}^T$ is the velocity vector of the dependent natural coordinates.

From the application of the Davies' method we have

$$ \hat{\mathbf{M}}_N = \begin{bmatrix} \hat{\$}_a & \hat{\$}_c & \hat{\$}_d & -\hat{\$}_b \end{bmatrix} \tag{184} $$

$$= \begin{bmatrix} 1 & 1 & 1 & -1 \\ 0 & y_C & y_D & -y_B \\ 0 & -x_C & -x_D & x_B \end{bmatrix}; \tag{185}$$

therefore

$$\begin{bmatrix} 1 & 1 & -1 \\ y_C & y_D & -y_B \\ -x_C & -x_D & x_B \end{bmatrix} \boldsymbol{\varphi} = - \begin{bmatrix} 1 \\ 0 \\ 0 \end{bmatrix} \omega_a, \tag{186}$$

where $\boldsymbol{\varphi} = \begin{bmatrix} \omega_c & \omega_d & \omega_b \end{bmatrix}^T$. Now using the Equation (181) we obtain:

$$\begin{bmatrix} 1 & 1 & -1 \\ y_C & y_D & -y_B \\ -x_C & -x_D & x_B \end{bmatrix} \boldsymbol{\alpha} = - \begin{bmatrix} 0 & 0 & 0 & 0 \\ 0 & \omega_c & 0 & \omega_d \\ -\omega_c & 0 & -\omega_d & 0 \end{bmatrix} \dot{\mathbf{q}} - \begin{bmatrix} 1 \\ 0 \\ 0 \end{bmatrix} \alpha_a, \tag{187}$$

where α_a is the input acceleration and $\boldsymbol{\alpha} = \begin{bmatrix} \alpha_c & \alpha_d & \alpha_b \end{bmatrix}^T$. Let us suppose that $x_A = 0$ [m], $y_A = 0$ [m], $x_B = 4$ [m], $y_B = 0$ [m], $a = 1$ [m], $b = 5$ [m], $c = 4$ [m], $\omega_a = 1$ [rad/s], $\alpha_a = 0$ rad/s^2.

Figure 42 compares the results between the proposed method and the GIM mechanism analysis program (PETUYA et al., 2014). Here, an exact match between the angular accelerations is evidenced. Although the example shown here is for illustrative purposes, the method can be applied to any planar or spatial mechanism.

Figure 42 – Relative angular accelerations.

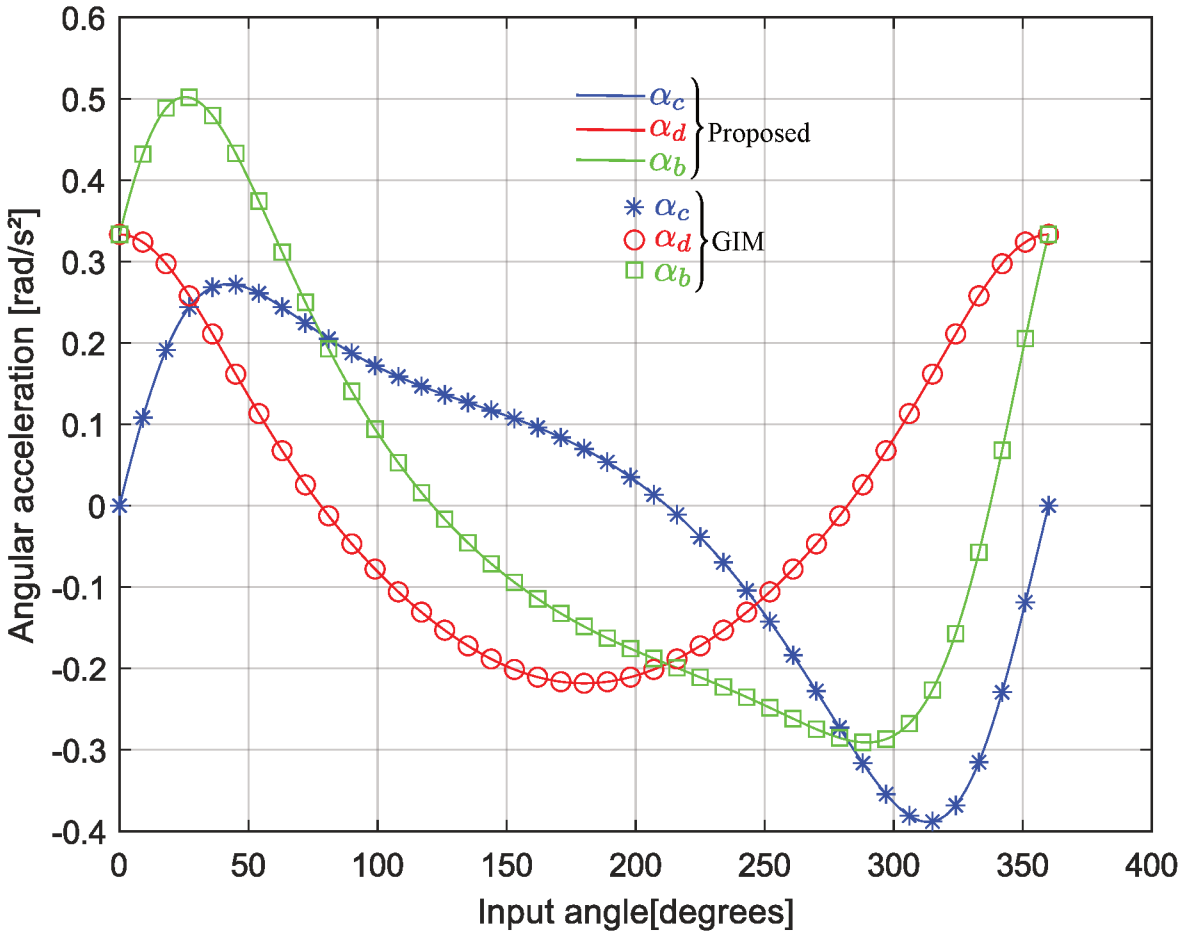

Source: The author.

5 SCREW THEORY-BASED STATIC BALANCING METHOD

This section shows a method for optimal static balancing of mechanisms. This approach is based on the minimization of the actuation forces necessary to keep the mechanism in equilibrium. These actuation forces are systematically computed using Davies' method (DAVIES, 2006). The objective function is formulated in a quadratic form, allowing an analytical approach to the sensitivities analysis, increasing the precision and efficiency of the optimization.

5.1 POSITION KINEMATIC ANALYSIS

Since a mechanism is composed of links interconnected by kinematic pairs, it is necessary to choose how to mathematically describe the relationship between the links before considering the optimal synthesis. This mathematical description constitutes the base of the optimal synthesis modeling. To model a mechanism, we need description variables to know the position of all the links. All these positions at a given moment constitute a linkage configuration. Description variables, also called generalized coordinates, can be independent or dependent. In fact, since bodies are interconnected by joints, their movements are not completely free and generate constraints between some generalized coordinates. Therefore kinematic modeling is crucial for the behavior of the optimal synthesis process. During the optimization, the model will be evaluated with various values of the dimensions (angles or lengths), leading to various configurations of the mechanism. For closed-loop linkages, these evaluations also involve the assembly of the mechanism and singularity problems.

Three types of generalized coordinates are generally used to describe the position kinematics of a mechanism as illustrated in Figure 43: reference point coordinates Figure 43(a), natural coordinates Figure 43(b) and relative coordinates Figure 43(c).

Figure 43 – Four-bar linkage modeled using three types of coordinates.

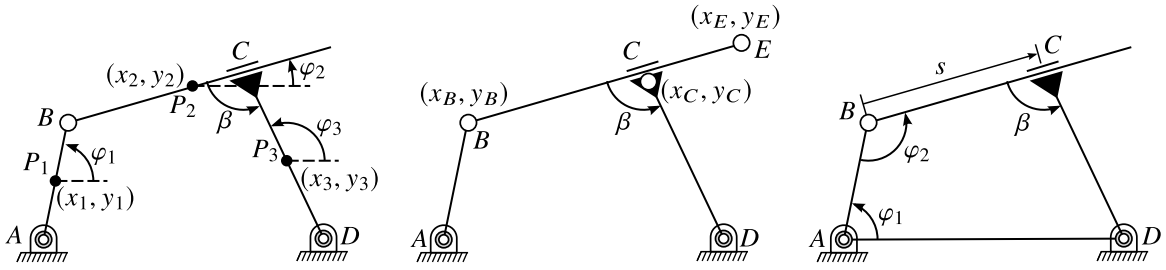

(a) Reference point coordinates (b) Natural coordinates (c) Relative coordinates

Source: The author.

Regardless of the type of generalized coordinates used to describe the mechanism, the position kinematics can be represented by a set of constraint equations:

$$\mathbf{\Phi}(\mathbf{q}) = \mathbf{0}, \tag{188}$$

where $\mathbf{\Phi}$ is the constraints vector and $\mathbf{q}$ is the generalized coordinates vector. Figure 44 shows a classification of the methods for solving the kinematic position problem, which is not intended to be an exhaustive classification but rather one that shows robust and simple to implement methods known to the authors.

Figure 44 – Classification of position analysis methods.

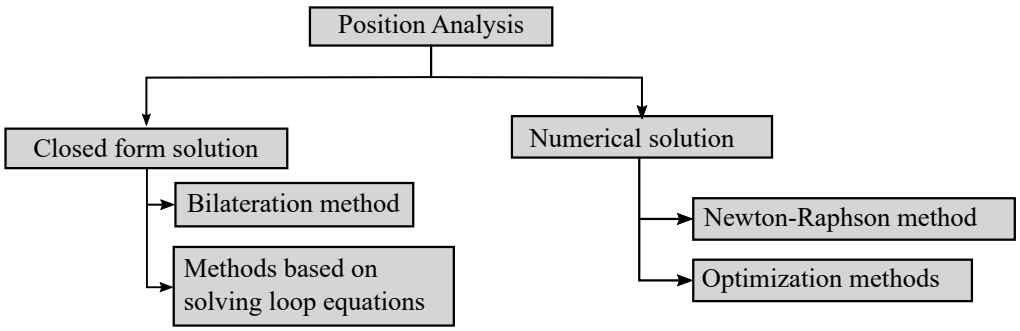

Source: The author.

Within the closed-form solution methods, we will focus on the bilateration method (ROJAS, NICOLAS, 2012), which allows modeling the position kinematics of planar mechanisms elegantly and compactly. Any point of interest of the mechanism will be determined by:

$$\begin{aligned} \mathbf{p}_l &= \mathbf{p}_k + \mathbf{\Omega}\mathbf{p}_{ij} \\ &= \mathbf{p}_k + \mathbf{\Omega}(\mathbf{p}_j - \mathbf{p}_i) \end{aligned}, \tag{189}$$

where: $\mathbf{p}_i$, $\mathbf{p}_j$ and $\mathbf{p}_k$ are known points, $\mathbf{p}_l$ is unknown point and $\mathbf{\Omega}$ is a bilateration matrix that depends only on distances. As shown, the kinematic position analysis using bilateration is quite simplified, see for instance (ROJAS; THOMAS, 2012; NANSAI; ELARA; IWASE, 2016).

The most direct way to obtain a numerical solution is through the Newton-Raphson method:

$$\mathbf{\Phi}_\mathbf{q}(\mathbf{q}_i)(\mathbf{q}_{i+1} - \mathbf{q}_i) = -\mathbf{\Phi}(\mathbf{q}_i), \tag{190}$$

where $\mathbf{\Phi}_\mathbf{q}$ is the Jacobian matrix of the constraint equations with respect to the generalized coordinates $\mathbf{q}$. This method is simple to implement, but has the following drawbacks: If the starting point solution is singular then the first iteration step cannot be performed because the Jacobian is not invertible. For a particular configuration, the starting point must be close enough to this configuration so as not to have problems of chaotic changing between different configurations, in the case that the assembly is not physically possible, the Newton-Raphson method will diverge, and it will not contain an efficient error measure to penalize the objective function in the optimal synthesis.

The above drawbacks can be solved if the position problem is solved by some suitable optimization method as shown in (JEAN-FRANÇOIS COLLARD, 2007). If an optimization method based on Newton's method is used then the computational cost is not a problem since, in

general, whether the starting point is sufficiently close to the minimum, the method will converge quadratically towards the solution (FRANDSEN; JONASSON, 2004).

5.1.1 Natural coordinates

Natural coordinates were originally introduced by García De Jalón and collaborators (JALÓN; BAYO, 1994), In planar mechanisms natural coordinates are mostly Cartesian coordinates located at kinematic pairs or points of interest. The main advantages of natural coordinates are: simplicity and intuitive physical interpretation, the position and orientation of each element are defined directly, and trigonometric functions do not appear in the constraint equations. Moreover, natural coordinates are particularly well adapted to sensitivity analysis and optimization (JEAN-FRANÇOIS COLLARD, 2007; ANA MAGDALENA DE JUAN DE LUNA, 2011; AVELLO, 2014).

Given the advantages of the natural coordinates mentioned above, they are chosen for the description mechanism in this work. Another advantage of this choice is that this type of coordinates can naturally be integrated into the screw theory, as will be shown in Section 5.2.

5.2 STATIC ANALYSIS

In this work, we adopt Davies' method for static analysis that uses graph theory to model the topology and screw theory to represent the physical behavior of the mechanisms. This method allows systematically obtaining the equations of statics regardless complexity of the mechanism. For more details of this method, we suggest the reader see (DAVIES, 1981, 2006; CAZANGI, 2008; MEJIA; SIMAS; MARTINS, 2016; LAUS; SIMAS; MARTINS, 2020).

5.2.1 Integration of natural coordinates in screw theory

Applying the Davies' method (DAVIES, 2006) to solve the static of a mechanism produces a system of equations written in a compact form as:

$$\hat{\mathbf{A}}_N \boldsymbol{\Psi} = \mathbf{0}\,, \tag{191}$$

where $\hat{\mathbf{A}}_N$ is the network unit action matrix of a coupling network and $\boldsymbol{\Psi}$ is the vector of magnitudes of action screws. The matrix $\hat{\mathbf{A}}_N$ is assembled from the unit action matrix $\hat{\mathbf{A}}_D$ as

$$\hat{\mathbf{A}}_N = \begin{bmatrix} \hat{\mathbf{A}}_D\mathbf{Q}_1 \\ \hat{\mathbf{A}}_D\mathbf{Q}_2 \\ \vdots \\ \hat{\mathbf{A}}_D\mathbf{Q}_k \end{bmatrix}, \tag{192}$$

where $\mathbf{Q}_i = \text{diag}([\mathbf{Q}_A]_i)$, $i = 1, 2, \cdots, k$ are diagonal matrices whose diagonal elements correspond to row i of cutset matrix $\mathbf{Q}_A$, derived from action graph G_A. A cut is equivalent to

disassembling parts of the mechanism as in the well known free body diagram. Unlike fundamental cuts, free-body diagrams can generate dependent equations in statics, which makes it necessary to change the free-body diagrams.

The unit action matrix is composed by one unit action screw for column:

$$\hat{\mathbf{A}}_D = \begin{bmatrix} \hat{\$}_a & \hat{\$}_b & \cdots & \hat{\$}_j & \cdots & \hat{\$}_C \end{bmatrix}, \tag{193}$$

where C is the gross degree of constraint, so that the j-th unit action screw $\hat{\$}_j$ is written in Plücker coordinates in ray formation (BOTTEMA; ROTH, 1990) as

$$\hat{\$}_j = \begin{bmatrix} \mathbf{s}_0 \times \mathbf{s} + h\mathbf{s} \\ \mathbf{s} \end{bmatrix}, \tag{194}$$

where $\mathbf{s}_0$ is a point on the axis of the action screw, $\mathbf{s}$ is a unit vector in the direction of the action screw and h is the pitch of the screw. Note that $\mathbf{s}_0$ corresponds to the Cartesian coordinates of a point on the axis of the action screw, therefore naturally $\mathbf{s}_0$ can be written as a function of the natural coordinate vector of the mechanism, that is $\mathbf{s}_0 = \mathbf{s}_0(\mathbf{q})$, in the same way, the unit vector $\mathbf{s}$ can also be written as a function of the vector $\mathbf{q}$ i.e, $\mathbf{s} = \mathbf{s}(\mathbf{q})$. Therefore, Equation (191) can be rewritten in the form

$$\hat{\mathbf{A}}_N(\mathbf{q})\boldsymbol{\Psi} = \mathbf{0}\,, \tag{195}$$

thus this expression combines natural coordinates and screw theory, thereby obtaining the advantages of both mathematical tools.

Let us split the vector $\boldsymbol{\Psi}$ into three vectors as follows: the vector of the internal forces acting in each kinematic pair ${}^{i}\boldsymbol{\Psi}$, the vector of the forces supply by each actuator ${}^{a}\boldsymbol{\Psi}$ and the vector of external forces ${}^{e}\boldsymbol{\Psi}$. Thus, Equation (195) is written as:

$$\begin{bmatrix} {}^{i}\hat{\mathbf{A}}_N(\mathbf{q}) & {}^{a}\hat{\mathbf{A}}_N(\mathbf{q}) & {}^{e}\hat{\mathbf{A}}_N(\mathbf{q}) \end{bmatrix} \begin{bmatrix} {}^{i}\boldsymbol{\Psi} \\ {}^{a}\boldsymbol{\Psi} \\ {}^{e}\boldsymbol{\Psi} \end{bmatrix} = \mathbf{0}\,, \tag{196}$$

where ${}^{i}\hat{\mathbf{A}}_N(\mathbf{q})$ is the network unit internal action matrix, ${}^{a}\hat{\mathbf{A}}_N(\mathbf{q})$ is the network unit actuator action matrix and ${}^{e}\hat{\mathbf{A}}_N$ is the network unit external action matrix. Rearranged the Equation (196) we can determine the internal forces and loads supplied by the actuators:

$${}^{r}\hat{\mathbf{A}}_N(\mathbf{q}){}^{r}\boldsymbol{\Psi} = -{}^{e}\hat{\mathbf{A}}_N(\mathbf{q}){}^{e}\boldsymbol{\Psi}\,, \tag{197}$$

where ${}^{r}\hat{\mathbf{A}}_N(\mathbf{q}) = \begin{bmatrix} {}^{i}\hat{\mathbf{A}}_N(\mathbf{q}) & {}^{a}\hat{\mathbf{A}}_N(\mathbf{q}) \end{bmatrix}$ is the resultant network unit action matrix and ${}^{r}\boldsymbol{\Psi} = \begin{bmatrix} {}^{i}\boldsymbol{\Psi}^T & {}^{a}\boldsymbol{\Psi}^T \end{bmatrix}^T$ is the resultant forces vector. Let us use a simple illustrative example which consists of a rotating bar with a constant force on one extreme, as shown in the Figure 45. Where, f_{ox}, f_{oy}, and τ are internal forces in joint o, and actuation torque, respectively Figure 45(a). Bar 1 can be modeled by the natural coordinates vector $\mathbf{q} = \begin{bmatrix} x & y \end{bmatrix}^T$ that corresponds to the

Cartesian coordinates of point P. Then, the unit action screws for f_{ox}, f_{oy}, τ, and $\mathbf{F}$ according Equation (194) are:

$$\hat{\$}_{ox}(\mathbf{q}) = \begin{bmatrix} 0 \\ 1 \\ 0 \end{bmatrix}, \quad \hat{\$}_{oy}(\mathbf{q}) = \begin{bmatrix} 0 \\ 0 \\ 1 \end{bmatrix}, \quad \hat{\$}_{\tau}(\mathbf{q}) = \begin{bmatrix} 1 \\ 0 \\ 0 \end{bmatrix}, \quad \hat{\$}_{p}(\mathbf{q}) = \begin{bmatrix} -x \\ 0 \\ -1 \end{bmatrix},$$

respectively. This simple case has only one cut, as shown in the actions and fundamental cutsets graph Figure 45(b), then the cutset matrix is $\mathbf{Q}_A = \begin{bmatrix} 1 & 1 & 1 & 1 \end{bmatrix}$. Applying Equation (192), yields

$$\hat{\mathbf{A}}_D(\mathbf{q}) = \begin{bmatrix} \hat{\$}_{ox}(\mathbf{q}) & \hat{\$}_{oy}(\mathbf{q}) & \hat{\$}_{\tau}(\mathbf{q}) & \hat{\$}_{p}(\mathbf{q}) \end{bmatrix},$$

and replacing the above equation in Equation (196) and rearranging according Equation (197) is obtained

Figure 45 – Illustrative example of static analysis: (a) actions and (b) cutset graph.

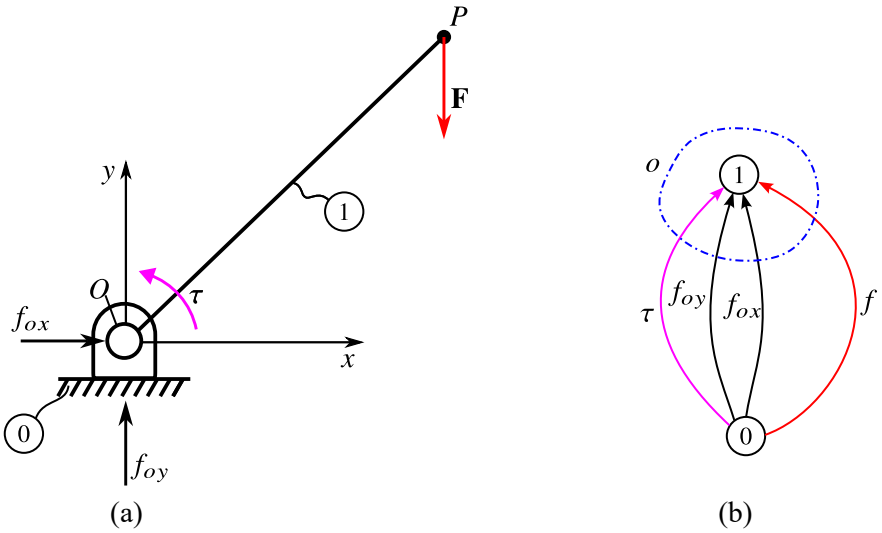

Source: The author.

$$\begin{bmatrix} \hat{\$}_{ox}(\mathbf{q}) & \hat{\$}_{oy}(\mathbf{q}) & \hat{\$}_{\tau}(\mathbf{q}) \end{bmatrix} \begin{bmatrix} f_{ox} \\ f_{oy} \\ \tau \end{bmatrix} = -\hat{\$}_{p}(\mathbf{q}) f \ .$$

Solving the previous equation, we obtain that $f_{ox} = 0$, $f_{oy} = f$, and $\tau = xf$.

This illustrative example shows the static analysis through integrating the natural coordinates in Davies' method, which produces simple equations and therefore facilitates the computation of derivatives in the optimization process.

5.2.2 Formulating the optimization problem

A mechanism is perfectly balanced if the weight of the links does not produce any torque or force on the actuators under static conditions for any configuration. (MOORE, 2009). The aim of this work is the approximate static balancing; hence our objective is to reduce the actuation forces, that is, minimize the sum of squares of the actuation forces:

$$f(\mathbf{z}) = \frac{1}{2}\sum_{j=1}^{n} {}^{a}\boldsymbol{\Psi}_j^T {}^{a}\boldsymbol{\Psi}_j, \tag{198}$$

where $\mathbf{z}$ is the design variables vector and n is the number of discretized configurations.

To avoid the magnitude of the objective function being influenced by the number of discretized configurations, one can replace the factor $\frac{1}{2}$ with $\frac{1}{n}$. However, all the subsequent development has been done for $\frac{1}{2}$ since this scaling factor affects only the value of the objective function but not the optimization result.

The optimization method used in this work is based on the analytical or approximate computing of the gradient of the objective function. For this reason, the objective function has been defined in quadratic form, since it satisfies the essential requirement of being differentiable. Various authors using a similar function can be found in the literature (ANGELES; BERNIER, 1987; COLLARD; DUYSINX; FISETTE, 2010; DE-JUAN; SANCIBRIAN; VIADERO, 2012).

Let $\underline{\mathbf{z}}$ and $\bar{\mathbf{z}}$ be lower and upper bounds of design variables respectively, let $\mathbf{g}(\mathbf{q},\mathbf{z}) \leq \mathbf{0}$ and $\mathbf{h}(\mathbf{q},\mathbf{z}) = \mathbf{0}$ be inequality and equality constraints vectors of the design variables and natural coordinates. Then, taking into account that in order to evaluate the objective function, the position problem and the equations of the statics must be solved, the optimization problem is written mathematically as:

$$\begin{aligned}
&\underset{\mathbf{z}}{\text{minimize}} \quad f(\mathbf{z}) = \frac{1}{2}\sum_{j=1}^{n} {}^{a}\boldsymbol{\Psi}_j^T {}^{a}\boldsymbol{\Psi}_j, \\
&\text{subject to} \quad \begin{cases} \mathbf{g}(\mathbf{q},\mathbf{z}) \leq \mathbf{0}, \\ \mathbf{h}(\mathbf{q},\mathbf{z}) = \mathbf{0}, \\ \underline{\mathbf{z}} \leq \mathbf{z} \leq \bar{\mathbf{z}}, \end{cases} \\
&\text{while solving} \quad \begin{cases} \boldsymbol{\Phi}(\mathbf{q},\mathbf{z}) = \mathbf{0}, \\ {}^{r}\hat{\mathbf{A}}_N(\mathbf{q},\mathbf{z}) {}^{r}\boldsymbol{\Psi}_j = -{}^{e}\hat{\mathbf{A}}_N(\mathbf{q},\mathbf{z}) {}^{e}\boldsymbol{\Psi}_j, \quad \text{where} \quad {}^{r}\boldsymbol{\Psi}_i = \begin{bmatrix} {}^{i}\boldsymbol{\Psi}_j \\ {}^{a}\boldsymbol{\Psi}_j \end{bmatrix}. \end{cases}
\end{aligned} \tag{199}$$

To evaluate the objective function, first, the position problem is solved for each configuration, then the static problem is solved, and finally, the objective function and constraints are evaluated. In practice, this procedure is done within a cycle, and the values are accumulated to obtain the total value of the objective function.

5.2.3 Analytical sensitivity analysis

Before using gradient-based optimization techniques, it is necessary to carry out a sensitivity analysis of the objective function. So, we derive Equation (198) with respect to the vector of design variables $\mathbf{z}$.

$$\frac{df}{d\mathbf{z}} = \sum_{j=1}^{n} {}^{a}\boldsymbol{\Psi}_j^T \left(\frac{\partial^a \boldsymbol{\Psi}_j}{\partial \mathbf{z}} + \frac{\partial^a \boldsymbol{\Psi}_j}{\partial \mathbf{q}} \frac{\partial \mathbf{q}}{\partial \mathbf{z}} \right), \tag{200}$$

and taking into account that the numerator layout is used here, the gradient of the objective function is $\nabla f = \left(\frac{df}{d\mathbf{z}}\right)^T$. Now to determine the change of the natural coordinates with respect to the design variables $\frac{\partial \mathbf{q}}{\partial \mathbf{z}}$, Equation (188) is derived with respect to the vector $\mathbf{z}$

$$\frac{\partial \boldsymbol{\Phi}}{\partial \mathbf{z}} + \boldsymbol{\Phi}_{\mathbf{q}} \frac{\partial \mathbf{q}}{\partial \mathbf{z}} = \mathbf{0}, \tag{201}$$

where $\boldsymbol{\Phi}_{\mathbf{q}}$ represents the Jacobian matrix of the constraint equations with respect to the natural coordinates. Rewriting the Equation (201) results the following linear system

$$\boldsymbol{\Phi}_{\mathbf{q}} \frac{\partial \mathbf{q}}{\partial \mathbf{z}} = -\frac{\partial \boldsymbol{\Phi}}{\partial \mathbf{z}}. \tag{202}$$

To compute $\frac{\partial^a \boldsymbol{\Psi}_j}{\partial \mathbf{z}}$ is derived Equation (197) with respect to $\mathbf{z} \in \mathbb{R}^m$. Here it is used the definition of matrix derivatives as in (VAN KHANG, 2010),

$${}^{r}\hat{\mathbf{A}}_N \frac{\partial^r \boldsymbol{\Psi}_j}{\partial \mathbf{z}} + \frac{\partial^r \hat{\mathbf{A}}_N}{\partial \mathbf{z}} ({}^{r}\boldsymbol{\Psi}_j \otimes \mathbf{I}_m) = -{}^{e}\hat{\mathbf{A}}_N \frac{\partial^e \boldsymbol{\Psi}_j}{\partial \mathbf{z}} - \frac{\partial^e \hat{\mathbf{A}}_N}{\partial \mathbf{z}} ({}^{e}\boldsymbol{\Psi}_j \otimes \mathbf{I}_m), \tag{203}$$

where $\mathbf{I}_m$ is a $m \times m$ identity matrix and $\otimes$ is the Kronecker product. Rearranging the Equation (203), yields

$${}^{r}\hat{\mathbf{A}}_N \frac{\partial^r \boldsymbol{\Psi}_j}{\partial \mathbf{z}} = -\left[{}^{e}\hat{\mathbf{A}}_N \frac{\partial^e \boldsymbol{\Psi}_j}{\partial \mathbf{z}} + \frac{\partial^e \hat{\mathbf{A}}_N}{\partial \mathbf{z}} ({}^{e}\boldsymbol{\Psi}_j \otimes \mathbf{I}_m) + \frac{\partial^r \hat{\mathbf{A}}_N}{\partial \mathbf{z}} ({}^{r}\boldsymbol{\Psi}_j \otimes \mathbf{I}_m) \right], \tag{204}$$

allows us to determine $\frac{\partial^a \boldsymbol{\Psi}_i}{\partial \mathbf{z}}$ by solving Equation (204), since that

$$\frac{\partial^r \boldsymbol{\Psi}_i}{\partial \mathbf{z}} = \begin{bmatrix} \frac{\partial^i \boldsymbol{\Psi}_j}{\partial \mathbf{z}} \\ \frac{\partial^a \boldsymbol{\Psi}_j}{\partial \mathbf{z}} \end{bmatrix}. \tag{205}$$

Now, deriving Equation (197) with respect to $\mathbf{q} \in \mathbb{R}^p$ and rearranging it, yields

$${}^{r}\hat{\mathbf{A}}_N \frac{\partial^r \boldsymbol{\Psi}_j}{\partial \mathbf{q}} = -\left[{}^{e}\hat{\mathbf{A}}_N \frac{\partial^e \boldsymbol{\Psi}_j}{\partial \mathbf{q}} + \frac{\partial^e \hat{\mathbf{A}}_N}{\partial \mathbf{q}} ({}^{e}\boldsymbol{\Psi}_j \otimes \mathbf{I}_p) + \frac{\partial^r \hat{\mathbf{A}}_N}{\partial \mathbf{q}} ({}^{r}\boldsymbol{\Psi}_j \otimes \mathbf{I}_p) \right], \tag{206}$$

$$\frac{\partial^r \boldsymbol{\Psi}_i}{\partial \mathbf{q}} = \begin{bmatrix} \frac{\partial^i \boldsymbol{\Psi}_j}{\partial \mathbf{q}} \\ \frac{\partial^a \boldsymbol{\Psi}_j}{\partial \mathbf{q}} \end{bmatrix}, \tag{207}$$

and therefore, solving this equation, we obtain the partial derivative $\frac{\partial^a \boldsymbol{\Psi}_j}{\partial \mathbf{q}}$.

Before solving the Equation (204) and Equation (207) the partial derivatives $\frac{\partial \boldsymbol{\Phi}}{\partial \mathbf{z}}$, $\frac{\partial^e \boldsymbol{\Psi}_j}{\partial \mathbf{z}}$, $\frac{\partial^e \boldsymbol{\Psi}_j}{\partial \mathbf{q}}$, $\frac{\partial^e \hat{\mathbf{A}}_N}{\partial \mathbf{z}}$, $\frac{\partial^e \hat{\mathbf{A}}_N}{\partial \mathbf{q}}$, $\frac{\partial^r \hat{\mathbf{A}}_N}{\partial \mathbf{z}}$ and $\frac{\partial^r \hat{\mathbf{A}}_N}{\partial \mathbf{q}}$ must be symbolically computed. These derivatives are relatively simple since most of the individual terms of each matrix are linear or quadratic.

5.2.4 Procedure for optimal static balancing

This section details the step by step of the optimal synthesis proposed method for static balancing which is summarized in Figure 46.

Step 1: The first step is to know the mechanism topology previously that is: kinematic structure, number of springs, their connectivity and attachment points and the number of counterweights and their location.

Step 2: The second step is kinematic modeling. First, we model the mechanism using natural coordinates. Then, as far as possible, the position is solved in closed form by means of bilateration, otherwise which is formulated as a numerical solution either by using Newton-Raphson or an optimization method.

Step 3: The next step is the static analysis, where the equations of statics are obtained through the integration of the natural coordinates in the Davies' method as explained in Section 5.2.

Step 4: The design variables are established, followed by the formulation of the objective function Equation (198). The lower and upper bounds of the design variables are also established. Finally, the constraints of equality and inequality are adequately formulated if they are necessary. The optimization problem is formulated mathematically as shown in Equation (199).

Step 5: Computing of the sensitivities of the objective function by using Equation (200) and the numerical solution of the linear Equation (197), Equation (202), Equation (204) and Equation (207) respectively.

Step 6: Before starting the optimization process, an initial mechanism must be established, which is previously analyzed to evaluate its performance. This first mechanism is represented by the initial design variables vector $\mathbf{z}_0$.

Step 7: The optimization process begins with the evaluation of the objective function and the restrictions by means of the previous solution of the position and the statics of the mechanism for each configuration through Equation (188) and Equation (197) respectively. If the optimality criteria are not met, the optimizer generates a new solution which is evaluated again and continues this cycle until the optimality criteria are met.

Step 8: Once an optimal solution is obtained, an analysis is carried out to detect kinematic problems and verify that the static balancing is adequate. If the solution obtained is not satisfactory, then the initial mechanism is changed and the process continue iteratively to obtain an adequate solution.

In summary, what is done is to mathematically formulate the position problem and the statics of the mechanism. Then the sensitivity analysis is performed, and the necessary derivatives

Figure 46 – Flowchart of the proposed procedure.

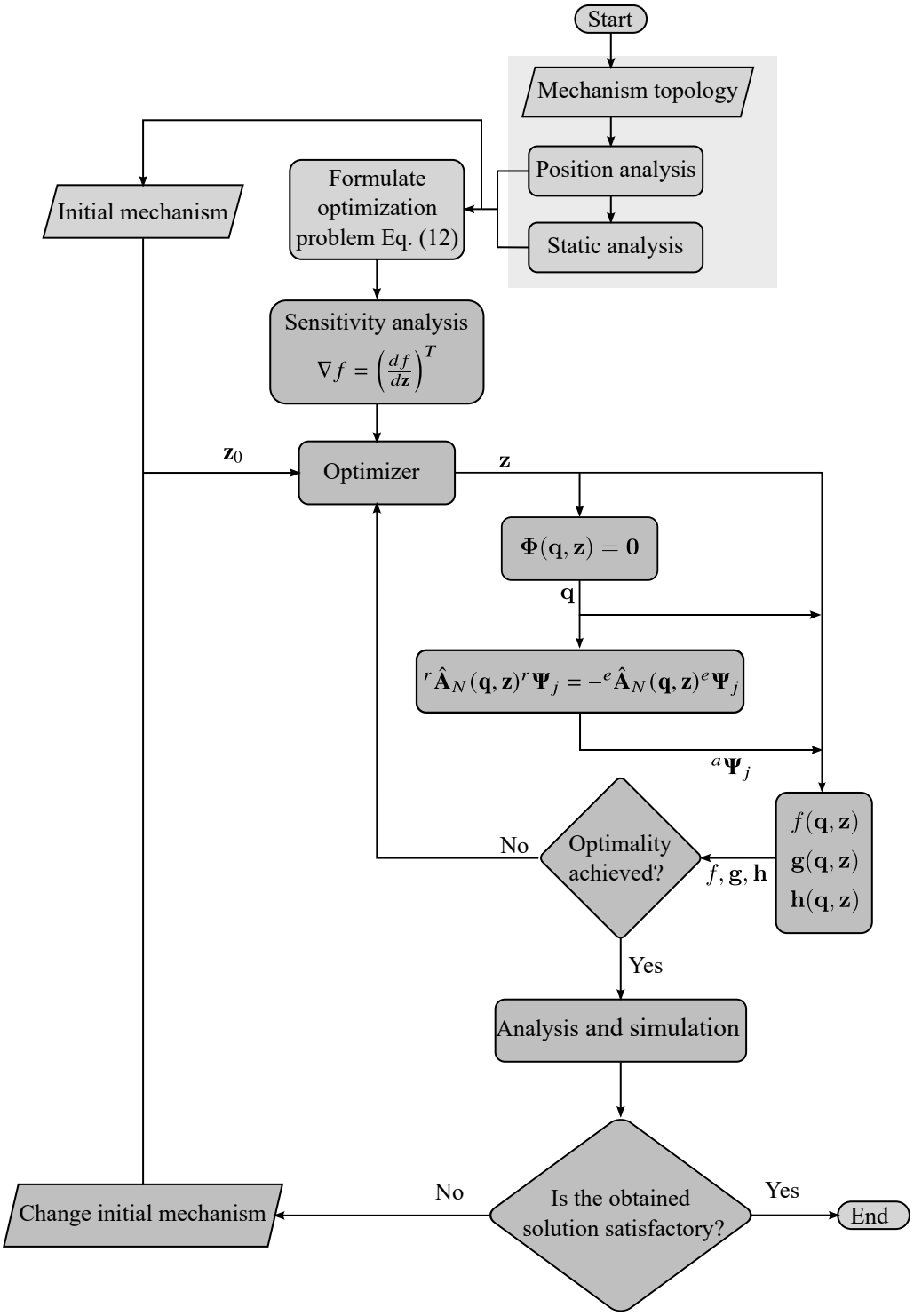

Source: The author.

are calculated symbolically. Then, in each iteration of the optimizer, the position problem is solved, the statics and the sensitivities equations are determined, and this cycle is continued until an optimum value is obtained. If the optimal value is not satisfactory, the initial guess is

modified, and the cycle repeats.

5.3 STATIC BALANCING OF A FOUR-BAR MECHANISM FOR VERTICAL STRAIGHT LINE MOTION OF AN EXTERNAL LOAD

Static balancing of an external load that moves in a vertical straight line is especially useful in devices where vertical adjustment of the payload is required with minimal efforts, such as, monitors with adjustable height, statically balanced shelves, writing-boards, and so forth. The first candidate mechanism that comes in mind is the four-bar mechanism with revolute joints, due to its versatility demonstrated to solve a wide variety of problems, moreover, of its relative simplicity. One application of the straight line four-bar mechanism is shown in Figure 47(a), which consists of a balanced writing-board with adjustable height. Another practical application is the 4-DoF support mechanism for desktop-monitor shown in Figure 47(b).

Figure 47 – Practical application of a straight line balancer four-bar mechanism.

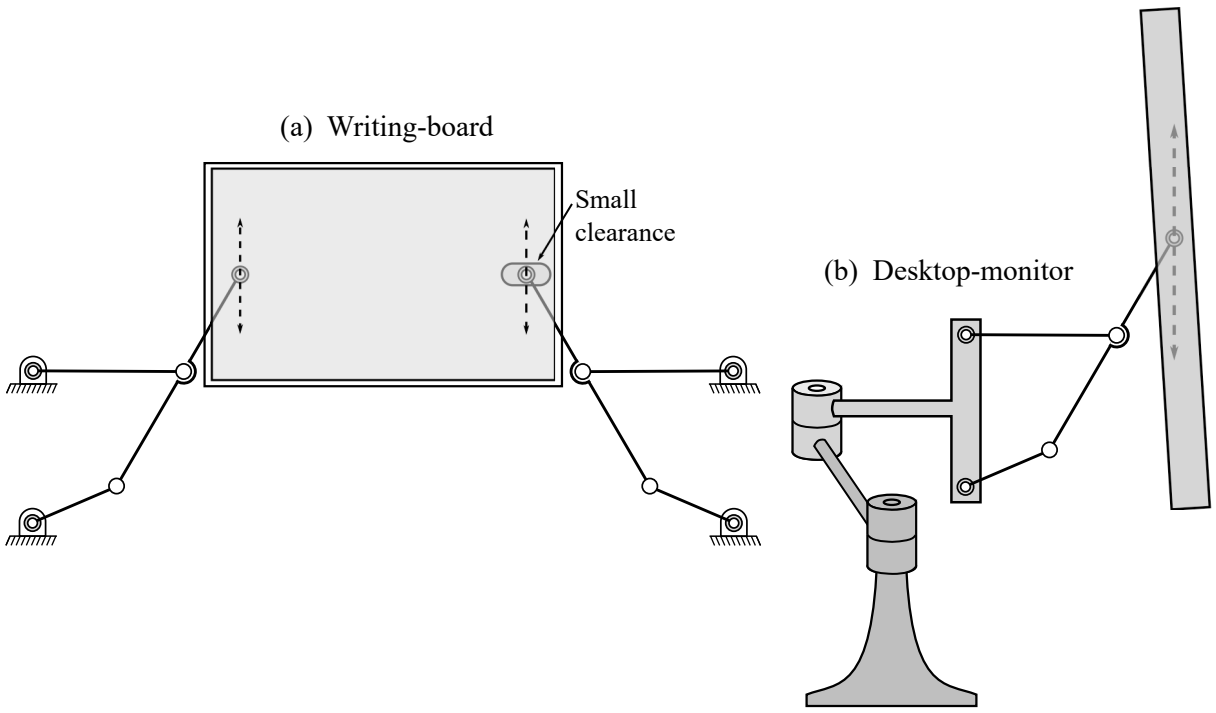

Source: The author.

5.3.1 Mechanism topology

A schematic of the straight line four-bar mechanism is shown in Figure 48. In this case study, the mechanisms is previously synthesized for a proximate straight line, and the mechanism is balanced after employing two non-zero free length springs attached to the input link.

Figure 48 – Straight line balancer four-bar mechanism (ARAVIND BASKAR, GURUNATHAN SARAVANA KUMAR, 2015).

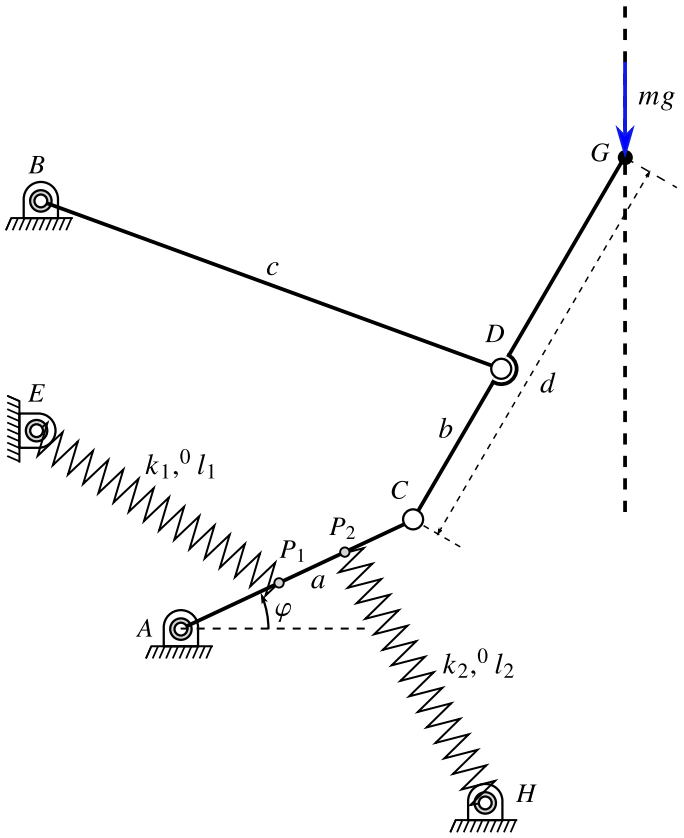

Source: The author.

5.3.2 Kinematic position analysis

The dimensions of the four-bar mechanism are taken from (ARAVIND BASKAR, GURUNATHAN SARAVANA KUMAR, 2015), for an approximate vertical straight line of 0.2m in the interval of the input angle of $-30° \leq \varphi \leq 30°$, where the numerical values are detailed in the Table 4.

Table 4 – Design parameters of the straight line four-bar mechanism.

Parameter	a	b	c	d	x_A	y_A	x_B	y_B
Value [m]	0.2	0.09	0.276	0.3	0	0	−0.08	0.09

Source: Adapted from (ARAVIND BASKAR, GURUNATHAN SARAVANA KUMAR, 2015).

In the first place the constraint equations vector of the mechanism is formulated

$$\mathbf{\Phi}(\mathbf{q},\mathbf{z}) = \begin{bmatrix} (x_D - x_C)^2 + (y_D - y_C)^2 - b^2 \\ (x_D - x_B)^2 + (y_D - y_B)^2 - c^2 \\ (x_C - x_A) - a\cos\varphi \\ (y_C - y_A) - a\sin\varphi \\ \varphi - \varphi_A(t) \end{bmatrix} = \mathbf{0}, \tag{208}$$

where the natural coordinates vector is $\mathbf{q} = \begin{bmatrix} x_C & y_C & x_D & y_D & \varphi \end{bmatrix}^T$ and $\varphi_A(t)$ is a law under which the mechanism moves. The first and second constraints correspond to the rigidity condition of links CD and BD, respectively, and the last three are driving constraints.

The natural coordinates x_C, y_C, x_D and y_D can be determined in a closed-form as functions of the input angle φ by using the bilateration method as in (ROMERO et al., 2019). Let us define the unit vector

$$\mathbf{u}_{AC} = \begin{bmatrix} \cos\varphi \\ \sin\varphi \end{bmatrix}, \tag{209}$$

then, point C is computed as

$$\mathbf{p}_C = \begin{bmatrix} x_C \\ y_C \end{bmatrix} = \mathbf{p}_A + a\mathbf{u}_{AC}\,, \tag{210}$$

where, a is the link AC length. Applying bilateration to the triangle $\triangle CBD$ is determined the point D

$$\mathbf{p}_D = \begin{bmatrix} x_D \\ y_D \end{bmatrix} = \mathbf{p}_C + \mathbf{N}_{CBD}(\mathbf{p}_B - \mathbf{p}_C), \tag{211}$$

where the bilateration matrix $\mathbf{N}_{CBD}$ is written as

$$\mathbf{N}_{CBD} = \frac{1}{d_{CB}} \begin{bmatrix} l_{CBD} & -h_{CBD} \\ h_{CBD} & l_{CBD} \end{bmatrix}, \tag{212}$$

and

$$d_{CB} = \sqrt{(\mathbf{p}_B - \mathbf{p}_C)^T(\mathbf{p}_B - \mathbf{p}_C)}, \qquad l_{CBD} = \frac{b^2 + d_{CB}^2 - c^2}{2d_{CB}}, \qquad h_{CBD} = -\sqrt{b^2 - l_{CBD}^2}\,.$$

Additionally, in the static analysis of Section 5.3.3, it is necessary to know the additional points G, P_1, and P_2. Where G is the point of application of the external load, P_1 and P_2 are the attachment points of the springs on link AC, respectively. This points are computed as

$$\mathbf{p}_G = \begin{bmatrix} x_G \\ y_G \end{bmatrix} = \mathbf{p}_C + \frac{d}{b}(\mathbf{p}_D - \mathbf{p}_C), \tag{213}$$

$$\mathbf{p}_1 = \begin{bmatrix} x_1 \\ y_1 \end{bmatrix} = \mathbf{p}_A + e\mathbf{u}_{AC}\,, \tag{214}$$

$$\mathbf{p}_2 = \begin{bmatrix} x_2 \\ y_2 \end{bmatrix} = \mathbf{p}_A + f\mathbf{u}_{AC}\,, \tag{215}$$

where, d, e and f are the distances of CG, AP_1 and AP_2 respectively.

5.3.3 Static analysis

The static analysis begins with the representation of internal and external actions present in the mechanism see Figure 49(a), from which the action graph and cutset are derived as shown in Figure 49(c). Where, f_1, f_2 are springs forces, f_g is the weight of the external load and τ_a is the actuation torque.The spring forces and their unit vectors are computed as

$$
\begin{aligned}
f_1 &= k_1(l_1 - {}^0l_1)\,, & f_2 &= k_2(l_2 - {}^0l_2)\,,\\
l_1 &= \sqrt{(\mathbf{p}_E - \mathbf{p}_1)^T(\mathbf{p}_E - \mathbf{p}_1)}\,, & l_2 &= \sqrt{(\mathbf{p}_H - \mathbf{p}_2)^T(\mathbf{p}_H - \mathbf{p}_2)}\,,\\
\mathbf{u}_1 &= \begin{bmatrix} u_{1x} \\ u_{1y} \end{bmatrix} = \frac{1}{l_1}(\mathbf{p}_E - \mathbf{p}_1)\,, & \mathbf{u}_2 &= \begin{bmatrix} u_{2x} \\ u_{2y} \end{bmatrix} = \frac{1}{l_2}(\mathbf{p}_H - \mathbf{p}_2)\,,
\end{aligned}
$$

where k_1 and k_2 are the springs stiffness, ${}^0l_1$ and ${}^0l_2$ are the springs free length.

Now, from the unit action screws of all the forces, the unit action matrix is obtained

$$
\hat{\mathbf{A}}_D = \begin{array}{c}
\begin{matrix} f_{ax} & f_{ay} & f_{bx} & f_{by} & f_{cx} & f_{cy} & f_{dx} & f_{dy} & f_g & f_1 \end{matrix}\\
\begin{bmatrix}
0 & 0 & -y_B & x_B & -y_C & x_C & -y_D & x_D & x_G & (x_1u_{1y} - y_1u_{1x}) \\
1 & 0 & 1 & 0 & 1 & 0 & 1 & 0 & 0 & u_{1x} \\
0 & 1 & 0 & 1 & 0 & 1 & 0 & 1 & 1 & u_{1y}
\end{bmatrix}
\end{array}
\begin{array}{cc}
f_2 & \tau_a \\
\begin{bmatrix}
(x_2u_{2y} - y_2u_{2x}) & 1 \\
u_{2x} & 0 \\
u_{2y} & 0
\end{bmatrix}.
\end{array}
\tag{216}
$$

Applying Equation (192) it is obtained the the network unit action matrix $\hat{\mathbf{A}}_N$ then splitting it as in Equation (196) and rearranging we obtained the static analysis equations (Equation (197)). Where the matrices ${}^r\hat{\mathbf{A}}_N$, ${}^e\hat{\mathbf{A}}_N$ and vectors ${}^r\mathbf{\Psi}$, ${}^e\mathbf{\Psi}$ are the following

$$
{}^r\hat{\mathbf{A}}_N(\mathbf{q},\mathbf{z}) = \begin{array}{c}
\begin{matrix} f_{ax} & f_{ay} & f_{bx} & f_{by} & f_{cx} & f_{cy} & f_{dx} & f_{dy} & \tau_a \end{matrix}\\
\begin{bmatrix}
0 & 0 & -y_B & x_B & 0 & 0 & 0 & 0 & 1 \\
1 & 0 & 1 & 0 & 0 & 0 & 0 & 0 & 0 \\
0 & 1 & 0 & 1 & 0 & 0 & 0 & 0 & 0 \\
0 & 0 & -y_B & x_B & -y_C & x_C & 0 & 0 & 0 \\
0 & 0 & 1 & 0 & 1 & 0 & 0 & 0 & 0 \\
0 & 0 & 0 & 1 & 0 & 1 & 0 & 0 & 0 \\
0 & 0 & y_B & -x_B & 0 & 0 & -y_D & x_D & 0 \\
0 & 0 & -1 & 0 & 0 & 0 & 1 & 0 & 0 \\
0 & 0 & 0 & -1 & 0 & 0 & 0 & 1 & 0
\end{bmatrix}
\end{array},
\tag{217}
$$

Figure 49 – Schematic representation of couplings and actions.

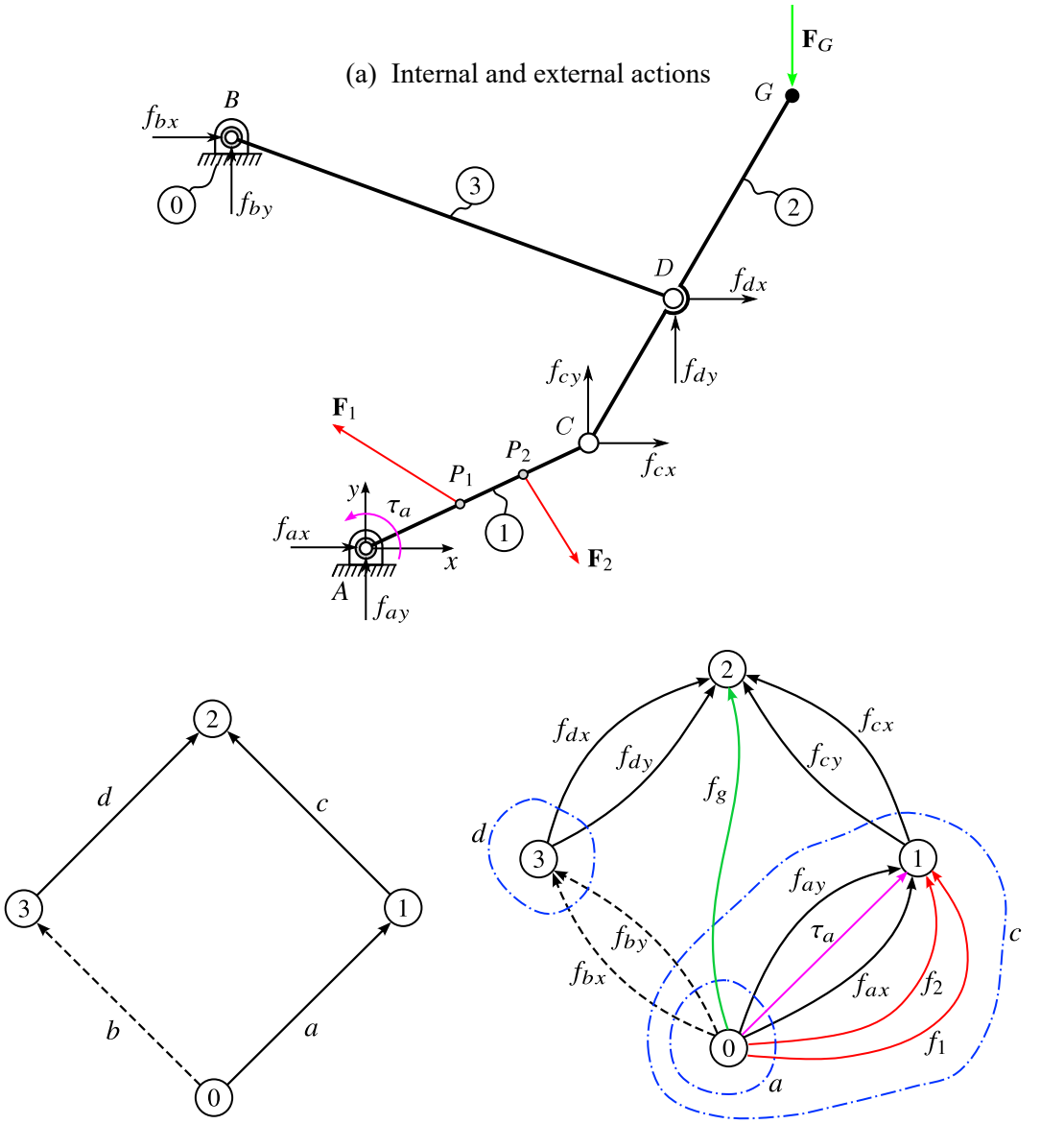

Source: The author.

$$
{}^{e}\hat{\mathbf{A}}_N(\mathbf{q},\mathbf{z}) = \begin{array}{c} \begin{matrix} f_g & f_1 & f_2 \end{matrix} \\ \begin{bmatrix} x_G & (x_1u_{1y} - y_1u_{1x}) & (x_2u_{2y} - y_2u_{2x}) \\ 0 & u_{1x} & u_{2x} \\ 1 & u_{1y} & u_{2y} \\ x_G & 0 & 0 \\ 0 & 0 & 0 \\ 1 & 0 & 0 \\ 0 & 0 & 0 \\ 0 & 0 & 0 \\ 0 & 0 & 0 \end{bmatrix} \end{array}, \tag{218}
$$

$$
{}^{r}\boldsymbol{\Psi} = \begin{bmatrix} f_{ax} & f_{ay} & f_{bx} & f_{by} & f_{cx} & f_{cy} & f_{dx} & f_{dy} & \tau_a \end{bmatrix}^T, \tag{219}
$$

and

$$
{}^{e}\boldsymbol{\Psi}(\mathbf{q},\mathbf{z}) = \begin{bmatrix} f_g & f_1 & f_2 \end{bmatrix}^T. \tag{220}
$$

5.3.4 Optimization problem formulation

In this example, the dimensions of the mechanism do not change because the mechanism was previously synthesized to perform an approximate straight line. Therefore, the design variables correspond to the location of the tension springs and their properties. Then the vector of design variables is defined as:

$$
\mathbf{z} = \begin{bmatrix} k_1 & k_2 & {}^{0}l_1 & {}^{0}l_2 & x_E & y_E & x_H & y_H & e & f \end{bmatrix}^T.
$$

Now the lower and upper bounds of the design variables are defined:

$$
\underline{\mathbf{z}} = \begin{bmatrix} 0\ \text{Nm} \\ 0\ \text{Nm} \\ 0.1\ \text{m} \\ 0.1\ \text{m} \\ -0.2\ \text{m} \\ -0.3\ \text{m} \\ -0.2\ \text{m} \\ -0.3\ \text{m} \\ 0.04\ \text{m} \\ 0.04\ \text{m} \end{bmatrix}, \qquad \bar{\mathbf{z}} = \begin{bmatrix} 10000\ \text{Nm} \\ 10000\ \text{Nm} \\ 0.3\ \text{m} \\ 0.3\ \text{m} \\ 0.2\ \text{m} \\ 0.3\ \text{m} \\ 0.2\ \text{m} \\ 0.3\ \text{m} \\ 0.16\ \text{m} \\ 0.16\ \text{m} \end{bmatrix},
$$

then, the optimization problem is formulated as

$$\begin{aligned} \underset{\mathbf{z}}{\text{minimize}} \quad & f(\mathbf{z}) = \frac{1}{2}\sum_{j=1}^{n} {}^{a}\boldsymbol{\Psi}_j^{T\,a}\boldsymbol{\Psi}_j \,, \\ \text{subject to} \quad & \underline{\mathbf{z}} \leq \mathbf{z} \leq \bar{\mathbf{z}} \,, \\ \text{while solving} \quad & \begin{cases} \boldsymbol{\Phi}(\mathbf{q},\mathbf{z}) = \mathbf{0}; \quad \text{Eq.(208)} \\ {}^{r}\hat{\mathbf{A}}_N(\mathbf{q},\mathbf{z})^{r}\boldsymbol{\Psi}_j = -{}^{e}\hat{\mathbf{A}}_N(\mathbf{q},\mathbf{z})^{e}\boldsymbol{\Psi}_j \,. \end{cases} \end{aligned} \tag{221}$$

where ${}^{a}\boldsymbol{\Psi}_j = [\tau_a]$. In this case, it was not necessary to define inequality and equality constraints.

5.3.5 Implementation and results

The optimization problem defined above is solved for the payload $m = 60$ kg, using the interior-point algorithm of the built-in `fmincon` function in the software Matlab®. Table 5, shows the optimal design parameters which are illustrated in Figure 50(b).The Figure 50(a) shows the initial mechanism that is represented by the initial vector of design variables

$$\mathbf{z}_0 = \begin{bmatrix} 100 & 100 & 0.05 & 0.05 & 0.1 & 0.3 & -0.2 & 0.2 & 0.04 & 0.14 \end{bmatrix}^T,$$

this initial mechanism was selected from a pre-analysis by setting iteratively different design parameters until to find adequate ones.

Table 5 – Optimal design parameters.

Design parameter	Value	Unit
k_1	9967.97129311232	[Nm]
${}^{0}l_1$	0.299493442996904	[m]
e	0.150391105503725	[m]
x_E	−0.188689683701425	[m]
y_E	−0.0943722256223178	[m]
k_2	9969.84992797751	[Nm]
${}^{0}l_2$	0.113609035840242	[m]
f	0.159760684640614	[m]
x_H	−0.0297426243905242	[m]
y_H	0.160610921414398	[m]

Source: The author.

Figure 51(a) shows the convergence of the objective function where a value of 0.022 was reached with 1226 iterations. Figure 51(b) shows the torque for the unbalanced and balanced mechanisms, in which the maximum torques are 117.8 Nm and 0.1104 Nm, respectively, indicating a reduction of 99.91%. Note that the torque range of the unbalanced mechanism is from 98 to 118 Nm, and the torque range of the balanced mechanism is from -0.08 to 0.12 Nm. In Figure 51(c), it can be seen that the total potential energy of the mechanism is practically constant throughout the range of motion.

Figure 50 – Optimization results: (a) initial mechanism and (b) optimal mechanism.

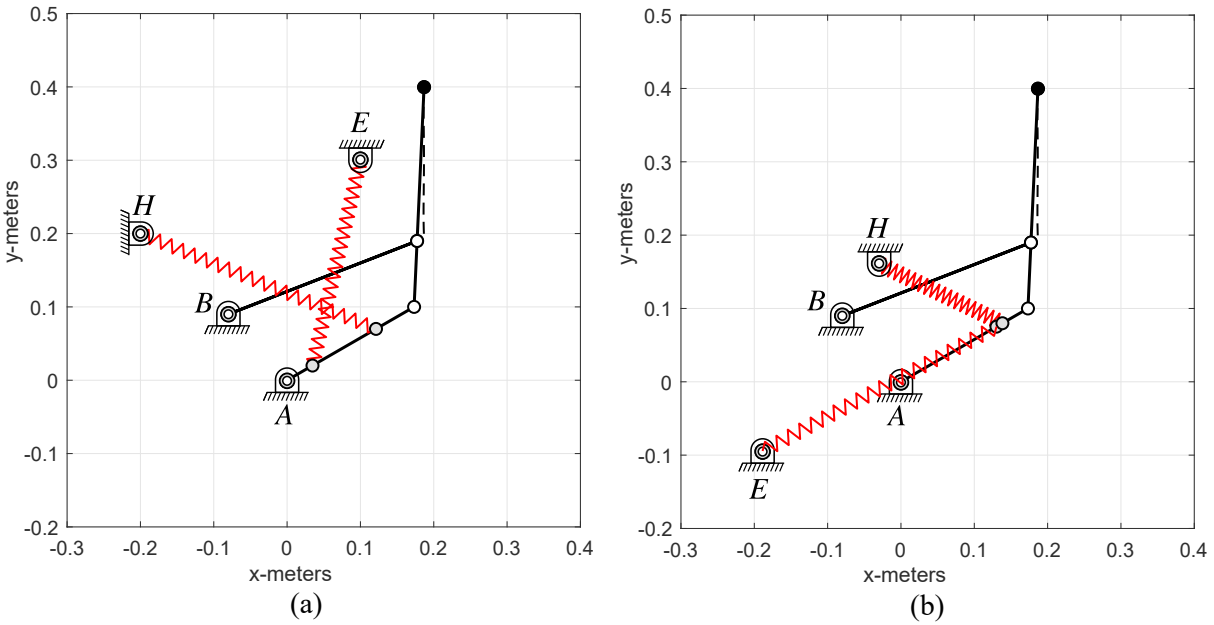

Source: The author.

5.4 STATIC BALANCING OF A RSSR-SS MECHANISM

This example presents the static balancing of a rigid-body guidance spatial mechanism named RSSR-SS, see Figure 52. The Revolution-Spherical-Spherical-Revolution-Spherical-Spherical (RSSR-SS) mechanism is a particular type of multi-loop spatial mechanism with greater structural stiffness than a four-bar spatial mechanism. This property makes it a good candidate for rigid body guidance due to its high capacity for loads (PATEL; BHATT, 2022). Another important application of the RSSR-SS mechanism is also the path generation as shown in (PREMKUMAR; KRAMER, 1990).

The literature has abundant works on the analysis and dimensional synthesis for path generation and rigid body guidance. Still, there is no evidence of works on the static balancing of RSSR-SS mechanism, so the author believes this proposed application is novel.

5.4.1 Mechanism topology

To balance the mechanism a tension spring is connected between the ground and the coupler as shown in Figure 53. The design parameters in the proposed topology are eight, corresponding to three coordinates of point P relative to the coupler, three coordinates of point H relative to the global reference system, and two spring parameters corresponding to the elastic constant and free length, respectively.

Figure 51 – Optimization results: (a) actuator torque τ_a unbalanced mechanism, (b) actuator torque τ_a balanced mechanism, (c) convergence of the objective function, and (d) potential energies of the optimal mechanism.

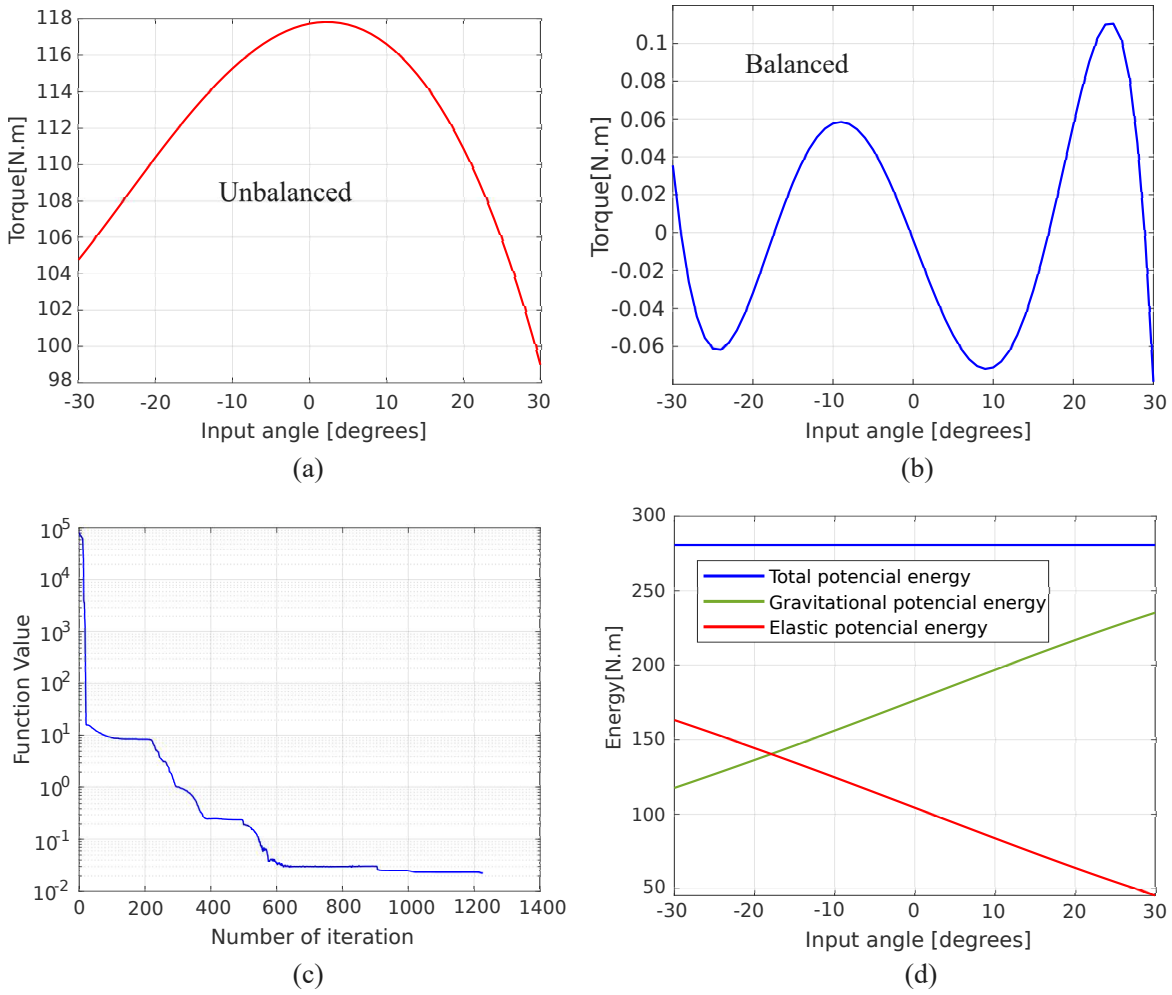

Source: The author.

5.4.2 Kinematic position analysis

The unit vector of revolute joint $\mathbf{u}_A$ can be parameterized using the rotation angles θ_{Az}, and θ_{Ay}. Then the unit vector is defined as $\mathbf{u}_A = \mathbf{R}(\theta_{Az}, \theta_{Ay})\mathbf{u}_{A0}$, where $\mathbf{u}_{A0} = \begin{bmatrix} 1 & 0 & 0 \end{bmatrix}^T$ is the initial orientation of $\mathbf{u}_A$, and $\mathbf{R}(\theta_{Az}, \theta_{Ay})$ is a successive rotation about the moving coordinate axes. The rotation matrix of the successive rotation angles θ_{Az}, and θ_{Ay} is computed as

$$\mathbf{R} = \begin{bmatrix} \mathrm{c}\,\theta_{Az}\,\mathrm{c}\,\theta_{Ay} & -\mathrm{s}\,\theta_{Az} & \mathrm{c}\,\theta_{Az}\,\mathrm{s}\,\theta_{Ay} \\ \mathrm{s}\,\theta_{Az}\,\mathrm{c}\,\theta_{Ay} & \mathrm{c}\,\theta_{Az} & \mathrm{s}\,\theta_{Az}\,\mathrm{s}\,\theta_{Ay} \\ -\mathrm{s}\,\theta_{Ay} & 0 & \mathrm{c}\,\theta_{Ay} \end{bmatrix}. \tag{222}$$

Similarly, the unit vector $\mathbf{u}_B$ of the revolute joint at B is defined. . The next step is to determine the position of point D as a function of input angle φ. For this, it is first necessary to

Figure 52 – RSSR-SS mechanism.

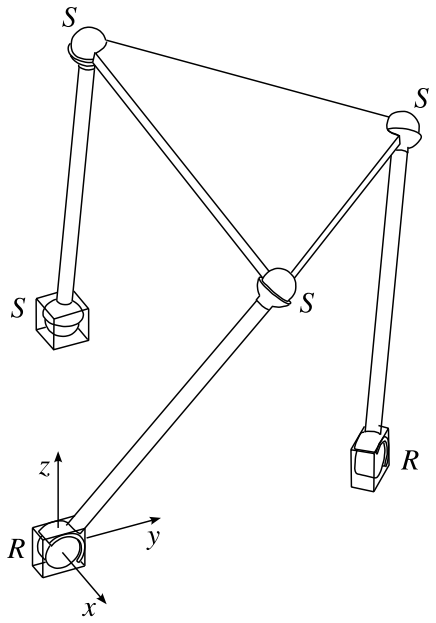

Source: The author.

Figure 53 – Topology of balancer RSSR-SS mechanism.

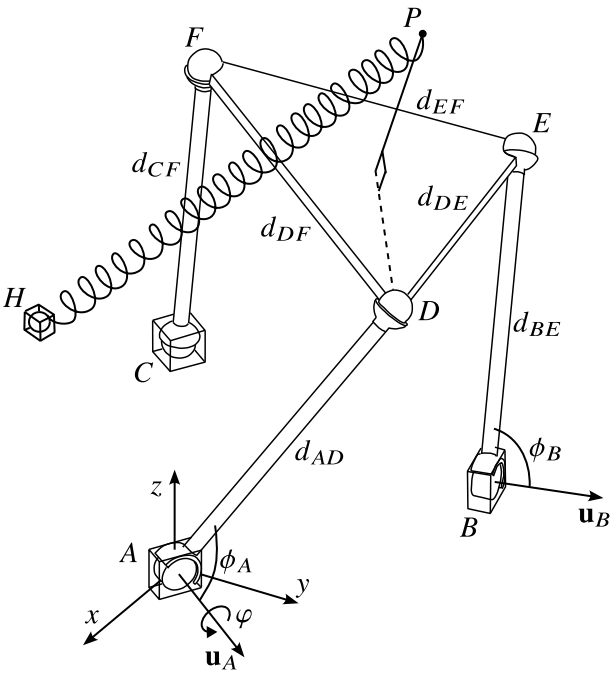

Source: The author.

determine the initial position of point D as follows,

$$\mathbf{r}_{D0} = \mathbf{R}(\theta_{Az}, \theta_{Ay}) \begin{bmatrix} d_{AD} \cos \phi_A \\ d_{AD} \sin \phi_A \\ 0 \end{bmatrix}, \tag{223}$$

and using the matrix form of Rodrigues' formula, we obtain the position of point D as a function of the input angle

$$\mathbf{r}_D = \mathbf{R}(\varphi)\mathbf{r}_{D0}\,, \tag{224}$$

where the elements of the rotation matrix $\mathbf{R}(\varphi)$ are given by:

$$\begin{aligned}
r_{11} &= (u_{Bx}^2 - 1)(1 - \mathrm{c}\,\varphi) + 1\,,\\
r_{12} &= u_{Bx}u_{By}(1 - \mathrm{c}\,\varphi) - u_{Bz}\,\mathrm{s}\,\varphi\,,\\
r_{13} &= u_{Bx}u_{Bz}(1 - \mathrm{c}\,\varphi) + u_{By}\,\mathrm{s}\,\varphi\,,\\
r_{21} &= u_{By}u_{Bx}(1 - \mathrm{c}\,\varphi) + u_{Bz}\,\mathrm{s}\,\varphi\,,\\
r_{22} &= (u_{By}^2 - 1)(1 - \mathrm{c}\,\varphi) + 1\,,\\
r_{23} &= u_{By}u_{Bz}(1 - \mathrm{c}\,\varphi) - u_{Bx}\,\mathrm{s}\,\varphi\,,\\
r_{31} &= u_{Bz}u_{Bx}(1 - \mathrm{c}\,\varphi) - u_{By}\,\mathrm{s}\,\varphi\,,\\
r_{32} &= u_{Bz}u_{By}(1 - \mathrm{c}\,\varphi) - u_{Bx}\,\mathrm{s}\,\varphi\,,\\
r_{33} &= (u_{Bz}^2 - 1)(1 - \mathrm{c}\,\varphi) + 1\,.
\end{aligned}$$

Now we defined the constraint vector Equation (225). These six constraint equations correspond to the five constant distances d_{CF}, d_{DE}, d_{EF}, d_{EF}, d_{BE}, and a constant angle constraint between $\mathbf{r}_{BE}$ and $\mathbf{u}_B$.

$$\mathbf{\Phi}(\mathbf{q},\mathbf{z}) = \begin{bmatrix}
\mathbf{r}_{CF}\cdot\mathbf{r}_{CF} - d_{CF}^2\\
\mathbf{r}_{DE}\cdot\mathbf{r}_{DE} - d_{DE}^2\\
\mathbf{r}_{DF}\cdot\mathbf{r}_{DF} - d_{DF}^2\\
\mathbf{r}_{EF}\cdot\mathbf{r}_{EF} - d_{EF}^2\\
\mathbf{r}_{BE}\cdot\mathbf{r}_{BE} - d_{BE}^2\\
\mathbf{r}_{BE}\cdot\mathbf{u}_B - d_{BE}\cos\phi_B
\end{bmatrix} = \mathbf{0}, \tag{225}$$

where the natural coordinates vector is $\mathbf{q} = \begin{bmatrix} x_E & y_E & z_E & x_F & y_F & z_F \end{bmatrix}^T$.The Eq. (225) is easily solved using the Newton-Raphson method as showed in Section 5.1.

To determine the position of point P in relation to the coupler, we define the coordinates μ_1, μ_2, and μ_3 with respect to the vector basis $\mathbf{u}_{DE}$, $\mathbf{u}_{DF}$, and $\mathbf{n}_D = \mathbf{u}_{DE}\times\mathbf{u}_{DF}$. Then the coordinates of point P with respect to the global reference frame are determined through the following expression

$$\mathbf{r}_P = \mathbf{r}_D + \mu_1\mathbf{u}_{DE} + \mu_2\mathbf{u}_{DF} + \mu_3\mathbf{n}_D \tag{226}$$

5.4.3 Static analysis

For spatial mechanisms, the static analysis is similar to that for planar mechanisms. The main difference is that the direction of the kinematic pairs must be considered in order to properly

define the actions in each pair. In spherical pairs, no special treatment of the unit vectors is necessary since the reactions are defined in the direction of the coordinate axes of the global reference system.

By simplicity, the reference frame is defined as coincident with point A. In the pair of revolution at A, we define a reference system formed by the unit vectors $\mathbf{u}_B$, $\mathbf{v}_B$, and $\mathbf{w}_B$ where the vector $\mathbf{v}_B$ is chosen so that it is perpendicular to the vector $\mathbf{w}_B$ and thus $\mathbf{w}_B = \mathbf{u}_B \times \mathbf{v}_B$. In the same way, a reference frame is defined in the pair of revolution in B. The internal and external actions are illustrated Figure 54.

Figure 54 – Internal and external actions.

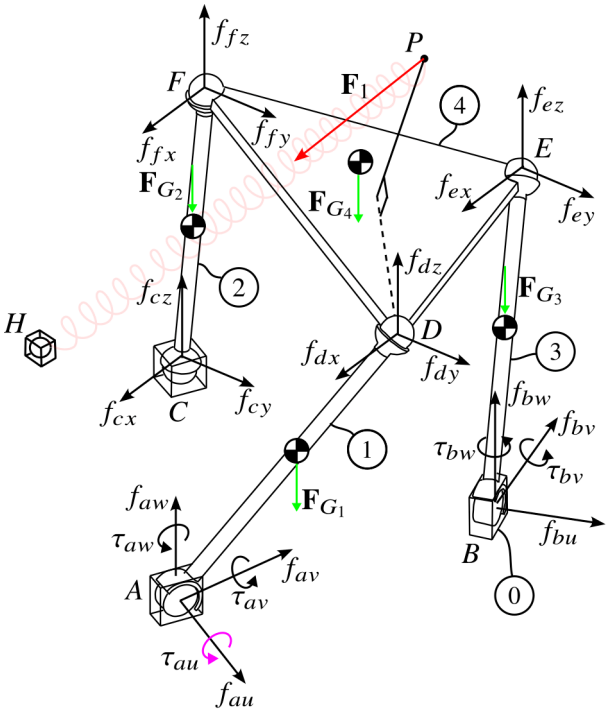

Source: The author.

The action graph and cutset are shown in Figure 55. From the actions shown in the Figure 54, the unit action matrix $[\mathbf{A}_D]_{4\times28}$ is determined, and from the fundamental cutsets graph Figure 55, the fundamental cutset matrix $[\mathbf{Q}_A]_{4\times28}$ is determined. Due to the size of these matrices it is not possible to show the elements here.

The constitutive equations of statics can be written in a compact form as:

$$\left[{}^{r}\hat{\mathbf{A}}_N\right]_{24\times23}\begin{bmatrix} {}^{i}\boldsymbol{\Psi} \\ {}^{a}\boldsymbol{\Psi} \end{bmatrix}_{23\times1} = -\left[{}^{e}\hat{\mathbf{A}}_N\right]_{24\times5}\left[{}^{e}\boldsymbol{\Psi}\right]_{5\times1}, \tag{227}$$

Figure 55 – (a) Directed coupling graph G_C, and (b) actions and fundamental cutsets graph G_A.

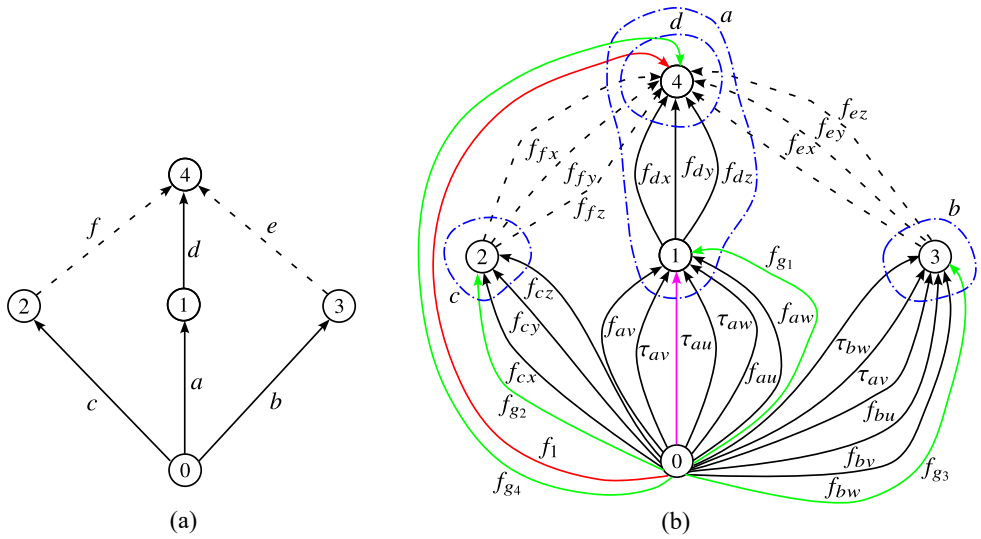

Source: The author.

where,

$$
\begin{aligned}
{}^{i}\boldsymbol{\Psi} &= \begin{bmatrix} f_{au} & f_{av} & f_{aw} & \tau_{av} & \tau_{aw} & f_{bu} & f_{bv} & f_{bw} & \tau_{bv} & \tau_{bw} & f_{cx} \\ f_{cy} & f_{cz} & f_{dx} & f_{dy} & f_{dz} & f_{ex} & f_{ey} & f_{ez} & f_{fx} & f_{fy} & f_{fz} \end{bmatrix}^T, \\
{}^{a}\boldsymbol{\Psi} &= \tau_{au}\,, \\
{}^{e}\boldsymbol{\Psi} &= \begin{bmatrix} f_{g_1} & f_{g_2} & f_{g_3} & f_{g_4} & f_1 \end{bmatrix}^T.
\end{aligned}
$$

5.4.4 Optimization problem formulation

The description of the design variables is shown in Table 6. These variables correspond to the spring properties: spring stiffness constant and free length and the spring attachment points with the coupler and the ground.

In this case, there are only constraints due to the upper and lower bounds of the design variables, so the optimization problem formulation is the same as in Section 5.3, see Equation 221. It is necessary to solve the position problem Equation 225 numerically at each iteration and for the discretized configurations during optimization.

5.4.5 Implementation and results

Table 7 shows the dimensions of two RSSR-SS balancer named mechanism i and mechanism ii. The masses of each link are: $m_1 = m_2 = m_3 = 10$ [kg], and $m_4 = 30$ [kg] for both mechanisms. We assume that the center of mass of each link is located at the geometric center. The values used in these example are arbitrary and do not correspond to any practical application, so they are illustrative. The input angle range for mechanism i is $45° \leq \varphi \leq 120°$

Table 6 – Design parameters of RSSR-SS balancer.

Design parameter	Description	Unit
k_1	Spring stiffness	[Nm]
${}^0l_1$	Spring free length	[m]
μ_1	$\mathbf{u}_{DE}$ coordinate of the point P relative to coupler	[m]
μ_2	$\mathbf{u}_{DF}$ coordinate of the point P relative to coupler	[m]
μ_3	$\mathbf{n}_D$ coordinate of the point P relative to coupler	[m]
x_H	x-coordinate of the point H	[m]
y_H	y-coordinate of the point H	[m]
z_H	z-coordinate of the point H	[m]

Source: The author.

and $20° \leq \varphi \leq 200°$ for mechanism ii. For mechanism i, $n = 76$ configurations were used and $n = 181$ configurations for mechanism ii; in both cases, the input angles had a constant increment of one degree.

Table 7 – Dimensions for RSSR-SS mechanism i and mechanism ii.

Variable	RSSR-SS i	RSSR-SS ii	Unit
$\mathbf{u}_A$	$\begin{bmatrix} 1 & 0 & 0 \end{bmatrix}^T$	$\begin{bmatrix} 1 & 0 & 0 \end{bmatrix}^T$	[m]
$\mathbf{u}_B$	$\begin{bmatrix} \frac{1}{\sqrt{2}} & \frac{1}{\sqrt{2}} & 0 \end{bmatrix}^T$	$\begin{bmatrix} \frac{1}{\sqrt{2}} & \frac{1}{\sqrt{2}} & 0 \end{bmatrix}^T$	[m]
$\mathbf{r}_A$	$\begin{bmatrix} 0 & 0 & 0 \end{bmatrix}^T$	$\begin{bmatrix} 0 & 0 & 0 \end{bmatrix}^T$	[m]
$\mathbf{r}_B$	$\begin{bmatrix} 0 & 4 & 0 \end{bmatrix}^T$	$\begin{bmatrix} 0 & 4 & 0 \end{bmatrix}^T$	[m]
$\mathbf{r}_C$	$\begin{bmatrix} -4 & 2 & 0 \end{bmatrix}^T$	$\begin{bmatrix} -4 & 2 & 0 \end{bmatrix}^T$	[m]
ϕ_A	90	90	[°]
ϕ_B	100	95.0316	[°]
d_{AD}	4	2	[m]
d_{CF}	4	4	[m]
d_{DF}	4	4.8989	[m]
d_{DE}	4	4.5	[m]
d_{EF}	4	4.0311	[m]
d_{BE}	4	4.0311	[m]

Source: The author.

Figure 56 shows the optimal mechanisms at a particular position. Table 8 and Table 9 show the optimal values of the design variables and the optimization parameters: limits and initial values of the design variables. Figure 57 shows the evolution of the objective function for both mechanisms, where 659 iterations were necessary to obtain a local optimum for mechanism i, and 258 iterations for mechanism ii.

Figure 58(a) and Figure 58(b) show the torques for the unbalanced and the balanced mechanism i which the maximum torques are 1467.818 [Nm] and 1.3667 [Nm] respectively, which indicates a reduction of 99.9%. Figures 58 (c) and Figure 58 (d) show the torques for the unbalanced and balanced mechanism ii, in which the maximum torques are 698.888 [Nm] and 0.749 [Nm], respectively, which indicates a reduction of 99.89%. Note that the torque range of the unbalanced mechanism i goes from -1500 to 1000 Nm, the torque range of the balanced mechanism i goes from -1.5 to 1.5 Nm, the torque range of the unbalanced mechanism ii goes

Figure 56 – Optimization results: (a) optimal mechanism i and (b) optimal mechanism ii.

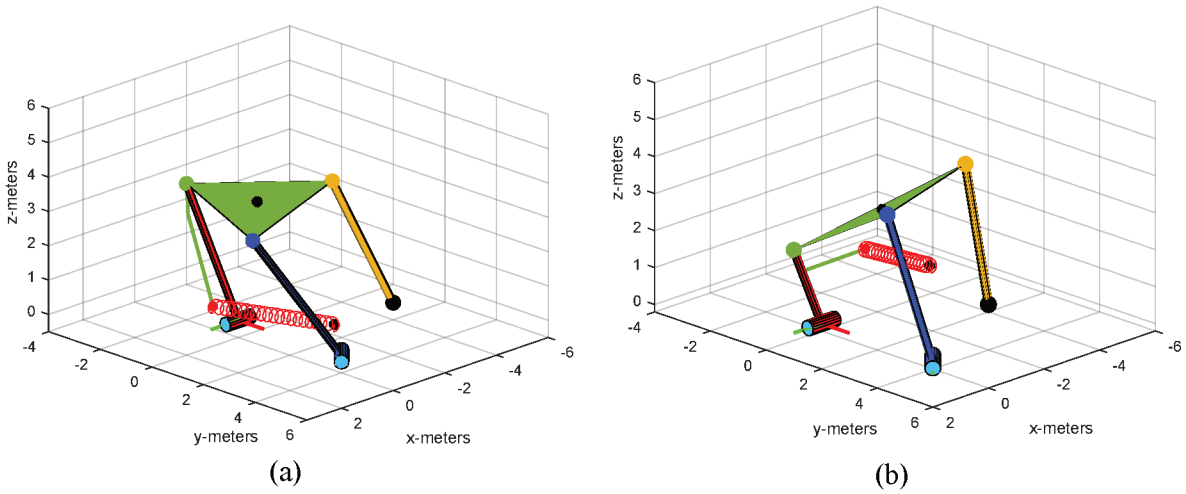

Source: The author.

Table 8 – Optimization parameters and optimal mechanism i.

z	z_0	$\underline{z}$	$\bar{z}$	**Optimal z**
k_1	100	10	10000	2399.59531353929
${}^0l_1$	0.2	0.1	3	2.99999188468730
μ_1	1	−10	10	6.31893554353017
μ_2	1	−10	10	−2.18508327366046
μ_3	1	−10	10	−1.11133462774918
x_H	5	−6	6	−2.24352423230350
y_H	5	−6	6	1.47709971193836
z_H	5	−6	6	−0.314246659719851

Source: The author.

Table 9 – Optimization parameters and optimal mechanism ii.

z	z_0	$\underline{z}$	$\bar{z}$	**Optimal z**
k_1	100	10	10000	839.584268727804
${}^0l_1$	0.5	0.1	3	2.72378059422542
μ_1	3	−10	10	3.44972233906328
μ_2	−1	−10	10	−0.309790680312529
μ_3	−1	−10	10	−0.762879644487900
x_H	0	−7	7	−3.58138339195359
y_H	0	−7	7	0.303901332795582
z_H	2	−7	7	0.725886920793986

Source: The author.

from -700 to 300 Nm, and the torque range of the balanced i-mechanism goes from -0.8 to 0.8 Nm. Figure 59(a) and Figure 59(b) show the elastic potential energy, gravitational potential energy, and total potential energy for mechanism i and mechanism ii, respectively. In both cases, the variation of the total potential energy is minimal, and therefore the mechanisms are satisfactorily

Figure 57 – convergence of the objective function: (a) mechanism i and (b) mechanism ii.

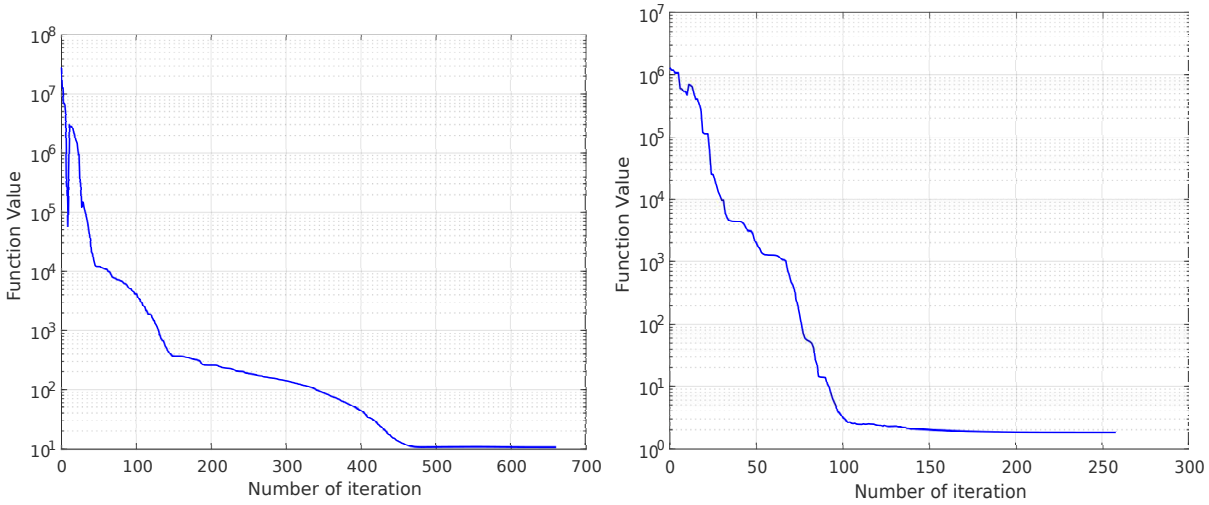

(a) (b)

Source: The author.

balanced.

5.5 STATIC BALANCING OF A KUKA KR 210 R3100 SERIAL MANIPULATOR

In this section, the proposed methodology is applied in the static balancing of the KUKA KR 210 R3100 serial manipulator using an auxiliary mechanism as shown in the Fig. 60. This example was inspired by Nguyen (NGUYEN, 2022) but here parallelogram linkages are not considered to make the balancing problem more generic. Shoulder O_1 and O_2 elbow joints are only taken into consideration because the first joint at the base aligns with the direction of gravity and the last three joints near the end-effector can be neglected. Therefore, the balancer robot can be treated as a planar mechanism.

5.5.1 Kinematic position analysis

The geometric parameters of the robot balancer are shown in the kinematic representation in Figure 61 and Table 10, that show the dimensional and mass parameters of the KUKA KR 210 R3100 robot. Where r_1, r_2 are the distances between O_1 and O_2, O_2 and O_3 respectively, $\bar{r}_1$ and $\bar{r}_2$ are the distances of the center of mass of link 1 and link 2 from O_1 and O_2, m_1, m_2, and m_3 are the masses of link 1, link 2 and the payload respectively. Moreover, $a_k = \|\mathbf{p}_{A_kB_k}\|$, $b_k = \|\mathbf{p}_{B_kC_k}\|$, $c_k = \|\mathbf{p}_{O_kC_k}\|$, $d_k = \|\mathbf{p}_{O_kA_k}\|$,$e_k = \|\mathbf{p}_{O_kE_k}\|$, $g_k = \|\mathbf{p}_{B_kD_k}\|$, $h_k = \|\mathbf{p}_{O_kH_k}\|$, $i_k = \|\mathbf{p}_{C_kD_k}\|$, $p_k = \|\mathbf{p}_{C_kE_k}\|$, $d_3 = \|\mathbf{p}_{O_2A_3}\|$ and $j = \|\mathbf{p}_{A_1A_3}\|$ are distances with $k = 1, 2$.

The following vector of constraint equations models the kinematics of the mechanism:

Figure 58 – Optimization results: (a) actuator torque τ_{au} unbalanced mechanism i, (b) actuator torque τ_{au} balanced mechanism i, (c) actuator torque τ_{au} unbalanced mechanism ii, (d) actuator torque τ_{au} balanced mechanism ii.

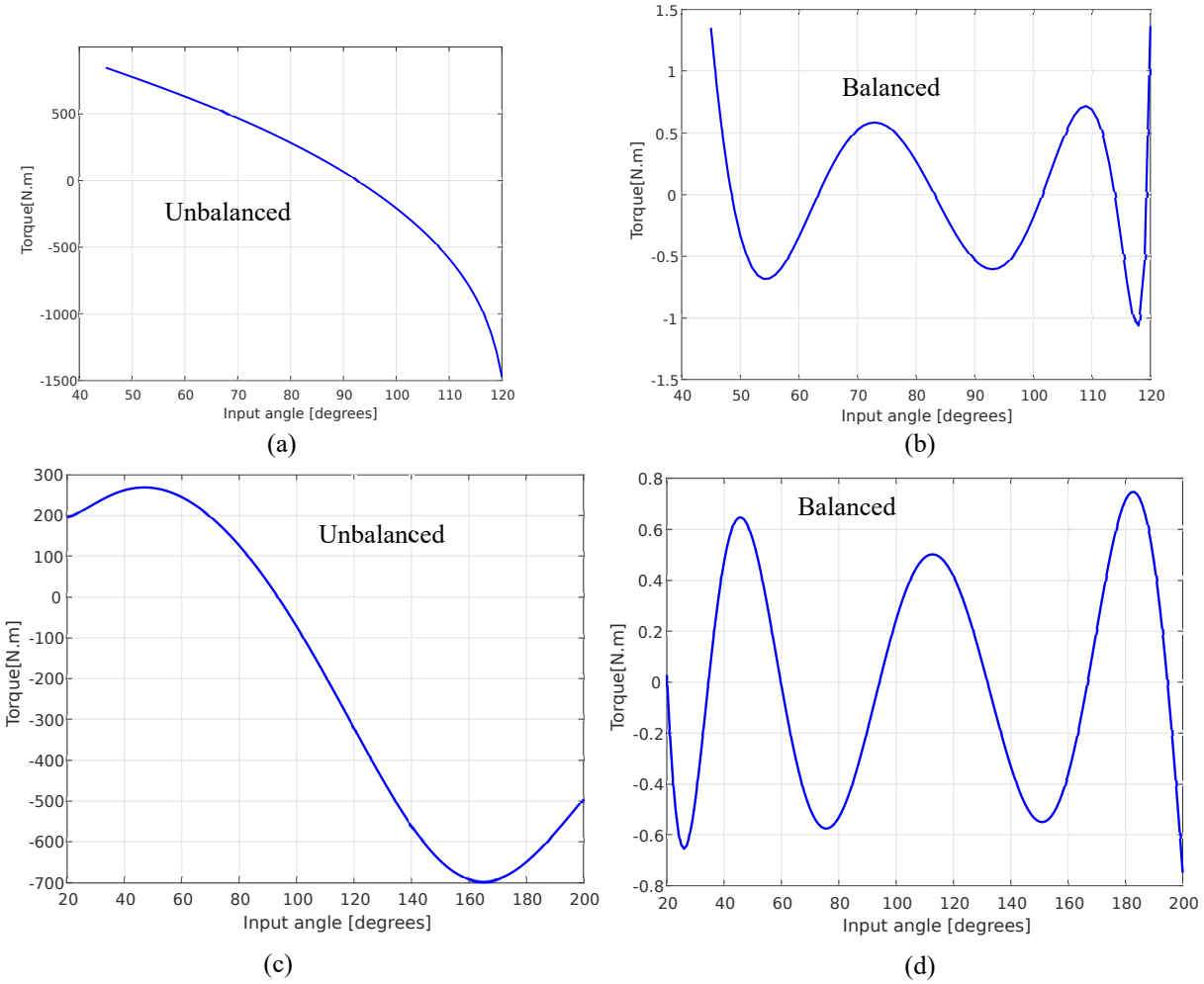

Source: The author.

$$\mathbf{\Phi}(\mathbf{q},\mathbf{z}) = \begin{bmatrix} (x_{B_1} - x_{A_1})^2 + (y_{B_1} - y_{A_1})^2 - a_1^2 \\ (x_{B_1} - x_{C_1})^2 + (y_{B_1} - y_{C_1})^2 - b_1^2 \\ (x_{A_3} - x_{A_1})^2 + (y_{A_3} - y_{A_1})^2 - j^2 \\ (x_{A_3} - x_{O_2})^2 + (y_{A_3} - y_{O_2})^2 - d_3^2 \\ (x_{B_2} - x_{A_2})^2 + (y_{B_2} - y_{A_2})^2 - a_2^2 \\ (x_{B_2} - x_{C_2})^2 + (y_{B_2} - y_{C_2})^2 - b_2^2 \\ (x_{D_1} - x_{B_1})^2 + (y_{D_1} - y_{B_1})^2 - g_1^2 \\ (x_{D_1} - x_{C_1})^2 + (y_{D_1} - y_{C_1})^2 - i_1^2 \\ (x_{D_2} - x_{B_2})^2 + (y_{D_2} - y_{B_2})^2 - g_2^2 \\ (x_{D_2} - x_{C_2})^2 + (y_{D_2} - y_{C_2})^2 - i_2^2 \\ (x_{A_3} - x_{O_2}) - \frac{d_3}{d_2}(x_{A_2} - x_{O_2}) \\ (y_{A_3} - y_{O_2}) - \frac{d_3}{d_2}(y_{A_2} - y_{O_2}) \end{bmatrix} = \mathbf{0}, \tag{228}$$

Figure 59 – Potential energies of the balanced mechanisms: (a) mechanism i and (b) mechanism ii.

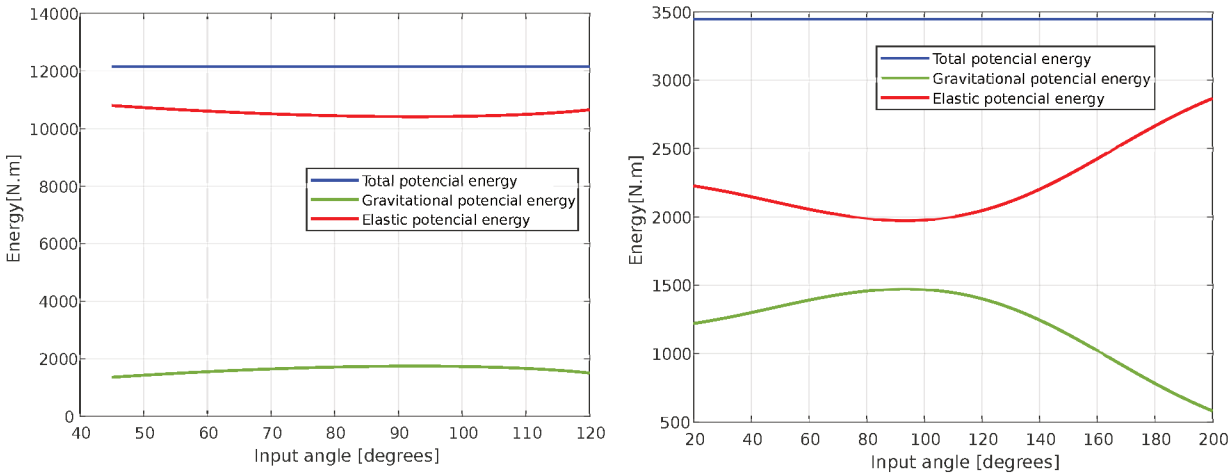

Source: The author.

Figure 60 – Balancer topology of the robot manipulator.

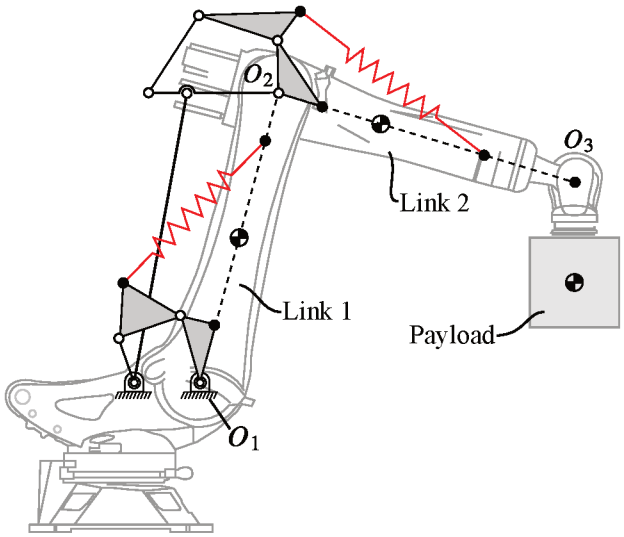

Source: Adapted from (NGUYEN, 2022).

where, the points A_2, A_3, B_1, B_2, D_1 and D_2 forms the natural coordinates vector

$$\mathbf{q} = \begin{bmatrix} \mathbf{p}_{A_2}^T & \mathbf{p}_{A_3}^T & \mathbf{p}_{B_1}^T & \mathbf{p}_{B_2}^T & \mathbf{p}_{D_1}^T & \mathbf{p}_{D_2}^T \end{bmatrix}^T. \tag{229}$$

In Equation (228), the first ten constraint equations correspond to the rigid body condition of the links, and the last two correspond to the alignment of points A_2, A_3, and O_2.

The point coordinates that define the vector $\mathbf{q}$ can be determined by using bilateration.

Figure 61 – Modeling using natural coordinates.

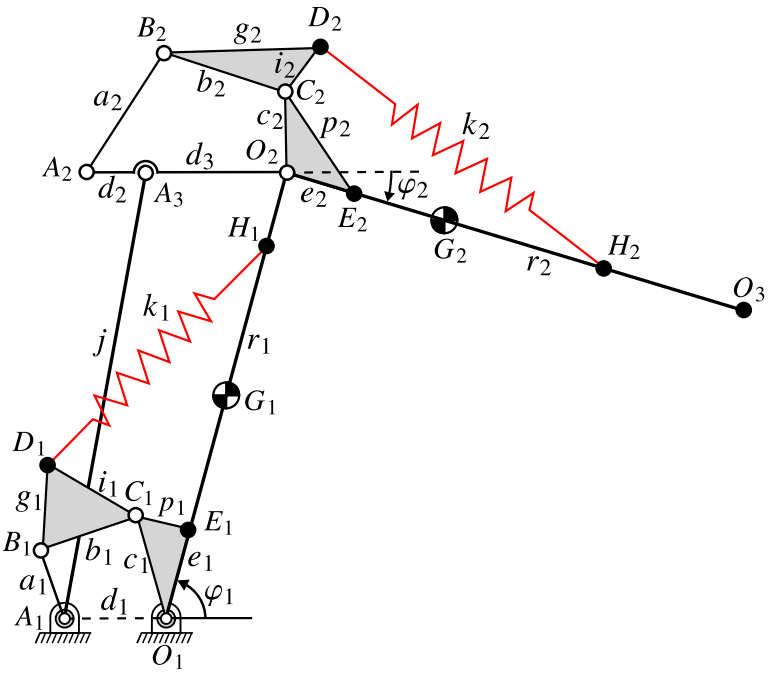

Source: The author.

Table 10 – Dimensional and mass parameters of the KUKA KR 210 R3100 robot (NGUYEN, 2022, 2021).

Parameters	Value	Unit
r_1	1.35	[m]
r_2	1.4	[m]
$\bar{r}_1$	0.525	[m]
$\bar{r}_2$	0.482	[m]
m_1	349	[kg]
m_2	324	[kg]
m_3	30	[kg]

Source: The author.

To this let us define the unit vectors

$$\mathbf{u}_{O_1O_2} = \begin{bmatrix} \cos\varphi_1 \\ \sin\varphi_1 \end{bmatrix}, \tag{230}$$

$$\mathbf{u}_{O_2O_3} = \begin{bmatrix} \cos\varphi_2 \\ \sin\varphi_2 \end{bmatrix}, \tag{231}$$

then, the coordinate points O_2, O_3, E_1, E_2, H_1, and H_2 are computed as

$$\mathbf{p}_{O_2} = \mathbf{p}_{O_1} + r_1\mathbf{u}_{O_1O_2}\,, \qquad \mathbf{p}_{O_3} = \mathbf{p}_{O_2} + r_2\mathbf{u}_{O_2O_3}\,,$$
$$\mathbf{p}_{E_1} = \mathbf{p}_{O_1} + e_1\mathbf{u}_{O_1O_2}\,, \qquad \mathbf{p}_{E_2} = \mathbf{p}_{O_2} + e_2\mathbf{u}_{O_2O_3}\,,$$
$$\mathbf{p}_{H_1} = \mathbf{p}_{O_1} + h_1\mathbf{u}_{O_1O_2}\,, \qquad \mathbf{p}_{H_2} = \mathbf{p}_{O_2} + h_2\mathbf{u}_{O_2O_3}\,,$$

and the rest of points are determined using bilateration as follows

$$\begin{aligned}
\mathbf{p}_{C_1} &= \mathbf{p}_{O_1} + \mathbf{N}_{O_1E_1C_1}(\mathbf{p}_{E_1} - \mathbf{p}_{O_1}),\\
\mathbf{p}_{A_2} &= \mathbf{p}_{O_2} + \left(\frac{d_2}{d_3}\right)(\mathbf{p}_{A_3} - \mathbf{p}_{O_2}),\\
\mathbf{p}_{B_1} &= \mathbf{p}_{A_1} + \mathbf{N}_{A_1C_1B_1}(\mathbf{p}_{C_1} - \mathbf{p}_{A_1}),\\
\mathbf{p}_{C_2} &= \mathbf{p}_{O_2} + \mathbf{N}_{O_2E_2C_2}(\mathbf{p}_{E_2} - \mathbf{p}_{O_2}),\\
\mathbf{p}_{D_1} &= \mathbf{p}_{B_1} + \mathbf{N}_{B_1C_1D_1}(\mathbf{p}_{C_1} - \mathbf{p}_{B_1}),\\
\mathbf{p}_{B_2} &= \mathbf{p}_{A_2} + \mathbf{N}_{A_2C_2B_2}(\mathbf{p}_{C_2} - \mathbf{p}_{A_2}),\\
\mathbf{p}_{A_3} &= \mathbf{p}_{O_2} + \mathbf{N}_{A_1O_2A_3}(\mathbf{p}_{O_2} - \mathbf{p}_{A_1}),\\
\mathbf{p}_{D_2} &= \mathbf{p}_{B_2} + \mathbf{N}_{B_2C_2D_2}(\mathbf{p}_{C_2} - \mathbf{p}_{B_2}),
\end{aligned}$$

where, the bilateration matrix $\mathbf{N}_{IJK}$ is computed as in Equation (212).

The centers of gravity G_1, G_2 ..., can be computed without much difficulty once the natural coordinates are known.

5.5.2 Static analysis

Figure 62 depicts the couplings and actions diagram. Actions and fundamental cutsets graph is shown in Figure 63, where black arrows represent internal forces, gravity forces are drawn in green color, the spring forces are represented by red arrows and the actuators are drawn in fuchsia color.

The fundamental cutset matrix $\mathbf{Q}_A$ of action graph G_A and the unit action matrix $\hat{\mathbf{A}}_D$ are obtained from the actions and coupling graph schematic, see Figure 62. Applying Equation (197) it is obtained a 24×24 linear system

$$\left[{}^{r}\hat{\mathbf{A}}_N\right]_{24\times24}\begin{bmatrix} {}^{i}\boldsymbol{\Psi} \\ {}^{a}\boldsymbol{\Psi} \end{bmatrix}_{24\times1} = -\left[{}^{e}\hat{\mathbf{A}}_N\right]_{24\times13}\left[{}^{e}\boldsymbol{\Psi}\right]_{13\times1}\,, \tag{232}$$

where, the actuation forces vector is composed as

$${}^{a}\boldsymbol{\Psi} = \begin{bmatrix} \tau_{o_1} \\ \tau_{o_2} \end{bmatrix},$$

and the internal forces vector is

$$
{}^{i}\boldsymbol{\Psi} = \begin{bmatrix} f_{a_{1x}} & f_{a_{1y}} & f_{a'_{1x}} & f_{a'_{1y}} & f_{a_{2x}} & f_{a_{2y}} & f_{a_{3x}} & f_{a_{3y}} & f_{b_{1x}} \\ f_{b_{1y}} & f_{b_{2x}} & f_{b_{2y}} & f_{c_{1x}} & f_{c_{1y}} & f_{c_{2x}} & f_{c_{2y}} & f_{o_{1x}} & f_{o_{1y}} & f_{o_{2x}} & f_{o_{2y}} \\ & & & & & & & & & f_{o'_{2x}} & f_{o'_{2y}} \end{bmatrix}^{T}.
$$

Figure 62 – Schematic representation of couplings and actions: (a) internal and external actions and (b) directed coupling graph.

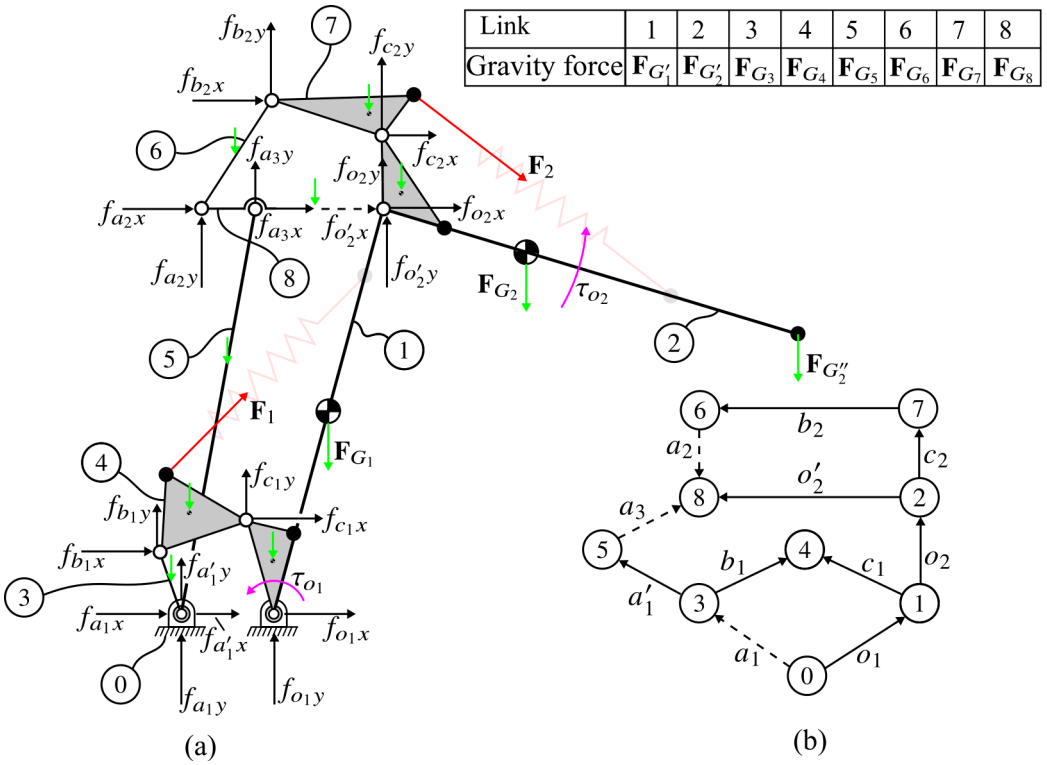

Source: The author

5.5.3 Optimization problem formulation

This example is substantially more complicated than the previous one since the dimensions of the mechanism are also design variables. The masses of the links of the mechanism are previously defined to simplify the optimization problem. Then the vector of design variables is defined as:

$$
\mathbf{z} = \begin{bmatrix} k_1 & k_2 & {}^{0}l_1 & {}^{0}l_2 & a_1 & a_2 & b_1 & b_2 & c_1 & c_2 & d_1 & d_2 & d_3 & e_1 & e_2 \\ g_1 & g_2 & h_1 & h_2 & i_1 & i_2 & j & p_1 & p_2 \end{bmatrix}^{T}.
$$

Figure 63 – Actions and fundamental cutsets graph G_A.

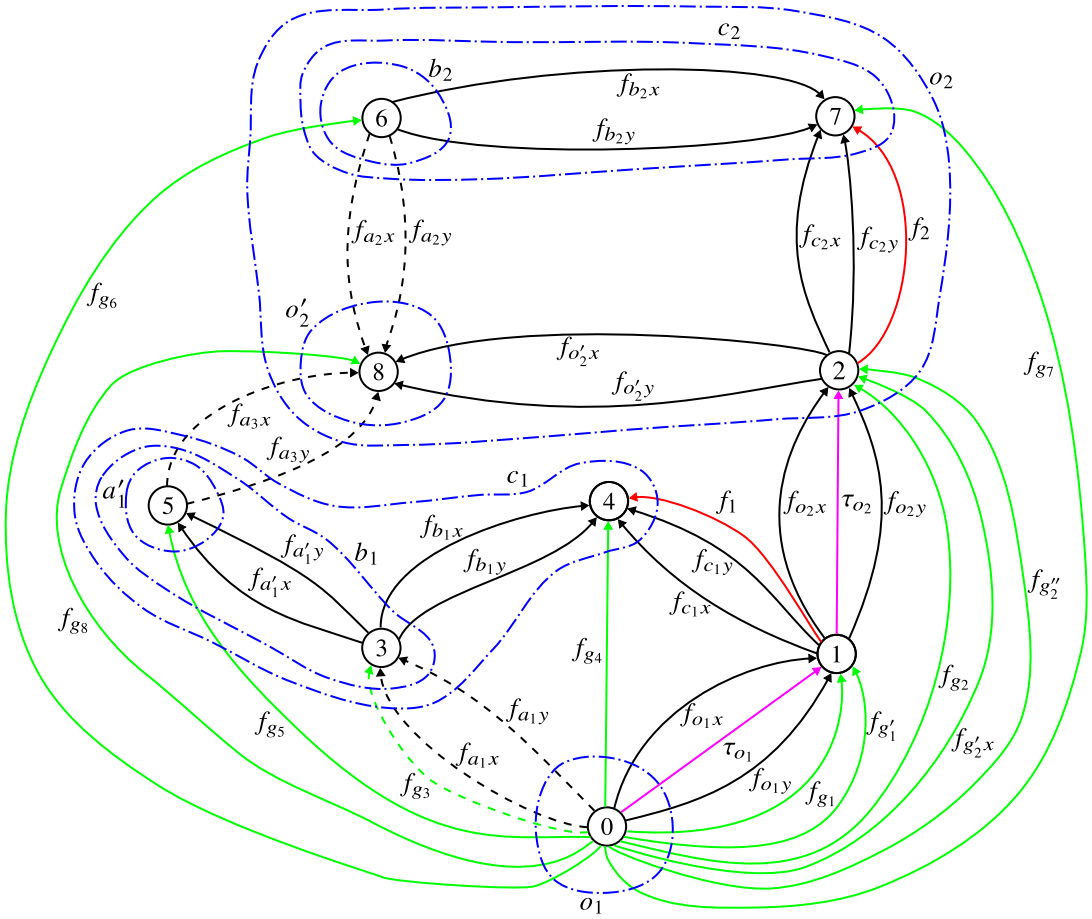

Source: The author.

Assembly of the mechanism may not be physically possible during the optimization process. Therefore, it is necessary to formulate constraints in order to avoid this type of problem. The distances sets: $\{c_1, e_1, p_1\}$, $\{b_1, g_1, i_1\}$, $\{c_2, e_2, p_2\}$, $\{b_2, g_2, i_2\}$, $\{a_1, b_1, d_{A_1C_1}\}$, $\{d_3, j, d_{A_1O_2}\}$, $\{a_2, b_2, d_{A_2C_2}\}$ must satisfy the triangle inequality that can be written in compact form as

$$\mathbf{g}_j(\mathbf{q}, \mathbf{z}) = \begin{bmatrix} (c_1 - e_1 + p_1)(c_1 + e_1 - p_1)(c_1 - e_1 - p_1) \\ (b_1 - g_1 + i_1)(b_1 + g_1 - i_1)(b_1 - g_1 - i_1) \\ (c_2 - e_2 + p_2)(c_2 + e_2 - p_2)(c_2 - e_2 - p_2) \\ (b_2 - g_2 + i_2)(b_2 + g_2 - i_2)(b_2 - g_2 - i_2) \\ (a_1 - b_1 + d_{A_1C_1})(a_1 + b_1 - d_{A_1C_1})(a_1 - b_1 - d_{A_1C_1}) \\ (d_3 - j + d_{A_1O_2})(d_3 + j - d_{A_1O_2})(d_3 - j - d_{A_1O_2}) \\ (a_2 - b_2 + d_{A_2C_2})(a_2 + b_2 - d_{A_2C_2})(a_2 - b_2 - d_{A_2C_2}) \end{bmatrix} \leq \mathbf{0}, \tag{233}$$

then, the optimization problem is formulated as

$$\begin{aligned} \underset{\mathbf{z}}{\text{minimize}} \quad & f(\mathbf{z}) = \frac{1}{2}\sum_{j=1}^{n} {}^{a}\boldsymbol{\Psi}_j^{T}\,{}^{a}\boldsymbol{\Psi}_j \,, \\ \text{subject to} \quad & \mathbf{g}_j(\mathbf{q},\mathbf{z}) \leq \mathbf{0} \,, \\ & \underline{\mathbf{z}} \leq \mathbf{z} \leq \bar{\mathbf{z}} \,, \\ \text{while solving} \quad & \begin{cases} \boldsymbol{\Phi}(\mathbf{q},\mathbf{z}) = \mathbf{0}; \quad \text{Eq.(228)} \\ {}^{r}\hat{\mathbf{A}}_N(\mathbf{q},\mathbf{z})\,{}^{r}\boldsymbol{\Psi}_j = -{}^{e}\hat{\mathbf{A}}_N(\mathbf{q},\mathbf{z})\,{}^{e}\boldsymbol{\Psi}_j \quad \text{Eq.(232).} \end{cases} \end{aligned} \tag{234}$$

5.5.4 Implementation and results

Table 11 shows the optimization parameters and the optimal values of the variables. Figure 64(a) shows the initial mechanism, and Figure 64(b) shows the optimized robot. Figure 65 shows the evolution of the objective function, and Figure 66(a) and Figure 66(b) show the actuators' torques in the unbalanced robot's shoulder and elbow. Figure 66(c) and Figure 66(d) show the torques of the balanced robot, and finally, Figure 67 shows the gravitational potential energy, elastic potential energy and total potential energy. The maximum actuation torque was considerably reduced from 8405[Nm] to 343.24[Nm], corresponding to a reduction of approximately 95.9%. Note that the torque range of the unbalanced robot goes from 0 to 10000 Nm and from 800 to 2000 Nm at the shoulder and elbow, respectively, and the torque range of the balanced robot goes from -400 to 200 Nm and from -200 to 200 Nm at the shoulder and elbow respectively.

Table 11 – Optimization parameters and solution of the balancing of the KUKA KR 210 R3100 robot.

z	$\mathbf{z}_0$	$\underline{\mathbf{z}}$	$\bar{\mathbf{z}}$	**Optimal z**	**z**	$\mathbf{z}_0$	$\underline{\mathbf{z}}$	$\bar{\mathbf{z}}$	**Optimal z**
k_1 [Nm]	600000	0	700000	600230.294658	d_3 [m]	0.551	0	0.8	0.505922
k_2 [Nm]	200000	0	700000	200253.348435	e_1 [m]	0.5	0	0.8	0.768402
${}^{0}l_1$ [m]	0.1	0	1	0.539316	e_2 [m]	0.5	0	0.8	0.381746
${}^{0}l_2$ [m]	0.1	0	1	0.950349	g_1 [m]	0.4	0	0.8	0.798099
a_1 [m]	0.5	0	0.8	0.795314	g_2 [m]	0.4	0	0.8	0.184379
a_2 [m]	0.5	0	0.8	0.746580	h_1 [m]	1	0.5	1.35	0.500382
b_1 [m]	0.5	0	0.8	0.799549	h_2 [m]	1	0.5	1.4	1.060447
b_2 [m]	0.5	0	0.8	0.65854	i_1 [m]	0.4	0	0.8	0.77282
c_1 [m]	0.5	0	0.8	0.378685	i_2 [m]	0.4	0	0.8	0.70796
c_2 [m]	0.25	0	0.8	0.543282	j [m]	1.35	2.5	0.5	1.451492
d_1 [m]	0.4	0	0.7	0.571242	p_1 [m]	0.25	0	0.8	0.389718
d_2 [m]	0.7	0	0.8	0.126921	p_2 [m]	0.5	0	0.8	0.198751

Source: The author.

Figure 64 – Optimization results: (a) initial mechanism and (b) optimal mechanism.

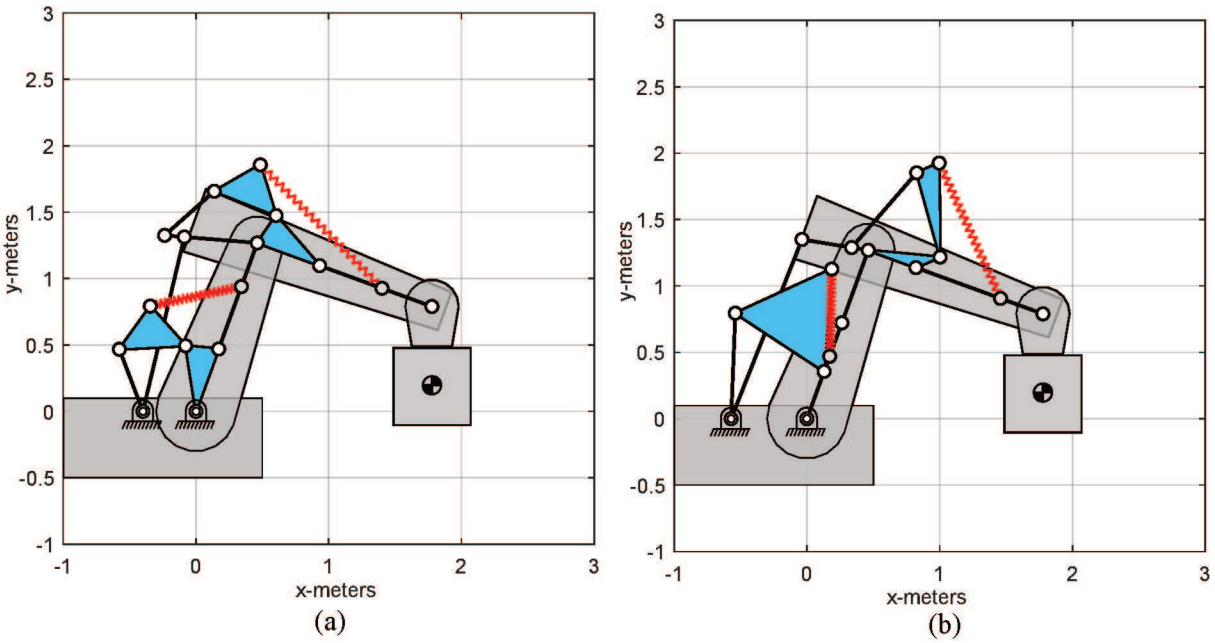

Source: The author.

Figure 65 – Convergence of the objective function.

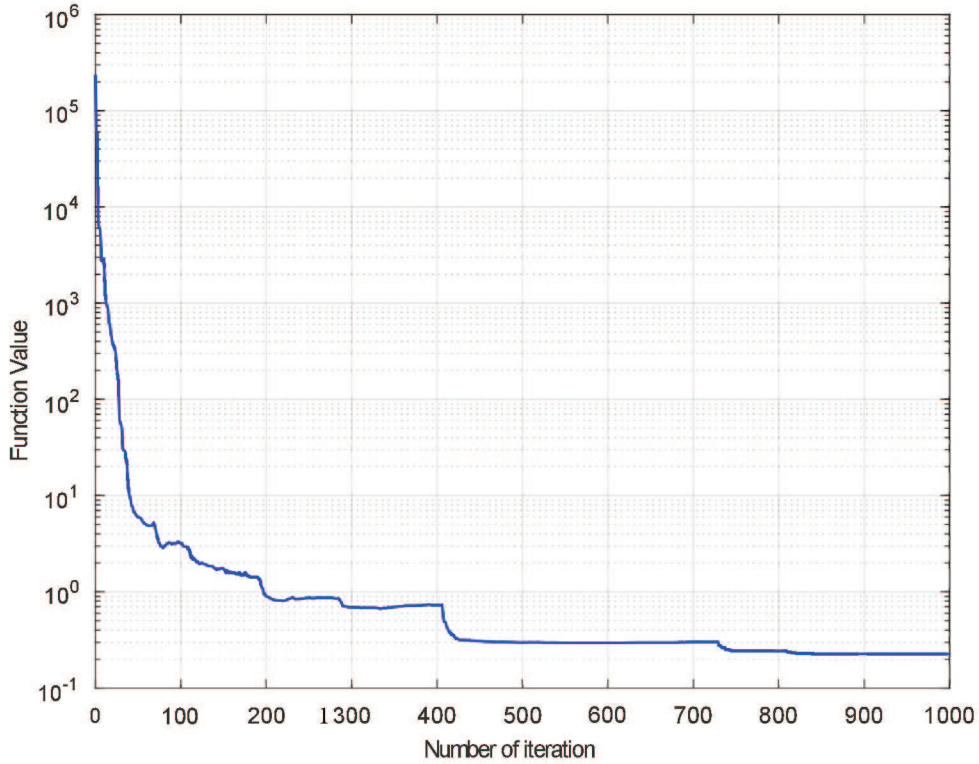

Source: The author.

Figure 66 – Actuator torques: (a) unbalanced torque at shoulder joint, (b) unbalanced a torque at elbow joint, (c) balanced torque at shoulder joint, and (d) balanced a torque at elbow joint.

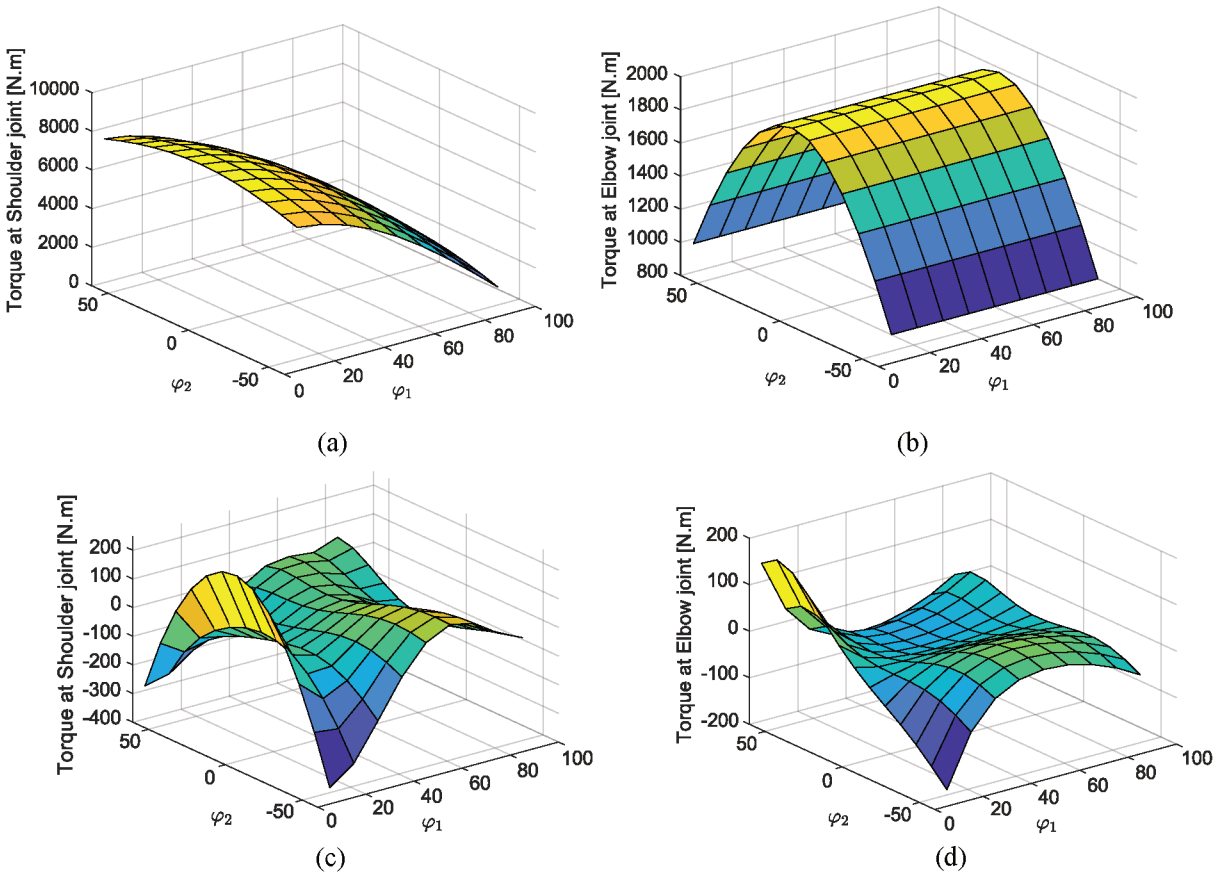

Source: The author.

Figure 67 – Potential energies of the balanced robot.

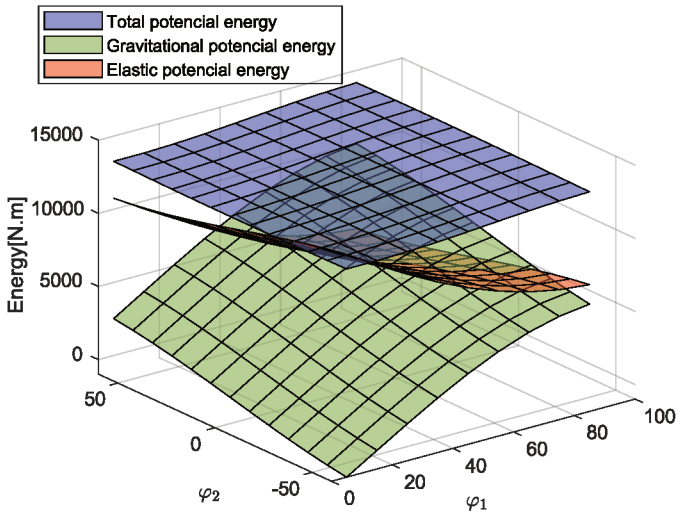

Source: The author.

6 EQUIMOMENTAL SYSTEMS REPRESENTATIONS OF POINT-MASSES OF PLANAR RIGID-BODIES

Equimomental point-mass systems facilitate the definition of the inertial properties of a rigid body and simplify the dynamic analysis of mechanisms and machines. In this work, the equimomental systems of three point-masses of planar rigid bodies are investigated using the concept of pseudo-inertia matrix. It is found that given a planar rigid body, it is always possible to determine an equimomental system of three equal masses located at the vertices of an isosceles triangle. A procedure is presented to determine equimomental systems with different masses, guaranteeing that the masses are positive. It is shown that it is always possible to choose an equimomental system of three point-masses located at the vertices of an isosceles triangle with a prescribed position of one mass. The conditions for prescribing the position of two and three point-masses are also investigated. A first idealized example shows the step-by-step procedure for determining an equimomental system of three point-masses of a planar rigid body. The proposed model is applied to a symmetric connecting rod in a second example due to its wide use in combustion engines. A third example shows an equimomental system of an asymmetric bucket of an excavator.

6.1 EQUIMOMENTAL SYSTEMS

A three-dimensional rigid body can always be modeled by a dynamically equivalent system of four rigidly connected point masses (SEYFERTH, 1974). However, in the case of planar rigid bodies, it is always possible to construct a dynamically equivalent system with a three point-mass (SOMMERVILLE, 1930). These systems having the same dynamic behavior are known as equimomental systems (SELIG, J. M., 2015). Wenglarz et al. (WENGLARZ; FOGARASY; MAUNDER, 1969) and Haung (HUANG, 1993) introduce the concept of equimomental systems. Equimomental systems help to define the inertial properties of rigid bodies and determine shaking forces, shaking moments, and input torques of mechanical systems (CHAUDHARY; SAHA, 2009; ROUTH, E. J., 1905). Laus and Selig (LAUS; SELIG, 2020) show formal proof of the existence of four point-mass equimomental to a given three-dimensional rigid body. The authors developed analytical expressions to determine the possible location and values of the masses using modern methods. They also derived the equation of motion based on the screw theory of a rigid body in space. Similarly, in Chica et al. (CHICA; POLO; MOLINA, 2014), the same result is derived in a more current language. The authors state that this important property seems to be forgotten, and up to the publication date of this paper, they had not found an appropriate demonstration.

Chaudhary and collaborators have extensively studied the equimomental systems of planar rigid bodies (CHAUDHARY; SAHA, 2007, 2008, 2009; CHAUDHARY; CHAUDHARY, 2014a, 2015). In the proposed models, it cannot be assured that the masses are always positive. However, this is not an obstacle for the rigid body representation process as long as the total mass and

the moment of inertia about the center of mass give positive values (SHERWOOD; HOCKEY, 1969). Jan de Jong et al. (JONG; DIJK; HERDER, 2017) propose a method to determine planar equimomental mechanisms through an inertia decomposition method. This method avoids infeasible solutions using constraints on the model parameters. The main disadvantage of this procedure is that it cannot be applied to mechanisms with more than one loop or to the mechanism where there are bodies connected with prismatic pairs. Gössner (GÖSSNER, 2021) proposes an equimomental model of point masses located at the vertices of a polygon. The author believes that this polygonal system approach is new to the best of his knowledge. Future work can focus on the negative masses that occur here and their avoidance.

Equimomental point-mass systems are especially advantageous in the dynamic balancing of mechanisms and machines (CHAUDHARY; SAHA, 2006; GUPTA; SAHA; CHAUDHARY, 2019), in the minimization of constraint forces and actuation moments (KUMANI; CHAUDHARY, 2018; GUPTA; CHAUDHARY; SAHA, 2015). Here, the equations of the dynamic model are greatly simplified and also allow a reduced use of design parameters. An interesting application of equimomental systems in the field of biophysics is shown in Fábián et al. (FÁBIÁN; THALLMAIR; HUMMER, 2022), where a simulation of the molecular dynamics of cholesterol is performed. The authors claim that with an equimomental arrangement, the convergence of the binding constraint is accelerated while preserving the original force field and the dynamics of cholesterol.

Another possible and interesting application of point-masses equimomental systems is dynamic synthesis, which consists of determining the shape of a body given inertial properties and some restrictions on the body's form and maximum allowable stresses (TISCHLER et al., 2000). Unfortunately, nowadays, dynamics is studied from the analytical point of view without a synthetic branch in the same way as in statics. Therefore, in inherently dynamic problems, a quasi-static behavior is assumed (SELIG; MARTINS, 2014).

The discussion of equimomental systems of point masses dates back to the 19th century (ROUTH, E., 1897). However, nowadays, few researchers have taken this approach despite its advantages in the dynamic analysis of mechanisms and machines. Laus and Selig (LAUS; SIMAS; MARTINS, 2020) have made significant advances in the case of three-dimensional rigid bodies, although the models developed have not yet been adapted to planar rigid bodies. These are the main reasons that motivated the realization of the present work, besides trying to simplify the dynamic analysis of mechanisms and machines.

Next, a study on the equimomental systems of point masses of a planar rigid body is presented. Using the formalism of the pseudo-inertia matrix, an equimomental system of three equal point masses always forms an isosceles triangle. If the radii of gyration are equal, the triangle formed by the three masses is equilateral; these results are stated as a theorem and a corollary with their respective proof. A procedure is also shown to determine equimomental systems with three different masses and always guarantee positive masses. Then a theorem on the possibility of prescribing the position of one of the point masses is shown, and the conditions

for prescribing the position of two and three masses are established. By means of a numerical example, the step-by-step procedure for determining a three-mass system equimomental to a planar rigid body is shown. An example is also shown where the results found are applied to determine an equimomental system of a symmetric connecting rod. Finally, in a third example, an equimomental system of three point-masses of an asymmetric plane rigid body is determined.

6.2 INERTIA MATRIX

Two rigid bodies are called equimomental if they have the same inertial properties; in other words, two equimomental bodies have the same mass, their centers of mass coincide, and their inertia matrices are equal with respect to a fixed coordinate system (SELIG, J. M., 2015). One of the ways to combine the inertial properties in a single matrix is through the *homogeneous plane-distance inertia matrix*, commonly known in a rather loose way as the *pseudo-inertia matrix*. The pseudo-inertia matrix appears naturally when determining mean-squared distance of a rigid body to a plane, as presented in Selig and Martins (SELIG; MARTINS, 2014).

The pseudo-inertia matrix of a body B is defined as:

$$\widetilde{\boldsymbol{\Xi}} = \int_B \widetilde{\mathbf{p}}\widetilde{\mathbf{p}}^T \, dm = \begin{bmatrix} \int_B x^2 \, dm & \int_B xy \, dm & \int_B xz \, dm & \int_B x \, dm \\ \int_B xy \, dm & \int_B y^2 \, dm & \int_B yz \, dm & \int_B y \, dm \\ \int_B xz \, dm & \int_B yz \, dm & \int_B z^2 \, dm & \int_B z \, dm \\ \int_B x \, dm & \int_B y \, dm & \int_B z \, dm & \int_B dm \end{bmatrix}, \tag{235}$$

where, $\widetilde{\mathbf{p}} = \begin{bmatrix} x & y & z & 1 \end{bmatrix}^T$ is the homogeneous position vector. Given the following definitions

$$\begin{aligned} I_{xx} &= \int_B (y^2 + z^2) \, dm & I_{xy} &= -\int_B xy \, dm & mx_C &= \int_B x \, dm \\ I_{yy} &= \int_B (x^2 + z^2) \, dm & I_{xz} &= -\int_B xz \, dm & my_C &= \int_B y \, dm \\ I_{zz} &= \int_B (x^2 + y^2) \, dm & I_{yz} &= -\int_B yz \, dm & mz_C &= \int_B z \, dm \end{aligned}$$

where, m is the mass of the body; I_{ij} corresponds to the elements of the traditional 3×3 inertia matrix $\mathbf{I}$ and x_C, y_C, z_C are the center of mass coordinates. Then, the pseudo-inertia matrix can be expanded to

$$\widetilde{\boldsymbol{\Xi}} = \begin{bmatrix} \frac{1}{2}\left(-I_{xx} + I_{yy} + I_{zz}\right) & -I_{xy} & -I_{xz} & mx_C \\ -I_{xy} & \frac{1}{2}\left(I_{xx} - I_{yy} + I_{zz}\right) & -I_{yz} & my_C \\ -I_{xz} & -I_{yz} & \frac{1}{2}\left(I_{xx} + I_{yy} - I_{zz}\right) & mz_C \\ mx_C & my_C & mz_C & m \end{bmatrix}, \tag{236}$$

since

$$\int_B x^2\,dm = \frac{1}{2}\int_B -(y^2+z^2)+(x^2+z^2)+(x^2+y^2)\,dm\,,$$
$$\int_B y^2\,dm = \frac{1}{2}\int_B (y^2+z^2)-(x^2+z^2)+(x^2+y^2)\,dm\,,$$
$$\int_B z^2\,dm = \frac{1}{2}\int_B (y^2+z^2)+(x^2+z^2)-(x^2+y^2)\,dm\,.$$

Laus and Selig (LAUS; SELIG, 2020) argue that this matrix is a unique property and two bodies will be equimomental if and only if they have the same homogeneous matrix. In a planar rigid body, the pseudo-inertia matrix Equation (236) loses the third row and the third column as the points of the body are constrained in the xy plane i.e. $z = 0$. Then, the pseudo-inertia matrix becomes

$$\widetilde{\boldsymbol{\Xi}} = \begin{bmatrix} \frac{1}{2}\left(-I_{xx}+I_{yy}+I_{zz}\right) & -I_{xy} & mx_C \\ -I_{xy} & \frac{1}{2}\left(I_{xx}-I_{yy}+I_{zz}\right) & my_C \\ mx_C & my_C & m \end{bmatrix}, \tag{237}$$

The pseudo-inertia matrix of planar body represented by n point-masses can be written as

$$\widetilde{\boldsymbol{\Xi}} = \sum_{i=1}^{n} m_i \widetilde{\mathbf{p}}_i \widetilde{\mathbf{p}}_i^T, \tag{238}$$

where, m_i is i-th point-mass, and $\widetilde{\mathbf{p}}_i$ is the homogeneous extended position vector of point $\mathbf{p}_i$ and has the form $\widetilde{\mathbf{p}}_i = \begin{bmatrix} x_i & y_i & 1 \end{bmatrix}^T$. The rigid transformation can be performing by standard homogeneous representation

$$\widetilde{\boldsymbol{\Xi}}' = \mathbf{G}\widetilde{\boldsymbol{\Xi}}\mathbf{G}^T \tag{239}$$

where, $\mathbf{G}$ is a homogeneous transformation matrix of the form

$$\mathbf{G} = \begin{bmatrix} \mathbf{R} & \mathbf{t} \\ 0 & 1 \end{bmatrix}, \tag{240}$$

with $\mathbf{R}$ the 2×2 rotation matrix and $\mathbf{t}$ its translation vector (SELIG, J. M., 2015).

The following section presents a procedure to determine a system of three equal point masses by scaling an equilateral triangle.

6.3 EQUIMOMENTAL SYSTEM WITH EQUAL POINT-MASSES

It is a classical theorem that there exists a translation that locates the center of mass at the origin of coordinates and a rotation that aligns the coordinate axes with the principal directions of inertia. That is, there is a homogeneous transformation $\mathbf{G}$ that diagonalizes a given pseudo-inertia matrix $\widetilde{\boldsymbol{\Xi}}'$. So the pseudo-inertia matrix can be written as

$$\widetilde{\boldsymbol{\Xi}} = \mathbf{G}\widetilde{\boldsymbol{\Xi}}'\mathbf{G}^{\mathrm{T}} = m\,\mathrm{diag}\left(a^2, b^2, 1\right)\,, \tag{241}$$

where a, b, are the gyration radii of the original system. The conditions for three points of equal masses to form an equimomental system will be deduced next.

We look for convenient canonical points $\widetilde{\mathbf{q}}_i$ that satisfy

$$\sum_{i=1}^{3} \tilde{\mathbf{q}}_i \tilde{\mathbf{q}}_i^T = 3\mathbf{I}_3. \tag{242}$$

These points $\widetilde{\mathbf{q}}_i$ can be scaled by the diagonal matrix $\widetilde{\mathbf{D}} = \text{diag}(a, b, 1)$, then the points $\widetilde{\mathbf{p}}_i = \widetilde{\mathbf{D}}\widetilde{\mathbf{q}}_i$ are an equimomental system since

$$\frac{m}{3}\sum_{i=1}^{3} \tilde{\mathbf{p}}_i \tilde{\mathbf{p}}_i^T = \frac{m}{3}\sum_{i=1}^{3} \widetilde{\mathbf{D}}\tilde{\mathbf{q}}_i \tilde{\mathbf{q}}_i^T \widetilde{\mathbf{D}}^{\mathrm{T}} = m\,\text{diag}\left(a^2, b^2, 1\right)$$

Consider three point-masses located at triangle's vertices $\mathbf{q}_1$, $\mathbf{q}_2$, and $\mathbf{q}_3$, see Figure 68. Following Equation (242), the extended vectors satisfy the following conditions

$$\tilde{\mathbf{q}}_i^T \tilde{\mathbf{q}}_j = 0 \text{ when } i \neq j\,, \tag{243}$$

$$\tilde{\mathbf{q}}_i^T \tilde{\mathbf{q}}_i = 3 \text{ for } i = 1, \ldots, 3\,. \tag{244}$$

Figure 68 – Three point-masses located at triangle's vertices.

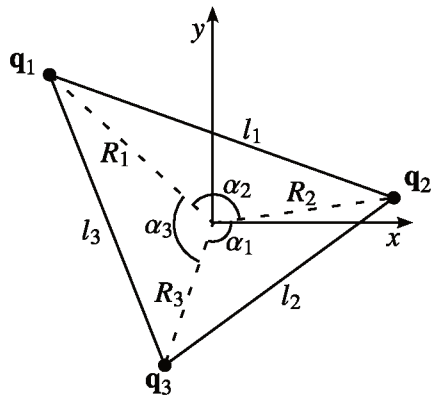

Source: The author.

As a consequence of the above relationships, it will be shown that $\sum_{i=1}^{3} \tilde{\mathbf{q}}_i \tilde{\mathbf{q}}_i^T = 3\mathbf{I}_3$ is satisfied. This will then be used to derive an equimomental system of three-point masses of a given planar rigid body. The first condition, Equation (243), yields the following constraint equations

$$\begin{aligned} x_1 x_2 + y_1 y_2 + 1 &= 0 \\ x_1 x_3 + y_1 y_3 + 1 &= 0 \end{aligned} \tag{245}$$

$$x_2x_3 + y_2y_3 + 1 = 0$$

and the second condition, Equation (244), yields

$$\begin{aligned} x_1^2 + y_1^2 &= 2 \\ x_2^2 + y_2^2 &= 2 \\ x_3^2 + y_3^2 &= 2 \end{aligned} \tag{246}$$

The three constraints in Equation (246) represent circles with radius $R_i = R = \sqrt{2}$ for $i = 1,2,3$. The three constraints in Equation (245) guarantee that the triangle is equilateral, since $\mathbf{q}_i^T\mathbf{q}_j^T + 1 = 0$ with $i \neq j$ that is $(\sqrt{2})(\sqrt{2})\cos\alpha_i + 1 = 0$ then $\alpha_i = 2\pi/3$, and $l_i = l$ for $i = 1,2,3$. The radius R and the length of the sides of the equilateral triangle l are related by the equation $R = l/\sqrt{3}$, then $l = \sqrt{6}$. Let us locate the equilateral triangle in an arbitrary orientation, as illustrated in Figure 69(a). Where the homogeneous extended position vector of triangle's vertices can be written as

Figure 69 – Equilateral triangle: (a) arbitrary orientation, and (b) symmetrical to y-coordinate axis.

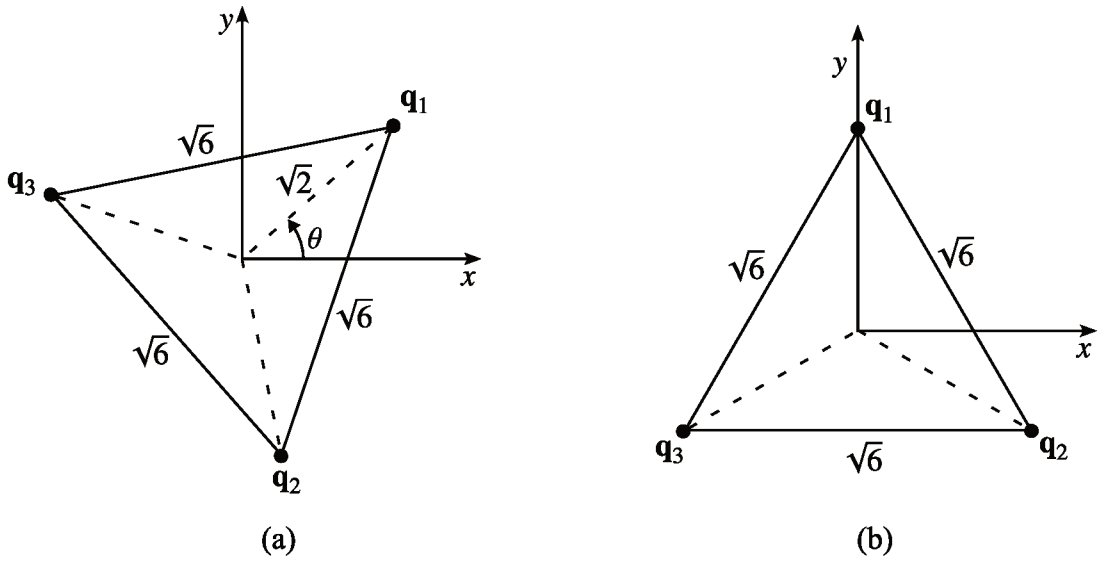

Source: The author.

$$\widetilde{\mathbf{q}}_1 = \begin{bmatrix} \sqrt{2}\cos\theta \\ \sqrt{2}\sin\theta \\ 1 \end{bmatrix}, \widetilde{\mathbf{q}}_2 = \begin{bmatrix} -\frac{\sqrt{2}}{2}\cos\theta + \frac{\sqrt{6}}{2}\sin\theta \\ -\frac{\sqrt{2}}{2}\sin\theta - \frac{\sqrt{6}}{2}\cos\theta \\ 1 \end{bmatrix}, \widetilde{\mathbf{q}}_3 = \begin{bmatrix} -\frac{\sqrt{2}}{2}\cos\theta - \frac{\sqrt{6}}{2}\sin\theta \\ -\frac{\sqrt{2}}{2}\sin\theta + \frac{\sqrt{6}}{2}\cos\theta \\ 1 \end{bmatrix}, \tag{247}$$

this homogeneous extended position vector satisfy

$$\sum_{i=1}^{3} \tilde{\mathbf{q}}_i\tilde{\mathbf{q}}_i^T = 3\mathbf{I}_3\,, \tag{248}$$

where, $\mathbf{I}_3$ is a 3×3 identity matrix.

Theorem 1 *Any planar rigid body is equimomental to a system of three equal point masses located at the vertices of an isosceles triangle.*

Proof. To facilitate calculations and without loss of generality, let us set the triangle's orientation to $\theta = \pi/2$, which means that the triangle in the new orientation is symmetric with respect to the y-coordinate axis, see Figure 69. Then, replacing $\theta = \pi/2$ in the extended position vectors Equation (247) yields,

$$\widetilde{\mathbf{q}}_1 = \begin{bmatrix} 0 \\ \sqrt{2} \\ 1 \end{bmatrix}, \quad \widetilde{\mathbf{q}}_2 = \begin{bmatrix} \frac{\sqrt{6}}{2} \\ -\frac{\sqrt{2}}{2} \\ 1 \end{bmatrix}, \quad \text{and} \quad \widetilde{\mathbf{q}}_3 = \begin{bmatrix} -\frac{\sqrt{6}}{2} \\ -\frac{\sqrt{2}}{2} \\ 1 \end{bmatrix}. \tag{249}$$

Using the transformation shown in Equation (239), it is always possible to find a transformation $\mathbf{G}$ that converts the pseudo-inertia matrix into a diagonal matrix of the form $\widetilde{\boldsymbol{\Xi}} = m\,\mathrm{diag}\left(a^2, b^2, 1\right)$. The points in Equation (249) can be moved using a non-rigid transformation $\widetilde{\mathbf{D}} = \mathrm{diag}(a, b, 1)$ so that the extended position vectors of the points become $\tilde{\mathbf{p}}_i = \widetilde{\mathbf{D}}\tilde{\mathbf{q}}_i$,

$$\widetilde{\mathbf{p}}_1 = \begin{bmatrix} 0 \\ \sqrt{2}b \\ 1 \end{bmatrix}, \quad \widetilde{\mathbf{p}}_2 = \begin{bmatrix} \frac{\sqrt{6}}{2}a \\ -\frac{\sqrt{2}}{2}b \\ 1 \end{bmatrix}, \quad \text{and} \quad \widetilde{\mathbf{p}}_3 = \begin{bmatrix} -\frac{\sqrt{6}}{2}a \\ -\frac{\sqrt{2}}{2}b \\ 1 \end{bmatrix}$$

Placing three equal masses $m/3$ at these points produces a system with the required inertia matrix,

$$\frac{m}{3}\sum_{i=1}^{3} \tilde{\mathbf{p}}_i \tilde{\mathbf{p}}_i^T = \frac{m}{3}\sum_{i=1}^{3} \widetilde{\mathbf{D}}\tilde{\mathbf{q}}_i \tilde{\mathbf{q}}_i^T \widetilde{\mathbf{D}}^{\mathrm{T}} = m\widetilde{\mathbf{D}}\mathbf{I}_3\widetilde{\mathbf{D}}^T = \widetilde{\boldsymbol{\Xi}}\,. \tag{250}$$

Then, all plane rigid body is equimomental to three equal points-masses, located at the vertices of a triangle, which are obtained by deforming the equilateral triangle by the transformation $\widetilde{\mathbf{D}} = \mathrm{diag}(a, b, 1)$; moreover, this triangle is isosceles since $\|\mathbf{p}_{12}\|^2 = 3(a^2+3b^2)/2$, $\|\mathbf{p}_{13}\|^2 = 3(a^2 + 3b^2)/2$, and $\|\mathbf{p}_{23}\|^2 = 6a^2$ as shown in Figure 70.

□

Corollary 1 *If a planar rigid body with inertia matrix $\widetilde{\boldsymbol{\Xi}} = m\,\mathrm{diag}\left(a^2, b^2, 1\right)$ respect to a reference frame with origin at the center of mass and coordinate axes coincident with the principal axes, where $a = b$, then the rigid body is equimomental to a system of three equal point masses located at the vertices of an equilateral triangle*

Proof. The system of three-point masses is equimomental to the planar rigid body with inertia matrix $\widetilde{\boldsymbol{\Xi}} = m\,\mathrm{diag}\left(a^2, b^2, 1\right)$, as shown in Equation (250). Furthermore, if $a = b$, then $\|\mathbf{p}_{12}\|^2 = \|\mathbf{p}_{13}\|^2 = \|\mathbf{p}_{23}\|^2 = 6a^2$ proving that the three point masses form an equilateral triangle. □

Figure 70 – Three point-masses located at isosceles triangle's vertices.

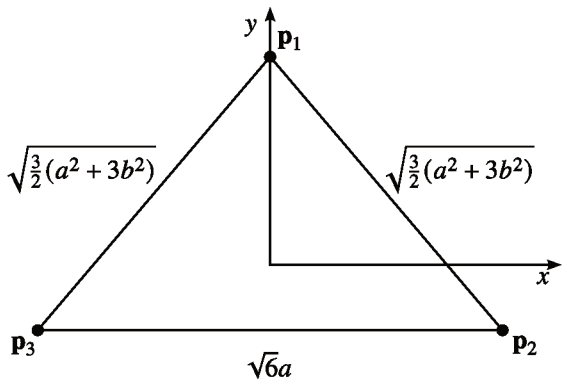

Source: The author.

It is possible to find solutions with different masses from the equimomental system of three equal point masses. These solutions with different masses will be analyzed in the next section.

6.4 EQUIMOMENTAL SYSTEM WITH UNEQUAL POINT-MASSES

This section shows that it is possible to determine equimomental systems of three different point masses not necessarily located at the vertices of an isosceles triangle.

If in Equation (250) we use $\tilde{\mathbf{p}}_i = \widetilde{\mathbf{D}}\mathbf{U}\tilde{\mathbf{q}}_i$ instead of $\tilde{\mathbf{p}}_i = \widetilde{\mathbf{D}}\tilde{\mathbf{q}}_i$, where $\mathbf{U} \in O(3)$ is a 3×3 orthogonal matrix, then the same pseudo-inertia matrix is obtained as in Equation (250),

$$\frac{m}{3}\sum_{i=1}^{3}\widetilde{\mathbf{D}}\mathbf{U}\tilde{\mathbf{q}}_i\tilde{\mathbf{q}}_i^T\mathbf{U}^T\widetilde{\mathbf{D}}^T = m\widetilde{\mathbf{D}}\mathbf{U}\mathbf{I}_3\,\mathbf{U}^T\widetilde{\mathbf{D}}^T = \widetilde{\boldsymbol{\Xi}}\,, \tag{251}$$

since that $\mathbf{U}\mathbf{U}^T = \mathbf{I}_3$. This property can be used to determine a family of point-mass solutions. For this, we will parameterize $\mathbf{U} = \mathbf{U}(\beta)$, where the parameter β is an angle around the y-axis. Let us define a 3D rotation around the y-axis,

$$\mathbf{U} = \begin{bmatrix} \cos\beta & 0 & \sin\beta \\ 0 & 1 & 0 \\ -\sin\beta & 0 & \cos\beta \end{bmatrix}, \tag{252}$$

and, performing the rotation $\mathbf{U}\widetilde{\mathbf{q}}_i$ for $i = 1,2,3$, yields,

$$\mathbf{U}\widetilde{\mathbf{q}}_1 = \begin{bmatrix} \sin\beta \\ \sqrt{2} \\ \cos\beta \end{bmatrix} = \cos\beta \begin{bmatrix} \tan\beta \\ \sqrt{2}\sec\beta \\ 1 \end{bmatrix}, \tag{253}$$

$$\mathbf{U}\widetilde{\mathbf{q}}_2 = \begin{bmatrix} \frac{\sqrt{6}}{2}\cos\beta + \sin\beta \\ -\frac{\sqrt{2}}{2} \\ -\frac{\sqrt{6}}{2}\sin\beta + \cos\beta \end{bmatrix}$$

$$= (\cos\beta - \frac{\sqrt{6}}{2}\sin\beta)\begin{bmatrix} (\frac{\sqrt{6}}{2}\cos\beta + \sin\beta)/(\cos\beta - \frac{\sqrt{6}}{2}\sin\beta) \\ -\sqrt{2}/2(\cos\beta - \frac{\sqrt{6}}{2}\sin\beta) \\ 1 \end{bmatrix}, \tag{254}$$

$$\mathbf{U}\widetilde{\mathbf{q}}_3 = \begin{bmatrix} -\frac{\sqrt{6}}{2}\cos\beta + \sin\beta \\ -\frac{\sqrt{2}}{2} \\ \frac{\sqrt{6}}{2}\sin\beta + \cos\beta \end{bmatrix}$$

$$= (\frac{\sqrt{6}}{2}\sin\beta + \cos\beta)\begin{bmatrix} (-\frac{\sqrt{6}}{2}\cos\beta + \sin\beta)/(\frac{\sqrt{6}}{2}\sin\beta + \cos\beta) \\ -\sqrt{2}/2(\frac{\sqrt{6}}{2}\sin\beta + \cos\beta) \\ 1 \end{bmatrix}. \tag{255}$$

The right side of above equations can be used to find the point-masses and their position since that,

$\sum_{i=1}^{3}(\mathbf{U}\widetilde{\mathbf{q}}_i)(\mathbf{U}\widetilde{\mathbf{q}}_i)^T = \cos^2\beta\widetilde{\mathbf{q}}_1'\widetilde{\mathbf{q}}_1'^T + (\cos\beta - \frac{\sqrt{6}}{2}\sin\beta)^2\widetilde{\mathbf{q}}_2'\widetilde{\mathbf{q}}_2'^T + (\frac{\sqrt{6}}{2}\sin\beta + \cos\beta)^2\widetilde{\mathbf{q}}_3'\widetilde{\mathbf{q}}_3'^T$,

then the masses are: $m_1 = \frac{m}{3}\cos^2\beta$, $m_2 = \frac{m}{3}(\cos\beta - \frac{\sqrt{6}}{2}\sin\beta)^2$, and $m_3 = \frac{m}{3}(\frac{\sqrt{6}}{2}\sin\beta + \cos\beta)^2$. The extended position vectors are then,

$$\widetilde{\mathbf{q}}_1' = \begin{bmatrix} \tan\beta \\ \sqrt{2}\sec\beta \\ 1 \end{bmatrix}, \tag{256}$$

$$\widetilde{\mathbf{q}}_2' = \begin{bmatrix} (\frac{\sqrt{6}}{2}\cos\beta + \sin\beta)/(\cos\beta - \frac{\sqrt{6}}{2}\sin\beta) \\ -\sqrt{2}/2(\cos\beta - \frac{\sqrt{6}}{2}\sin\beta) \\ 1 \end{bmatrix}, \tag{257}$$

$$\widetilde{\mathbf{q}}_3' = \begin{bmatrix} (-\frac{\sqrt{6}}{2}\cos\beta + \sin\beta)/(\frac{\sqrt{6}}{2}\sin\beta + \cos\beta) \\ -\sqrt{2}/2(\frac{\sqrt{6}}{2}\sin\beta + \cos\beta) \\ 1 \end{bmatrix}. \tag{258}$$

by eliminating the parameter β in vector $\mathbf{q}_1'$ it is determined that the mass m_1 describes a hyperbola defined by equation $\frac{y^2}{2} - x^2 = 1$, see Fig. 71. Similarly, it is concluded that the masses m_2 and m_3 describe the same hyperbola defined by equation $\frac{y^2}{1/5} - x^2 = 1$, see Figure 71.

Varying the parameter β from 0 to 2π, it starts with the masses that form the equilateral triangle studied above. One point at a time moves to infinity and reappears on the opposite side. When the parameter reaches the value of π, an equilateral triangle is formed again, but with points reflected with respect to the x-axis in relation to the initial triangle. Once the parameter reaches the value of 2π the points return to the original position. Figure 72 shows the variation of the normalized mass; note that the sum is constant and equal to 1.

Figure 71 – The effect of a 3D rotation on a triangle of point-masses.

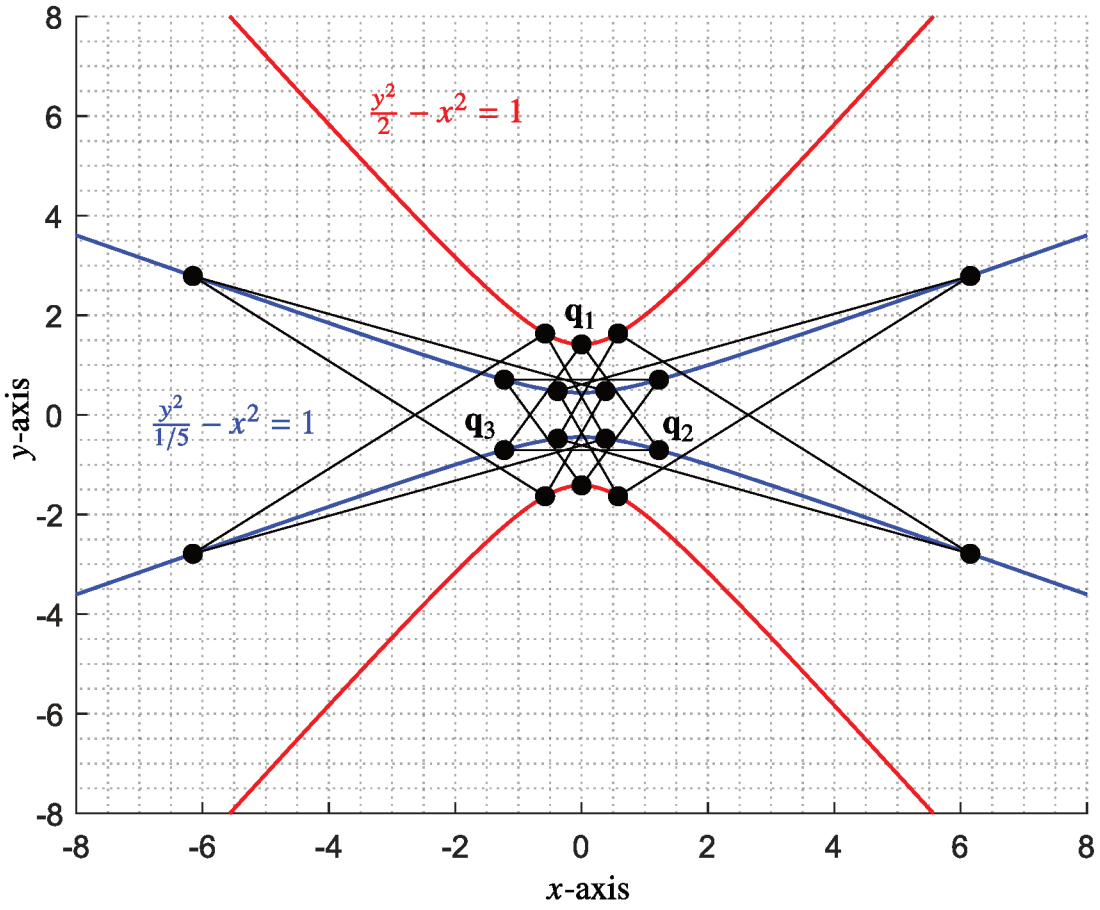

Source: The author.

Figure 72 shows the possible values of the masses for a fixed orientation of the equilateral triangle shown in Figure 69(b). In order to determine all possible values of the masses it is necessary to use two parameters, namely θ and β. Now we will use the transformation $\tilde{\mathbf{p}}_i(\theta,\beta) = \widetilde{\mathbf{D}}\mathbf{U}(\beta)\tilde{\mathbf{q}}_i(\theta)$, then the masses and the position vectors become a function of two parameters, that is, $m_i = m_i(\theta,\beta)$ and $\widetilde{\mathbf{q}}_i' = \widetilde{\mathbf{q}}_i'(\theta,\beta)$. The masses are transformed according to

$$m_1 = \frac{m}{3}\left(\cos\beta - \sqrt{2}\sin\beta\cos\theta\right)^2, \tag{259}$$

$$m_2 = \frac{m}{3}\left[\cos\beta + \sin\beta\left(\frac{\sqrt{2}}{2}\cos\theta - \frac{\sqrt{6}}{2}\sin\theta\right)\right]^2, \tag{260}$$

$$m_3 = \frac{m}{3}\left[\cos\beta + \sin\beta\left(\frac{\sqrt{2}}{2}\cos\theta + \frac{\sqrt{6}}{2}\sin\theta\right)\right]^2, \tag{261}$$

and the Figure 73 illustrates the normalized mass. The three points will move according to

Figure 72 – Variation of normalized masses form 0 to 2π.

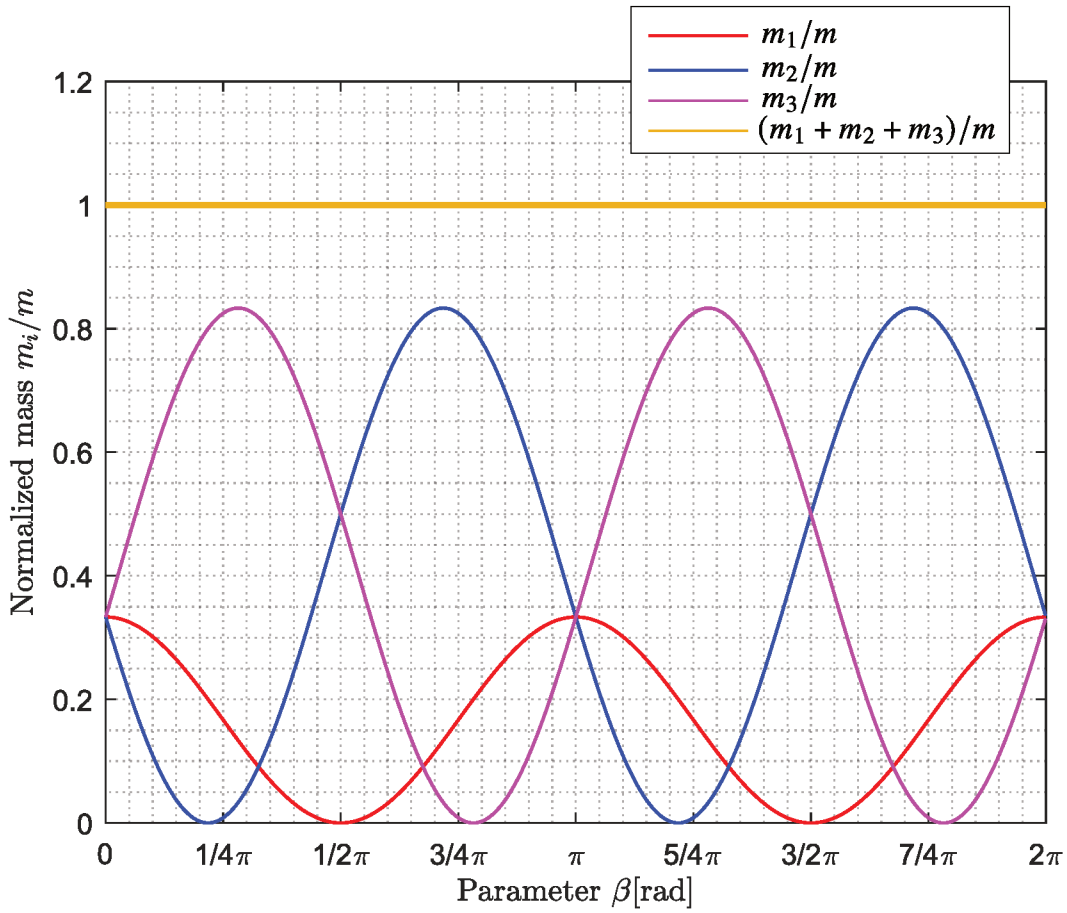

Source: The author.

$$\widetilde{\mathbf{q}}_1' = \begin{bmatrix} \frac{\sin\beta+\sqrt{2}\cos\beta\cos\theta}{\cos\beta-\sqrt{2}\sin\beta\cos\theta} \\ \frac{\sqrt{2}\sin\theta}{\cos\beta-\sqrt{2}\sin\beta\cos\theta} \\ 1 \end{bmatrix}, \tag{262}$$

$$\widetilde{\mathbf{q}}_2' = \begin{bmatrix} \frac{\sin\beta-\cos\beta\left(\frac{\sqrt{2}}{2}\cos\theta-\frac{\sqrt{6}}{2}\sin\theta\right)}{\cos\beta+\sin\beta\left(\frac{\sqrt{2}}{2}\cos\theta-\frac{\sqrt{6}}{2}\sin\theta\right)} \\ \frac{-\frac{\sqrt{2}}{2}\sin\theta-\frac{\sqrt{6}}{2}\cos\theta}{\cos\beta+\sin\beta\left(\frac{\sqrt{2}}{2}\cos\theta-\frac{\sqrt{6}}{2}\sin\theta\right)} \\ 1 \end{bmatrix}, \tag{263}$$

$$\widetilde{\mathbf{q}}_3' = \begin{bmatrix} \frac{\sin\beta-\cos\beta\left(\frac{\sqrt{2}}{2}\cos\theta+\frac{\sqrt{6}}{2}\sin\theta\right)}{\cos\beta+\sin\beta\left(\frac{\sqrt{2}}{2}\cos\theta+\frac{\sqrt{6}}{2}\sin\theta\right)} \\ \frac{\frac{\sqrt{6}}{2}\cos\theta-\frac{\sqrt{2}}{2}\sin\theta}{\cos\beta+\sin\beta\left(\frac{\sqrt{2}}{2}\cos\theta+\frac{\sqrt{6}}{2}\sin\theta\right)} \\ 1 \end{bmatrix}. \tag{264}$$

Figure 73 – Three point-masses located at isosceles triangle's vertices.

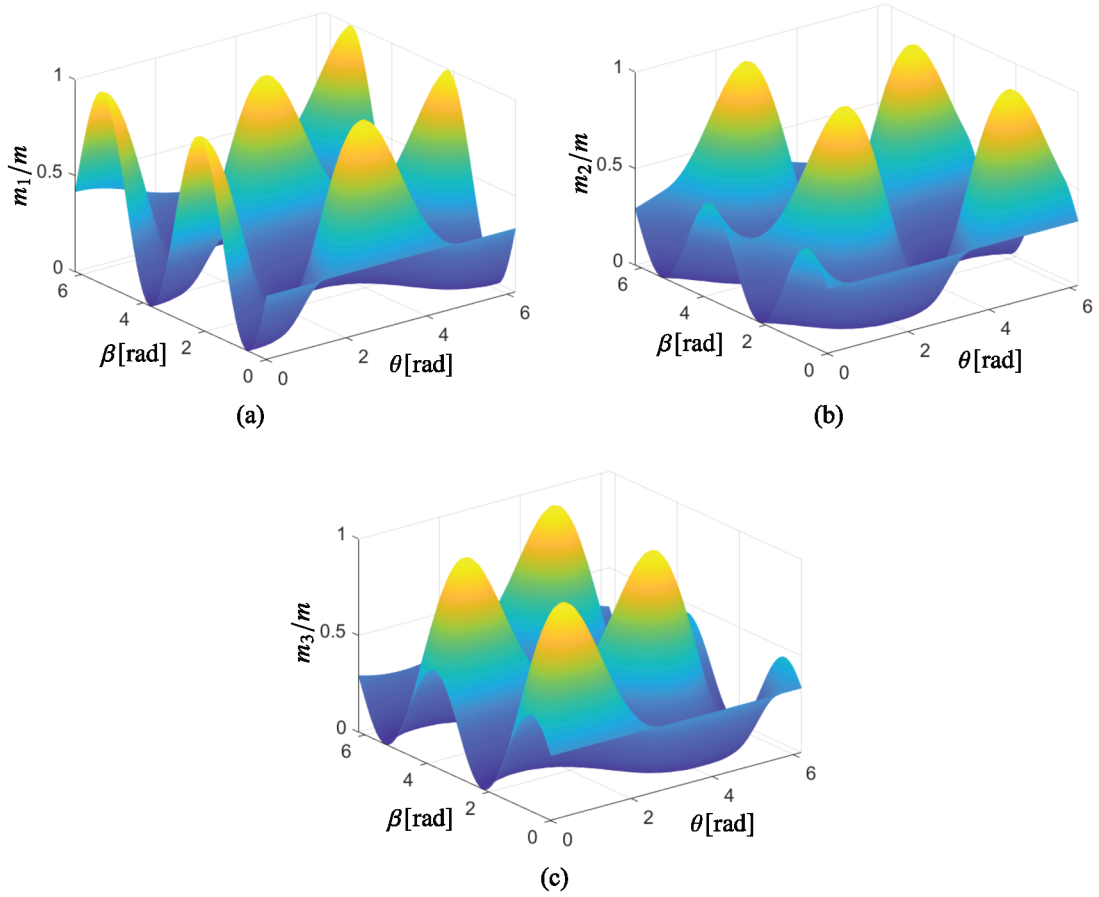

Source: The author.

6.5 EQUIMOMENTAL SYSTEMS WITH PRESCRIBED POINT-MASSES

In this section, we study the possibility of prescribing the position of one mass while guaranteeing that all masses are positive. In addition, the conditions for prescribing the position of two and three point-masses are also presented.

6.5.1 One prescribed point

Lemma 1 *An equimomental system of three-point masses can always be chosen for a planar rigid body if one of the points is prescribed on one of the principal axes.*

Alternatively, Lemma 1 can be rewritten as: "For any inertial system, if you prescribe a first point along one of the principal axes, there is always an equimomental system of three-point masses by a proper selection of the positions of two extra points."

Proof. Consider a rigid body with an inertia matrix $\widetilde{\boldsymbol{\Xi}} = m\,\mathrm{diag}\left(a^2, b^2, 1\right)$ relative to a reference frame with origin at the center of mass and coordinate axes coincident with the principal axes.

Let us define an xy coordinate system coincident with the principal axes. If the rotation angle $\theta = 0$, then the point $\mathbf{q}_1$ is on the x-axis according to Equation (262). Now, if we fix the point $\mathbf{p}_1$, it obtains the following relation

$$\beta = \arctan\left(\frac{x_1 - \sqrt{2}a}{a + \sqrt{2}x_1}\right), \tag{265}$$

then, the points $\widetilde{\mathbf{q}}_1$ and $\widetilde{\mathbf{q}}_2$ of the non-scaled triangle can be written as

$$\widetilde{\mathbf{q}}_2 = \begin{bmatrix} \frac{\sin\beta - \frac{\sqrt{2}}{2}\cos\beta}{\cos\beta + \frac{\sqrt{2}}{2}\sin\beta} \\ \frac{-\sqrt{6}}{2(\cos\beta + \frac{\sqrt{2}}{2}\sin\beta)} \\ 1 \end{bmatrix}, \widetilde{\mathbf{q}}_3 = \begin{bmatrix} \frac{\sin\beta - \frac{\sqrt{2}}{2}\cos\beta}{\cos\beta + \frac{\sqrt{2}}{2}\sin\beta} \\ \frac{\sqrt{6}}{2(\cos\beta + \frac{\sqrt{2}}{2}\sin\beta)} \\ 1 \end{bmatrix}. \tag{266}$$

From Equation (259), Equation (260), and Equation (261) we have that the masses are

$$m_1 = \frac{m}{3}(\cos\beta - \sqrt{2}\sin\beta)^2, \tag{267}$$

$$m_2 = m_3 = \frac{m}{3}(\cos\beta + \frac{\sqrt{2}}{2}\sin\beta)^2, \tag{268}$$

and according to Equation (251) we have that $\sum_{i=1}^{3} \tilde{\mathbf{p}}_i \tilde{\mathbf{p}}_i^T = m\,\mathrm{diag}\left(a^2, b^2, 1\right)$ then the three point-masses form a system equimomental to the given rigid body. □

Note that points $\widetilde{\mathbf{p}}_1$ and $\widetilde{\mathbf{p}}_2$ are symmetric with respect to the x-coordinate axis; therefore, the system of point masses forms an isosceles triangle with two equal masses, $m_2 = m_3$.

Theorem 2 *For a planar rigid body, an equimomental system of three point masses located at the vertices of an isosceles triangle can always be chosen with a mass at an arbitrary point.*

Proof. Suppose that a point is prescribed, and its coordinates are written relative to a fixed coordinate system on the body. In that case, it is clear that the point coordinates can be written relative to a reference system with the origin at the center of mass and coordinate axes coincident with the principal axes. In this coordinate system, the point can be rotated at an angle θ around the center of mass so that it is on the x-axis. It is now possible to determine an equimomental system with three-point masses located at the vertices of an isosceles triangle, as shown in Lemma 1. Finally, the prescribed point at the current position is rotated at an angle $-\theta$ that locates it at the original position. □

6.5.1.1 Symmetrical planar rigid bodies

In the case of a planar rigid body with at least one axis of symmetry, the determination of an equimomental system is substantially facilitated since it is sufficient to define a point on an axis of symmetry exempt from the center of mass, then we obtain an isosceles triangle with two equal masses symmetrical to the axis of symmetry.

6.5.2 Two prescribed point

According to Theorem 2, two points can be prescribed as long as they are symmetric to an axis passing through the center of mass of the body. If the body is symmetric, then the two points must be symmetric to the axis of symmetry.

6.5.3 Three prescribed point

Some models, such as the one presented by Chaudhary (CHAUDHARY; SAHA, 2009), allow prescribing three point-masses with some restrictions, but it cannot be guaranteed that the masses are positive. It is clear that it is impossible to define three general points arbitrarily since the position of the masses must obey Equation (262), Equation (263), and Equation (264).

6.6 EXAMPLES

In the following, we first show an idealized example to demonstrate the procedure for determining an equimomental system of a planar rigid body. In the two subsequent examples, we consider a symmetric and an asymmetric rigid body, respectively.

6.6.1 Six point-masses rigidly connected

This idealized example shows the procedure to determine an equimomental system of three-point masses of a given rigid body.

Next we show the step-by-step procedure for determining the equivalent three-point-mass system given a pseudo-inertia matrix. The pseudo-inertia matrix of a set of six point-masses, summing $m = 1$, located in the positions:

$$\widetilde{\mathbf{q}}_1 = \begin{bmatrix} -4 \\ 6 \\ 1 \end{bmatrix}, \widetilde{\mathbf{q}}_2 = \begin{bmatrix} 3 \\ 8 \\ 1 \end{bmatrix}, \widetilde{\mathbf{q}}_3 = \begin{bmatrix} 3 \\ 5 \\ 1 \end{bmatrix}, \widetilde{\mathbf{q}}_4 = \begin{bmatrix} -6 \\ -1 \\ 1 \end{bmatrix}, \widetilde{\mathbf{q}}_5 = \begin{bmatrix} 1 \\ -2 \\ 1 \end{bmatrix}, \widetilde{\mathbf{q}}_6 = \begin{bmatrix} 5 \\ -4 \\ 1 \end{bmatrix},$$

is

$$\widetilde{\boldsymbol{\Xi}} = \frac{1}{6}\sum_{i=1}^{6} \tilde{\mathbf{q}}_i \tilde{\mathbf{q}}_i^T = \begin{bmatrix} 16.0000 & -0.1667 & 0.3333 \\ -0.1667 & 24.3333 & 2.0000 \\ 0.3333 & 2.0000 & 1.0000 \end{bmatrix}, \tag{269}$$

here we are using equal masses for simplicity but we have no loss of generality. To determine the transformation $\mathbf{G}$ that converts the matrix $\widetilde{\boldsymbol{\Xi}}$ into a diagonal one, we must first translate the body center of mass. Then the eigenvectors of the matrix $\mathbf{I}$ that form a rotation matrix $\mathbf{R}$ are determined (SELIG, J., 2005). Therefore, the transformation matrix has the form,

$$\mathbf{G} = \begin{bmatrix} \mathbf{R}^T & -\mathbf{R}^T\mathbf{t}_C \\ 0 & 1 \end{bmatrix}, \tag{270}$$

where $\mathbf{t}_C$ is the position of the center of mass. Following the above procedure, we have

$$\mathbf{G} = \begin{bmatrix} -0.1784 & 0.9840 & -1.9084 \\ -0.9840 & -0.1784 & 0.6848 \\ 0 & 0 & 1.0000 \end{bmatrix}, \tag{271}$$

then the diagonal pseudo-inertia matrix is

$$\widetilde{\boldsymbol{\Xi}}' = \mathbf{G}\widetilde{\boldsymbol{\Xi}}\mathbf{G}^{\mathrm{T}} = \begin{bmatrix} 20.4844 & 0 & 0 \\ 0 & 15.7378 & 0 \\ 0 & 0 & 1 \end{bmatrix}, \tag{272}$$

and remember that the diagonal matrix is written as $\widetilde{\boldsymbol{\Xi}}' = m\,\mathrm{diag}\left(a^2, b^2, 1\right)$, and the non-rigid transformation of the triangle is $\widetilde{\mathbf{D}} = \mathrm{diag}(a, b, 1)$; therefore, we have that

$$\widetilde{\mathbf{D}} = \begin{bmatrix} 4.5260 & 0 & 0 \\ 0 & 3.9671 & 0 \\ 0 & 0 & 1 \end{bmatrix}, \tag{273}$$

then, using $\tilde{\mathbf{p}}'_i = \widetilde{\mathbf{D}}\tilde{\mathbf{q}}_i$ for $i = 1, 2, 3$. it is computed the position of vertices' triangle in the current reference frame,

$$\widetilde{\mathbf{p}}'_1 = \begin{bmatrix} 0 \\ 5.6103 \\ 1.0000 \end{bmatrix}, \quad \widetilde{\mathbf{p}}'_2 = \begin{bmatrix} 5.5432 \\ -2.8052 \\ 1.0000 \end{bmatrix}, \quad \text{and} \quad \widetilde{\mathbf{p}}'_3 = \begin{bmatrix} -5.5432 \\ -2.8052 \\ 1.0000 \end{bmatrix}.$$

The above points are written in the original reference frame using the transformation $\tilde{\mathbf{p}}_i = \mathbf{G}^{-1}\tilde{\mathbf{p}}'_i$,

$$\widetilde{\mathbf{p}}_1 = \begin{bmatrix} -5.1869 \\ 0.9990 \\ 1.0000 \end{bmatrix}, \quad \widetilde{\mathbf{p}}_2 = \begin{bmatrix} 2.1044 \\ 7.9547 \\ 1.0000 \end{bmatrix}, \quad \text{and} \quad \widetilde{\mathbf{p}}_3 = \begin{bmatrix} 4.0825 \\ -2.9537 \\ 1.0000 \end{bmatrix},$$

The pseudo-inertia matrix is calculated with these points, confirming that the two systems are equimomental Equation (274). Figure 74 shows in red the set of six points, the undeformed triangle in blue, in green the deformed triangle representing the equimomental system, and the black point is the position of the center of mass.

$$\widetilde{\boldsymbol{\Xi}} = \frac{1}{3}\sum_{i=1}^{3} \tilde{\mathbf{p}}_i \tilde{\mathbf{p}}_i^T = \begin{bmatrix} 16.0000 & -0.1667 & 0.3333 \\ -0.1667 & 24.3333 & 2.0000 \\ 0.3333 & 2.0000 & 1.0000 \end{bmatrix} \tag{274}$$

Figure 74 – Equimomental system.

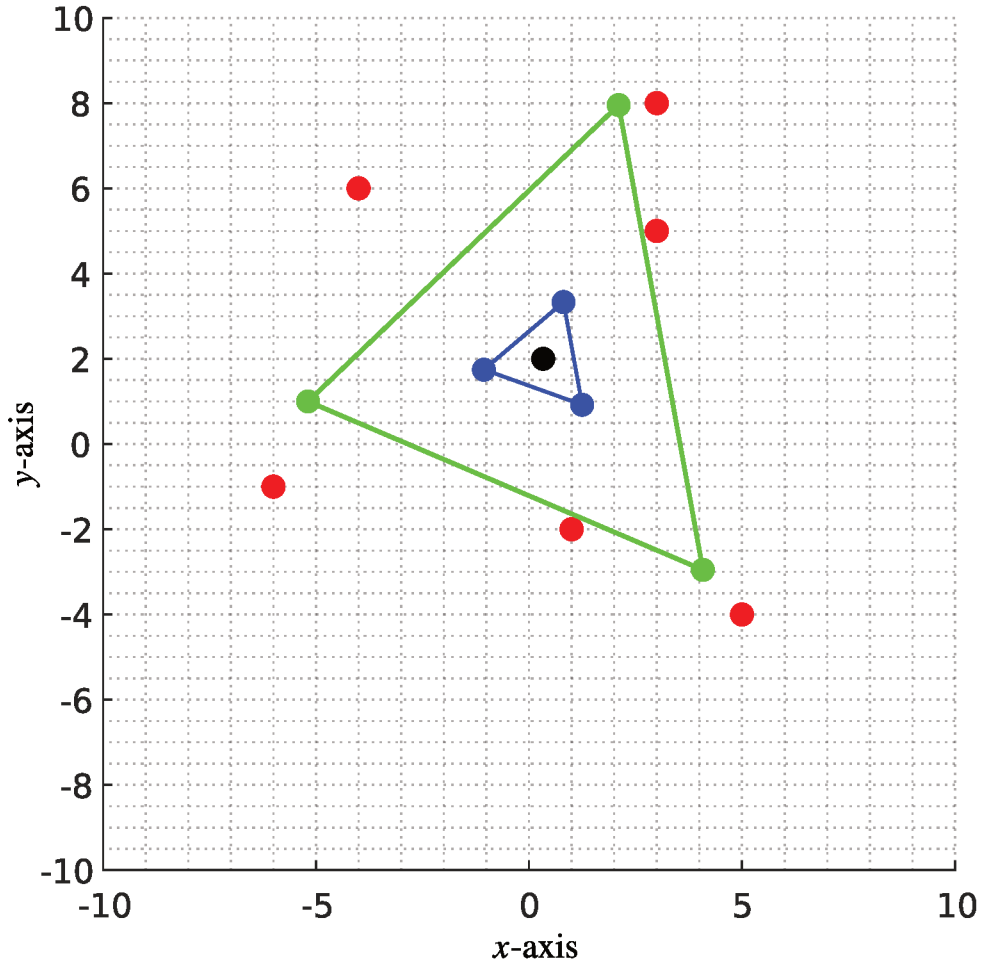

Source: The author.

6.6.2 Symmetric connecting rod

Connecting rods are a component of machines and mechanisms to transmit motion between different bodies. Connecting rods are commonly used in internal combustion engines and compressors to convert reciprocating motion into circular motion and vice versa. Generally, connecting rods are symmetrical, which allows defining an equimomental system of two point masses positioned along the axis of symmetry, as shown hereafter.

If the connecting rod is considered a straight rod with negligible diameter or width and thickness, see Figure 75(b), then we have $I_{xy} = I_{xx} = 0$, and $I_{yy} = I_{zz}$. Furthermore, the pseudo-inertia matrix with respect to the center of mass becomes $\widetilde{\boldsymbol{\Xi}} = \text{diag}\,(I_{zz}, 0, m)$ according to Equation (237), and the scaling matrix is therefore $\widetilde{\mathbf{D}} = \text{diag}\left(\sqrt{I_{zz}/m}, 0, 1\right) = \text{diag}\,(a, 0, 1)$. Now fixing the mass m_1 at the point A with the coordinates $(x_1, 0)$ and comparing this point with Equation (262) we have that $\theta = 0$ and the following relation is obtained

Figure 75 – Symmetric connecting rod.

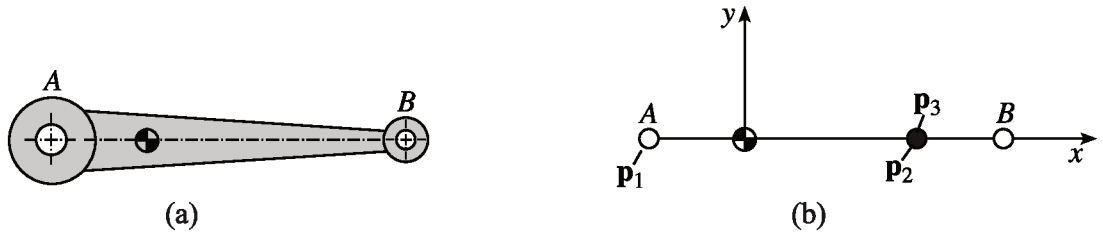

Source: The author.

$$\tan\beta = \frac{x_1 - \sqrt{2}a}{a + \sqrt{2}x_1}, \tag{275}$$

where, $a = \sqrt{I_{zz}/m}$. The scaling of point at Equation (262), Equation (263), and Equation (264) by means of $\tilde{\mathbf{p}}_i = \widetilde{\mathbf{D}}\tilde{\mathbf{q}}_i$ produces

$$\widetilde{\mathbf{p}}_1 = \begin{bmatrix} x_1 \\ 0 \\ 1 \end{bmatrix}, \ \widetilde{\mathbf{p}}_2 = \widetilde{\mathbf{p}}_3 = \begin{bmatrix} \frac{a(\tan\beta - \frac{\sqrt{2}}{2})}{1+\frac{\sqrt{2}}{2}\tan\beta} \\ 0 \\ 1 \end{bmatrix} = \begin{bmatrix} -\frac{I_{zz}}{mx_1} \\ 0 \\ 1 \end{bmatrix}. \tag{276}$$

The masses m_2 and m_3 collapse at the same point along the segment AB so this system of three more point masses can be seen as an equimomental system of two point masses, see Fig. 75(b). Where, the first and second mass are

$$m_1 = \frac{m}{3}\left(\frac{1 - 2\sqrt{2}\tan\beta + 2\tan^2\beta}{1 + \tan^2\beta}\right) = \frac{I_{zz}m}{mx_1^2 + I_{zz}}, \tag{277}$$

$$m_2 + m_3 = \frac{2m}{3}\left(\frac{2 + 2\sqrt{2}\tan\beta + \tan^2\beta}{2(1 + \tan^2\beta)}\right) = \frac{m^2x_1^2}{mx_1^2 + I_{zz}}, \tag{278}$$

respectively, and located in the position with coordinates x_1, and $x_2 = -I_{zz}/(mx_1)$. This model deduced with modern techniques is equivalent to the one shown in the classical literature as in (BARANOV; ROJAS, et al., 1979).

6.6.3 Asymmetric planar body

Often the rigid bodies that conform to a machine have complex geometry and, in some cases, are asymmetric. Thus, in the following example, a system of three masses is determined that is equimomental to the bucket of a Komatsu PC400 (KOMATSU, 2017) excavator. Figure 76(a) shows a side view of the excavator, and Figure 76(b) shows the isometric drawing of the bucket generated in Solidworks.

Figure 76 – Komatsu PC400 excavator: (a) side view, and (b) Solidworks CAD of the bucket.

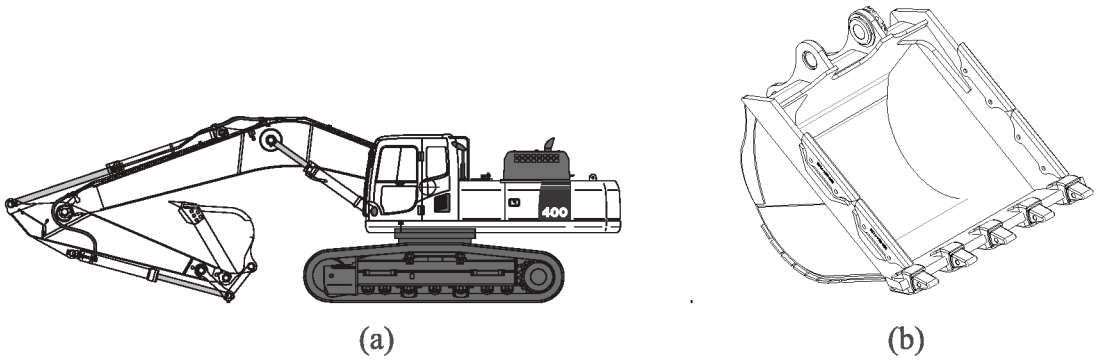

Source: The author.

The inertial properties were obtained using Solidworks software and considering a steel alloy with a density of 7850 kg/m^3; where the computed mass of the bucket is m = 1787.17469476 kg, and the coordinates of the center of mass are x_C = 0.70554017 m, and y_C = 0.11310906 m. Moreover, the numerical entries of the inertia matrix with respect to the origin of coordinates O(see Figure 77) are:

$$\mathbf{I} = \begin{bmatrix} 701.00983325 & 23.86484464 & -0.45099906 \\ 23.86484464 & 1860.876545 & -3.51307961 \\ -0.45099906 & -3.51307961 & 1674.58542686 \end{bmatrix}, \tag{279}$$

and, applying Eq. 237 we calculate the pseudo-inertia matrix

$$\widetilde{\mathbf{\Xi}} = \begin{bmatrix} 1417.226069305 & -23.86484464 & 1260.92353796 \\ -23.86484464 & 257.35935755 & 202.14564978 \\ 1260.92353796 & 202.14564978 & 1787.17469476 \end{bmatrix}. \tag{280}$$

Following the same procedure as in Section 6.6.1, we find the matrix $\mathbf{G}$ that diagonalizes the pseudo-inertia matrix.

$$\mathbf{G} = \begin{bmatrix} -0.91124435 & 0.41186614 & 0.59633370 \\ -0.41186614 & -0.91124435 & 0.39365810 \\ 0 & 0 & 1.00000000 \end{bmatrix}, \tag{281}$$

So, the diagonal pseudo-inertia matrix is

$$\widetilde{\mathbf{\Xi}}' = \mathbf{G}\widetilde{\mathbf{\Xi}}\mathbf{G}^{\mathrm{T}} = \mathrm{diag}\,(602.84288196,\ 159.24583313,\ 1787.17469476),$$

then, the scaling matrix becomes $\widetilde{\mathbf{D}}$ = diag(0.58078924, 0.29850426, 1). Thus, the position of the point masses in relation to the reference system Oxy is calculated by means of the equation $\tilde{\mathbf{p}}_i = \mathbf{G}^{-1}\widetilde{\mathbf{D}}\tilde{\mathbf{q}}_i$,

$$\widetilde{\mathbf{p}}_1 = \begin{bmatrix} 0.53167 \\ -0.27157 \\ 1.00000 \end{bmatrix}, \quad \widetilde{\mathbf{p}}_2 = \begin{bmatrix} 0.14428 \\ 0.59841 \\ 1.00000 \end{bmatrix}, \quad \text{and} \quad \widetilde{\mathbf{p}}_3 = \begin{bmatrix} 1.44065 \\ 0.01248 \\ 1.00000 \end{bmatrix}.$$

Figure 77 shows in blue the undeformed equilateral triangle and in green the position of the point masses at the vertices of an isosceles triangle after the deformation of the equilateral triangle.

Figure 77 – Equimomental system of backhoe bucket.

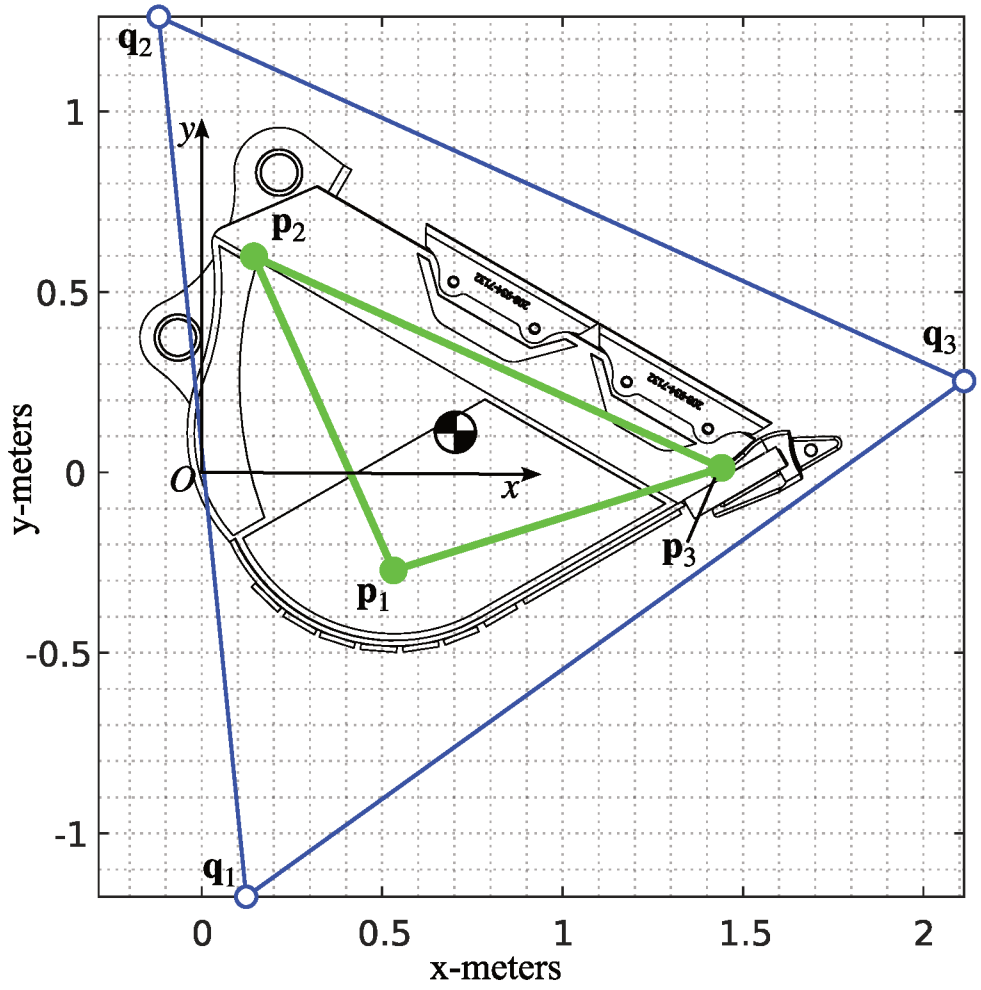

Source: The author.

In this section, novel results on the equimomental systems of three point-masses of planar rigid bodies are presented. The ideas studied here can contribute to the dynamics of planar rigid bodies and the concept of inertial synthesis (TISCHLER et al., 2000), a less explored topic.

In the developed model, it is considered that the rigid body does not have a constant density and thickness; therefore, the expressions obtained are general. First, it is determined that the formed triangle is isosceles for an equimomental system of equal masses. Then, all possible

solutions with unequal masses are determined, and the values of the normalized masses are shown graphically. Also, a procedure is developed to determine an equimomental system with the position of a prescribed mass. Conditions are given to prescribing the position of two and three point-masses. Finally, three examples of application of the ideas explored in this work are presented.

7 DYNAMIC BALANCING OF PLANAR MECHANISMS USING EQUIMOMENTAL SYSTEMS OF POINT-MASSES

In this chapter, the proposed method is adapted for the dynamic balancing of planar mechanisms. First, we use the representation of the inertial properties by an equimomental system as proposed in Chapter 6. The Davies method is then used to solve the inverse dynamic problem to formulate the optimization problem. Finally, an example application is presented. The method proposed in this work can be expanded to balance spatial mechanisms, but this topic will be addressed in future work.

7.1 SCREW BASED DYNAMIC OF PLANAR RIGID BODY

In this section, the equation of motion of a planar rigid body is written concisely using screw theory (BALL, 1998), and natural coordinates (JALÓN; BAYO, 1994).

Firstly, it shows the constitutive equations describing the state of accelerations of a planar rigid body. Let us consider an inertial reference frame Oxy and a local reference frame $O^e x^e y$ attached to the rigid body, see Figure 78. The position and orientation of the body are defined using natural coordinates vector $\mathbf{q} = \begin{bmatrix} x_i & y_i & x_j & y_j \end{bmatrix}^T$, which corresponds to two points P_i and P_j attached to the body. Then, the matrix transformation that relates the local reference frame with respects to inertial frame can be written as,

Figure 78 – Equimomental system.

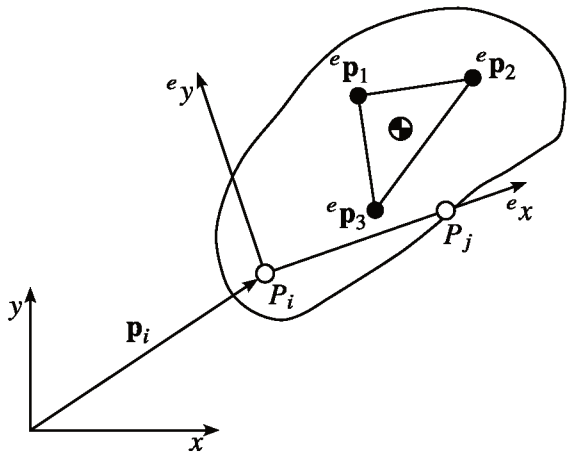

Source: The author.

$$\mathbf{R}_e(\mathbf{q}) = \frac{1}{d_{ij}} \begin{bmatrix} (x_j - x_i) & -(y_j - y_i) \\ (y_j - y_i) & (x_j - x_i) \end{bmatrix}, \tag{282}$$

where, d_{ij} is the distance between the points P_i and P_j.

Now, the position of point-masses ${}^{e}\mathbf{p}_k$ for $k = 1,2,3$ written in the inertial reference frame can be computed as,

$$\mathbf{p}_k = \mathbf{p}_i + \mathbf{R}_e {}^{e}\mathbf{p}_k \,, \tag{283}$$

and deriving twice with respect to time yields

$$\ddot{\mathbf{p}}_k = \ddot{\mathbf{p}}_i + \ddot{\mathbf{R}}_e {}^{e}\mathbf{p}_k \,. \tag{284}$$

According to Laus and Selig (2020), the total wrench acting in the body is equal to the sum of the inertial wrenches of the point masses of the equimomental system,

$$\begin{bmatrix} \boldsymbol{\tau} \\ \mathbf{F} \end{bmatrix} = m_1 \begin{bmatrix} (\mathbf{S}\mathbf{p}_1)^T \ddot{\mathbf{p}}_1 \\ \ddot{\mathbf{p}}_1 \end{bmatrix} + m_2 \begin{bmatrix} (\mathbf{S}\mathbf{p}_2)^T \ddot{\mathbf{p}}_2 \\ \ddot{\mathbf{p}}_2 \end{bmatrix} + m_3 \begin{bmatrix} (\mathbf{S}\mathbf{p}_3)^T \ddot{\mathbf{p}}_3 \\ \ddot{\mathbf{p}}_3 \end{bmatrix}, \tag{285}$$

where, $\mathbf{S} = \begin{bmatrix} 0 & -1 \\ 1 & 0 \end{bmatrix}$ represents a $\pi/2$ radian counterclockwise rotation, $\boldsymbol{\tau}$ and $\mathbf{F}$ are the total moment and force acting on the body.

This formulation is suitable for solving the inverse dynamics of mechanisms since the accelerations are calculated a priori. In the next section, we show an application of the use of equimomental point-masses systems to solve the inverse dynamics of a slider-crank linkage.

7.2 SHAKING FORCE AND SHAKING MOMENT ANALYSIS

This section shows an application of equimomental systems in analyzing forces and shaking moments. As an illustrative example, the slider crank mechanism was selected as it is widely used in internal combustion engines and compressors, see Figure 79.

Davies' method was developed to solve the kinematics and statics of planar and spatial mechanisms systematically, see (DAVIES, 1981, 2006; CAZANGI, 2008; MEJIA; SIMAS; MARTINS, 2016; LAUS; SIMAS; MARTINS, 2020). To adapt the technique to the solution of inverse dynamics is sufficient to apply the D'Alembert principle (GOLDSTEIN; POOLE; SAFKO, 2002), whereby the screw of inertia (FRANTZ et al., 2018) of the body considering equal masses can be written as follows:

$$\$_i^{in} = \begin{bmatrix} \tau_i \\ f_{ix} \\ f_{iy} \end{bmatrix} = -\frac{m_i}{3} \left(\begin{bmatrix} (\mathbf{S}\mathbf{p}_1^i)^T \ddot{\mathbf{p}}_1^i \\ \ddot{\mathbf{p}}_1^i \end{bmatrix} + \begin{bmatrix} (\mathbf{S}\mathbf{p}_2^i)^T \ddot{\mathbf{p}}_2^i \\ \ddot{\mathbf{p}}_2^i \end{bmatrix} + \begin{bmatrix} (\mathbf{S}\mathbf{p}_3^i)^T \ddot{\mathbf{p}}_3^i \\ \ddot{\mathbf{p}}_3^i \end{bmatrix} \right), \tag{286}$$

where, τ_i is inertial torque in the body i, f_{ix} and f_{iy} are the x and y components of the inertial force of body i, $\mathbf{p}_j^i$ for $j = 1,2,3.$ is the inertial screw position j of body i, and $\ddot{\mathbf{p}}_j^i$ is the acceleration of point j of body i.

Figure 79 – Slider crank mechanism.

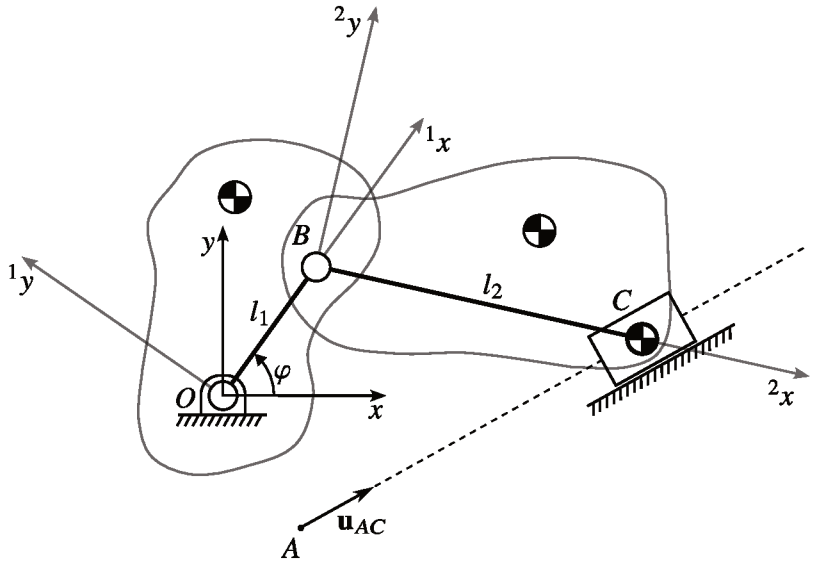

Source: The author.

Before applying the Davies' method it is necessary to determine the accelerations of the point-masses. For this we first formulate the constraint equations in natural coordinates that define the kinematics of the mechanism. So the constraint equations can be written as,

$$\mathbf{\Phi}(\mathbf{q}) = \begin{bmatrix} (x_C - x_B)^2 + (y_C - y_B)^2 - l_2^2 \\ (x_C - x_A)y_{\mathbf{u}_{AC}} - (y_C - y_A)x_{\mathbf{u}_{AC}} \\ (x_B - x_O) - l_1 \cos\varphi \\ (y_B - y_O) - l_1 \sin\varphi \end{bmatrix} = \mathbf{0}\,. \tag{287}$$

where, $\mathbf{q} = \begin{bmatrix} x_B & y_B & x_C & y_C & \varphi \end{bmatrix}^T$. Now, deriving the above equation twice, we obtain

$$\mathbf{\Phi}_\mathbf{q}\dot{\mathbf{q}} = \mathbf{0}\,, \tag{288}$$

$$\mathbf{\Phi}_\mathbf{q}\ddot{\mathbf{q}} = -\dot{\mathbf{\Phi}}_\mathbf{q}\dot{\mathbf{q}}\,, \tag{289}$$

here, $\mathbf{\Phi}_\mathbf{q}$ is the Jacobian of the constraint vector Equation (287).

$$\ddot{\mathbf{p}}_j^i(\ddot{\mathbf{q}}) = \ddot{\mathbf{p}}_k(\ddot{\mathbf{q}}) + \ddot{\mathbf{R}}_i(\ddot{\mathbf{q}})^i\mathbf{p}_j\,. \tag{290}$$

In this expression, $\ddot{\mathbf{p}}_k$ with $k = O, B$ represents the acceleration of reference frame origin.

The dynamic analysis begins with the representation of internal and external actions present in the mechanism, see Figure 80(a). From the directed coupling graph G_C as shown in Figure 80(b) it is constructed the action and fundamental cutsets graph G_A, see Figure 80(c). where, f_{bx}, f_{by}, f_{cx}, f_{cy}, f_{ox}, f_{oy}, f_d, and τ_d are internal reactions, τ is the input torque required

to achieve the specified accelerations, f_p is the external force acting in the piston, f_1^{in}, f_2^{in}, and f_3^{in} are inertial forces.

Figure 80 – Davies method.

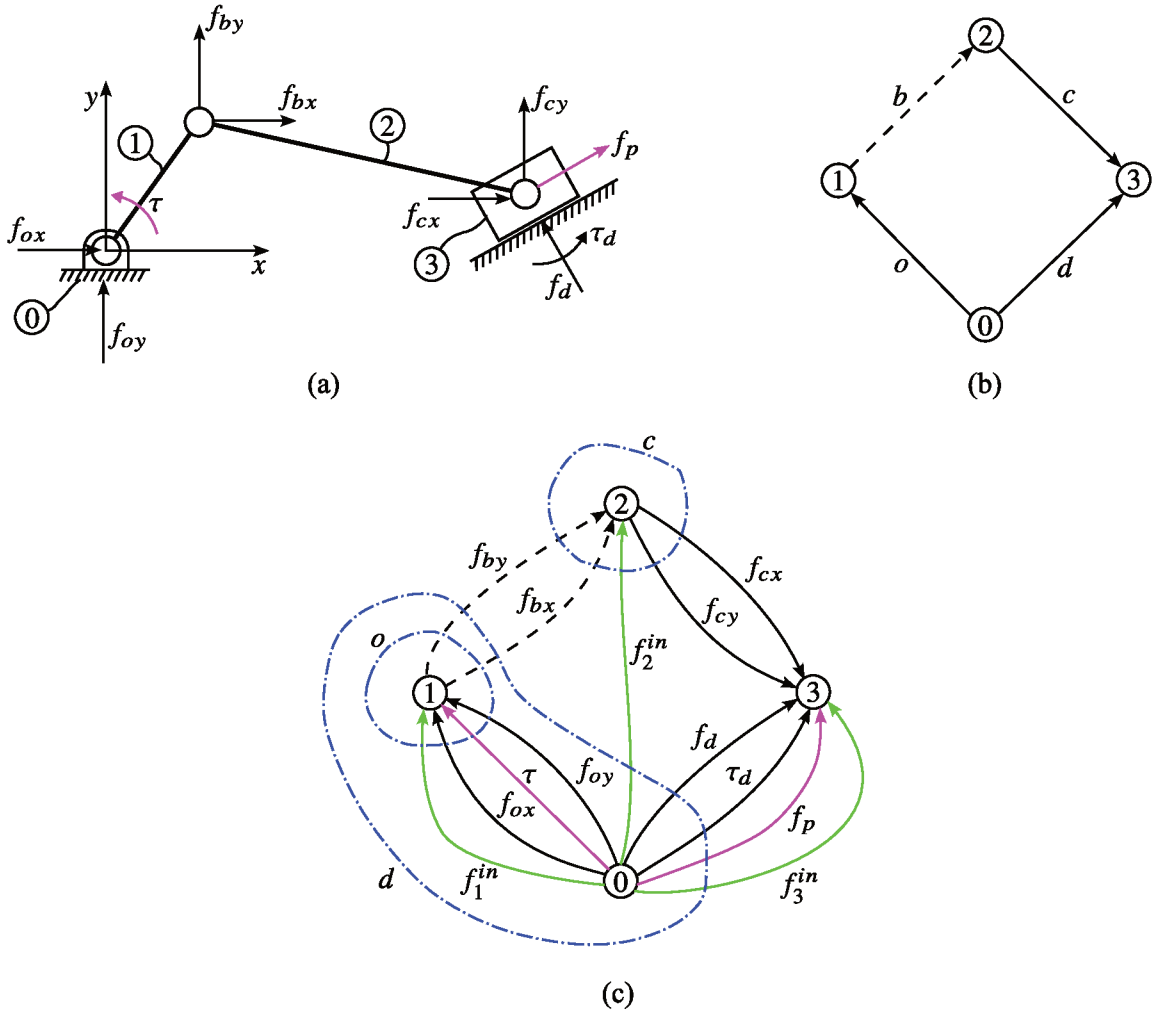

Source: The author.

Now, the fundamental cutset matrix of action graph G_A is,

$$\mathbf{Q}_A = \begin{array}{c} \\ c \\ d \\ o \end{array} \begin{array}{c} \begin{array}{cccccccccccc} f_{bx} & f_{by} & f_{cx} & f_{cy} & f_d & \tau_d & f_{ox} & f_{oy} & \tau & f_p & f_1^{in} & f_2^{in} & f_3^{in} \end{array} \\ \begin{bmatrix} -1 & -1 & 1 & 1 & 0 & 0 & 0 & 0 & 0 & 0 & 0 & -1 & 0 \\ 1 & 1 & 0 & 0 & 1 & 1 & 0 & 0 & 0 & 1 & 0 & 1 & 1 \\ -1 & -1 & 0 & 0 & 0 & 0 & 1 & 1 & 1 & 0 & 1 & 0 & 0 \end{bmatrix} \end{array}. \tag{291}$$

and, from the unit action screws of all the forces, the unit action matrix is obtained

$$\hat{\mathbf{A}}_D = \begin{array}{c} \begin{matrix} f_{bx} & f_{by} & f_{cx} & f_{cy} & f_d & \tau_d & f_{ox} & f_{oy} & \tau & f_p \end{matrix} \\ \begin{bmatrix} -y_B & x_B & -y_C & x_C & x_C y_{\mathbf{u}_d} - y_C x_{\mathbf{u}_d} & 1 & 0 & 0 & 1 & x_C y_{\mathbf{u}_A} - y_C x_{\mathbf{u}_A} \\ 1 & 0 & 1 & 0 & x_{\mathbf{u}_d} & 0 & 1 & 0 & 0 & x_{\mathbf{u}_A} \\ 0 & 1 & 0 & 1 & y_{\mathbf{u}_d} & 0 & 0 & 1 & 0 & y_{\mathbf{u}_A} \end{bmatrix} \end{array} \begin{array}{ccc} f_1^{in} & f_2^{in} & f_3^{in} \\ \hat{\tau}_1 & \hat{\tau}_2 & \hat{\tau}_3 \\ x_{\mathbf{u}_1} & x_{\mathbf{u}_2} & x_{\mathbf{u}_3} \\ y_{\mathbf{u}_1} & y_{\mathbf{u}_2} & y_{\mathbf{u}_3} \end{array} \tag{292}$$

then, the constitutive equations of the dynamics can be written compactly as

$$\hat{\mathbf{A}}_N(\mathbf{q})\boldsymbol{\Psi} = \mathbf{0}\,, \tag{293}$$

where, $\hat{\mathbf{A}}_N$ is the network unit action matrix of a coupling network and $\boldsymbol{\Psi}$ is the vector of magnitudes of action screws. The matrix $\hat{\mathbf{A}}_N$ is assembled from the unit action matrix $\hat{\mathbf{A}}_D$ as

$$\hat{\mathbf{A}}_N = \begin{bmatrix} \hat{\mathbf{A}}_D\mathbf{Q}_1 \\ \hat{\mathbf{A}}_D\mathbf{Q}_2 \\ \vdots \\ \hat{\mathbf{A}}_D\mathbf{Q}_k \end{bmatrix}, \tag{294}$$

where $\mathbf{Q}_i = \text{diag}([\mathbf{Q}_A]_i)$, $i = 1, 2, \cdots, k$ are diagonal matrices whose diagonal elements correspond to row i of cutset matrix $\mathbf{Q}_A$, derived from action graph G_A.

Let us split the vector $\boldsymbol{\Psi}$ into three vectors as follows: the vector of the internal forces acting in each kinematic pair ${}^{i}\boldsymbol{\Psi}$, the vector of the forces supply by each actuator ${}^{a}\boldsymbol{\Psi}$ and the vector of external forces ${}^{e}\boldsymbol{\Psi}$. Thus, Equation (293) is written as:

$$\begin{bmatrix} {}^{i}\hat{\mathbf{A}}_N(\mathbf{q}) & {}^{a}\hat{\mathbf{A}}_N(\mathbf{q}) & {}^{e}\hat{\mathbf{A}}_N(\mathbf{q}) \end{bmatrix} \begin{bmatrix} {}^{i}\boldsymbol{\Psi} \\ {}^{a}\boldsymbol{\Psi} \\ {}^{e}\boldsymbol{\Psi} \end{bmatrix} = \mathbf{0}, \tag{295}$$

where ${}^{i}\hat{\mathbf{A}}_N(\mathbf{q})$ is the network unit internal action matrix, ${}^{a}\hat{\mathbf{A}}_N(\mathbf{q})$ is the network unit actuator action matrix and ${}^{e}\hat{\mathbf{A}}_N$ is the network unit external action matrix. Rearranged the Equation (295) we can determine the internal forces and loads supplied by the actuators:

$${}^{r}\hat{\mathbf{A}}_N(\mathbf{q}){}^{r}\boldsymbol{\Psi} = -{}^{e}\hat{\mathbf{A}}_N(\mathbf{q}){}^{e}\boldsymbol{\Psi}, \tag{296}$$

where ${}^{r}\hat{\mathbf{A}}_N(\mathbf{q}) = \begin{bmatrix} {}^{i}\hat{\mathbf{A}}_N(\mathbf{q}) & {}^{a}\hat{\mathbf{A}}_N(\mathbf{q}) \end{bmatrix}$ is the resultant network unit action matrix and ${}^{r}\boldsymbol{\Psi} = \begin{bmatrix} {}^{i}\boldsymbol{\Psi}^T & {}^{a}\boldsymbol{\Psi}^T \end{bmatrix}^T$ is the resultant forces vector.

The dimensions of the slider crank mechanisms and their inertial properties are summarized in the Table 12. The mechanism is moved by a motor located at point O, rotating at a constant angular velocity $\dot{\varphi}$ of 2π rad/s. Moreover, the point A coincides with point O, and the unit vector $\mathbf{u}_{AC}$ is parallel to x-axis and same sense.

Table 12 – Dimensions and inertial properties (CHAUDHARY; CHAUDHARY, 2014b).

Body i	1	2	3	**Unit**
Mass m_i	2	3	4	[kg]
Length l_i	0.292	0.427	–	[m]
Inertia I_{zz_i}	0.03	0.14	0	[kg · m^2]
Center of mass ${}^e x_{C_i}$	0.146	0.214	0	[m]
Center of mass ${}^e y_{C_i}$	0	0	0	[m]

Source: The author.

The proposed kinematic and dynamic model was implemented in Matlab. The Figure 81(a) shows the mechanism in an arbitrary configuration, where the triangles in green represent the equimomental point masses of the crank and connecting rod. The Figure 81(b) and Figure 81(c) show the shaking forces components, and Figure 81(d) shows the shaking moment. The shaking screw is computed using the equation. The shaking screw is computed using the equation,

$$\$_{sh} = \begin{bmatrix} \boldsymbol{\tau}_{sh} \\ \mathbf{F}_{sh} \end{bmatrix} = - \begin{bmatrix} \tau + \tau_d + (\mathbf{S}\mathbf{p}_{OC})^T \mathbf{F}_d \\ \mathbf{F}_o + \mathbf{F}_d \end{bmatrix} \tag{297}$$

where, $\mathbf{F}_o$ is the reaction force in point O, $\mathbf{F}_d$ is the reaction force in slider pair, and $\mathbf{p}_{OC}$ is the position of point C relative to point O.

A simulation was performed in the kinematic and dynamic analysis software of planar and spatial mechanisms GIM (PETUYA et al., 2014; HERNÁNDEZ et al., n.d.) to validate the proposed model. The Figure 82 shows the comparison of the input torque of the proposed method and the one calculated in GIM, where the two plots are a close match.

7.3 DYNAMIC BALANCING METHOD

In this section, a method for dynamic balancing of planar mechanisms is proposed. The proposed method is a dating method developed for static balancing in which the dynamic problem is transformed into a static problem by considering inertial forces. The balancing is achieved by minimizing the forces and shaking moments; therefore, we deal with a multi-objective optimization problem. The steps of the proposed method are the following:

Step 1: First, the position problem is formulated using natural coordinates, as in Section 4.1.1.

Step 2: The second step is the computing of the accelerations. It is achieved by deriving the constraint vector twice, see Equation (288) and Equation (289).

Figure 81 – Shaking forces and shaking moment analysis.

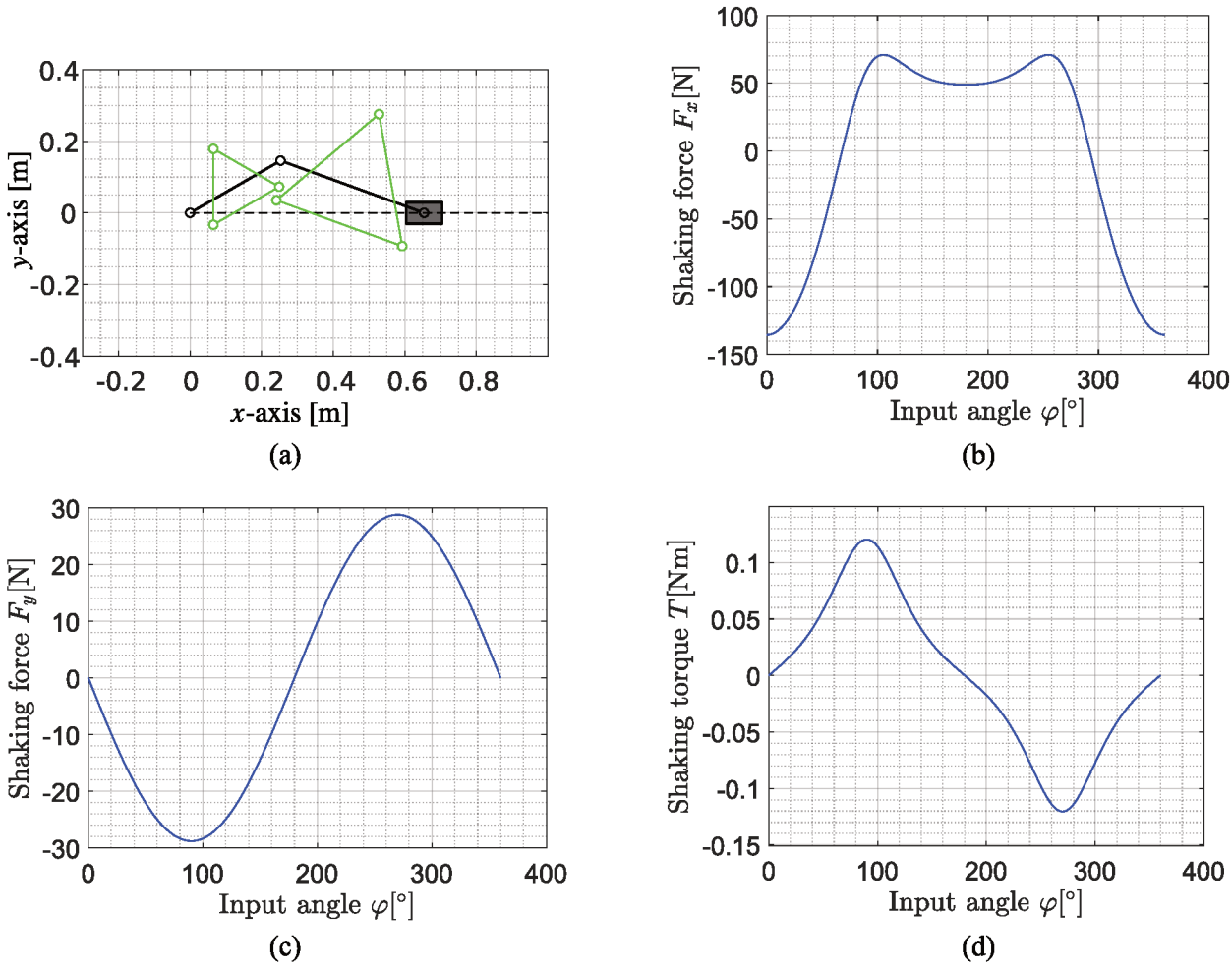

Source: The author.

Step 3: The next step is determining an equimomental system of three point-masses using the local reference frame for each link. Equation (283) is used to determine the positions in the global reference frame.

Step 4: We now determine the accelerations of the three point-masses for each link using the Equation (284).

Step 5: Next, the inertia screw is determined for each link by means of Equation (286).

Step 6: The next step is to solve the inverse dynamic problem, which is solved as if it were a static problem, see Equation (296).

Figure 82 – Input torque and its comparison with GIM result (PETUYA et al., 2014).

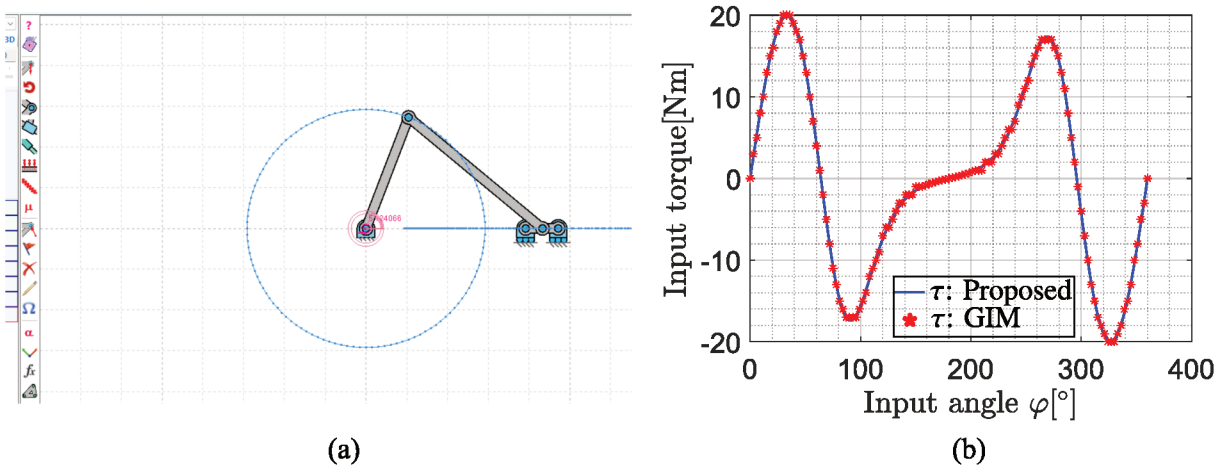

Source: The author.

Step 7: We now determine the shaking screw through the equations:

$$\$_{sh} = \begin{bmatrix} \boldsymbol{\tau}_{sh} \\ \mathbf{F}_{sh} \end{bmatrix} = -\sum_{i=1}^{n_f} \begin{bmatrix} \mathbf{s}_0^i \times \mathbf{F}_i^* \\ \mathbf{F}_i^* \end{bmatrix} - \sum_{i=1}^{n_t} \begin{bmatrix} \boldsymbol{\tau}_i^* \\ \mathbf{0} \end{bmatrix} \tag{298}$$

where $\mathbf{F}_i^*$ and $\boldsymbol{\tau}_i^*$ are the i-th force reaction and the i-th torque reaction in the base, respectively.

Step 8: The next step is formulating the optimization problem, which can be mathematically written as

$$\begin{aligned} \underset{\mathbf{z}}{\text{minimize}} \quad & f(\mathbf{z}) = \sum_{j=1}^{n} \$_{sh_j}^T \boldsymbol{\eta}\boldsymbol{\nu}\$_{sh_j}, \\ \text{subject to} \quad & \begin{cases} \mathbf{g}(\mathbf{q},\mathbf{z}) \leq \mathbf{0}, \\ \mathbf{h}(\mathbf{q},\mathbf{z}) = \mathbf{0}, \\ \underline{\mathbf{z}} \leq \mathbf{z} \leq \bar{\mathbf{z}}, \end{cases} \\ \text{while solving} \quad & \begin{cases} \boldsymbol{\Phi}(\mathbf{q}) = \mathbf{0}, \\ {}^r\hat{\mathbf{A}}_N(\mathbf{q},\mathbf{z})^r\boldsymbol{\Psi}_j = -{}^e\hat{\mathbf{A}}_N(\mathbf{q},\mathbf{z})^e\boldsymbol{\Psi}_j. \end{cases} \end{aligned} \tag{299}$$

In Equation (299) the normalization matrix $\boldsymbol{\eta}$ is defined as

$$\boldsymbol{\eta} = \begin{bmatrix} 1/\eta_1 & 0 & 0 \\ 0 & 1/\eta_2 & 0 \\ 0 & 0 & 1/\eta_2 \end{bmatrix} \tag{300}$$

where η_1 is a positive number that normalizes the shaking torque and η_2 normalizes the shaking force. The weight matrix $\boldsymbol{\nu}$ is defined as

$$\boldsymbol{\nu} = \begin{bmatrix} \nu & 0 & 0 \\ 0 & (1-\nu) & 0 \\ 0 & 0 & (1-\nu) \end{bmatrix} \tag{301}$$

when $\nu = 0$, the problem becomes a shaking force balancing, and shaking torque balancing for $\nu = 1$.

Step 9: Finally, the optimization problem is solved either by gradient-based techniques or evolutionary algorithms.

Figure 83 shows a flow chart that illustrates the proposed procedure for dynamic balancing of planar mechanisms.

7.4 DYNAMIC BALANCING OF A SLIDER CRANK MECHANISM

In this section, the dynamic balancing of a slider crank mechanism is presented. The dimensions of the mechanism and the masses of the links are the same as those used in Section 7.2.

7.4.1 Position analysis

First, the position of the point B is calculated as a function of the input angle using the expression $\mathbf{p}_B = [\ l_1 \cos\varphi \quad l_1 \sin\varphi\ ]^T$. The position of point C is easily determined by bilateration as follows:

$$\mathbf{p}_C = \mathbf{p}_A + \mathbf{Y}_{ABC}\mathbf{u}_{AC}, \tag{302}$$

where

$$\mathbf{Y}_{ABC} = \begin{bmatrix} \mathbf{p}_{AB}\cdot\mathbf{u}_{AC} + \sqrt{s_{BC} - s_{AB} + (\mathbf{p}_{AB}\cdot\mathbf{u}_{AC})^2} & 0 \\ 0 & \mathbf{p}_{AB}\cdot\mathbf{u}_{AC} + \sqrt{s_{BC} - s_{AB} + (\mathbf{p}_{AB}\cdot\mathbf{u}_{AC})^2} \end{bmatrix}. \tag{303}$$

7.4.2 Acceleration analysis

Before solving the acceleration problem, it is necessary to solve the velocity problem. By applying Equation (145) and dividing the velocity vector into dependent and independent

Figure 83 – Flowchart of the proposed procedure for dynamic balancing.

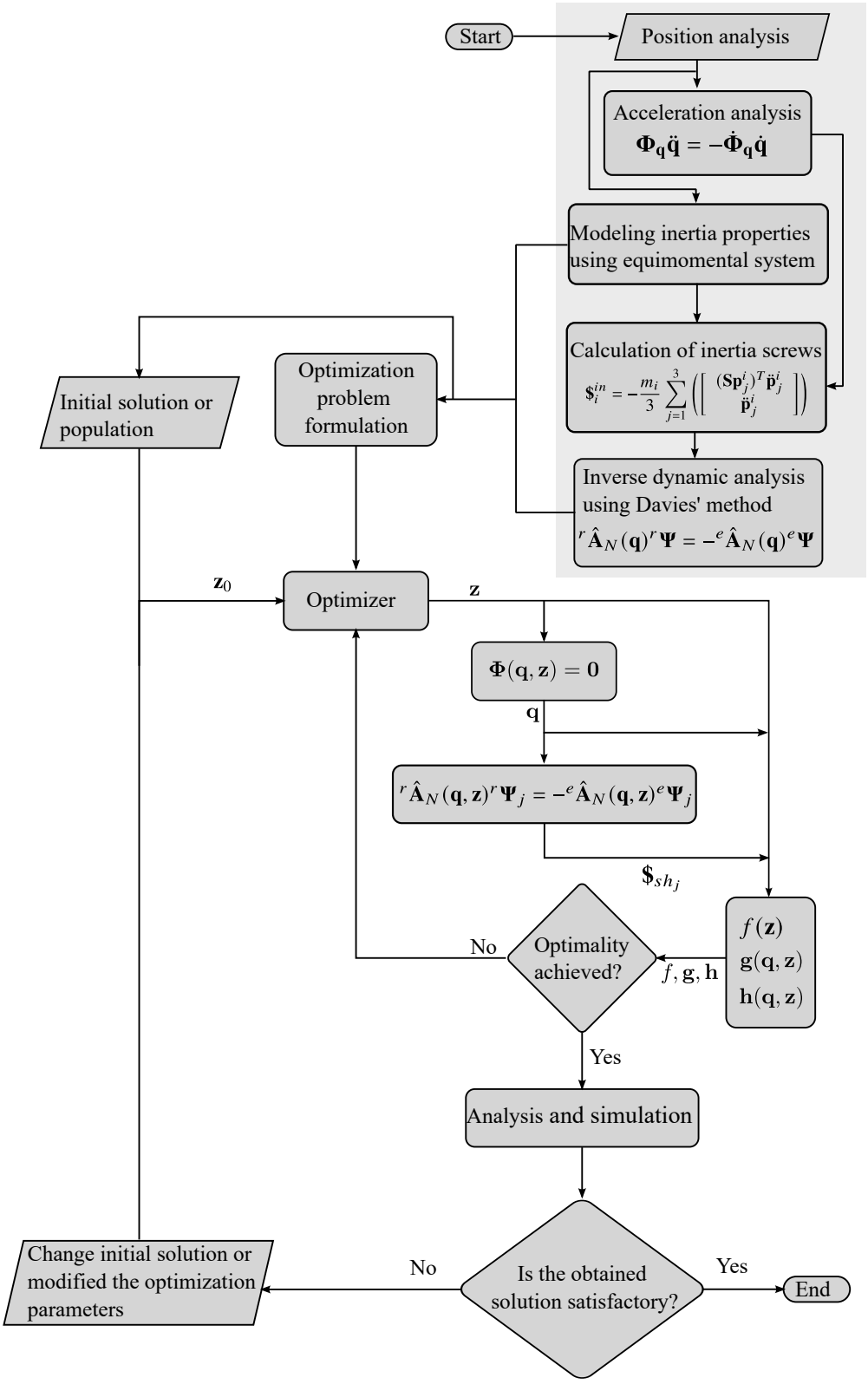

Source: The author.

velocities, we can write the velocity problem in expanded form as

$$\begin{bmatrix} -(x_C - x_B) & -2(y_C - y_B) & 2(x_C - x_B) & 2(y_C - y_B) \\ 0 & 0 & y_{\mathbf{u}_{AC}} & -x_{\mathbf{u}_{AC}} \\ 1 & 0 & 0 & 0 \\ 0 & 1 & 0 & 0 \end{bmatrix} \begin{bmatrix} \dot{x}_B \\ \dot{y}_B \\ \dot{x}_C \\ \dot{y}_C \end{bmatrix} = - \begin{bmatrix} 0 \\ 0 \\ l_1 \sin\varphi \\ -l_1 \cos\varphi \end{bmatrix} \dot{\varphi} \,. \quad (304)$$

Now the acceleration problem can be written in expanded form as follows.

$$\begin{bmatrix} -(x_C - x_B) & -2(y_C - y_B) & 2(x_C - x_B) & 2(y_C - y_B) \\ 0 & 0 & y_{\mathbf{u}_{AC}} & -x_{\mathbf{u}_{AC}} \\ 1 & 0 & 0 & 0 \\ 0 & 1 & 0 & 0 \end{bmatrix} \begin{bmatrix} \ddot{x}_B \\ \ddot{y}_B \\ \ddot{x}_C \\ \ddot{y}_C \end{bmatrix} = -\dot{\mathbf{\Phi}}_{\mathbf{q}} \begin{bmatrix} \dot{x}_B \\ \dot{y}_B \\ \dot{x}_C \\ \dot{y}_C \\ \dot{\varphi} \end{bmatrix}, \quad (305)$$

where

$$\dot{\mathbf{\Phi}}_{\mathbf{q}} = \begin{bmatrix} -2(\dot{x}_C - \dot{x}_B) & -2(\dot{y}_C - \dot{y}_B) & 2(\dot{x}_C - \dot{x}_B) & 2(\dot{y}_C - \dot{y}_B) & 0 \\ 0 & 0 & 0 & 0 & 0 \\ 0 & 0 & 0 & 0 & l_1 \cos\varphi\, \dot{\varphi} \\ 0 & 0 & 0 & 0 & l_1 \sin\varphi\, \dot{\varphi} \end{bmatrix}. \quad (306)$$

7.4.3 Optimization problem formulation

Considering that the masses of the links are previously known and that the objective is to distribute the masses in each link so that the shaking forces and shaking torques are minimized, we can define the vector of design variables as follows.

$$\mathbf{z} = \begin{bmatrix} I_{zz_1} & x_{C_1} & y_{C_1} & I_{zz_2} & x_{C_2} & y_{C_2} \end{bmatrix}^T, \quad (307)$$

where I_{zz_i} for $i = 1, 2$ are the mass moments of inertia with respect to the center of mass. In this optimization, we are not interested in the shape of the links. Therefore, we can consider in the optimization that the links are symmetric and that $I_{xy} = 0$, and $I_{xx} = I_{yy} = I_{zz}/2$. In future work, the shape of the links can be considered in the optimization using the equimomental systems formalism proposed in this work.

In this case, the only constraints in the optimization are the bounding values of the design variables, so the optimization problem is substantially simplified. Then in the dynamic balancing

of the slider crank mechanism, we can write the optimization problem as

$$\begin{aligned} \underset{\mathbf{z}}{\text{minimize}} \quad & f(\mathbf{z}) = \sum_{j=1}^{n} \$_{sh_j}^{T} \boldsymbol{\eta\nu} \$_{sh_j}, \\ \text{subject to} \quad & \underline{\mathbf{z}} \leq \mathbf{z} \leq \bar{\mathbf{z}}, \\ \text{while solving} \quad & \begin{cases} \boldsymbol{\Phi}(\mathbf{q}) = \mathbf{0}, \\ {}^{r}\hat{\mathbf{A}}_N(\mathbf{q},\mathbf{z})^{r}\boldsymbol{\Psi}_j = -{}^{e}\hat{\mathbf{A}}_N(\mathbf{q},\mathbf{z})^{e}\boldsymbol{\Psi}_j. \end{cases} \end{aligned} \tag{308}$$

7.4.4 Numerical results

Table 13 presents the masses and lengths of the links in which we consider that the piston moves horizontally and that its mass is zero. The above assumptions are made for simplicity but do not represent any loss of generality since the model allows to optimize the mechanism in any arrangement and also considering external forces on the piston. The consideration of external forces on the piston due to gas pressure is an important issue in the design of compressors and internal combustion engines; this issue will be studied in future work as it is not the focus of this work.

Table 13 – Dimensions and masses of links.

Body i	1	2	3	**Unit**
Mass m_i	1.64346901	2.51946901	0	[kg]
Length l_i	0.25	0.4	–	[m]

Source: María Teresa Orvañanos Guerrero (2022).

The mechanism is moved by a motor located at point O, rotating at a constant angular velocity $\dot{\varphi}$ of 500 [rpm]. Table 14 shows the limit values of the design variables, the initial values of the design variables, and the optimum solution. The interior-point algorithm of the Matlab toolbox was used to solve the optimization problem. The normalization values η_1 and η_2 were calculated relative to the initial solution, that is, the squared sum of the shaking torques and the squared sum of the shaking forces, respectively. In the optimization the same weight was given to the two objective functions, that is, $\nu = 0.5$. Figure 84 shows the convergence of the objective function in which a value of 3.147426×10^{-2} was reached in 31 iterations.

Table 14 – Optimization parameters and results.

Variables	$\underline{\mathbf{z}}$	$\bar{\mathbf{z}}$	$\mathbf{z}_0$	**Optimal**	**Units**
I_{zz_1}	0	1	0.01109156672	0.499933107990787	[kg · m^2]
x_{C_1}	-0.25	0.25	0.125	-0.249999863527270	[m]
y_{C_1}	-0.25	0.25	0	3.49115728996315e-08	[m]
I_{zz_2}	0	1	0.0394565196	0.0715844690734737	[kg · m^2]
x_{C_2}	-0.4	0.4	0.2	0.0923548465403011	[m]
y_{C_2}	-0.4	0.4	0	4.27135932507908e-10	[m]

Source: The author.

Figure 84 – Convergence of objective function for the dynamic balancing of slider-crank mechanism.

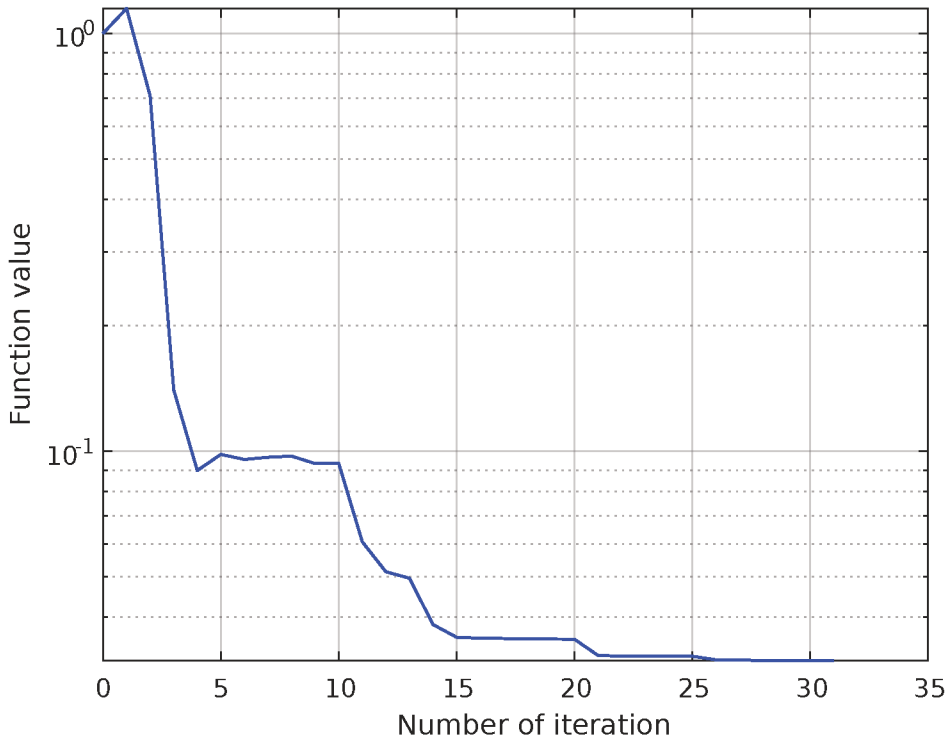

Source: The author.

The Figure 85(a) compares the shaking torque of the initial mechanism and the shaking torque of the balanced mechanism. The absolute maximum shaking torque was reduced from 134.6024 [Nm] to 0.0000067778 [Nm], representing a reduction of 99.99%. Figure 85(b) and Figure 85(c) compare the x-component of shaking force and y-component of shaking force between the initial and optimum mechanism, respectively. The shaking force was reduced from 2829.65504 [N] to 849.5889 [N], representing a reduction of 69.97%.

Figure 85 – Comparison between initial solution and optimal balancing of the slider-crank mechanism: (a) shaking torque, (b) x-component of shaking force, and (c) y-component of shaking force.

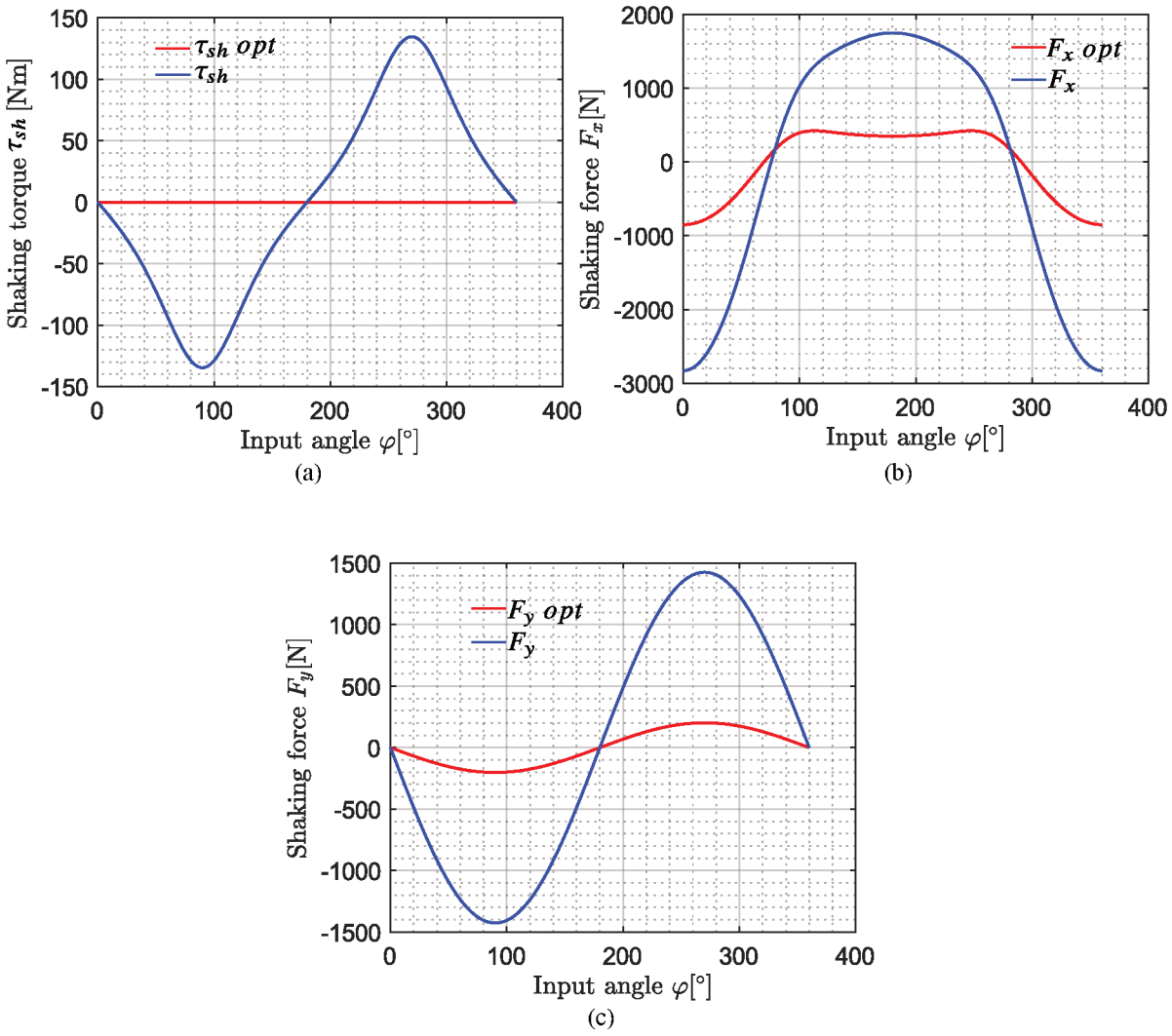

Source: The author.

8 CONCLUSIONS

First, this thesis proposes a systematic method for the dimensional synthesis of statically balanced mechanisms. Unlike the methods found in the literature, the developed method is general enough to deal with static balancing problems of planar and spatial mechanisms regardless of their complexity. The proposed method is based on the integration of natural coordinates in screw theory, which allows the advantages of both tools. The main advantages of natural coordinates are simplicity and intuitive physical interpretation; the position and orientation of each element are directly defined, and trigonometric functions do not appear in the constraint equations. In addition, natural coordinates are particularly well suited for sensitivity analysis and optimization. The main advantage of the screw theory is that it has a geometrical interpretation that allows dealing with both the kinematics and the statics of the mechanisms. In this thesis, the constitutive equations of statics are obtained systematically through Davies' method. The proposed method was applied to static balancing of a four-bar mechanism for vertical straight-line motion of an external load. Step by step descriptions are shown so that the reader can reproduce this study. The straight-line four-bar balance mechanism achieved a 99.9% reduction in the actuation torque. Next, a static balancing of an RSSR-SS mechanism was considered. In this case, a reduction in actuation torque of 99.9% and 99.89% was achieved for mechanism i and mechanism ii, respectively. A third example shows the balancing of the KUKA KR 210 R3100 manipulator robot, achieving a 95.9% reduction in the actuation torque. The examples shown are illustrative; therefore, the values found should not be used as appropriate for manufacturing a physical model, since some data were assumed and do not represent actual data.

This thesis explores the equimomental systems of three point-masses in planar rigid bodies using the concept of pseudo-inertia matrix. The research shows that it is always possible to identify an equimomental system of three equal masses located at the vertices of an isosceles triangle for a planar rigid body. The procedure presented guarantees that the masses are positive while determining equimomental systems with different masses. It is also possible to select an equimomental system of three point-masses in an isosceles triangle with a prescribed position for one of the masses. The research also investigates the conditions for prescribing the position of two and three point-masses. The process for determining an equimomental system of three point-masses of a planar rigid body is demonstrated in the first example. The second example applies the proposed model to a symmetric connecting rod due to its extensive use in combustion engines. The third example shows an equimomental system of an asymmetric bucket of an excavator.

Based on the representation of equimomental systems and with the support of the integration of natural coordinates in the screw theory, it was possible to adapt the static balancing method to the dynamic balancing of planar mechanisms. In formulating the optimization problem, the concept of a shaking screw was introduced, allowing an elegant and compact definition of the objective function. The method was applied to balancing a sliding crank mechanism where

an improvement in the shaking force of 69.97% and an improvement in the shaking torque of 99.99% was achieved.

This thesis proposes new approaches for the kinematic analysis of mechanisms based on Davies' method, natural coordinates, and the bilateration method. The study reviews kinematic analysis techniques using natural coordinates, bilateration, and screw theory. In addition, it suggests integrating natural coordinates and screw theory to simplify the analysis of velocities and accelerations in mechanisms. Incorporating natural coordinates into Davies' method allows the relative angular accelerations to be determined directly, thus facilitating the analysis of accelerations. Furthermore, the study proposes a simultaneous solution to the position and velocity problem. In this thesis an alternative formulation of the bilateration method using complex numbers is presented. This formulation shows that certain properties can be easily demonstrated using the complex form of bilateration matrices, known as bilaterators. In addition, a bilateration matrix for a planar RRRP mechanism is proposed, which is helpful in solving the position kinematics of more complex planar mechanisms.

8.1 FUTURE WORK

Future works on this thesis includes:

- In this work, the problem of structural synthesis of statically balanced mechanisms was not addressed. This problem can be dealt with using the techniques developed in Laboratory of Applied Robotics Raul Guenther (LAR), particularly the techniques proposed by Murai (2019).
- To extend the static balancing method to planar and spatial compliant mechanisms.
- Develop user-friendly and intuitive software that allows the engineering designer to explore a wide number of possible solutions.
- To explore the problem of dimensional synthesis of dynamic balancing of spatial mechanisms using equimomental systems of point-masses.
- To develop a dynamic synthesis method, i.e., given the inertial properties of a rigid body, to synthesize the rigid body subject to constraints on the shape and stresses supported. Inertia from a geometrical perspective, as studied in (TISCHLER et al., 2000; SELIG; MARTINS, 2014), seems to be a promising approach to solving the above problem.
- To study the relationship between the Jacobian calculated using natural coordinates and the geometric Jacobian constructed with screws. If it is possible to determine the Jacobian in natural coordinates using screws directly, it will facilitate the kinematic analysis of position, velocity analysis, and acceleration analysis of mechanisms.
- To extend the bilateration method to spherical mechanisms. For this, it is necessary to determine a matrix expression in terms of the arcs that form the links.

8.2 PUBLISHED AND SUBMITTED PAPERS

This work yielded several papers for journals and conferences:

- NUÑEZ, Neider Nadid Romero; VIEIRA, Rodrigo S.; MARTINS, Daniel. Equimomental systems representations of point-masses of planar rigid-bodies. Acta Mechanica, [S. l.], p. 1-16, 18 Aug. 2023.
- NUÑEZ, Neider Nadid Romero; CUTA, Carlos Humberto Pinzón; VIEIRA, Rodrigo S.; MARTINS, Daniel. Optimal dimensional synthesis of central-lever steering linkage using natural coordinates as design variables. 27th International Congress of Mechanical Engineering COBEM, A Associação Brasileira de Engenharia e Ciências Mecânicas – ABCM, n. 27, p. 1-10, 7 nov. 2023.
- NUÑEZ, Neider Nadid Romero; ZHAO, Jing-Shan; MISYURI, Sergey Yurievich; VIEIRA, Rodrigo S.; MARTINS, Daniel. A Screw Theory-based Method for Approximate Static Balancing of a RSSR-SS Mechanism. 16th World Congress of the International Federation for the Promotion of Mechanism and Machine Science, Mechanisms and Machine Science, n. 16, p. 1-10, 5 nov. 2023.
- NUÑEZ, Neider Nadid Romero; ZHAO, Jing-Shan; NICOLAZZI, Lauro Cesar; VIEIRA, Rodrigo S.; MARTINS, Daniel. Double Butterfly Steering Linkage. 16th World Congress of the International Federation for the Promotion of Mechanism and Machine Science, Mechanisms and Machine Science, n. 16, p. 1-10, 5 nov. 2023.
- NUÑEZ, Neider Nadid Romero; FLOREZ, Anderson Romero; VIEIRA, Rodrigo S.; MARTINS, Daniel. Dimensional synthesis of rack-and-pinion steering mechanism using a novel synthesis equation. Journal of the Brazilian Society of Mechanical Sciences and Engineering, [S. l.], p. 1-10, 20 jun. 2023.
- Neider Nadid Romero; CONTRERAS, Gonzalo Moreno; TOLOZA , Sonia Carolina Mantilla; MARTINS, Daniel. Balanceo estático de un mecanismo de rehabilitación de miembro inferior para reducir los requerimientos de actuación. XV Congreso Iberoamericano de Ingeniería Mecánica, Universidad Nacional de Educación a Distancia, p. 1-7, 22 nov. 2022.
- BUZZI, B.F.; ROMERO, N.N.; MARTINS, D.; de Souza Vieira, R. Dimensional Synthesis of a Two-Axles Steering System. In: Pucheta, M., Cardona, A., Preidikman, S., Hecker, R. (eds) Multibody Mechatronic Systems. MuSMe 2021. Mechanisms and Machine Science, vol 94. Springer, Cham.
- NUÑEZ, Neider Nadid Romero; CAMPOS, Alexandre; MARTINS, Daniel; VIEIRA , Rodrigo S. A new approach for the optimal synthesis of four-bar path generator linkages. SN Applied Sciences, [S. l.], v. 1, n. 11, p. 1-8, 28 out. 2019.

REFERENCES

ALABUZHEV, PM. **Vibration protection and measuring systems with quasi-zero stiffness**. [S.l.]: CRC Press, 1989.

ALAMDARI, Aliakbar; HAGHIGHI, Reza; KROVI, Venkat. Gravity-Balancing of Elastic Articulated-Cable Leg-Orthosis Emulator. **Mechanism and Machine Theory**, v. 131, p. 351–370, Jan. 2019. ISSN 0094114X. DOI: 10.1016/j.mechmachtheory.2018.09.019.

ANA MAGDALENA DE JUAN DE LUNA. **METODOLOGÍA DE SÍNTESIS ÓPTIMA DIMENSIONAL DE MECANISMOS INCLUYENDO OBJETIVOS DE POSICIÓN Y VELOCIDAD**. 2011. s. 228. PhD thesis – Universidad de Cantabria.

ANGELES, J.; BERNIER, A. The Global Least-Square Optimization of Function-Generating Linkages. **Journal of Mechanisms, Transmissions, and Automation in Design**, v. 109, p. 204–209, 2 June 1987. ISSN 0738-0666. DOI: 10.1115/1.3267439.

ARAVIND BASKAR, GURUNATHAN SARAVANA KUMAR, Sandipan Bandyopadhyay. Design of a static balancing mechanism for coordinated motion of an external load. In: INDIAN INSTITUTE OF TECHNOLOGY KANPUR (Ed.), DECEMBER. **2nd International and 17th National Conference on Machines and Mechanisms**. Kanpur: iNaCoMM2015, 2015. p. 1–9.

ARORA, Jasbir. **Introduction to Optimum Design**. [S.l.]: Elsevier, 2012. ISBN 9780123813756. DOI: 10.1016/C2009-0-61700-1.

ARORA, Rajesh Kumar. **Optimization: algorithms and applications**. [S.l.]: CRC Press, 2015.

AVELLO, Alejo. **Teoría de Máquinas**. 2. ed. Pamplona, España: [s.n.], 2014. p. 394. ISBN 9788480812504.

BALL, Robert Stawell. **A Treatise on the Theory of Screws**. [S.l.]: Cambridge university press, 1998.

BANALA, Sai K. et al. Gravity-balancing leg orthosis and its performance evaluation. **IEEE Transactions on Robotics**, v. 22, n. 6, p. 1228–1239, 2006. ISSN 15523098. DOI: 10.1109/TRO.2006.882928.

BARANOV, GG; ROJAS, G, et al. **Curso de la Teoría de Mecanismos y Máquinas**. [S.l.]: Mir, 1979. v. 2.

BEER, F.P. **Vector Mechanics for Engineers: Statics**. [S.l.]: McGraw-Hill Higher Education, 2010. (Vector Mechanics for Engineers). ISBN 9780073529233.

BOTTEMA, Oene; ROTH, Bernard. **Theoretical kinematics**. New York: Dover Publication, 1990.

BUSTOS, Igor Fernández de. **Síntesis cinemática dimensional de mecanismos mediante algoritmos genéticos**. 2004. PhD thesis – PhD Dissertation, University of the Basque Country.

CARRABOTTA, Roberto et al. Optimal static balancing of a spatial palletizing robot. **Proceedings of the ECCOMAS Thematic Conference on Multibody Dynamics 2015, Multibody Dynamics 2015**, p. 817–827, 2015.

CAZANGI, Humberto Reder. **Aplicação do método de Davies para análise cinemática e estática de mecanismos com múltiplos graus de liberdade**. 2008. PhD thesis – UNIVERSIDADE FEDERAL DE SANTA CATARINA.

CHAUDHARY, Himanshu; SAHA, Subir Kumar. Balancing of four-bar linkages using maximum recursive dynamic algorithm. **Mechanism and Machine Theory**, v. 42, p. 216–232, 2 Feb. 2007. ISSN 0094114X. DOI: 10.1016/j.mechmachtheory.2006.02.008.

CHAUDHARY, Himanshu; SAHA, Subir Kumar. Balancing of shaking forces and shaking moments for planar mechanisms using the equimomental systems. **Mechanism and Machine Theory**, v. 43, p. 310–334, 3 Mar. 2008. ISSN 0094114X. DOI: 10.1016/j.mechmachtheory.2007.04.003.

CHAUDHARY, Himanshu; SAHA, Subir Kumar. **Dynamics and Balancing of Multibody Systems**. [S.l.]: Springer Berlin Heidelberg, 2009. v. 37. ISBN 978-3-540-78178-3. DOI: 10.1007/978-3-540-78179-0.

CHAUDHARY, Himanshu; SAHA, Subir Kumar. Equimomental System and Its Applications. In: VOLUME 3: Dynamic Systems and Controls, Symposium on Design and Analysis of Advanced Structures, and Tribology. [S.l.]: ASMEDC, Jan. 2006. p. 33–42. DOI: 10.1115/ESDA2006-95066.

CHAUDHARY, Kailash; CHAUDHARY, Himanshu. Dynamic balancing of planar mechanisms using genetic algorithm. **Journal of Mechanical Science and Technology**, v. 28, p. 4213–4220, 10 Oct. 2014. ISSN 1738-494X. DOI: 10.1007/s12206-014-0934-4.

CHAUDHARY, Kailash; CHAUDHARY, Himanshu. Optimal dynamic balancing and shape synthesis of links in planar mechanisms. **Mechanism and Machine Theory**, v. 93, p. 127–146, Nov. 2015. ISSN 0094114X. DOI: 10.1016/j.mechmachtheory.2015.07.006.

CHAUDHARY, Kailash; CHAUDHARY, Himanshu. Optimum Balancing of Slider-crank Mechanism Using Equimomental System of Point-masses. **Procedia Technology**, v. 14, p. 35–42, 2014. ISSN 22120173. DOI: 10.1016/j.protcy.2014.08.006.

CHICA, F. J. Gil; POLO, M Pérez; MOLINA, M Pérez. Note on an apparently forgotten theorem about solid rigid dynamics. **European Journal of Physics**, v. 35, p. 045003, 4 July 2014. ISSN 0143-0807. DOI: 10.1088/0143-0807/35/4/045003.

COLLARD, Jean-François; DUYSINX, Pierre; FISETTE, Paul. Optimal synthesis of planar mechanisms via an extensible-link approach. **Structural and Multidisciplinary Optimization**, v. 42, p. 403–415, 3 Sept. 2010. ISSN 1615-147X. DOI: 10.1007/s00158-010-0500-3.

DAVIES, T H. Dual coupling networks. **Proceedings of the Institution of Mechanical Engineers, Part C: Journal of Mechanical Engineering Science**, v. 220, n. 8, p. 1237–1247, Aug. 2006. ISSN 0954-4062. DOI: 10.1243/09544062C09405.

DAVIES, T H. Kirchhoff's circulation law applied to multi-loop kinematic chains. **Mechanism and Machine Theory**, v. 16, p. 171–183, 3 Jan. 1981. ISSN 0094114X. DOI: 10.1016/0094-114X(81)90033-1.

DAVISON, JK; HUNT, KH. **Robotics and Screw Theory, Application of Kinematics and Statics to Robots**. [S.l.]: Oxford Univ. Press, 2004.

DEEPAK, Sangamesh R.; ANANTHASURESH, G.K. Static balancing of a four-bar linkage and its cognates. **Mechanism and Machine Theory**, v. 48, p. 62–80, Feb. 2012. ISSN 0094114X. DOI: 10.1016/j.mechmachtheory.2011.09.009.

DENIZHAN, Onur. **Three-Position Four-Bar Linkage Mechanism Synthesis , Static Balancing and Optimization of Automotive Engine Hood**. 2015. s. 98. PhD thesis – Lehigh University.

ERTHAL, JORGE LUIZ. **Modelo cinestático para análise de rolagem em veículos**. 2010. PhD thesis – Universidade Federal de Santa Catarina.

FÁBIÁN, Balázs; THALLMAIR, Sebastian; HUMMER, Gerhard. Optimal bond-constraint topology for molecular dynamics simulations of cholesterol. **Theoretical and Computational Chemistry**, 2022. DOI: 10.26434/chemrxiv-2022-t41rx.

FOIX, Salvador Cardona. **Teoría de máquinas**. [S.l.]: Univ. Politéc. de Catalunya, 2000. v. 95.

FRANDSEN, P.E.; JONASSON, K. **Unconstrained optimization. Lecture note for the course "Optimization and Data Fitting"**. Denmark: Technical University of Denmark, 2004.

FRANTZ, Julio Cesar et al. **A New Methodology for the Balancing of Mechanisms Using the Davies' Method**. [S.l.]: Springer International Publishing, 2018. v. 54, p. 203–212. ISBN 978-3-319-67566-4. DOI: 10.1007/978-3-319-67567-1_19.

FREAKLEY, Philip K; PAYNE, Arthur Robert. **Theory and practice of engineering with rubber**. [S.l.]: Applied Science Publishers, 1978.

GALLEGO SANCHEZ, Juan Andrés. **Statically Balanced Compliant Mechanisms**. 2013. s. 232. PhD thesis – Technische Universtiteit Delft. ISBN 9789461862150. DOI: 10.13140/2.1.3093.2163.

GALLEGO, Juan A; HERDER, Just L. Buckling as a new perspective on static balancing of mechanisms. **13th World Congress in Mechanism and Machine Science**, November, p. 19–25, 2011.

GARCÍA-MARINA, V. et al. Using nodal coordinates as variables for the dimensional synthesis of mechanisms. **Meccanica**, v. 53, n. 8, p. 1981–1996, 2018. ISSN 15729648. DOI: 10.1007/s11012-017-0799-6.

GOLDSTEIN, H.; POOLE, C.P.; SAFKO, J.L. **Classical Mechanics**. [S.l.]: Addison Wesley, 2002. (Addison-Wesley series in physics). ISBN 9780321188977.

GOLDSTEIN, H.; POOLE, C.P.; SAFKO, J.L. **Classical Mechanics**. [S.l.]: Pearson, 2013. ISBN 9781292026558.

GÖSSNER, Stefan. Equimomental Polygonal Systems. **Duisburg-Essen Publications online**, p. 1–7, 1 Feb. 2021. ISSN 0094114X. DOI: 10.17185/duepublico/74044.

GUPTA, Vinay; CHAUDHARY, Himanshu; SAHA, Subir K. Dynamics and actuating torque optimization of planar robots. **Journal of Mechanical Science and Technology**, v. 29, p. 2699–2704, 7 July 2015. ISSN 1738-494X. DOI: 10.1007/s12206-015-0517-z.

GUPTA, Vinay; SAHA, Subir Kumar; CHAUDHARY, Himanshu. Optimum Design of Serial Robots. **Journal of Mechanical Design**, v. 141, 8 Aug. 2019. ISSN 1050-0472. DOI: 10.1115/1.4042623.

HERDER, JL; VAN DEN BERG, FPA. Statically balanced compliant mechanisms (SBCM's), an example and prospects. In: PROCEEDINGS of the 26th ASME DETC biennial, mechanisms and robotics conference. [S.l.: s.n.], 2000.

HERDER, Justus Laurens. **Energy-free Systems. Theory, conception and design of statically balanced spring mechanisms**. 2001. s. 248. PhD thesis – Delft University of Technology. ISBN 9789037001921. DOI: 10.13140/RG.2.1.3942.8966.

HERNÁNDEZ, Alfonzo et al. **general purpose software for the kinematics and dynamics analysis of planar and spatial mechanisms, GIM**. [S.l.]: University of the Basque Country. Available from: https://www.ehu.eus/compmech/software/.

HIBBELER, R.C. **Engineering Mechanics: Statics and dynamics**. [S.l.]: Prentice-Hall, 2010. (Engineering Mechanics). ISBN 9780138149291.

HORN, Roger A; JOHNSON, Charles R. **Matrix analysis**. [S.l.]: Cambridge university press, 2012.

HUANG, N. C. Equimomental system of rigidly connected equal particles. **Journal of Guidance, Control, and Dynamics**, v. 16, p. 1194–1196, 6 Nov. 1993. ISSN 0731-5090. DOI: 10.2514/3.21150.

JALÓN, J.García De; UNDA, J.; AVELLO, A. Natural coordinates for the computer analysis of multibody systems. **Computer Methods in Applied Mechanics and Engineering**, v. 56, p. 309–327, 3 July 1986. ISSN 00457825. DOI: 10.1016/0045-7825(86)90044-7.

JALÓN; BAYO, Eduardo. **Kinematic and dynamic simulation of multibody systems**. [S.l.]: Springer-Verlag, 1994. p. 452. ISBN 0387940960.

JEAN-FRANÇOIS COLLARD. **Geometrical and kinematic optimization of closed-loop multibody systems**. 2007. s. 203. Ph.D – Université Catholique de Louvain.

JONG, Jan de; DIJK, Johannes van; HERDER, Just. **On the Dynamic Equivalence of Planar Mechanisms, an Inertia Decomposition Method**. [S.l.]: Springer International Publishing, 2017. p. 51–59. DOI: 10.1007/978-3-319-44156-6_6.

DE-JUAN, A.; SANCIBRIAN, R.; VIADERO, F. Optimal synthesis of function generation in steering linkages. **International Journal of Automotive Technology**, v. 13, p. 1033–1046, 7 Dec. 2012. ISSN 1229-9138. DOI: 10.1007/s12239-012-0106-4.

KAPLAN, W. **Advanced Calculus**. [S.l.]: Addison-Wesley, 2002. (Addison-Wesley higher mathematics). ISBN 9780201799378.

KIM, Chang-Kyun et al. Three-Degrees-of-Freedom Passive Gravity Compensation Mechanism Applicable to Robotic Arm With Remote Center of Motion for Minimally Invasive Surgery. **IEEE Robotics and Automation Letters**, v. 4, p. 3473–3480, 4 Oct. 2019. ISSN 2377-3766. DOI: 10.1109/LRA.2019.2926953.

KOMATSU. **Hydraulic excavator PC400**. [S.l.: s.n.], 2017. Accessed: 2022-12-19. Available from: https://www.komatsu.com.

KUMANI, Devi Singh; CHAUDHARY, Himanshu. Minimizing constraint forces and moments of manipulators using teaching–learning-based optimization and octahedron point mass model. **Proceedings of the Institution of Mechanical Engineers, Part C: Journal of Mechanical Engineering Science**, v. 232, p. 3500–3511, 19 Oct. 2018. ISSN 0954-4062. DOI: 10.1177/0954406217736341.

KUO, Chin-Hsing; LAI, Shao-Jung. Design of a Novel Statically Balanced Mechanism for Laparoscope Holders With Decoupled Positioning and Orientating Manipulation. **Journal of Mechanisms and Robotics**, v. 8, 1 Feb. 2016. ISSN 1942-4302. DOI: 10.1115/1.4029789.

KUO, Chin-Hsing; NGUYEN, Vu Linh, et al. Statically Balancing a Reconfigurable Mechanism by Using One Passive Energy Element Only: A Case Study. **Journal of Mechanisms and Robotics**, v. 13, 4 Aug. 2021. ISSN 1942-4302. DOI: 10.1115/1.4050682.

LAUB, A.J. **Matrix Analysis for Scientists and Engineers**. [S.l.]: Society for Industrial and Applied Mathematics, 2005. (Other Titles in Applied Mathematics). ISBN 9780898715767.

LAUS, L. P.; SELIG, J. M. Rigid body dynamics using equimomental systems of point-masses. **Acta Mechanica**, Springer, v. 231, p. 221–236, 1 Jan. 2020. ISSN 0001-5970. DOI: 10.1007/s00707-019-02543-3.

LAUS, L.P.; SIMAS, H.; MARTINS, D. Machine efficiency determined using graph and screw theories with application in robotics. **Mechanism and Machine Theory**, v. 148, p. 103748, June 2020. ISSN 0094114X. DOI: 10.1016/j.mechmachtheory.2019.103748.

LAVAL UNIVERSITY ROBOTICS LABORATORY. **Static and dynamic balancing of parallel mechanisms**. [S.l.: s.n.], 2002. Available from: https://robot.gmc.ulaval.ca/en/research/research-thrusts/parallel-mechanisms/equilibrage-statique-et-dynamique-de-mecanismes-paralleles/. Visited on: 2020.

LIN, Po Yang; SHIEH, Win Bin; CHEN, Dar Zen. A stiffness matrix approach for the design of statically balanced planar articulated manipulators. **Mechanism and Machine Theory**, Elsevier Ltd, v. 45, n. 12, p. 1877–1891, 2010. ISSN 0094114X. DOI: 10.1016/j.mechmachtheory.2010.08.003.

LIN, Po-Yang; SHIEH, Win-Bin; CHEN, Dar-Zen. A theoretical study of weight-balanced mechanisms for design of spring assistive mobile arm support (MAS). **Mechanism and Machine Theory**, v. 61, p. 156–167, Mar. 2013. ISSN 0094114X. DOI: 10.1016/j.mechmachtheory.2012.11.003.

MA, Ou. **An innovative 6-DOF platform for testing a space robotic system to perform contact tasks in zero-gravity environment**. [S.l.], 2013.

MA, Yiwei et al. Kinetostatic Modelling and Gravity Compensation of the TriMule Robot. **Mechanisms and Machine Science**, p. 1731–1740, 2019. DOI: 10.1007/978-3-030-20131-9_171.

MARÍA TERESA ORVAÑANOS GUERRERO. **Análisis y optimización de mecanismos para el balanceo dinámico utilizando coordenadas naturales**. 2022. s. 197. PhD thesis – Universidad Panamericana.

MARTINI, Alberto; TRONCOSSI, Marco; RIVOLA, Alessandro. Algorithm for the static balancing of serial and parallel mechanisms combining counterweights and springs: Generation, assessment and ranking of effective design variants. **Mechanism and Machine Theory**, Elsevier Ltd, v. 137, p. 336–354, 2019. ISSN 0094114X. DOI: 10.1016/j.mechmachtheory.2019.03.031.

MEJIA, L.; SIMAS, H.; MARTINS, D. Wrench capability in redundant planar parallel manipulators with net degree of constraint equal to four, five or six. **Mechanism and Machine Theory**, v. 105, p. 58–79, Nov. 2016. ISSN 0094114X. DOI: 10.1016/j.mechmachtheory.2016.06.020.

MOORE, Brian. **Dynamic balancing of linkages by algebraic methods**. 2009. s. 87. PhD thesis – Johannes-Kepler University Linz.

MURAI, Estevan Hideki. **Number synthesis methods for mechanism design: an alternative approach**. 2019. PhD thesis – Universidade Federal de Santa Catarina.

NANSAI, Shunsuke; ELARA, Mohan Rajesh; IWASE, Masami. Speed Control of Jansen Linkage Mechanism for Exquisite Tasks. **Journal of Advanced Simulation in Science and Engineering**, v. 3, p. 47–57, 1 2016. ISSN 2188-5303. DOI: 10.15748/jasse.3.47.

NGUYEN, Vu Linh. A design approach for gravity compensators using planar four-bar mechanisms and a linear spring. **Mechanism and Machine Theory**, v. 172, p. 104770, June 2022. ISSN 0094114X. DOI: 10.1016/j.mechmachtheory.2022.104770.

NGUYEN, Vu Linh. Gravity Compensation of Articulated Robots Using Spring Four-Bar Mechanisms. In: SPRINGER. INTERNATIONAL Symposium on Multibody Systems and Mechatronics. [S.l.: s.n.], 2021. p. 201–209. DOI: 10.1007/978-3-030-88751-3_21.

NIKRAVESH, Parviz E. **Planar multibody dynamics: formulation, programming and applications**. Ed. by CRC press. [S.l.]: CRC press, 2007.

NIKRAVESH, Parviz E. **Computer-aided analysis of mechanical systems**. Ed. by CRC press. [S.l.]: Prentice-Hall, 1988. p. 370. ISBN 0131642200.

NIKRAVESH, Parviz E. **Planar Multibody Dynamics**. Second edition. | Boca Raton : Taylor & Francis, CRC Press, CRC Press, Sept. 2018. ISBN 9781315105437. DOI: 10.1201/b22302.

PARK, ST; LUU, TT. Techniques for optimizing parameters of negative stiffness. **Proceedings of the Institution of Mechanical Engineers, Part C: Journal of Mechanical Engineering Science**, SAGE Publications Sage UK: London, England, v. 221, n. 5, p. 505–510, 2007.

PATEL, Kaushik; BHATT, Pina M. Modeling and dynamic analysis of multi-loop RSSR-SS parallel manipulator. **Materials Today: Proceedings**, v. 66, p. 2001–2007, 2022. ISSN 22147853. DOI: 10.1016/j.matpr.2022.05.443.

PERREAULT, Simon; CARDOU, Philippe; GOSSELIN, Clément. Approximate static balancing of a planar parallel cable-driven mechanism based on four-bar linkages and springs. **Mechanism and Machine Theory**, Elsevier Ltd, v. 79, p. 64–79, 2014. ISSN 0094114X. DOI: 10.1016/j.mechmachtheory.2014.04.008.

PETUYA, Víctor et al. Educational software tools for the kinematic analysis of mechanisms. **Computer Applications in Engineering Education**, v. 22, p. 72–86, 1 Mar. 2014. ISSN 10613773. DOI: 10.1002/cae.20532.

PLATUS, David L. Vibration isolation system. **The Journal of the Acoustical Society of America**, Acoustical Society of America, v. 94, n. 2, p. 1177–1177, 1993.

PLATUS, DL. Smoothing out bad vibes. **Machine design**, v. 65, n. 4, p. 123, 1993.

PREMKUMAR, P.; KRAMER, S. Synthesis of Multi-Loop Spatial Mechanisms by Iterative Analysis: The RSSR-SS Path Generator. **Journal of Mechanical Design**, v. 112, p. 69–73, 1 Mar. 1990. ISSN 1050-0472. DOI: 10.1115/1.2912580.

RADAELLI, Giuseppe; GALLEGO, Juan A.; HERDER, Just L. An energy approach to static balancing of systems with torsion stiffness. **Journal of Mechanical Design, Transactions of the ASME**, v. 133, n. 9, p. 1–8, 2011. ISSN 10500472. DOI: 10.1115/1.4004704.

RAO, R Venkata; WAGHMARE, Gajanan. Optimum static balancing of a robot manipulator using TLBO algorithm. **Advances in Robotics Research**, v. 2, n. 1, p. 13–31, 2018.

REDDY, Junuthula Narasimha. **Energy principles and variational methods in applied mechanics**. [S.l.]: John Wiley & Sons, 2017.

RIVIN, Eugene. **Stiffness and damping in mechanical design**. [S.l.]: CRC Press, 1999.

RIVIN, Eugene I. **Passive vibration isolation**. [S.l.: s.n.], 2003.

ROJAS, NICOLAS. **Distance-based formulations for the position analysis of kinematic chains**. 2012. s. 159. Ph.D – Universitat Politècnica de Catalunya.

ROJAS, Nicolas. **Distance-based formulations for the position analysis of kinematic chains**. 2012. s. 159. PhD thesis – Universitat Politècnica de Catalunya.

ROJAS, Nicolás; THOMAS, Federico. On closed-form solutions to the position analysis of Baranov trusses. **Mechanism and Machine Theory**, v. 50, p. 179–196, Apr. 2012. ISSN 0094114X. DOI: 10.1016/j.mechmachtheory.2011.10.010.

ROMERO NUÑEZ, Neider Nadid et al. Optimal Synthesis of a Theo Jansen Mechanism. **International Review of Mechanical Engineering (IREME)**, v. 12, n. 12, p. 981, Dec. 2018. ISSN 2532-5655. DOI: 10.15866/ireme.v12i12.16457.

ROMERO, Neider Nadid et al. A new approach for the optimal synthesis of four-bar path generator linkages. **SN Applied Sciences**, Springer, v. 1, p. 1504, 11 Nov. 2019. ISSN 2523-3963. DOI: 10.1007/s42452-019-1511-3.

ROSYID, Abdur; EL-KHASAWNEH, Bashar; ALAZZAM, Anas. Gravity compensation of parallel kinematics mechanism with revolute joints using torsional springs. **Mechanics Based Design of Structures and Machines**, v. 48, p. 27–47, 1 Jan. 2019. ISSN 1539-7734. DOI: 10.1080/15397734.2019.1619579.

ROUTH, E.J. **The Elementary Part of A Treatise on the Dynamics of a System of Rigid Bodies: Being Part I. of a Treatise on the Whole Subject. With Numerous Examples**. [S.l.]:

Macmillan and Company, limited, 1897. (The Elementary Part of A Treatise on the Dynamics of a System of Rigid Bodies).

ROUTH, Edward John. **A Treatise on the Dynamics of a System of Rigid Bodies. Elemementary part I**. [S.l.]: Dover Publication Inc, 1905. v. 1.

RUSSO, Andrea; SINATRA, Rosario; XI, Fengfeng. Static balancing of parallel robots. **Mechanism and Machine Theory**, v. 40, n. 2, p. 191–202, 2005. ISSN 0094114X. DOI: 10.1016/j.mechmachtheory.2004.06.011.

SEGLA, S.; KALKER-KALKMAN, C.M.; SCHWAB, A.L. Statical balancing of a robot mechanism with the aid of a genetic algorithm. **Mechanism and Machine Theory**, v. 33, n. 1-2, p. 163–174, Jan. 1998. ISSN 0094114X. DOI: 10.1016/S0094-114X(97)00012-8.

SELIG, J. M. Equimomental Systems and Robot Dynamics. In: PROCEEDINGS of the IMA Conference on Mathematics of Robotics. [S.l.]: Institute of Mathematics and its Applications, 2015. p. 1–8. DOI: 10.19124/ima.2015.001.21.

SELIG, J. M.; MARTINS, D. On the line geometry of rigid-body inertia. **Acta Mechanica**, v. 225, p. 3073–3101, 11 Nov. 2014. ISSN 0001-5970. DOI: 10.1007/s00707-014-1103-7.

SELIG, J.M. **Geometric Fundamentals of Robotics**. [S.l.]: Springer New York, 2005. ISBN 978-0-387-20874-9. DOI: 10.1007/b138859.

SEYFERTH, W. Massenersatz durch punktmassen in räumlichen Getrieben. **Mechanism and Machine Theory**, v. 9, p. 49–59, 1 Mar. 1974. ISSN 0094114X. DOI: 10.1016/0094-114X(74)90007-X.

SHABANA, Ahmed A. **Dynamics of multibody systems**. Cambridge: Cambridge University Press, 2013. p. 1–27. ISBN 9781107337213. DOI: 10.1017/CBO9781107337213.

SHEKARFOROUSH, S. M. Mehdi; EGHTESAD, Mohammad; FARID, Mehrdad. Kinematic and Static Analyses of Statically Balanced Spatial Tensegrity Mechanism with Active Compliant Components. **Journal of Intelligent & Robotic Systems**, v. 71, p. 287–302, 3-4 Sept. 2013. ISSN 0921-0296. DOI: 10.1007/s10846-012-9784-4.

SHERWOOD, A.A.; HOCKEY, B.A. The optimisation of mass distribution in mechanisms using dynamically similar systems. **Journal of Mechanisms**, v. 4, p. 243–260, 3 Sept. 1969. ISSN 00222569. DOI: 10.1016/0022-2569(69)90005-6.

SHIN, E.; STREIT, D. A. An energy efficient quadruped with two-stage equilibrator. **Journal of Mechanical Design, Transactions of the ASME**, v. 115, n. 1, p. 156–163, 1993. ISSN 10500472. DOI: 10.1115/1.2919313.

SHIN, Eungsoo; STREIT, Donald A. Spring equilibrator theory for static balancing of planar pantograph linkages. **Mechanism and Machine Theory**, v. 26, n. 7, p. 645–657, 1991. ISSN 0094114X. DOI: 10.1016/0094-114X(91)90027-2.

SIMIONESCU, Ion; CIUPITU, Liviu. Static balancing of the industrial robot arms. Part I: discrete balancing. **Mechanism and Machine Theory**, v. 35, n. 9, p. 1287–1298, 2000. ISSN 0094114X. DOI: 10.1016/S0094-114X(99)00067-1.

SIMIONESCU, Ion; CIUPITU, Liviu. Static balancing of the industrial robot arms. Part II: continuous balancing. **Mechanism and Machine Theory**, v. 35, n. 9, p. 1299–1311, 2000. ISSN 0094114X. DOI: 10.1016/S0094-114X(99)00068-3.

SIMIONESCU, Ion; CIUPITU, Liviu; IONITA, Luciana Cristina. Static balancing with elastic systems of DELTA parallel robots. **Mechanism and Machine Theory**, Elsevier B.V., v. 87, p. 150–162, 2015. ISSN 0094114X. DOI: 10.1016/j.mechmachtheory.2014.11.008.

SOMMERVILLE, D. M. Y. Equimomental Tetrads of a Rigid Body. **Mathematical Notes**, v. 26, p. x–xi, Oct. 1930. ISSN 1757-7489. DOI: 10.1017/S1757748900002127.

STAPEL, Aa¨ ron; HERDER, Just L. Feasibility study of a fully compliant statically balanced laparoscopic grasper. In: INTERNATIONAL Design Engineering Technical Conferences and Computers and Information in Engineering Conference. [S.l.: s.n.], 2004. p. 635–643.

STREIT, D. A.; SHIN, E. Equilibrators for planar linkages. **Journal of Mechanical Design, Transactions of the ASME**, v. 115, n. 3, p. 604–611, 1993. ISSN 10500472. DOI: 10.1115/1.2919233.

SUH, Chung Ha; RADCLIFFE, Charles W. **Kinematics and mechanisms design**. [S.l.]: Wiley, 1978.

TAKAHASHI, Takuto et al. Computational Design of Statically Balanced Planar Spring Mechanisms. **IEEE Robotics and Automation Letters**, IEEE, v. 4, n. 4, p. 4438–4444, 2019. ISSN 23773766. DOI: 10.1109/LRA.2019.2929984.

TISCHLER, CR et al. Rigid-body inertia and screw geometry. In: PROCEEDINGS of a Symposium Commemorating the Legacy, Works, and Life of Sir Robert Stawell Ball Upon the 100th Anniversary of A Treatise on the Theory of Screws. [S.l.: s.n.], 2000.

TOLOU, Nima; HENNEKEN, Vincent A; HERDER, Just L. Statically balanced compliant micro mechanisms (SB-MEMS): Concepts and simulation. In: INTERNATIONAL Design Engineering Technical Conferences and Computers and Information in Engineering Conference. [S.l.: s.n.], 2010. p. 447–454.

TREASE, Brian; DEDE, E. Statically-balanced compliant four-bar mechanism for gravity compensation. **ASME Student Mechanism Design Competition**, p. 1–13, 2004.

TSENG, Tzu Yu et al. A novel reconfigurable gravity balancer for lower-limb rehabilitation with switchable hip/knee-only exercise. **Journal of Mechanisms and Robotics**, v. 9, n. 4, 2017. ISSN 19424310. DOI: 10.1115/1.4036218.

VAN KHANG, Nguyen. Consistent definition of partial derivatives of matrix functions in dynamics of mechanical systems. **Mechanism and Machine Theory**, Elsevier Ltd, v. 45, n. 7, p. 981–988, 2010. ISSN 0094114X. DOI: 10.1016/j.mechmachtheory.2010.03.005.

VEER, Sushant; SUJATHA, S. Approximate spring balancing of linkages to reduce actuator requirements. **Mechanism and Machine Theory**, Elsevier Ltd, v. 86, p. 108–124, Apr. 2015. ISSN 0094114X. DOI: 10.1016/j.mechmachtheory.2014.11.014.

WALDRON, Kenneth J; KINZEL, Gary L; AGRAWAL, Sunil K. **Kinematics, dynamics, and design of machinery**. [S.l.]: John Wiley & Sons, 2016.

WALSH, G. J.; STREIT, D. A.; GILMORE, B. J. Spatial spring equilibrator theory. **Mechanism and Machine Theory**, v. 26, n. 2, p. 155–170, 1991. ISSN 0094114X. DOI: 10.1016/0094-114X(91)90080-N.

WANG, Jiegao. **Kinematic analysis, dynamic analysis and static balancing of planar and spatial parallel mechanisms or manipulators with revolute actuators**. 1997. PhD thesis – LAVAL LXIVERSITÉ.

WANG, Jieyu; KONG, Xianwen. A geometric approach to the static balancing of mechanisms constructed using spherical kinematic chain units. **Mechanism and Machine Theory**, v. 140, p. 305–320, Oct. 2019. ISSN 0094114X. DOI: 10.1016/j.mechmachtheory.2019.06.003.

[S.l.]. **An Optimization Method for the Static Balancing of Manipulators Using Springs**. [S.l.]: American Society of Mechanical Engineers, Aug. 2020. p. 1–8. ISBN 978-0-7918-8399-0. DOI: 10.1115/DETC2020-22217.

WENGLARZ, RA; FOGARASY, AA; MAUNDER, L. Simplified dynamic models. **Engineering**, DESIGN COUNCIL PO BOX 167, SITTINGBOURNE ME10 1BR, KENT, ENGLAND, v. 208, n. 5391, p. 194, 1969.

WIKIPEDIA. **Anglepoise lamp model 1227**. [S.l.: s.n.], 2020. Available from: https://en.wikipedia.org/wiki/Anglepoise%7B%5C_%7Dlamp. Visited on: 2020.

WOO, Jaehong; SEO, Jong Tae; YI, Byung Ju. A static balancing method for variable payloads by combination of a counterweight and spring and its application as a surgical platform. **Applied Sciences (Switzerland)**, v. 9, n. 19, 2019. ISSN 20763417. DOI: 10.3390/app9193955.

ZHOU, Libo et al. Design of a passive lower limb exoskeleton for walking assistance with gravity compensation. **Mechanism and Machine Theory**, v. 150, p. 103840, Aug. 2020. ISSN 0094114X. DOI: 10.1016/j.mechmachtheory.2020.103840.

Appendix

APPENDIX A – MATHEMATICAL TOOLS

A.1 PARTIAL DERIVATIVES OF A SCALAR, A VECTOR AND A MATRIX WITH RESPECT TO A VECTOR

Definition 2 (Partial derivatives of a scalar with respect to a vector) *Let scalar $\varphi = \varphi(\mathbf{x})$ be a function of column vector $\mathbf{x} \in \mathbb{R}^n$. The partial derivative of the scalar $\varphi(\mathbf{x})$ with respect to vector $\mathbf{x}$ is defined by (NIKRAVESH, Parviz E., 2018; SHABANA, 2013; VAN KHANG, 2010)*

$$\frac{\partial \varphi}{\partial \mathbf{x}} = \begin{bmatrix} \frac{\partial \varphi}{\partial x_1} & \frac{\partial \varphi}{\partial x_2} & \cdots & \frac{\partial \varphi}{\partial x_n} \end{bmatrix} \tag{309}$$

Definition 3 (Partial derivatives of a vector with respect to a vector) *Let vector $\boldsymbol{\varphi} = \boldsymbol{\varphi}(\mathbf{x}) \in \mathbb{R}^m$ be a function of vector $\mathbf{x} \in \mathbb{R}^n$. The partial derivative of the vector $\boldsymbol{\varphi}(\mathbf{x})$ with respect to vector $\mathbf{x}$ is defined by (NIKRAVESH, Parviz E., 2018; SHABANA, 2013; VAN KHANG, 2010)*

$$\frac{\partial \boldsymbol{\varphi}}{\partial \mathbf{x}} = \begin{bmatrix} \frac{\partial \varphi_1}{\partial \mathbf{x}} \\ \frac{\partial \varphi_2}{\partial \mathbf{x}} \\ \vdots \\ \frac{\partial \varphi_m}{\partial \mathbf{x}} \end{bmatrix} = \begin{bmatrix} \frac{\partial \varphi_1}{\partial x_1} & \frac{\partial \varphi_1}{\partial x_2} & \cdots & \frac{\partial \varphi_1}{\partial x_n} \\ \frac{\partial \varphi_2}{\partial x_1} & \frac{\partial \varphi_2}{\partial x_2} & \cdots & \frac{\partial \varphi_1}{\partial x_n} \\ \vdots & \vdots & \ddots & \vdots \\ \frac{\partial \varphi_m}{\partial x_1} & \frac{\partial \varphi_m}{\partial x_2} & \cdots & \frac{\partial \varphi_m}{\partial x_n} \end{bmatrix} \tag{310}$$

Definition 4 (Partial derivatives of a matrix with respect to a vector) *Let matrix $\mathbf{A} = \mathbf{A}(\mathbf{x}) \in \mathbb{R}^{m \times p}$ be a function of vector $\mathbf{x} \in \mathbb{R}^n$. The partial derivative of the matrix $\mathbf{A}(\mathbf{x})$ with respect to vector $\mathbf{x}$ is defined by (VAN KHANG, 2010)*

$$\begin{aligned} \frac{\partial \mathbf{A}}{\partial \mathbf{x}} &= \begin{bmatrix} \frac{\partial \mathbf{a}_1}{\partial \mathbf{x}} & \frac{\partial \mathbf{a}_2}{\partial \mathbf{x}} & \cdots & \frac{\partial \mathbf{a}_p}{\partial \mathbf{x}} \end{bmatrix} = \begin{bmatrix} \frac{\partial a_{11}}{\partial \mathbf{x}} & \frac{\partial a_{12}}{\partial \mathbf{x}} & \cdots & \frac{\partial a_{1p}}{\partial \mathbf{x}} \\ \frac{\partial a_{21}}{\partial \mathbf{x}} & \frac{\partial a_{22}}{\partial \mathbf{x}} & \cdots & \frac{\partial a_{2p}}{\partial \mathbf{x}} \\ \vdots & \vdots & \ddots & \vdots \\ \frac{\partial a_{m1}}{\partial \mathbf{x}} & \frac{\partial a_{m2}}{\partial \mathbf{x}} & \cdots & \frac{\partial a_{mp}}{\partial \mathbf{x}} \end{bmatrix} \\ &= \begin{bmatrix} \frac{\partial a_{11}}{\partial x_1} & \cdots & \frac{\partial a_{11}}{\partial x_n} & \frac{\partial a_{12}}{\partial x_1} & \cdots & \frac{\partial a_{12}}{\partial x_n} & \cdots & \frac{\partial a_{1p}}{\partial x_1} & \cdots & \frac{\partial a_{1p}}{\partial x_n} \\ \frac{\partial a_{21}}{\partial x_1} & \cdots & \frac{\partial a_{21}}{\partial x_n} & \frac{\partial a_{12}}{\partial x_1} & \cdots & \frac{\partial a_{22}}{\partial x_n} & \cdots & \frac{\partial a_{2p}}{\partial x_1} & \cdots & \frac{\partial a_{2p}}{\partial x_n} \\ \vdots & \ddots & \vdots & \vdots & \ddots & \vdots & \ddots & \vdots & \ddots & \vdots \\ \frac{\partial a_{m1}}{\partial x_1} & \cdots & \frac{\partial a_{m1}}{\partial x_n} & \frac{\partial a_{m2}}{\partial x_1} & \cdots & \frac{\partial a_{12}}{\partial x_n} & \cdots & \frac{\partial a_{mp}}{\partial x_1} & \cdots & \frac{\partial a_{mp}}{\partial x_n} \end{bmatrix} \end{aligned} \tag{311}$$

Definition 5 (Kronecker product of two matrices) *The Kronecker product of two matrices $\mathbf{A}(\mathbf{x}) \in \mathbb{R}^{m \times p}$ and $\mathbf{B}(\mathbf{x}) \in \mathbb{R}^{q \times s}$, denoted by $\mathbf{A} \otimes \mathbf{B}$, is a $mq \times ps$ matrix defined as (LAUB, 2005; VAN KHANG, 2010)*

$$\mathbf{A} \otimes \mathbf{B} = \begin{bmatrix} a_{11}\mathbf{B} & a_{12}\mathbf{B} & \cdots & a_{1p}\mathbf{B} \\ a_{21}\mathbf{B} & a_{22}\mathbf{B} & \cdots & a_{2p}\mathbf{B} \\ \vdots & \vdots & \ddots & \vdots \\ a_{m1}\mathbf{B} & a_{m2}\mathbf{B} & \cdots & a_{mp}\mathbf{B} \end{bmatrix} \tag{312}$$

Theorem 3 (Time derivative of a matrix) *When matrix* $\mathbf{A}(\mathbf{x}) \in \mathbb{R}^{m \times p}$ *is a function of vector* $\mathbf{x} \in \mathbb{R}^n$*, and* $\mathbf{x}(t)$ *is a function of the time, we have the following rule (VAN KHANG, 2010)*

$$\frac{d\mathbf{A}(\mathbf{x})}{dt} = \frac{\partial \mathbf{A}(\mathbf{x})}{\partial \boldsymbol{x}}(\mathbf{I}_n \otimes \dot{\mathbf{x}}) \tag{313}$$

Theorem 4 (Partial derivative of the product of two matrices) *Let the matrices* $\mathbf{A}(\mathbf{x}) \in \mathbb{R}^{m \times p}$ *and* $\mathbf{B}(\mathbf{x}) \in \mathbb{R}^{q \times s}$ *be functions of vector* $\mathbf{x} \in \mathbb{R}^n$*. Then the partial derivative of the matrix product* $\mathbf{A}(\mathbf{x})\mathbf{B}(\mathbf{x})$ *with respect to vector* $\mathbf{x}$ *is given by (VAN KHANG, 2010)*

$$\frac{\partial(\mathbf{AB})}{\partial \mathbf{x}} = \frac{\partial \mathbf{A}}{\partial \mathbf{x}}(\mathbf{B} \otimes \mathbf{I}_n) + \mathbf{A}\frac{\partial \mathbf{B}}{\partial \mathbf{x}} \tag{314}$$